

PhD Thesis

School of Chemistry
Cardiff University



Promoting Supported Noble Metal Catalysts for Enhanced Activity and Selectivity

Thesis submitted in accordance with the requirements of Cardiff
University for the degree of Doctor of Philosophy by:

Alexandra Barnes
2024

Abstract

In this thesis two important reactions in the area of heterogeneous catalysis are explored, the chemoselective hydrogenation of 3-nitrostyrene and the direct synthesis of hydrogen peroxide.

It was found that by tuning the platinum sites of low loading (0.05 – 0.5wt% Pt/TiO₂) through heat treatment that highly active and selective catalysts could be produced for the chemoselective hydrogenation of 3-nitrostyrene to 3-vinylaniline. From a range of characterisation techniques, it was found that by employing an oxidative treatment prior to a second reductive step, a detrimental SMSI (strong metal-support interaction) effect could be prevented, due to the stabilisation of the nanoparticles during calcination. This work resulted in a highly active and selective 0.2wt% Pt/TiO₂ (calcination then reduced at 450°C) catalyst.

This work also investigated the effect of low-level doping of non-precious transition metals to enhance the performance of AuPd-supported catalysts towards the direct synthesis of H₂O₂. In particular, 1%AuPd_(0.975)X_(0.025)/TiO₂ (where X = Cu, Ni, Zn) catalysts prepared by sol-immobilisation were found to be particularly active towards the synthesis of H₂O₂, improving upon the activities seen for the bimetallic analogue 1wt% AuPd/TiO₂ without compromising on the H₂ selectivity towards H₂O₂. It was also observed that increasing the concentration of the tertiary metal above 0.025wt% resulted in a substantial decrease in reactivity, with all catalytic performance dropping below that seen for the bimetallic at a dopant loading of 0.1 wt%.

Developing upon this a 1%AuPd_(0.975)Cu_(0.025)/ZSM-5 catalyst prepared by an excess chloride co-impregnation method, was found to give superior activity to the aforementioned catalysts. The success of these trimetallic catalysts was attributed to electronic modification of the Pd species through the introduction of the dopant metal, as well as changes in the surface composition of the nanoalloys.

Acknowledgements

First, I would like to thank the MaxNet Cardiff Centre on the Fundamentals of Heterogeneous Catalysis for funding this PhD and the EPSRC Centre for Doctoral Training in Catalysts for funding the initial MRes year of this programme. The research in this thesis would not have been possible without this financial support.

Many people have supported me throughout the journey of my PhD, the first person I would like to thank is my academic supervisor Professor Graham Hutchings who welcomed me into the CCI (Cardiff Catalysis Institute), providing laboratory space, equipment, guidance, and endless knowledge.

To my post-doc supervisor Dr Rich Lewis, you went above and beyond the call of duty. You have been a fountain of knowledge in the area of hydrogen peroxide synthesis, you were always available to help, and diligently proof-read this thesis. However, it is the support that you have provided outside the project I am most thankful for, you provided endless coffee, laughs, and a shoulder to cry on through the difficult times. I can't thank you enough for everything you have done.

During my undergraduate research project in the CCI I was supervised by Nikos Dimitratos and Stefano Cattaneo, both of whom encouraged me during my formative studies and to continue in research and pursue a PhD, for their kindness and support I am very grateful.

Thank you to everyone in Team Peroxide, in particular Alba Santos, Joe Brehm, Fenglou Ni, Tom Richards and the MaxNet lab, in particular Naomi Lawes, Anna Lazaridou, and Tanja Parmentier, you all made time in the lab so much fun. Thank you also to Gigi Ososki, who I have studied alongside since undergraduate.

A special thanks must go to the analytical chemists in the department who work tirelessly and without whom a substantial amount of characterisation in this thesis would not have been possible. Dr Thomas Davies provided TEM images, Mr Simon Waller performed ICP-MS analysis and Dr David Morgan provided XPS analysis. I would also like to thank the members of the workshop, who work so hard to keep our labs and equipment running, Mr Steve Morris, Mr Lee Wescombe and Mr Mark Reece. Thanks also to Dr Greg Shaw who works constantly throughout the CCI to make the labs run seamlessly.

The third chapter in this thesis, chemoselective hydrogenation of 3-nitrostyrene, was a large collaboration, so I would like to thank everyone who contributed to this work, Margherita Macino, Sultan Althahban, Ruiyang Qu, Emma K. Gibson, David Morgan, Simon Freakley, Nikolaos Dimitratos, Christopher Kiely, Xiang Gao, Andrew Beale, Donald Bethell, Qian He, Meenakshisundaram Sankar and Graham Hutchings.

Thank you to everyone in the CCI, there are so many of you that it is impossible to mention everyone by name, but you have made this PhD enjoyable as well as educational.

Additionally, I would also like to express my thanks to Ms George Summers and Miss Caru Shanahan in the postgraduate office, both of you are always there to help with a smile on your face.

I would like to thank my friends outside of the lab that have been there for me throughout this PhD. Briony Munslow, you have been there for me since we met at university, our friendship means so much to me. Thank you also to Becky Slinger, Dave Whelan and Brad Saunders. Bethany Harteveld and Joe Macginley, thank you for the many games nights we have had over the past few years. Thank you to Oishee Kundu who has kept me company when also working-from-home.

To my family, none of this would have been possible without you. Mum and Dad; you have always supported me and are my biggest cheerleaders. Vicky Rawlins-Barnes; my sister, you have always been by my side, and I loved having you in Cardiff with me. I would also like to thank my loving grandparents, aunts and uncles.

Finally, thank you to the best writing companions in the whole world, my beautiful cats Heidi and Lily (yes, I will be blaming any typos on you both!)

Publications

1. Tuning of catalytic sites in Pt/TiO₂ catalysts for the chemoselective hydrogenation of 3-nitrostyrene

M Macino, A. J. Barnes, S. M. Althahban, R. Qu, E. Gibson, D. J Morgan, S. J. Freakley, N. Dimitratos, C. J. Kiely, X. Gao, A. M. Beale, D. Bethell, Q. He, M. Sankar and G. J. Hutchings, *Nat Catal.*, 2019, **2**, 873–881.

2. Probing Composition Distributions in Nanoalloy Catalysts with Correlative Electron Microscopy

S. Liu, I. Gow, T. Davies, A. Barnes, M. Sankar, X. Gong, A. G. R. Howe, M. Dixon, G. J. Hutchings, C. J. Kieley and Q. He, *J. Mater. Chem. A*, 2020, **8**, 15725-15733.

3. Lanthanum modified Fe-ZSM-5 zeolites for selective methane oxidation with hydrogen peroxide

S. Sun, A. J. Barnes, X. Gong, R. J. Lewis, N. F. Dummer, T. Bere, G. Shaw, N. Richards, D. J. Morgan and G. J. Hutchings, *Catal. Sci. Technol.*, 2021, **11**, 8052-8064.

4. Selective oxidation of methane to methanol and methyl hydroperoxide over palladium modified MoO₃ photocatalyst under ambient conditions

S. Sun, N. F. Dummer, T. Bere, A. J. Barnes, G. Shaw, M. Douthwaite, S. Patisson, R. J. Lewis, N. Richards, D. J. Morgan and G. J. Hutchings, *Catal. Sci. Technol.*, 2022, **12**, 3727-3736.

5. Enhancing catalytic performance of AuPd catalysts towards the direct synthesis of H₂O₂ through incorporation of base metals

A. J. Barnes, R. J. Lewis, D. J. Morgan, T. E. Davies and G. J. Hutchings, *Catal. Sci. Technol.*, 2022, **12**, 1986-1995.

6. Improving Catalytic Activity towards the Direct Synthesis of H₂O₂ through Cu Incorporation into AuPd Catalysts

A. J. Barnes, R. J. Lewis, D. J. Morgan, T. E. Davies and G. J. Hutchings, *Catalysts*, 2022, **12**, 1396.

Table of Contents

| | |
|--|----|
| Chapter 1: Introduction..... | 1 |
| 1.1 Basics of Catalysis..... | 1 |
| 1.1.1 What is catalysis? | 1 |
| 1.1.2 Catalyst Deactivation..... | 4 |
| 1.1.3 Catalytic Mechanisms | 4 |
| 1.1.4 Sabatier's Principle..... | 6 |
| 1.1.5 Rate Order Kinetics | 7 |
| 1.2 Chemoselective hydrogenation of nitrostyrene and other substituted nitroarenes | 8 |
| 1.2.1 Selective reduction of substituted nitroaromatics..... | 8 |
| 1.2.2 Proposed mechanisms of nitroarene reduction | 9 |
| 1.2.3 Hydrogen Source..... | 11 |
| 1.2.4 Catalyst Selectivity | 15 |
| 1.2.5 Monometallic Catalysts..... | 17 |
| 1.2.6 Catalysts incorporating non-precious metals..... | 19 |
| 1.2.7 Bimetallic Catalysts | 22 |
| 1.2.8 Single Atom Catalysts and Nanocluster Catalysts | 26 |
| 1.2.9 Summary of Pt catalysts of the Selective Hydrogenation of 3-Nitrostyrene..... | 28 |
| 1.3 Hydrogen Peroxide..... | 30 |
| 1.3.1 Uses of H ₂ O ₂ | 31 |
| 1.3.2 The Anthraquinone Oxidation Process | 32 |
| 1.3.3 Alternative Methods of H ₂ O ₂ Production..... | 36 |
| 1.3.4 Direct Hydrogen Peroxide Synthesis | 37 |
| 1.3.5 Solvents and Gas Dilutants for Direct H ₂ O ₂ Synthesis..... | 40 |
| 1.3.6 Catalyst Preparation Methods | 42 |
| 1.3.7 AuPd Bimetallic Catalysts for Direct H ₂ O ₂ Synthesis | 44 |
| 1.3.8 Incorporation of Non-Precious Metals into Pd Catalysts | 48 |
| 1.3.9 Trimetallic Catalysts for Direct H ₂ O ₂ Synthesis..... | 51 |

| | |
|---|----|
| 1.4 References..... | 57 |
| Chapter 2: Experimental | 64 |
| 2.1 Reagents..... | 64 |
| 2.2 Catalyst Preparation..... | 66 |
| 2.2.1 Wet Impregnation | 66 |
| 2.2.2 Sol-Immobilisation | 66 |
| 2.2.3 Excess Chloride Wet Co-Impregnation..... | 67 |
| 2.2.4 Catalyst Precursors..... | 67 |
| 2.3 Catalyst Testing..... | 68 |
| 2.3.1 3-Nitrostyrene Hydrogenation | 68 |
| 2.3.2 Direct Hydrogen Peroxide Synthesis | 69 |
| 2.3.3 Time-on-Line Experiments for the Direct Hydrogen Peroxide Synthesis | 70 |
| 2.3.4 Gas Replacement Experiments for the Direct Synthesis of H ₂ O ₂ | 70 |
| 2.3.5 Catalyst Reusability in the Direct Synthesis and Degradation of H ₂ O ₂ | 70 |
| 2.3.6 Hydrogen Peroxide Degradation | 70 |
| 2.4 Characterisation Techniques | 71 |
| 2.4.1 GC (Gas Chromatography)..... | 71 |
| 2.4.2 UV-Vis (Ultraviolet-Visible Spectroscopy) | 73 |
| 2.4.3 FT-IR (Fourier Transform Infra-Red Spectroscopy) | 76 |
| 2.4.4 CO-DRIFTS (Diffuse Reflectance Infrared Fourier Transform Spectroscopy) | 77 |
| 2.4.5 Chemisorption..... | 79 |
| 2.4.6 N ₂ Physisorption Isotherms (N ₂ adsorption/ desorption Isotherms) | 81 |
| 2.4.7 TEM and STEM (Transmission Electron Microscopy and Scanning Transmission Electron Microscopy)..... | 82 |
| 2.4.8 ICP-MS (Inductively Coupled Plasma Mass Spectrometry) | 86 |
| 2.4.9 XRD (X-Ray Diffraction)..... | 87 |
| 2.4.10 XPS (X-Ray Photoelectron Spectroscopy)..... | 89 |
| 2.4.11 XAS (X-Ray Absorption Spectroscopy)..... | 93 |
| 2.5 References..... | 96 |

| | |
|---|-----|
| Chapter 3: Tuning of Catalytic Sites in Pt/TiO ₂ Catalysts for the Chemoselective Hydrogenation of 3-Nitrostyrene | 98 |
| 3.1 Introduction | 98 |
| 3.2 Results and Discussion | 100 |
| 3.2.1 Hydrogenation of 3-Nitrostyrene | 100 |
| 3.2.2 Electron Microscopy Studies | 107 |
| 3.2.3 X-ray Photoelectron Spectroscopy Studies | 113 |
| 3.2.4 X-ray Absorption Spectroscopy Studies | 116 |
| 3.2.5 CO-DRIFTS (CO Diffuse Reflectance Infrared Fourier Transform Spectroscopy) and Chemisorption Analysis..... | 120 |
| 3.3 Conclusions | 125 |
| 3.4 References..... | 126 |
| Chapter 4: Enhancing catalytic performance of AuPd catalysts towards the direct synthesis of H ₂ O ₂ through incorporation of base metals. | 128 |
| 4.1 Introduction | 128 |
| 4.2 Results and Discussion | 130 |
| 4.2.1 Investigating the effect of tertiary metal incorporation on the direct synthesis of H ₂ O ₂ . . | 130 |
| 4.2.2 Optimising the tertiary metal loading in AuPdNi, AuPdZn and AuPdCu supported catalysts | 136 |
| 4.2.3 Further Study and Characterisation of the optimised 1wt% AuPd _(0.975) X _(0.025) /TiO ₂ catalysts. | 139 |
| 4.2.4 Investigating 1wt% AuPd _(0.975) X _(0.025) /TiO ₂ Over Prolonged Reaction Times | 146 |
| 4.2.5 Reusability of trimetallic catalysts..... | 150 |
| 4.3 Conclusions | 156 |
| 4.4 References..... | 157 |
| Chapter 5: Improving Catalytic Activity towards the Direct Synthesis of H ₂ O ₂ through Cu Incorporation into AuPd/ZSM-5 Catalysts..... | 159 |
| 5.1 Introduction | 159 |
| 5.2 Results and Discussion | 161 |
| 5.2.1 Screening the tertiary metal | 161 |
| 5.2.2 Optimisation of Cu loading in 1wt% AuPd _(1-x) Cu _(x) /ZSM-5 for the Direct Synthesis of H ₂ O ₂ | 169 |
| 5.2.3 Further Study and Characterisation of 1wt% AuPd _(0.975) Cu _(0.025) /ZSM-5..... | 174 |

| | |
|--|-----|
| 5.2.4 Reusability of trimetallic catalysts..... | 179 |
| 5.3 Conclusions | 187 |
| 5.4 References..... | 189 |
| Chapter 6: Conclusions and Future Work | 191 |
| 6.1 Tuning Pt/TiO ₂ Catalysts for the Chemoselective Hydrogenation of 3-Nitrostyrene | 191 |
| 6.1.1 Conclusions | 191 |
| 6.1.2 Future Work | 193 |
| 6.2 Direct Synthesis of H ₂ O ₂ using Transition Metal Incorporated AuPd Catalysts | 194 |
| 6.2.1 Conclusions | 194 |
| 6.2.2 Future Work | 197 |
| 6.3 References..... | 199 |

Chapter 1: Introduction

1.1 Basics of Catalysis

1.1.1 What is catalysis?

Catalysis was first described by Berzelius in 1835:

*The property of exerting on other bodies an action which is very different from chemical affinity. By means of this action, the produce decomposition in bodies, and form new compounds into the composition of which they do not enter.*¹

Essentially, a catalyst provides an alternate pathway for a reaction to proceed at a lower activation energy, and hence increases the rate at which the reaction can reach equilibrium, while not being consumed in the reaction,^{2,3} as shown pictographically in Figure 1.1. The alternate pathway provided by the catalyst can involve multiple transition and intermediate states.³ Transition states last for one bond vibration cycle, it is the association of atoms at the highest energy point of the reaction.^{4,5} Whereas intermediate states are more stable than the transition state and can be isolated, though not all intermediates will be stable as they can include radicals for example.⁴

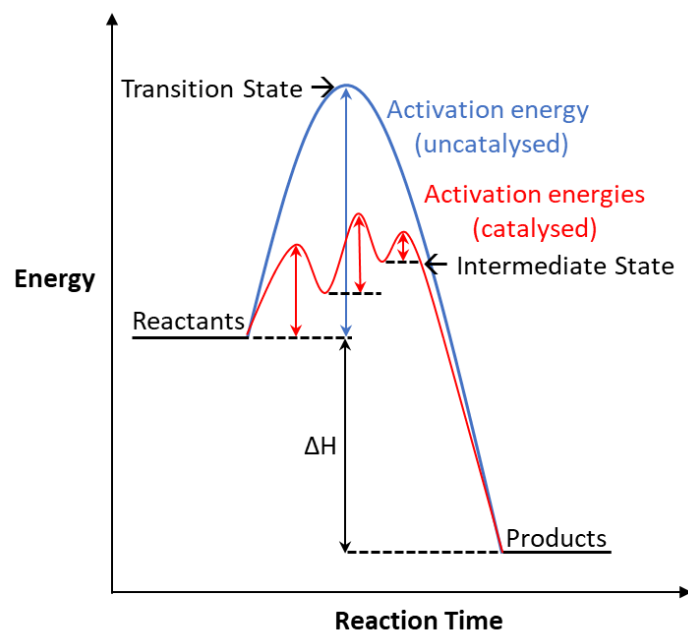


Figure 1.1: Effect of a catalyst on a reaction energy profile.

As the catalyst is unchanged by the reaction, it can be used for many consecutive reactions and only a small quantity is required compared to the substrate. It is important to note that a catalyst will not change the position of equilibrium, this can be altered by temperature or pressure.^{2,3} Catalyst efficiency can be measured by turnover number (TON), which is essentially the amount of product per unit catalyst or turnover frequency (TOF), which is the amount of product per number of catalyst active sites per unit time, however units can vary.^{2,3}

Catalysis is a useful tool in green chemistry, also known as sustainable chemistry. The aim of green chemistry is to reduce the impact of chemical processes on the environment. This is achieved through 12 main principles:^{3,6}

1. Prevention of waste production.
2. Increased atom economy, to maximise the reactants used to make the desired product.
3. Synthesis of less hazardous chemicals to both health and the environment.
4. Design of safer chemicals
5. Use of safer solvents and other auxiliary substances such as separating agents.
6. Energy efficiency to minimise environmental impact.
7. Use of renewable feedstocks and raw materials, rather than having to mine for materials and deplete stocks.
8. Reduce derivatives (e.g. blocking groups, modifications etc) as these extra steps have an additional environmental impact in addition to the necessary process.
9. Use catalysts (not stoichiometric reagents).
10. Design chemicals for easy degradation so as not to have a lasting impact and presence in the environment.
11. Reduce pollution in chemical processes.
12. Safer chemical procedures to minimise hazardous accidents.

It is notable that although catalysis is listed as one of the main principles it contributes to many of the other aspects as it allows chemical reactions to be performed at much milder (hence, safer) conditions, namely lower temperatures, while improving selectivity and reducing waste products.

There are three types of catalysts, heterogeneous, homogeneous and enzymes. A heterogeneous catalyst is in a different phase to the reactants and at least one of the reactants will be adsorbed onto the catalyst surface, for example a solid catalyst in a liquid or gaseous phase reaction mixture, this is particularly advantageous in terms of catalyst separation.³ Common examples of heterogeneous catalysts include Fe used to catalyse the Haber process (to produce ammonia) and catalytic converters to convert exhaust emissions into less toxic pollutants.^{2,3}

A homogeneous catalyst will be in the same phase as the reactants (and products).³ During the catalytic cycle the catalyst itself will change and form catalytic intermediates, but it will have returned to its original form by the end of the reaction and can then be reused in the next cycle.³ Many homogeneous catalysts consist of a transition metal stabilised by a ligand (often an organic molecule), and by altering the ligand, and addressing factors such as stereochemical and electronic properties, the catalyst selectivity, activity, and stability can be tuned.³ For example Wilkinson's catalyst $[\text{RhCl}(\text{PPh}_3)_3]$ is used to catalyse the hydrogenation of alkenes.³

Enzymes are biological catalysts made from nitrous organic compounds (proteins), and the reaction will occur at a specific active site on the protein.³ Some enzymes require a cofactor (non-protein) to function.³ Advantages include that they are naturally selective as the enzyme will only make a specific product, this can even extend to chirality whereby a specific enantiomer can be synthesised.³ Additionally, mild conditions are typical to prevent denaturing and they give a very high turnover.³ However, due to the lower stability of enzymes they can be undesirable industrially as they can be particularly sensitive to temperature and pH and can denature, for example enzymes in the human body work best at 310 K.³ There are six main groups of enzymes: oxidoreductases, transferases, hydrolases, lyases, isomerases and ligases.³ When the substrate (reactant) binds with the enzyme an intermediate enzyme substrate complex is formed, there are various mechanisms proposed for how this intermediate is formed, namely the lock-and-key and induced-fit models.^{3,5} One example of an enzyme is lactase which breaks down lactose into glucose and galactose, another is trypsin which converts proteins to amino acids (in the small intestine).

1.1.2 Catalyst Deactivation

It is often observed that as a reaction progresses or upon reuse of a catalyst it can become less active. In heterogeneous catalysis thermal degradation and sintering (agglomeration of metal particles) are common issues.³ High temperatures can cause structural changes to the support and the pores, additionally, metal particles can undergo changes to their shape, size and oxidation state, also metal leaching from the catalyst support can occur.³ These factors result in a decrease in catalytic surface area and the number of available active sites.³

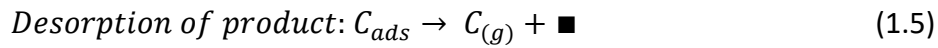
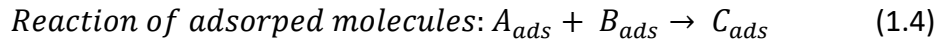
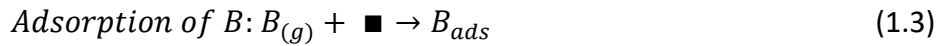
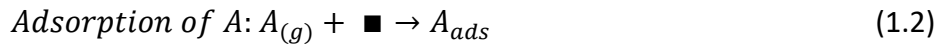
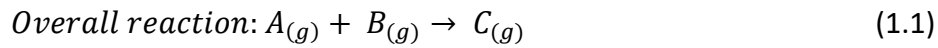
Catalysts can also suffer from competitive inhibition, this occurs largely in enzymatic processes, however it can also occur in homogeneous and heterogeneous catalysis, where is more commonly referred to as competitive adsorption.^{2,3} This involves a different molecule competing with the reactant for the active site, to combat this an excess of reactant(s) can be used.³ In enzyme catalysis non-competitive inhibition can also occur whereby a molecule will bind to an allosteric site and denature the catalyst by changing the properties of the active site.³

Irreversible catalyst inhibition is referred to as catalyst poisoning, in heterogeneous catalysis there are two types of poisoning, permanent and temporary.³ Temporary poisoning of a catalyst can be overcome by regenerating the catalyst, usually achieved by high temperature treatment such as recalcination.³

1.1.3 Catalytic Mechanisms

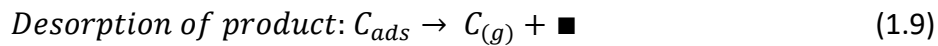
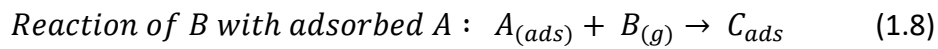
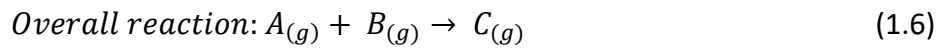
Various mechanisms have been proposed to describe how molecules in different catalytic systems interact on a catalyst surface to form the product, three predominant mechanisms include Langmuir-Hinshelwood, Eley-Rideal and Mars-Van Krevelen.⁷

The Langmuir-Hinshelwood mechanism states that in certain bimolecular reactions (two molecules in the rate-determining step), both molecules adsorb (separately) onto the catalyst surface at adjacent sites, where the reaction then occurs, and the product is then desorbed from the catalyst surface.^{2,3,7} This can also apply to a unimolecular reaction (where there is only one reactant involved in the rate-determining step) and can often describe enzyme kinetics.⁷ Equations 1.1-1.5 describe the Langmuir-Hinshelwood mechanism.⁷



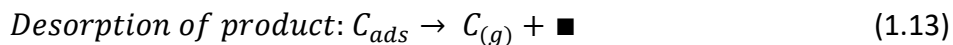
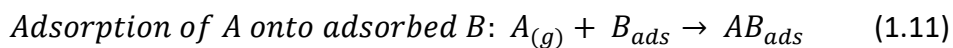
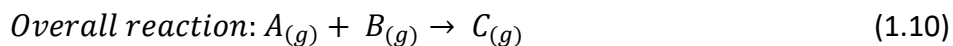
Where \blacksquare is a vacant site on the catalyst.

In the Eley-Rideal mechanism one reactant is absorbed onto the catalyst and the other reacts directly with the adsorbed molecule from the gas or liquid phase.^{2,3,7} This mechanism was originally used to describe hydrogenation of metals.⁷ Equations 1.6-1.9 describe the Eley-Rideal mechanism.⁷



Where \blacksquare is a vacant site on the catalyst.

For the Mars-Van Krevelen mechanism, absorption of molecule occurs on top of a previously adsorbed molecule.⁷ This mechanism was first developed as a way to kinetically describe the oxidation of SO₂ by a molten V/K on porous silica.⁷ However, it is assumed for many oxidation reactions, such as the selective oxidation of hydrocarbons, and has also been applied to reactions including hydrodesulfurisation and NO_x removal.⁷ Equations 1.10-1.14 describe the Mars-Van Krevelen mechanism.⁷





Where \blacksquare is a vacant site on the catalyst.

1.1.4 Sabatier's Principle

An important consideration in catalysis is the phenomenon described by Sabatier's principle.³ This concept demonstrates (Figure 1.2) in the form of a volcano plot, the importance of the interaction between the substrate and the catalysts. A weak interaction could result in losing contact with the substrate with no reaction taking place, causing the reaction to be adsorption limited (adsorption of the reactants onto the catalyst surface is the rate determining step), whereas too strong an interaction could cause the substrate or product to not leave the catalyst, (desorption limiting) causing inhibition/ poisoning.³ Sabatier optimisation is the point at the top of the volcano plot where the interaction between both the reactants and products with the catalyst surface results in the highest reaction rate.³ Factors such as the type of metals incorporated in a catalyst can effect this interaction, an example of this is cyclohexane dehydrogenation where the position in the periodic table of the metal in transition metal sulphides for hydrodesulfurisation reaction seen in Figure 1.2(b).³

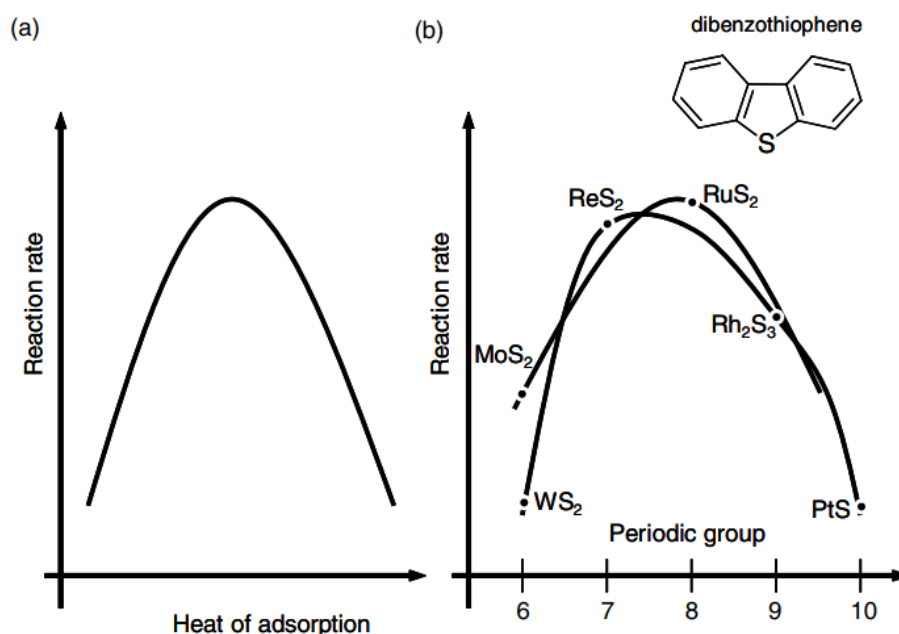


Figure 1.2: (a) Sabatier's Principle showing the reaction rate as a function of heat of adsorption and (b) activity of 2nd row and 3rd row transition metal sulfides for hydrodesulfurization of dibenzothiophene.³

1.1.5 Rate Order Kinetics

Catalytic reactions often follow zero, first and second order rate laws. If a reaction is zero order, then the rate of reaction is constant and independent of the concentration of reactants, and the reaction will continue at a constant rate until the limiting reactant is consumed.^{2,3,7} For a first order reaction the rate of the reaction is linearly dependent upon the concentration of one reactant.^{2,3,7} In a second order reaction the rate of concentration is proportional to the concentration of two reacting molecules.^{3,7} This is shown in Figure 1.3 with the respective integrated rate laws (k = rate constant).³

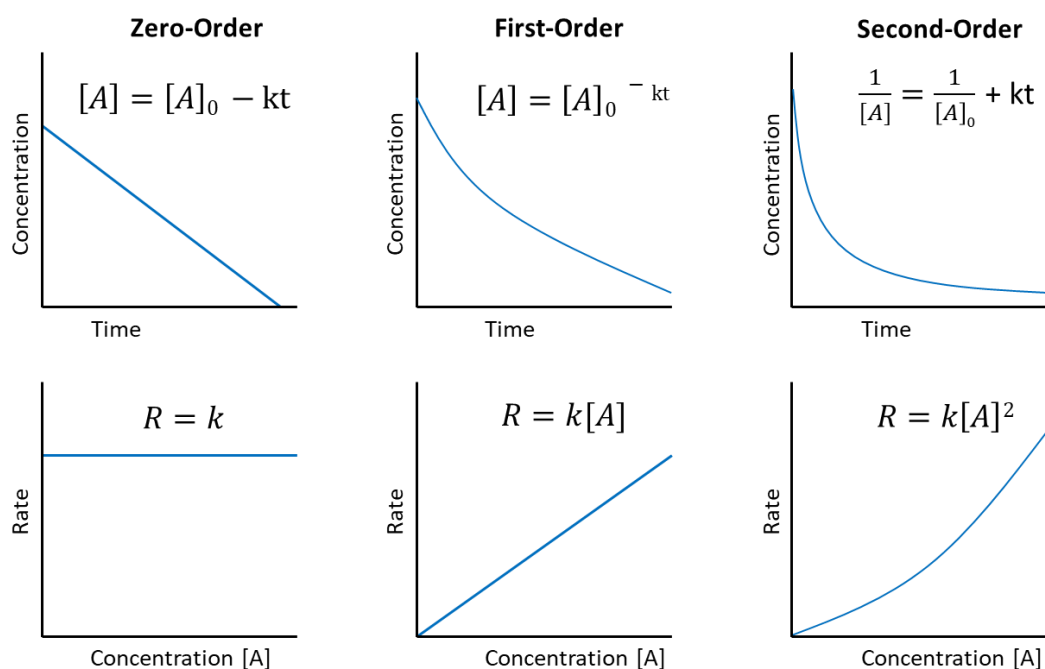


Figure 1.3: Zero-Order, First-Order and Second-Order Rate kinetics.

1.2 Chemoselective hydrogenation of nitrostyrene and other substituted nitroarenes

1.2.1 Selective reduction of substituted nitroaromatics

The selective hydrogenation of substituted nitroaromatics to their corresponding anilines is important, with functionalised anilines used in pharmaceuticals, agrochemicals, dyes, and fine chemicals.⁸ However, in nitroarenes with additional reducible groups (including $-C=C-X-$, $C=O$, $-C\equiv C$ and $-C\equiv N$), selectivity can be an issue as many heterogeneous catalysts will reduce both the intended nitro group and the other reducible site.⁸ For example, in 3-nitrostyrene (used in this thesis) there is a reducible $C=C$ functional group that is thermodynamically and kinetically favourable compared to the nitro group, and for the desired product, 3-vinylaniline, this must be avoided. Therefore, to avoid unwanted byproducts which will reduce the yield and selectivity, a selective catalyst towards the nitro group must be created. Not only is selective hydrogenation of nitrostyrene an important reaction in itself to produce functionalised anilines, but it is also a useful model reaction for investigating the selectivity of catalysts, due to the presence of the $C=C$ functional group.

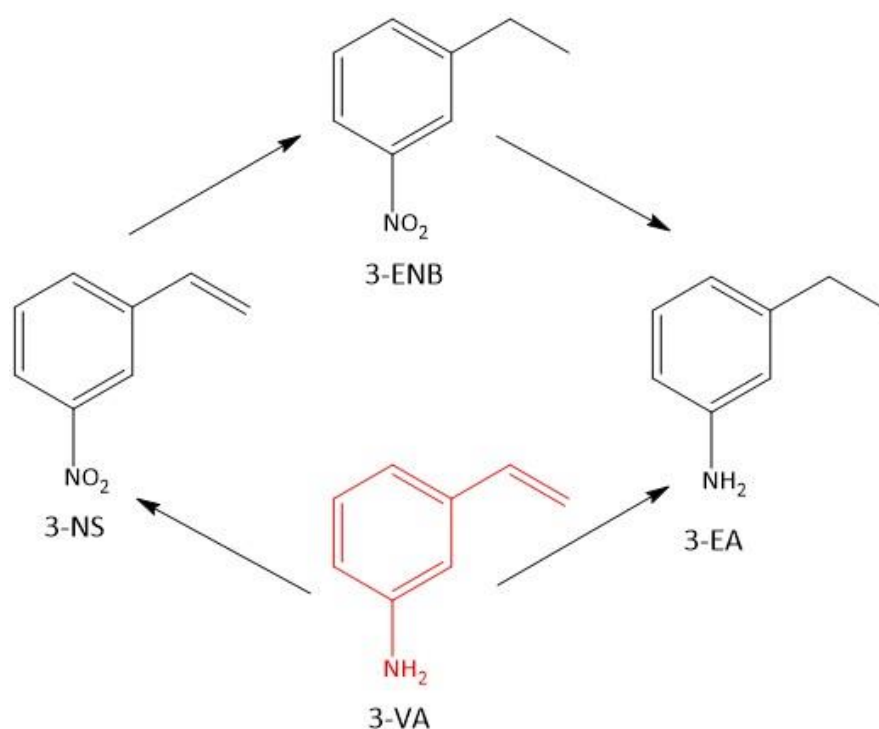


Figure 1.4: Chemoselective hydrogenation of 3-nitrostyrene (3-NS) to 3-vinylaniline (3-VA), including side products 3-ethylnitrobenzene (3-ENB) and 3-ethylaniline (3-EA).

Initial research into the reduction of nitroarenes was performed in 1854 by Bechamp where a metal and acid were used to reduce the nitro group.⁹ Obvious disadvantages to this methodology include toxicity and difficult separation of the product from the reaction medium.

1.2.2 Proposed mechanisms of nitroarene reduction

It is widely accepted the mechanism devised by Haber for the reduction of a nitroarenes to the corresponding amine.^{8,10} Figure 1.5 shows the two proposed reaction pathways.

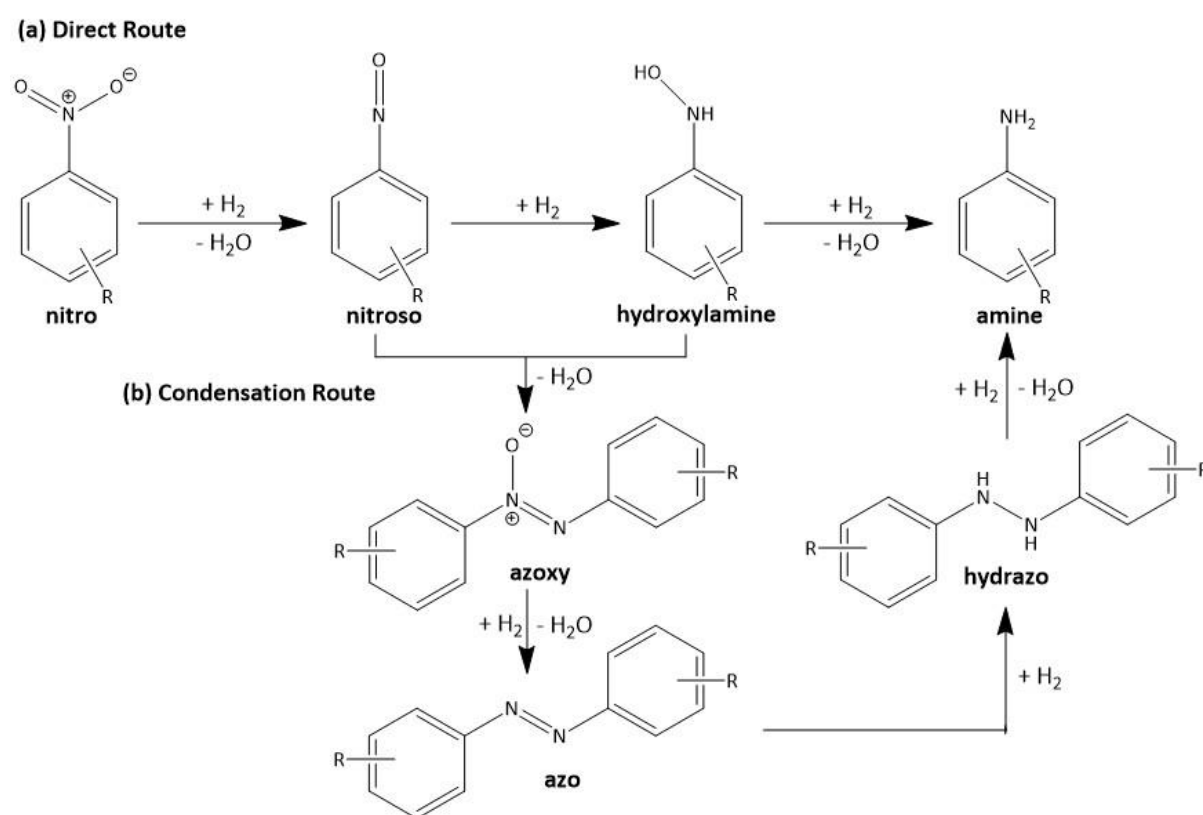


Figure 1.5: Haber mechanisms for the chemoselective hydrogenation of nitroarenes by (a) the direct route and (b) the condensation route.

The direct route is the most obvious pathway, first the nitro group is reduced to a nitroso group, it is then further reduced to form a hydroxyl amine, and then reduced again to form the amine.⁸ For the formation of the amine from the hydroxylamine cleavage of the N-O is needed, this is a slow step comparably, and therefore an active catalyst is required to prevent large build-up of the hydroxylamine and the potential result of unwanted by-products from

competing side-reactions.⁸ The second pathway, known as the condensation pathway, the aforementioned nitroso and hydroxylamine complexes undergo a condensation reaction to form an azoxy species, which then undergoes reduction to form an azo, another reduction to form a hydrazo, then further reduced whereby the molecule is split to form two amines, this pathway occurs under alkaline conditions.⁸ Examples of catalytic nitroarene reductions following the direct pathway over Co–Mo₂C/AC¹¹ (AC = activated carbon) and Pd₁/GDY/G¹² (GDY/G = graphdiyne/graphene) catalysts have been reported. While a Pd/Fe₃O₄@C¹² catalyst has been reported to follow the condensation route.

Interestingly Corma *et al.*,¹³ have shown that the direct route can also bypass production of the nitroso group and instead form the hydroxylamine compound directly from the nitro group. In this instance an Au/TiO₂ catalyst was used for the reduction of nitrobenzene and nitroso-benzene, it was found that the quantity of the intermediate phenylhydroxylamine was higher when nitrobenzene was the starting material as opposed to nitroso-benzene. This indicated that the primary source of phenylhydroxylamine is coming directly from the nitrobenzene and any produced from the formation of the nitroso species is merely a secondary source. It has also been reported by Nie *et al.*¹⁴ that nitro reduction over a Pt/RGO-EG (RGE = reduced graphene oxide, EG = prepared by ethylene glycol reduction) catalyst follows the direct route where the nitroso species is bypassed.

DFT (Density Functional Theory) calculations were performed by Sheng *et al.*¹⁵ for the reduction of nitrobenzene over a Pt(111) model catalyst. Calculations indicated that the energy of double H-induced dissociation of the N-O bond is considerably lower than either direct dissociation or single H-induced dissociation. This suggests that the most favourable mechanism for nitrobenzene hydrogenation according to these calculations is shown in Figure 1.6.

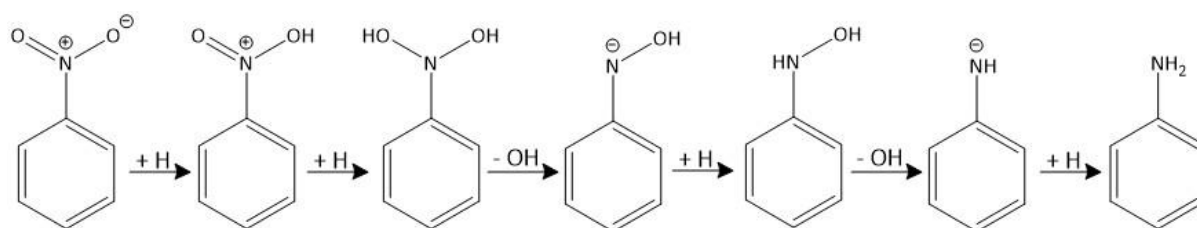


Figure 1.6: Mechanism for chemoselective hydrogenation of 3-nitrobenzene by double H-induced dissociation of the N-O bond.

Supporting this mechanism are reactions over $\text{Fe}_1/\text{N-C}$ ¹⁶ (N-C = mesoporous nitrogen doped carbon) and $\text{Fe}_3\text{O}_4@\text{SiO}_2\text{-NH}_2\text{-FeCu}$ ¹⁷ nanoparticle catalysts. It can be deduced that due to a number of observed mechanisms for this reaction, the environmental conditions (including catalyst) have an effect of the mechanism and therefore the intermediates.⁸ Different mechanisms can give rise to different intermediates and possible side products. It is therefore important to tailor the conditions to optimise the mechanism and get the most selective conversion of nitroarenes to their corresponding anilines.

1.2.3 Hydrogen Source

In terms of green chemistry use of hydrogen gas (when it is from a green source) as the hydrogen source is advantageous due to the only by-product being water. However, catalytic transfer hydrogenation (CTH) can be performed by other hydrogen donors for the hydrogenation of nitroarenes, including methanol (CH_3OH), formic acid (HCOOH), sodium borohydride (NaBH_4), ammonia borane ($\text{NH}_3\cdot\text{BH}_3$), or hydrazine (N_2H_4).^{8,18} The hydrogen donor selected for the reaction can affect selectivity and activity of the reduction. For example, Furukawa *et al*¹⁹ investigated the reduction of 4-nitrostyrene to 4-vinylaniline with a $\text{RhPb}_2/\text{SiO}_2$ catalyst, when molecular hydrogen was used as the reductant selectivity was 91% at 36% conversion, compared to methanol as the reductant with a selectivity of 93% at 94% conversion.

The superior selectivity of the donor hydrogen molecules stems from the ease of formation of the active hydrogen compared to formation by dissociation of molecular H_2 . Activation of molecular hydrogen can occur in one of two ways, the first being homolytic dissociation where cleavage of the hydrogen bond forms two hydrides, this process involves the catalyst accepting the σ electrons of the H_2 molecule and providing d-electrons to its σ^* antibonding orbital.^{8,20,21} The alternative is heterolytic dissociation where cleavage of the hydrogen bond forms H^+ and H^- due to either the presence of a nucleophilic atom or a strong electric field, in this instance the H^+ binds to the proton acceptor and then hydrogenates a polar group, in this case NO_2 .^{8,20-22} Both methods of producing active hydrogen on the catalyst surface from molecular hydrogen give a high activity but low selectivity.⁸

Sodium borohydride and ammonia borane are a common choice for catalytic transfer hydrogenation as both have a high hydrogen content, also they have good stability and can be transported easily.^{23–25} However, NaBH_4 is a toxic chemical and therefore not an ideal hydrogen source for use in green chemistry, and both hydrogen donors will produce side products that decrease atom economy of the process compared to pure H_2 . For a catalyst to produce activated hydrogen from a molecule a negative hydrogen reagent is required, with the electronegativity of hydrogen being 2.2 compared to boron being 2.04 and hence both aforementioned molecules fit this criterion.⁸ NaBH_4 is highly reactive and will react with aldehydes, ketones and olefins without a catalyst, and is therefore selective to these groups, however reduction of the nitro group requires a catalyst, in particular a catalyst that is selective to reduction of the nitro groups over other reducible/ unsaturated groups.⁸

Formic acid is another hydrogen rich donor that can be synthesised renewably from either lignocellulosic biomass or by electrochemical reduction of carbon dioxide.²⁶ The active hydrogen species is formyl hydrogen and the protonic hydrogen on the carboxyl group is involved in the reaction.²⁷ However, there is a poor hydrogenation activity due to the rapid proton exchange that occurs in protic solvents. There are two proposed reaction pathways for formic acid as a hydrogen donor to the nitro group.²⁶

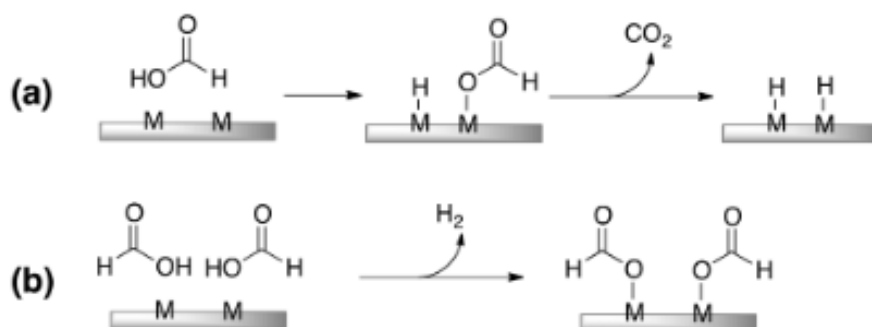
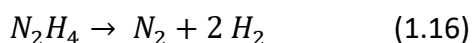
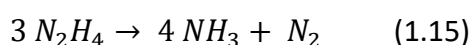


Figure 1.7: Reaction pathways for formic acid as a hydrogen donor (a) via adsorbed hydrogen (b) formate reacts directly with the nitro group.²⁶

The first proposal is that the formic acid produces adsorbed hydrogen and carbon dioxide on the catalyst surface, the hydrogen then can react with an adsorbed nitro group adjacent on the catalyst surface.²⁶ The alternative proposal is that the formate species directly reacts with

the nitro group, this latter proposal could be more selective because the activation of the species does not require dissociation of the hydrogen.²⁶

Hydrazine hydrate ($N_2H_4 \cdot H_2O$) is highly active as a hydrogen donor and is able to reduce a nitroarene without the presence of a catalyst.²⁸ It also has the highest natural selectivity towards the nitro- group compared to the aforementioned hydrogen donors.^{8,29} However, it should be noted that use of hydrazine should be limited for green chemistry applications due to its high toxicity. The presence of a catalyst is able to improve the selective utilisation of hydrazine. It has been found that for the reduction of *o*-chloronitrobenzene to *o*-chloroaniline over Pt catalysts (with complete *o*-chloronitrobenzene conversion), that hydrazine was far more selective than hydrogen.³⁰ Notably using a 2% Pt/CMK-3-HQ catalyst (mesoporous carbon support) with hydrazine gave 100% selectivity, whereas hydrogen gave 96.2% selectivity towards the aniline.³⁰ Wei *et al.*²⁹ reported the reduction of 4-methoxynitrobenzene to 4-methoxyaniline over a 0.5% Ru/OMS-IL catalyst (mesoporous silica support) using hydrazine gave > 99% selectivity whereas $NaHB_4$ gave 64% selectivity. It has also been reported that for the reduction of 3-nitrostyrene to 3-aminostyrene over a Rh/ α -FeOOH catalyst, with hydrazine as the hydrogen source a selectivity of 97% was achieved even after increasing the hydrazine concentration and continuing the reaction past 100% conversion, meaning that further hydrogenation of the other functional groups still did not occur.²⁹ This reiterates the selectivity of hydrazine specifically to the nitro group. There are two proposed pathways for the decomposition of hydrazine shown in Equation 1.15 and 1.16:³¹



For the reduction of nitroarenes the ideal pathway is the second equation, where there are 4 possible active hydrogens produced.^{32,33} This pathway would make hydrazine a green reducing agent as the only by-product is nitrogen. Sheng *et al.*³⁰ have proposed that over a Pt catalyst, the heterolytic cleavage of hydrazine hydrate makes an intermediate Pt-H⁻ species which then reduces the nitro- group.

For the reduction of nitrostyrene (and other nitroarenes) it is important to consider what reducible groups are most susceptible to reduction by the various hydrogen donors, and

therefore, which would give the best selectivity. In the presence of a catalyst molecular hydrogen (H_2) is able to reduce a range of functional groups including $-NO_2$ $-C=C$ $-X$ $-C=O$ $-C\equiv C$ and $-C\equiv N$ indicating that H_2 has poor natural selectivity.⁸ Therefore, a finely tuned catalyst is required to tailor selectivity to the desired functional group while multiple reducible groups are present. $NaBH_4$ and $NH_3\cdot BH_3$ both have similar reactivity with reducible functional groups, they both are able to spontaneously react with $-C=O$ groups (in the absence of a catalyst) and they catalytically react with $-NO_2$ $-X$ and $-C\equiv N$ groups.⁸ Additionally, $NaBH_4$ is also able to spontaneously reduce electron deficient $-C=C$ bonds such as nitroalkenes, and catalytically reduce electron-rich $-C=C$ groups.⁸ Formic acid catalytically reacts with $-NO_2$ $-C=O$ and $-C\equiv N$ functional groups, however, will not react with $-C=C$ or $-X$ groups.⁸ It has been well established that $N_2H_4\cdot H_2O$ will react catalytically with the $-NO_2$ functional group to form $-NH_2$ and it is also able to undergo a substitution reaction with a halogen ($-X$ group), and reacts with $-C=O$ and $-C\equiv N$ functional groups.⁸ However, even catalytically it will not react (or reacts very poorly) with $-C=C$ groups.⁸ The selectivity of hydrazine to the nitro group over the alkene functional group makes this hydrogen donor very desirable to reduction of nitrostyrene and it will be highly selective to the aniline product.⁸ Other notable reductants that have not been mentioned are isopropanol (C_3H_7OH) which reacts catalytically with $-NO_2$ and $-C\equiv N$ groups however is non-reactive to $-C=C$ and $-X$ groups, and it reacts catalytically with $-C=O$ groups via the Meerwein-Ponndorf-Verley reaction.⁸ Lithium aluminium hydride ($LiAlH_4$) has a natural selectivity towards a variety of reducible groups and reacts non-catalytically with $-NO_2$ $-C=C$ $-X$ $-C=O$ and $-C\equiv N$.⁸

To rationalise the selectivity of the hydrogen donors, we can look at the type of active hydrogens present in each case. Hydrazine has 4 highly selective protic hydrogens (hydrogen bonded to an oxygen or nitrogen).⁸ Formic acid also has a protic hydrogen and an additional available hydrogen from the central carbon.⁸ Whereas $NaBH_4$, $NH_3\cdot BH_3$ and H_2 have no protonated active hydrogens, however the active hydrogens that are obtained from these molecules by heterolytic cleavage of the respective H-B or H-H bonds have high activity.⁸ From this rationalisation it could be suggested that the presence of protic active hydrogen is crucial in natural selectivity towards the nitro group, in terms of selectivity towards the desired nitro group it could be suggested that the hydrogen donors can be ranked as: $N_2H_4\cdot H_2O > HCOOH > NaBH_4, NH_3\cdot BH_3 > H_2$.⁸

1.2.4 Catalyst Selectivity

The chemoselective hydrogenation of nitrostyrene to vinylaniline is a challenging reaction due to the presence of the reducible C=C functional group which is both kinetically and thermodynamically more favourable than the reduction of the nitro group.⁸ Unfortunately, many catalysts that are active for reduction of the nitro group are also active for the reduction of the olefin group.⁸ There are two important factors that will affect the selectivity of a catalyst, the first being intrinsic selectivity and the second being preferential adsorption.⁸ For the reduction of nitrostyrene the catalyst must have a high intrinsic selectivity for hydrogenation of the nitro group (over any other functional groups present), and a preferential adsorption towards the nitro group.

Studies by Boronat *et al.*³⁴ utilised a Au/TiO₂ catalyst with a high chemoselectivity towards the reduction of nitrostyrene (and other nitroaromatics) to their corresponding anilines. It was found by kinetic testing and in-situ IR spectroscopy that there was preferential adsorption of the reactant to the catalyst via the nitro group. It was found that nitro and olefin groups adsorb weakly on Au(111) and Au(001), and adsorption on low co-ordinated Au is stronger but unselective. However, it was also discovered that at the interface between the gold nanoparticles and the titania support there is an energetically and geometrically favoured adsorption of the nitro group. Interestingly this was not observed for the Au/SiO₂ catalyst indicating that the high chemoselectivity of the titania catalyst is due to the interaction between gold nanoparticles and the titania support that gives rise to preferential adsorption of the nitro group.

Studies by Wei *et al.*³⁵ utilised Pt/FeOx single atom catalysts (SAC) and pseudo-SAC, for the reduction of nitrostyrene. It was found that 0.08wt% Pt/FeOx-R200 (SAC) and 0.08wt% Pt/FeOx-R250 (pseudo-SAC) were able to achieve 98-99% selectivity towards vinylaniline. A strong interaction between the Pt and the support was found to favour the preferential adsorption of nitroarenes, additionally the positively charged Pt centres and the absence of Pt-Pt metallic bonding were found to enhance the preferential adsorption. To support the preferential adsorption of the nitro group (over the olefin) onto these catalysts, reduction of styrene and nitrobenzene in the same reaction showed a lower activity of styrene reduction and an increased activity of nitrobenzene reduction.

Gao *et al.*³⁶ used density functional theory (DFT) calculations for a nickel phosphate catalyst used for the chemoselective reduction of 4-nitrobenzaldehyde. They predicted that the nitro group was preferentially adsorbed onto the P-doped carbon support due to geometric hindrance of the Ni₂P clusters, which results in good chemoselectivity.

Sheng *et al.*³⁰ studied 2% Pt/CMK-3 (mesoporous carbon support) and 2% Pt/CMK-3-HQ catalysts for the dechlorination of chlorobenzene to benzene with hydrazine. It was found when nitrobenzene was added to the reaction mixture with the chlorobenzene, the activity for the dechlorination reaction decreased over the 2% Pt/CMK-3 catalyst and no dechlorination activity was seen for the 2% Pt/CMK-3-HQ catalyst. This indicates a competitive adsorption between the nitro and chloro groups, where the preferential adsorption is to the nitro group.

Intrinsic selectivity differs from preferential adsorption in that there is no competition from other groups as the catalyst is only active towards the nitro group (and inert to the other functional groups present).⁸ Tan *et al.*³⁷ demonstrated this with a Au₂₅/ZnAl-HT-300 catalyst for nitrostyrene reduction, where there was no competitive adsorption and subsequent reaction from the C=C group on the surface of the catalyst. Control experiments with styrene showed almost no conversion supporting the hypothesis that there was no reaction with the C=C functional group, and therefore an intrinsic selectivity towards the nitro group for the reaction with nitrostyrene.

The importance of selective adsorption and intrinsic selectivity is evident and therefore catalyst design should be tailored to enhance these phenomena. The work in this thesis focuses specifically on the chemoselective hydrogenation of 3-nitrostyrene to 3-vinylaniline using H₂ as the hydrogen source. The challenge for this reaction is that many catalysts are active for the reduction of the olefin functional group in addition to the nitro group, subsequently decreasing the selectivity. There are many ways that catalysts can be modified to enhance their geometric and electronic properties, for example modification of metal-support interactions by changing the support and incorporating specific heat treatments, metal doping with non-metallic elements (e.g. P as seen above), incorporation of multiple metals to form alloys, and using single atom catalysts amongst others. The following catalyst review will cover these catalysts specifically designed for nitrostyrene reduction with H₂.

1.2.5 Monometallic Catalysts

It is often found that precious metals make very active catalysts but can lack selectivity, this applies to chemoselective reduction of nitrostyrene. Therefore, there has been a lot of research into improving selectivity, by employing techniques to alter electronic and structural characteristics of the catalyst.

As mentioned in the catalyst selectivity discussion Boronat *et al.*³⁴ studied the effect of support for Au catalysts on the chemoselective hydrogenation of nitrostyrene. It was found for a 1.5wt% Au/TiO₂ catalyst that the interaction between the metal and the support resulted in preferential adsorption of the nitro group. The 4.5wt% Au/Fe₂O₃ catalyst showed far lower activity but similar selectivity, while SiO₂ and Carbon supported catalysts were both inactive and unselective towards the chemoselective reduction of nitrostyrene. It was also shown that a 1.5wt% Au/TiO₂ catalyst was much more selective than a 2wt% Pt/TiO₂ catalyst. Reactions with styrene and nitrobenzene as reactants (separately) demonstrated that 1.5wt% Au/TiO₂ was more active for nitrobenzene reduction than styrene, demonstrating intrinsic activity for hydrogenation of the nitro group. When nitrobenzene and styrene were reduced in one-pot, the rate of styrene reduction decreased whilst the activity towards nitrobenzene reduction was maintained, demonstrating the preferential adsorption of the nitro group.

In development of this work Corma *et al.*³⁸ prepared TiO₂ supported Au, Pt, Ni and Ru catalysts whereby strong metal-support interactions (SMSI) were formed by consecutive calcination and reductive heat treatments, decorating the exposed (111) and (100) crystal faces of the metal. This resulted in highly selective monometallic catalysts for reduction of 3-nitrostyrene to 3-vinylniline: 1.5wt% Au/TiO₂ 99% (solvent: toluene, 9 bar H₂, 6 hrs, 120°C), 0.2wt% Pt/TiO₂ 95% (solvent: toluene, 3 bar H₂, 6.5 hrs, 40°C), 5wt% Ni/TiO₂ 93% (solvent: toluene, 15 bar H₂, 3 hrs, 120°C) and 1wt% Ru/TiO₂ 95% (solvent: toluene, 15 bar H₂, 1.5 hrs, 120°C). What is particularly notable is the mild conditions that the 0.2wt% Pt/TiO₂ catalyst was able to operate under.

Matsushima *et al.*³⁹ synthesised a boronate microparticles via esterification as a support for Au catalysts. A highly selective (91%) Au-BP catalyst was prepared by deposition reduction. It was found that the boronate support promoted nitro group access to the Au active site, and the synergistic effect between the metal and the support resulted in high chemoselectivity. It

is notable that this catalyst also completely suppressed reduction of the olefin group, contributing to the high selectivity.

Tamura *et al.*⁴⁰ prepared Ru/SiO₂ catalysts modified with WO_x, MoO_x, and ReO_x metal oxides in order to enhance the catalytic activity and selectivity for chemoselective reduction of 3-nitrostyrene. The reaction was run under mild, solventless conditions (0.3 MPa H₂, 30°C, 2 hrs) and extremely high selectivities towards 3-vinylaniline were achieved Ru–WO_x/SiO₂ (~100%), Ru–MoO_x/SiO₂ (99%), Ru–ReO_x/SiO₂ (98%). Analysis of Ru–MoO_x/SiO₂ showed an active site the interface where Ru adsorbed strongly onto MoO_x, and an active hydride species being formed on Ru resulting in the catalytic performance seen.

Beier *et al.*⁴¹ synthesised small nanoparticles with an ionic liquid immobilised on a variety of supports. It was found that the pH of the reaction medium had a strong influence on the outcome of 3-nitrostyrene hydrogenation, with acidic conditions favouring 3-ethylnitrobenzene production and basic conditions favouring 3-nitrostyrene.

Makosch *et al.*⁴² used various organic thiols to modify an unselective (towards vinylaniline) Pt/TiO₂ catalyst. Whilst the unmodified Pt catalyst showed no selectivity towards the desired product, modification with thioglycerol, 1,6-dithiolhexane and α -lipoic acid were able to achieve 97-100% desired chemoselectivity. Modification of the catalyst surface inhibited the intrinsic activity of the Pt catalyst towards the olefin, thus improving the selectivity towards the nitro group.

Wu *et al.*⁴³ investigated how the selectivity between the nitro and the olefin groups of 3-nitrostyrene can be tuned using a 0.5wt% Pt/C catalyst. It was found that low temperature reductive treatments favoured the selective reduction of the olefin functional group, while high temperature reductive treatments favoured reduction of the nitro group. The presence of acidic groups on the surface of the catalyst facilitated the reduction of the olefin, whereas Pt-PO_x composite sites (formed from surface P species) promoted the reduction of the nitro group.

It is clear that precious metals (Pt, Au, Ru) that can originally seem unselective towards the chemoselective hydrogenation of nitrostyrene can be altered drastically through the use of different supports and heat treatments which alter the metal-support interactions, also addition of modifiers such as organic thiols and metal oxides. It had been demonstrated how

these metals can be used effectively without the addition of additional metals or alternative metal catalysts.

1.2.6 Catalysts incorporating non-precious metals

Non-precious metal catalysts have a much lower intrinsic activity towards the selective reduction of nitroarenes than precious metal alternatives, this can often be improved by increasing the hydrogen pressure in the reaction.^{8,44,45} However, these catalysts often have good chemical selectivity especially when paired with an appropriate hydrogen donor.⁸ Another advantage commercially is the lower cost and higher abundance of non-precious metals.

Transition metals supported on nitrogen-doped carbon (M-N-C catalysts) have been found to give high catalytic activities and selectivities for the selective hydrogenation of nitroaromatics such as nitrostyrene.^{8,21} These catalysts can be synthesised by pyrolyzing the metal, nitrogen and carbon precursors under inert gas.^{8,21} The M-N (metal-nitrogen) sites are the active sites of the catalyst, the M-N sites modify the electronic structure of the metal which in turn is able to facilitate both the preferential adsorption of the nitro group and activation of the nitro group.^{8,46,47}

Wei *et al.*⁴⁸ designed an amphiphilic (both hydrophobic and hydrophilic properties) 'sandwich-structured' Co@Co-N-C@SBA-15 catalyst using this M-N-C model, with cobalt as the chosen transition metal, for the chemoselective reduction of 4-nitrostyrene. The catalyst is comprised of hydrophilic external mesoporous silica support which allowed for good dispersion in water and promoted water-mediated hydrogen spillover. The inner N-C layers are hydrophobic and adsorb the 4-nitrostyrene, which is selectively activated and subsequently reduced at the Co-N active sites within the N-C layers. This catalyst was found to achieve 98% conversion of nitrostyrene and 99% selectivity of vinylaniline (1hr, 5 bar H₂, solvent: water). The metallic cobalt nanoparticles within the catalyst allows for effective catalyst recovery by magnetic separation, and the catalyst was found to be reusable with 87% nitrostyrene conversion and 99% vinylaniline selectivity upon the fourth use. A variety of solvents were also tested, and it was found that much lower nitrostyrene conversions were achieved in methyl alcohol (22%), triethylamine (17%) and toluene (21%) when compared to

water (98%). The use of water as the solvent was thought to improve catalyst dispersion and enhanced water-mediated hydrogen spillover. Additionally, reactions with nitrobenzene and styrene (separately) showed 100% conversion for the former and only 6% for the latter indicating the intrinsic selectivity of the Co-N sites towards the nitro group, not the C=C functional group.

Wang and Li⁴⁹ also utilised Co on nitrogen doped carbon catalysts, supported on a ZIF-67 MOF (metal organic framework). The catalyst was prepared by pyrolysis of ZIF-67 under an inert atmosphere. It was found that at Co/C-N-600 catalyst converted >99% of 4-nitrostyrene to 4-vinylaniline with 97% selectivity (solvent: methanol, 1MPa H₂, 100°C). ATR-IR analysis determined that C-N centres of the catalyst promoted the preferential adsorption of the nitro group resulting in the high selectivity.

Metal sulphide catalysts can also be used to selectively reduce nitrostyrene, typical formulations of the metal sulphides (MS₂) include transition metals such as Fe, Co, Ni and W.^{8,50}

Wei *et al.*⁴⁹ synthesised a cobalt sulphide catalyst supported on a porous carbon (CoS₂/PC), with terdentate and tetrahedral coordinated Co atoms. It was deduced that these face-to-face Co₃ and Co₄ sites form a 'synergic active pair site' where the Co₃ is occupied by 3-nitrostyrene and the Co₄ site is occupied by H₂. For the reduction of 3-nitrostyrene this catalyst achieved a conversion >99% over 8 hours with a vinylaniline selectivity of 99% (Solvent: methanol, 3MPa H₂). This work also utilised an FeS₂/PC catalyst that took 12 hours to reach full conversion, with 99% selectivity. However, NiS₂/PC was found to only reach 51% conversion after 12 hours, with a selectivity of 50%. It is important to note that although the Co (and Fe) catalyst shows excellent selectivity, a long reaction time is required to reach full conversion. It is also notable that the cobalt catalyst upon reuse did decrease in activity but chemoselectivity was maintained. Hydrogenation of nitrobenzene and styrene was also conducted using CoS₂/PC and it was observed that the catalyst has intrinsic selectivity towards the nitro group due to the much lower reaction rate seen for styrene. Preferential adsorption was also seen when a mixture of nitrobenzene and styrene was used as the reactant and the styrene reduction was completely prevented. This is supported by DFT calculations which showed a larger E_{ads} (energy of adsorption) for the nitro group (-0.08 eV) compared to the

olefin functional group (-0.36 eV). Evidently both intrinsic selectivity and preferential adsorption are working alongside each other and both contributing to the catalyst selectivity.

Sun *et al.*⁵⁰ used colloidal WS₂ nanostructures for the hydrogenation of nitrostyrene and other nitroarenes. This catalyst was used as a model 2-D TMD (2-dimensional transition metal dichalcogenide) system, which is essentially materials composed of a few-layers (or single-layer) of nanosheets. Studies showed the abundance of sulphur vacant-rich basal planes and tungsten terminated-edges present in the flower-like nanostructure of the WS₂ (not in the bulk counterpart), that are responsible for the chemoselectivity. This is due to these sites favouring the vertical adsorption of nitroarenes, which due to geometric effects enables hydrogen transfer specifically to the nitro group with a lower kinetic barrier. To this end, the WS₂ nanostructure catalyst achieved >99% conversion of 3-nitrostyrene to 3-vinylaniline with 98% selectivity (8 hr, solvent: H₂O, 50 bar H₂).

Gao *et al.*⁵⁰ used steric effect and organic chelation to change electronic structure in order to make a selective catalyst for nitrostyrene reduction. A SPhF-Ni₂P catalyst was made from Ni₂P chelated with *p*-fluorothiophenol. For the hydrogenation of 3-nitrostyrene excellent conversion (41.6%) and selectivity (100%) were achieved (70°C, 200 min). The way this catalyst achieves this high selectivity is that the ordered SPhF-arrays confines the flat adsorption of 3-nitrostyrene, this prevents hydrogenation of the olefin functional group. The SPhF-arrays push the d-band centre of Ni₂P away from the Fermi level, and this promotes the activation of the molecular hydrogen over Ni₂P sites.

It is evident that many highly chemoselective catalysts can be synthesis from non-precious metals for the reduction of nitrostyrene. However, there is often a drawback with regards to the activity of these catalysts and therefore reaction times, with some catalysts needing 12 hours to achieve full conversion. What is interesting is the various techniques that have been employed to enhance the selectivity of these catalysts: incorporating layers into the catalysts, use of porous supports, chelation to manipulate the active sites.

1.2.7 Bimetallic Catalysts

Another way of improving catalytic selectivity is by introducing an additional metal to form a bimetallic catalyst. By incorporating another metal catalyst active site properties can be modified by changes in electronic and structural properties such as rearrangement of the metals of the catalyst and enhancing metal-support interactions. The addition of secondary metals can enhance the performance of the original monometallic and can also lead to reactions needing much milder conditions to operate.

Mao *et al.*⁵¹ incorporated Co with Ru nanoparticles to produce a novel 'dumbbell-shaped' nanocatalyst for the chemoselective hydrogenation of 4-nitrostyrene to 4-vinylaniline. The nano catalyst consists of a Co nanorod capped at both ends with Ru nanoplates. It was found that the introduction of the Co connection in the centre of the Ru, resulted in compression of the lattice strain of Ru. It was found that for the nanocatalyst where Ru had a 3% lattice compression (composition: Co_{0.23}-Ru_{0.77}) almost complete conversion of 4-nitrostyrene was achieved with 99% selectivity towards vinylaniline. In comparison the Ru-only achieved just 66% selectivity. The Co_{0.23}-Ru_{0.77} was also able to maintain the selectivity upon 4 uses. It was shown by DFT calculations that the small lattice compression was responsible for the activity enhancement due to promoting the reduction of the nitro group and hindering reduction of the olefin group. It is notable that the Ru lattice strain was optimised at 3% and when a larger lateral compression of 6% is used the reaction may be blocked.

Furukawa *et al.*⁵² also synthesised a RuPb₂/SiO₂ catalysts for the selective reduction of 4-nitrostyrene, that has a low conversion of 36% and a selectivity of 91% selectivity (Solvent: THF, H₂, 0.5 hr). Although a relatively short reaction time, conversion was low, and the selectivity is comparable poor to other bimetallics reviewed here. However, it is notable that this catalyst was found to work more effectively using methanol as a hydrogen source for a CTH reaction rather than using molecular hydrogen.

Pt is a commonly used precious metal for this reaction however can suffer from low selectivity, therefore there have been many attempts to enhance the selectivity through introduction of non-precious metals. Sn, Bi, Pb, Co and Zn, amongst others have been used successfully to improve the selectivity towards vinylaniline.⁵³⁻⁵⁷

Pei *et al.*⁵⁷ produced Pt-based intermetallic nanoparticles (iNPs) encapsulated in shells of mesoporous silica and synthesised in a way to remove capping agents. Intermetallic compounds are an alloy with ordered atoms and specific crystal structure. PtSn@mSiO₂ was shown to be the most selective catalyst albeit with low activity, for the selective 3-nitrostyrene reduction, achieving >99% conversion and >99% selectivity to 3-vinylaniline in 9 hrs (solvent: toluene, 20 bar H₂, 80°C). Comparatively, PtPb@mSiO₂ achieved 98% conversion and >99% selectivity over 12 hours, and PtZn@mSiO₂ achieved 31% conversion and >99% selectivity over 12 hours. The Zn incorporated catalyst was far less active than the Sn and Pd, however was still highly selective. The catalysts had a Pt₃X@mSiO₂ (where X = Sn, Zn) counterparts however, these catalysts although far more active had either no selectivity or decreased selectivity towards the desired product, the same was also seen for a Pt@mSiO₂ catalyst. It was determined that the high selectivity of PtSn@mSiO₂ comes from the geometric structure of the intermetallic PtSn nanoparticles that have no Pt threefold sites that are present in Pt₃Sn. Elimination of these sites impede the adsorption and dissociation of H₂, and this results in a non-Horiuti-Polanyi hydrogenation pathway, whereas for the Pt₃Sn intermetallic species and Pt nanoparticles these surfaces are saturated with atomic hydrogen. Additionally, DFT calculations predict preferential adsorption of the nitro group onto PtSn intermetallic sites.

Shu *et al.*⁵⁸ produced bimetallic Pt-Sn catalysts supported on hydrogenated MoOx (H-MoOx) for the selective hydrogenation of 4-nitrostyrene. A highly active and selective Pt₄₀Sn₆₀/H-MoOx-400 (reduced 400°C) reached almost complete conversion after 120 minutes with a selectivity towards 4-vinylaniline of approx. 93% (30°C, 1 atm H₂). Not only is this catalyst efficient but it is also active under mild reaction conditions, which is another great advantage of this catalyst. The introduction of Sn into the catalyst resulted in structural variation giving rise to ultra-small nanoparticles and the atom-rearranged bimetallic Pt-Sn surface promoted selective adsorption of the nitro group. It was found that strong metal support interactions of this catalyst resulted in good hydrogenation on small positively charged nanoparticles.

Another use of bimetallics to enhance Pt catalyst is by Lan *et al.*⁵⁶ where Bi was incorporated. For Pt/TiO₂ only 20% selectivity towards vinylaniline as this was further hydrogenated to ethylaniline over the catalyst (solvent: H₂O, 2 MPa H₂, 85°C, 1.5 hr). Small quantities of Bi increased the selectivity, with an optimum Bi content of between 1-1.5% achieving selectivity

of ~96% with conversions of nitrostyrene ranging from 62-69%, but the activity decreased upon addition of Bi to 1.9%. For elongated reactions full conversion could be achieved and for 1.5%Bi/TiO₂ selectivity was maintained demonstrating the prohibition of further hydrogenation to ethylaniline that Pt/TiO₂ allowed. It was observed that upon addition of Bi there was an increase in the number of low co-ordinated Pt sites where the preferential adsorption of the nitro group could occur, instead of the terrace sites that are seen in the Pt/TiO₂ catalyst.

Wu *et al.*⁴³ used Co to modify Pt catalysts on a P-containing activated charcoal support. It was found that the Co incorporation decreased catalyst activity (complete conversion took 20 hrs) but improved selectivity towards 3-vinylaniline from 92% to >99% (solvent: toluene, 4 MPa H₂, 100°C). The high selectivity was a result of preferential nitro group adsorption on the Pt-POx interface layer over the supported Pt nanoparticles. This interface was a result of the Co addition. Interestingly in the product solution very small quantities of azo compounds were detected suggesting that the reaction mechanism could go via the Haber condensation route mechanism.

Yarulin *et al.*⁵⁴ investigated the effect of using Zn to promote Pt based catalysts resulting in a 2wt% Pt/ZnO. It was confirmed by XPS and XRD analysis that intermetallic (alloyed) nanoparticles were formed between the Pt metal and ZnO support interactions. These intermetallic particles were formed via reductive heat treatments (300 °C). This catalyst was able to achieve 97% conversion of 3-nitrostyrene and 100% selectivity towards 3-vinylaniline (solvent: ethanol, 10 bar H₂, 75°C), with the selectivity attributed to the intermetallic active phase. It was also determined that altering the partial pressure of H₂ (2-15 bar) did not significantly affect the selectivity, though activity did increase, in agreement with first order kinetics. By experimenting with solvent choice, it was found that in more polar solvents such as ethanol and methanol higher selectivity could be achieved, than in less polar solvents such as toluene.

In further work by this group,⁵³ it was found that by preparing PtZn bimetallic catalysts within a hypercross-linked polystyrene (HPS) support, size control of the PtZn nanoparticle could be achieved. The cavities in the support were in the range of 4-5 nm and TEM imaging found a mean metal particle size of 4.7 nm. Selectivity toward 3-vinylaniline of 97% was achieved, compared to Pt/HPS with selectivity of only 16% (solvent: ethanol, 10 bar H₂, 75°C). The

enhanced selectivity was attributed to the electronic and surface modifications of the Pt from the introduction of Zn. Notably, azo compounds were observed at points throughout the reaction indicating that the condensation mechanism may be used.

A series of IrFe bimetallic nanomaterials was synthesised by Lu *et al.*⁵⁹ with various morphologies and compositions which affected the activities and selectivities. Most notable are IrFe alloyed bimetallic nanoparticles and Ir/Fe₂O₃ (flakes) which were tuned by altering the molar ratio of Ir/Fe. It was found that Ir₁Fe₄ ratio was excellent for 3-nitrostyrene reduction, being highly active, highly selective and recyclable. This was determined to be due to a synergistic effect of the two metals, with the Ir nanoparticles as the active species for hydrogenation and the Fe₂O₃ favouring the preferential adsorption of the nitro group.

Synergistic effects have also been seen for AuNi and NiSn bimetallics, with Ni being active for the reduction of nitroarenes and unselective towards other reducible groups.^{60,61} It was found by Yamanaka *et al.*⁶¹ that incorporation electropositive Sn into Ni catalysts enhanced selectivity towards reduction of the nitro group.

However, it has also been found that some bimetallic catalysts favour selective reduction of the C=C (olefin) functional group. Zhang *et al.*⁶² produced Cu-Pd concave tetrahedral nanocrystals that exhibited 99% selectivity to the C=C group of nitrostyrene and was highly active at atmospheric H₂ pressure. Additionally, Wu *et al.*⁶³ synthesised Ph-doped Pd nanocubes with >99% selectivity towards 3-ethylnitrobenzene, with enhanced activity compared to Pd nanocubes. Introduction of Rh strengthened adsorption of 3-nitrostyrene resulting in improved activity and induced the unique adsorption that inhibited the hydrogenation of NO₂ and was therefore responsible for the excellent C=C selectivity.

It is evident that by addition of non-precious metals into precious metal catalysts the selectivity of the former and the activity of the later can be combined. This is largely achieved through the formation of specific intermetallic sites and metal support interactions that are selective towards hydrogenation of the nitro group.

1.2.8 Single Atom Catalysts and Nanocluster Catalysts

Single atom catalysts and nanoclusters have different electronic and geometric properties compared to nanoparticles and bulk metals. Single atom catalysts have excellent dispersion of active particles and often exhibit great activities and selectivities, and this has been reported for nitrostyrene hydrogenation.

Wei *et al.*³⁵ reported the use of Pt/FeO_x single atom catalysts (SAC) and pseudo-SAC. Very high activity was exhibited for both 0.08wt%FeO_x-R200 (SAC reduced at 200°C) and 0.08wt%FeO_x-R250 (pseudo-SAC reduced at 250°C) with 96% conversion of 3-nitrostyrene being achieved in 50 minutes, with 98% selectivity towards 3-vinylaniline under mild conditions (40°C, 3 bar H₂, solvent: toluene). A pseudo single atom structure is comprised of up to tens of atoms that are loosely and randomly combined, however they are very similar both structurally and functionally to individual single atoms and no strong Pt-Pt metal bonds are formed. The high selectivity of these catalysts was attributed to the absence of the Pt-Pt metallic bonding and the existence of positively charged Pt centres which facilitated the preferential adsorption of the nitro functional group. However, it was found that the two catalysts exhibit different intrinsic activities. For the hydrogenation of nitrobenzene and styrene (separately) the 0.08wt%FeO_x-R200 (SAC) catalyst showed higher intrinsic activity towards nitrobenzene reduction, whereas the 0.08wt%FeO_x-R250 (pseudo-SAC) catalyst exhibited similar activities towards both reactants, the activity towards the C=C group in the styrene could be due to the clusters of Pt atoms in the pseudo-SAC catalyst or the presence of Pt-Fe metal interactions, however there is clearly preferential absorption of the nitro group indicated by the high selectivity of nitrostyrene. Interestingly this work also investigated the interaction between the Pt and the FeO_x support, and it was found that stronger metal-support interactions were observed for the lower loading 0.08wt% catalysts, favouring the chemoselectivity to nitroarenes. When other supports were used (SiO₂ and Al₂O₃) selectivities decreased significantly (47% and 28% respectively). Unfortunately, the disadvantage of single atom catalysts (and pseudo-SAC) is the high probability of aggregation that occurs in for higher metal loadings which ultimately results in decreased selectivity.

However, the issue of high loading selectivity depletion was also tackled by Wei *et al.*⁶⁴ via the addition of alkali metal cations (e.g. Li⁺, Ni⁺ and K⁺). An optimised 5% Na–2.16% Pt/FeO_x catalyst improved the chemoselectivity selectivity towards 3-vinylaniline from 66%

to 97 whilst maintaining the high activity of the Pt monometallic (almost complete conversion in approx. 35 minutes). It was proposed that the addition of Na^+ produced a Pt–O–Na–O–Fe surface species, preventing the formation of Pt crystals and producing low co-ordinated and isolated positively charged Pt centres that are intrinsically selective toward the nitro group instead of the olefin.

It is possible to anchor single atoms onto a support to lower energy barriers and improve selectivity. Peng *et al.*⁶⁵ produced catalysts whereby single Pt atoms were embedded in the surface of Ni nanocrystals (P_1/Ni nanocrystals). This catalyst was able to achieve a high TOF (based on Pt surface atoms) of 1800 h^{-1} (40°C , 3 atm H_2 , 100 min) which was far more active than seen for Pt supported on activated-C, TiO_2 , SiO_2 and ZSM-5. It was found that the catalyst provided a high enough H_{ads} as a result of the spontaneous dissociation of the H_2 on the Pt and Ni atoms of the P_1/Ni nanocrystals which gave rise to a good hydrogen supply, in addition to easy diffusion of hydrogen on the P_1/Ni nanocrystals. There was also favourable selective adsorption towards the hydrogenation of the nitro group identified.

Tan *et al.*³⁷ used small and uniformly sized thiolate Au_{25} nanoclusters supported on ZnAl-hydroxalcalite (ZnAl-HT). Even with high calcination treatments extremely small nanoparticles were maintained $300^\circ\text{C} = 1.7 \text{ nm}$ and $500^\circ\text{C} = 2.0 \text{ nm}$ (average Au NPs). It was determined that residual sulphur and epitaxial interactions occurring between the Au and the ZnAl-HT support stabilised the catalyst even when it underwent high temperature calcination. The $\text{Au}_{25}/\text{ZnAl-HT-300}$ catalyst was found to achieved 100% conversion over a long reaction time and 99% selectivity towards 3-vinylaniline (90°C , 10 atm H_2 , 9 hrs). Interestingly the Au catalyst is only active towards the nitro group and is inert to the olefin group, showing an intrinsic selectivity towards NO_2 .

Following from this work, Tan *et al.*⁶⁶ studied how changing the metal (M^{2+}) in the hydroxalcalite support (MAI where $\text{M} = \text{Zn}, \text{Mg}, \text{Ni}$) would affect a nanocluster $\text{Au}_{25}/\text{MAI-HT-300}$ catalyst. It was found that although the $\text{Au}_{25}/\text{ZnAl-HT-300}$ gave the best selectivity towards 3-vinylaniline, the $\text{Au}_{25}/\text{NiAl-HT-300}$ catalyst was the most active, this coincided with this catalyst having a larger Au nanoparticle size (3.2 nm). The (reduced) metallic Ni species present in the catalyst suggested that Ni interacts with Au and is reduced, this resulted in the high activity of the catalyst and low selectivity (due to over hydrogenation). The reduced Ni species is also responsible for the hydrogenation going via the direct route and the

condensation route, whereas the Au₂₅/ZnAl-HT-300 and Au₂₅/MgAl-HT-300 catalysts only followed the condensation pathway.

Shimizu *et al.*⁶⁷ synthesised silver (Ag) clusters on a θ -Al₂O₃ support for the reduction of 4-nitrostyrene, which demonstrated good activity and selectivity. It was observed that smaller nanoparticle size resulted in a higher intrinsic activity and, acid-base bifunctional supports such as Al₂O₃ gave rise to higher activities than either acidic or basic supports. H⁺/H⁻ pairs were yielded at metal-support interfaces and the basic sites on the Al₂O₃ support are the nitro adsorption sites. Preferential transfer of the H⁺/H⁻ pair to the polar nitro group resulted in high selectivity towards 4-vinylaniline.

1.2.9 Summary of Pt catalysts of the Selective Hydrogenation of 3-Nitrostyrene

It is evident from the numerous studies on chemoselective hydrogenation of nitrostyrene and that Pt catalysts can show not only good activities of hydrogenation, but also good selectivities towards preferential reduction of the nitro group over the olefin functional group. A summary of some key Pt catalysts for the chemoselective hydrogenation of 3-nitrostyrene to 3-vinylaniline are given in Table 1.1.

Table 1.1: Summary of key Pt catalysts for the chemoselective hydrogenation (with H₂) of 3-nitrostyrene to 3-vinyllaniline.

| Catalyst (Heat Treatment) | Reaction Conditions | 3-NS Conversion / % (3-VA Selectivity / %) | TOF / h ⁻¹ | Ref |
|--|---|---|-----------------------|-----|
| 0.08wt% PtFeO_x (Reduced 200°C) | 3-NS/Pt = 1250 Temp = 40°C Pressure = 3 bar Time = 49 min | 96 (98) | 1494 | 35 |
| 0.08wt% PtFeO_x (Reduced 250°C) | 3-NS/Pt = 1250 Temp = 40°C Pressure = 3 bar Time = 50 min | 97 (99) | 1514 | 35 |
| 0.08wt% PtFeO_x (Reduced 250°C) | 3-NS/Pt = 1250 Temp = 80°C Pressure = 10 bar Time = 7 min | 89 (91) | 1514 | 35 |
| 0.2wt% Pt/TiO₂ (Reduced 450°C) | 3-NS/Pt = 323 Temp = 40°C Pressure = 3 bar Time = 390 min | 95 (93) | N/A | 38 |
| 0.2wt% Pt/TiO₂ (Reduced 450°C) | 3-NS/Pt = 1250 Temp = 40°C Pressure = 3 bar Time = 840 min | 97 (94) | 88 | 35 |
| 1.4wt% Pt/ZnO (Reduced 300°C) | 3-NS/Pt = 150 Temp = 75°C Pressure = 10 bar | ~99 (97) | 44640 | 68 |
| 0.1wt% Pt/TiO₂ (Reduced 300°C) | 3-NS/Pt = 150 Temp = 75°C Pressure = 10 bar | ~99 (53) | 24120 | 68 |
| 2wt% Pt/ZnO (Reduced 300°C) | 3-NS/Pt = 100 Temp = 75°C Pressure = 10 bar | ~99 (97) | 3840 | 54 |

1.3 Hydrogen Peroxide

Hydrogen peroxide (H_2O_2) was initially discovered in 1818 by Jacques Thenard being the product of the reaction between barium peroxide and nitric acid.^{69,70}



However it wasn't until 1914 that Henkel and Weber first proposed the direct synthesis of hydrogen peroxide using noble metal catalysts, which became the basis for the Anthraquinone Oxidation Process.⁶⁹⁻⁷¹

The synthesis of H_2O_2 is of huge industrial importance, due to its wide scale use in green chemistry as a strong oxidant for both inorganic and organic substances, operating under mild conditions with the only by-product of its degradation being water and molecular oxygen, making it environmentally safe.^{69,71} H_2O_2 is stable and safe under the correct conditions and is soluble in water and many organic solvents. For storage and transport as aqueous solutions (i.e. in water) the common concentrations of H_2O_2 are 35, 50, and 70 wt%.⁶⁹

The low molecular weight of H_2O_2 compared to other oxidants gives higher efficiency and better atom economy. Table 1.2 shows the efficiency of H_2O_2 compared to other common industrial oxidants, with H_2O_2 having the second largest wt% of active oxygen (the only exception being O_2 itself).⁶⁹ Additionally, Table 1.2 gives the by-products of these oxidants, and it is evident that in this regards H_2O_2 is the most environmental option (aside from O_2), with the only by-product water. In comparison, many stoichiometric oxidants such as t-BuOOH, N_2O and permanganate (MnO_4^-) produce waste products that require separation from the desired product.

Table 1.2: Common industrial oxidants.⁶⁹

| Oxidant | Active Oxygen / % wt/wt | By-Product |
|-------------------------------|-------------------------|---|
| H ₂ O ₂ | 47.1 | H ₂ O |
| O ₂ | 100 | - |
| <i>t</i> BuOOH | 17.8 | <i>t</i> BuOH |
| HNO ₃ | 25.0 | NO _x N ₂ O N ₂ |
| N ₂ O | 36.4 | N ₂ |
| NaClO | 21.6 | NaCl |
| NaClO ₂ | 35.6 | NaCl |
| NaBrO | 13.4 | NaBr |
| KHSO ₅ * | 10.5 | KHSO ₄ |
| NaIO ₄ | 29.9** | NaI |
| PhIO | 7.3 | PhI |

*Stabilised 2 KHSO₅·KHSO₄·K₂SO₄ **Assuming all 4 oxygen atoms are utilised.

1.3.1 Uses of H₂O₂

Primary industrial uses include bleaches and disinfectants, waste water treatment to remove hydrogen sulphide, chemical synthesis (including fine chemicals) metallurgy, the electronics and textiles industry amongst others, largely replacing the need for chlorine-based solutions, which are particularly hazardous to the environment.^{69,71-75}

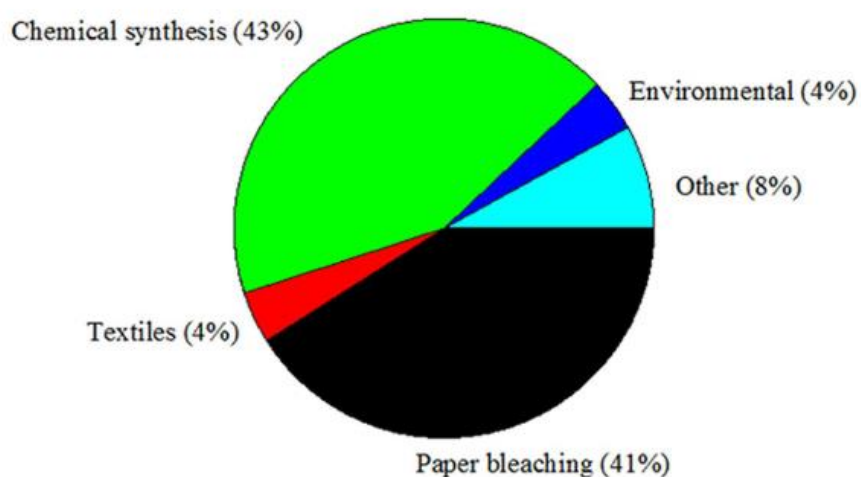


Figure 1.8: Industrial uses of H₂O₂.⁷¹

A crucial use of hydrogen peroxide is in pulp and paper bleaching, where it provides an alternative to chlorine-based bleaches and hence avoids halogenated waste products.^{71,76} As a bleach, the (nucleophilic) hydrogen peroxide anion (HO_2^-) is in an alkaline media which eliminates the chromophores (responsible for colour) in the lignin structures.⁶⁹ In the bleaching of recycled paper H_2O_2 is used alongside sodium hydrosulphite (NaS_2O_4) in a reductive bleaching process to remove printing dyes.⁶⁹

In the textiles industry, stable precursors such as sodium perborate (NaH_2BO_4) and sodium percarbonate ($\text{Na}_2\text{H}_3\text{CO}_6$) are used, which release H_2O_2 in water.⁶⁹ These are now being used preferentially to hypochlorite (NaOCl) and sodium hydrosulphite ($\text{Na}_2\text{S}_2\text{O}_4$) which not only contains toxic compounds (halogens and sulphur respectively), but hypochlorite can also cause yellowing and darkening of fabrics, whereas the peroxide compounds are colour safe.⁶⁹ Additionally, H_2O_2 is an effective disinfectant against bacteria and viruses, has no severe toxicity, corrosivity or effluent problems.⁶⁹ It is notable that of the peroxide precursors, sodium percarbonate is favourable compared to sodium perborate due to its lower dissolution temperature in water (can be used at lower temperatures), which is preferable in laundry detergents.⁶⁹

Another main use of H_2O_2 is in municipal wastewater treatment for the removal of hydrogen sulphide (H_2S) formation in sewer pipes.⁶⁹ It is also used to clean industrial waste streams of harmful chemicals including cyanide, thiocyanate, nitrates, chlorides, hypochlorite and organic matter.^{69,71}

1.3.2 The Anthraquinone Oxidation Process

Industrially, large-scale hydrogen peroxide production is almost exclusively performed by the Anthraquinone Oxidation Process,^{69,71} which was first developed Riedl and Pfeleiderer of BASF in 1939.⁷⁷ This process involves the sequential oxidation and hydrogenation of the precursor, alkyl anthraquinone, whereby the hydrogen and oxygen gases are kept separate.^{69,78} This multi-step process includes various organic solvents and liquid-liquid extraction to obtain the hydrogen peroxide.^{69,78} Generally, a stabiliser such as water is added and the resultant aqueous solution is sold primarily in concentrations of 35, 50, and 70 wt.%.⁶⁹ In itself, this is not a particularly economic or green process, due to the use of organic solvents, by-products and high energy input.⁶⁹ Furthermore, a stoichiometric amount of anthraquinone is required

in each cycle, and even though it is recovered a small amount undergoes non-selective reduction and therefore requires replacement, adding to the expense of the process.⁶⁹ However, one advantage is the separation of hydrogen and oxygen gases which prevents the formation of an explosive reaction environment. Figure 1.9 shows the sequential auto-oxidation of anthraquinone.^{69,78}

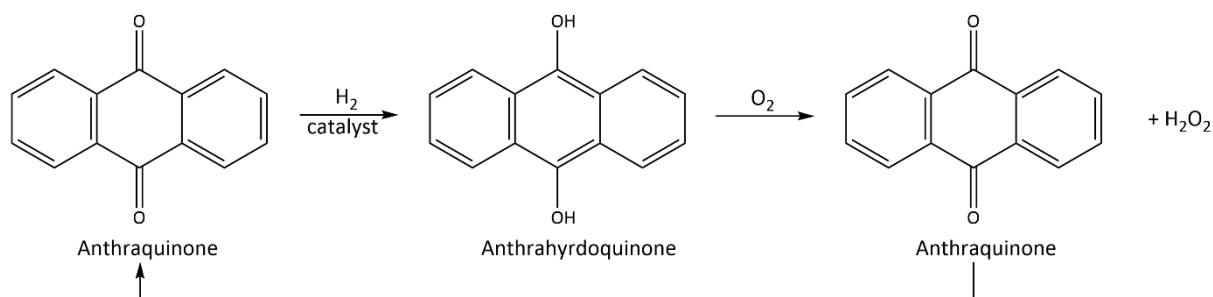


Figure 1.9: Anthraquinone auto-oxidation to produce hydrogen peroxide.

1.3.2.1 Hydrogenation step

The initial step in the Anthraquinone Oxidation Process is the catalytic reduction of anthraquinone to anthrahydroquinone, where the two carbonyl (C=O) groups are converted into alcohol (OH) groups.⁶⁹ The working conditions are temperatures between 40-50 °C with a hydrogen partial pressure up to 4 bar.⁶⁹ This reaction requires a catalyst and both Ni and Pd-supported catalysts have been used.^{79,80}

Originally Raney Ni catalysts were used for the reaction however, they promoted over-hydrogenation of the anthrahydroquinone and they rapidly deactivated.⁶⁹ The over-hydrogenation results in the use of excess consumption of both hydrogen and anthraquinone. Pd catalysts were found to be more selective than the Raney Ni catalyst however some by-products are still formed.⁶⁹ However, modifications to both Ni and Pd catalysts have been developed using promoters and use of different catalyst supports (e.g. Pd supported on SiO₂, Al₂O₃ and SiO₂/Al₂O₃).⁸⁰

The conversion of anthraquinone to anthrahydroquinone is maintained below 60% in order to decrease the chances of secondary hydrogenation reactions.⁶⁹ One such example is shown in Figure 1.10. The synthesised anthrahydroquinone can undergo ring hydrogenation to form 5,6,7,8-tetrahydroanthrahydroquinone.⁶⁹ As also shown in the reaction scheme, this can also

be oxidised alongside anthrahydroquinone when it is separated from the catalyst for the next step of the reaction to produce tetrahydroanthraquinone and the desired produce hydrogen peroxide.⁶⁹

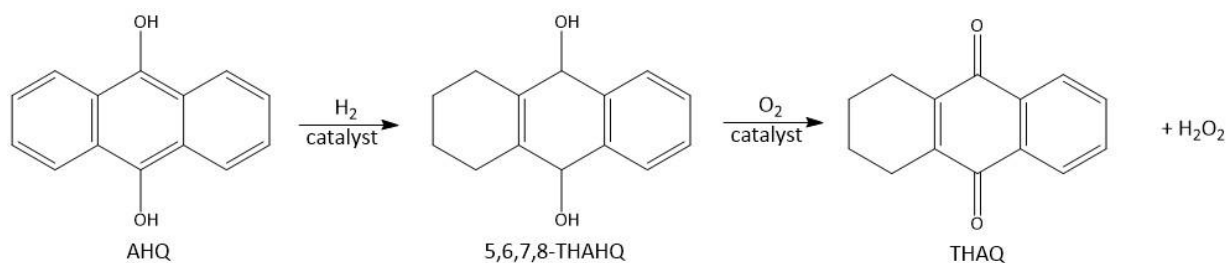


Figure 1.10: Catalytic ring hydrogenation of anthrahydroquinone (AHQ) to 5,6,7,8-tetrahydroanthrahydroquinone (5,6,7,8-THAHQ), followed by the subsequent oxidation to produce tetrahydroanthraquinone (THAQ) and hydrogen peroxide.

1.3.2.2 Oxidation Step

The hydroquinone solution is oxidised non-catalytically by the bubbling of air through the aqueous solution between 30-60 °C, at (close to) atmospheric pressure.⁶⁹ Figure 1.11 shows the free-radical chain mechanism by which anthraquinone is oxidised to produce H₂O₂.^{69,81}

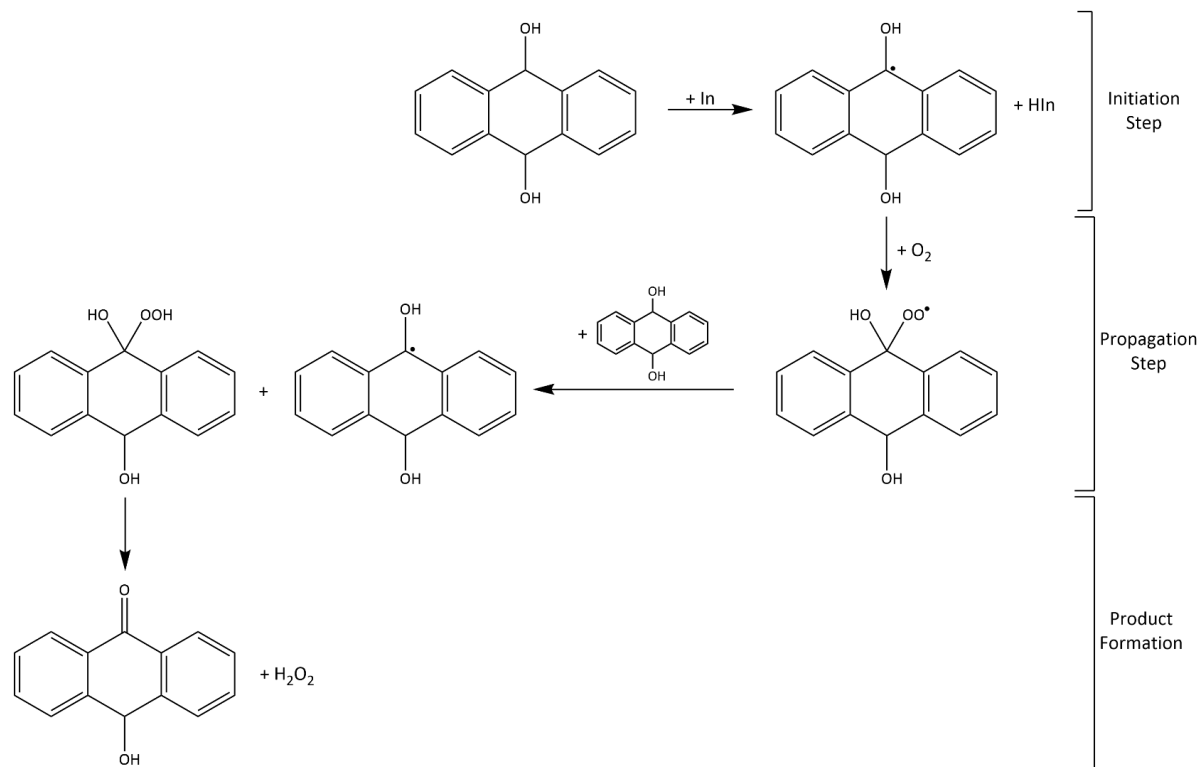


Figure 1.1: Oxidation pathway of hydroquinone to produce hydrogen peroxide and regenerate anthraquinone

In the first step (the initiation step), an initiator (In) reacts with a tertiary hydrogen on the anthraquinone molecule to produce a radical. The radical then reacts with oxygen to form a hydroperoxyl radical. In the propagation step of the reaction, the hydroperoxyl radical then reacts with a molecule of anthraquinone to produce an anthraquinone radical and an unstable molecule with an alcohol group and a peroxide group on the same carbon. The latter of which decomposes to a ketone (C=O) resulting in the production of the product, a H₂O₂ molecule.⁶⁹

1.3.3 Alternative Methods of H₂O₂ Production

1.3.3.1 Oxidation of Alcohols

Alternative approaches to synthesising hydrogen peroxide include the partial oxidation of primary or secondary alcohols, the by-product of this reaction being an aldehyde or ketone respectively, as shown in Figure 1.12.⁸²

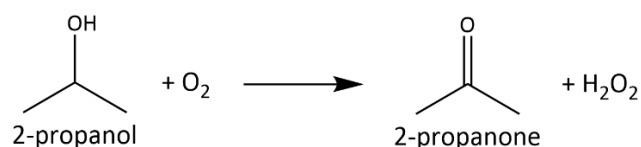


Figure 1.12: The oxidation of 2-propanol to 2-propanone and hydrogen peroxide.

This liquid-phase auto-oxidation reaction was utilised by Shell Chemical from 1957-1980.⁶⁹ An azeotrope mixture of 2-propanol (isopropanol) and water is oxidised by an 80-90 % O₂ gas source, between 10 - 20 bar at 90-140 °C, to produce 2-propanone (acetone) and hydrogen peroxide.⁶⁹ The oxidation is performed over several steps at decreasing temperature, with the conversion of 2-propanol per reaction cycle maintained below 15% to prevent the formation of by-products such as ethanoic acid (acetic acid).⁶⁹ The H₂O₂ is extracted from the solution by evaporation to leave behind the peroxide, and the water and organic compound solution is distilled to recover 2-propanol and 2-propanone.⁶⁹ The H₂O₂ must be diluted < 50% and purified in a counter current solvent-extraction column.⁶⁹ However, this process produces less pure hydrogen peroxide than recovered from the anthraquinone process due to the solubility of alcohols in the peroxide phase.⁶⁹

Another example of a secondary alcohol oxidation to produce hydrogen peroxide is methylbenzyl alcohol (MBA) oxidation to acetophenone, as shown in Figure 1.13.

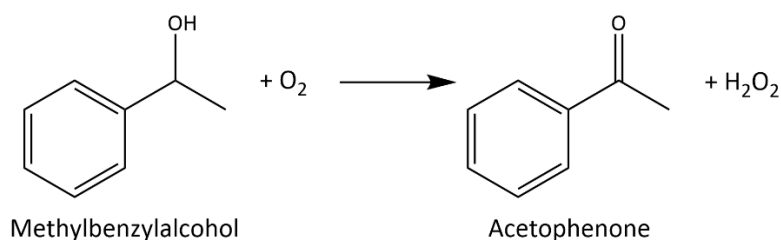


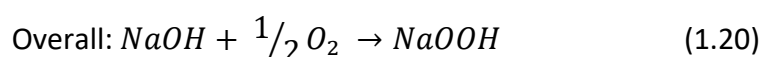
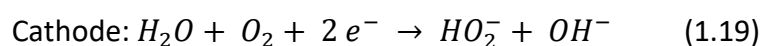
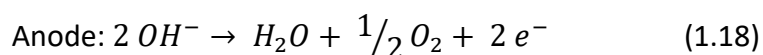
Figure 1.13: The oxidation of methylbenzyl alcohol to acetophenone and hydrogen peroxide.

This liquid-phase reaction was patented by ARCO Chemicals, a non-catalytic oxidation under conditions of 120-180 °C and 3-10 bar with 32% MBA converted and H₂O₂ selectivity of 97%.⁸³ The H₂O₂ is extracted from the product solution and purified, and the acetophenone is re-hydrogenated to reform MBA.

This process can also be performed catalytically by homogeneous Ni(II) b-diketone complexes, which have the benefit of not catalysing the degradation of hydrogen peroxide.⁶⁹ The ligand type of these complexes are very important as cyclic b-diketones, (e.g. 2-acetylcyclopentanoate and 2-acetylcyclohexanoate) increase H₂O₂ yield and selectivity, however basic ligands inhibit the oxidation and hence H₂O₂ production.⁶⁹

1.3.3.2 Electrochemical cells

Another method used to produce H₂O₂ is by electrolysis of a dilute NaOH solution in an electrochemical cell to produce an alkaline peroxide (NaOOH). Equations 1.18 and 1.19 show the reactions taking place at the anode and cathode of the electrochemical cell, with Equation 1.20 showing the overall reaction.⁶⁹



The basic set-up of the electrochemical cell is an anode in which the anolyte (a solution of NaOH) is fed, and a trickle bed cathode comprised from graphite, carbon black and a fluorocarbon binder which facilitates oxygen transfer for the cathodic reduction of O₂ to produce an alkaline peroxide (NaOOH).⁸⁴ Incorporation of an ion-exchange membrane can be used to improve the efficiency of this process. As this process produces an alkaline peroxide (rather than pure H₂O₂) it is most suited to applications in pulp bleaching so that separation of the product is not required.⁶⁹

1.3.4 Direct Hydrogen Peroxide Synthesis

The most direct way to produce hydrogen peroxide is the synthesis from hydrogen and oxygen, and the first patent for catalysts used for this reaction was granted in 1914 to Henkel

and Weber.⁸⁵ However, the direct synthesis route can give rise to problems due to the gas mixture being highly explosive, therefore, the gas mixture must be diluted with nitrogen, carbon dioxide or argon, to overcome this issue, however, this in turn will affect productivity.^{78,86–88}

Another issue in the direct synthesis is a number of subsequent reactions that can reduce selectivity. Figure 1.14 shows the enthalpies of reaction for the direct synthesis of hydrogen peroxide and the subsequent hydrogenation and decomposition reactions.⁶⁹

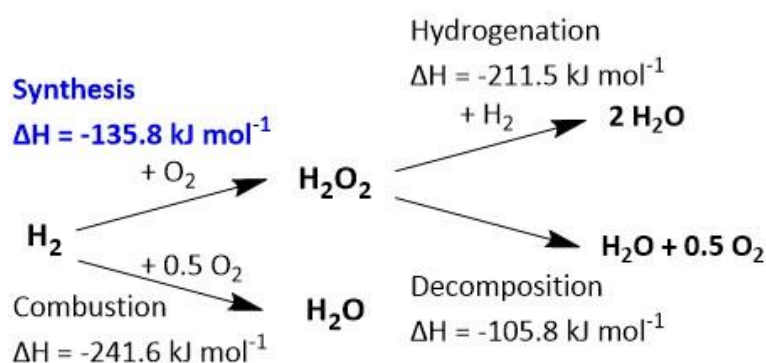
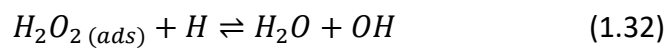
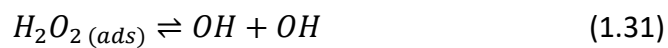
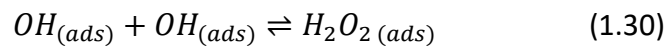
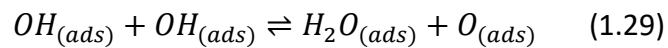
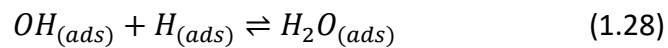
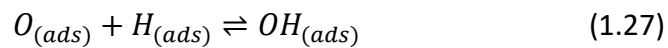
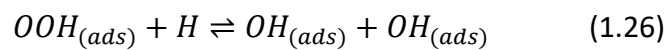
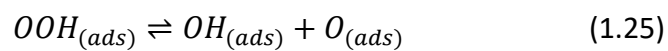
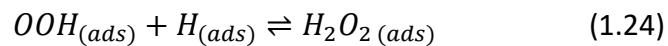
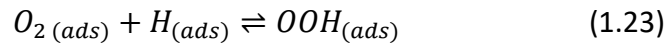
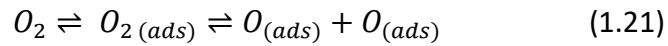


Figure 1.14: The direct synthesis of hydrogen peroxide and subsequent hydrogenation and degradation reactions, including the enthalpies of each reaction.

All reactions are thermodynamically favourable due to their exothermic nature. However, due to the production of H_2O being more thermodynamically favourable than H_2O_2 synthesis it is important to find a catalyst that favours the production of H_2O_2 .^{69,71} Not only that but it is ideal to produce a catalyst that not only favours the desired pathway but could also inhibit the subsequent reactions.

It was widely thought that the direct synthesis of H_2O_2 , by the successive hydrogenation of molecular O_2 , proceeds by a Langmuir-Hinshelwood mechanism.^{89–91} However other groups such as Flaherty and co-workers⁹² have proposed an alternative mechanism where the reaction occurs by a water-mediated proton-electron transfer. In this process, protic solvents are involved in the formation of surface-bound intermediates that transport the protons and electrons to the catalyst active sites.

It is generally assumed that the direct synthesis of H₂O₂ occurs by a 2-step hydrogenation mechanism.^{93,94} A proposed mechanism for the catalytic direct synthesis of H₂O₂ from O₂ and H₂, including potential side reactions is described:



Ads = adsorbed species on the surface of the catalyst

The main reactions steps in the synthesis of H₂O₂ are the hydrogenation shown in Equations 1.23 and 1.26, where the adsorbed atomic hydrogen (H_(ads)) and adsorbed oxygen (O_{2(ads)}) species react to form the peroxy (OOH_(ads)), which is then further hydrogenated to form the desired H₂O_{2(ads)} which must then desorb from the catalyst surface. Equations 1.21, 1.22 and 1.25 show the dissociation of O₂, H₂ and OOH. Cleavage of the O-O bond occurs in Equations 1.21 and 1.25, as does the hydrogenation reaction in Equation 1.26. Formation of the hydroxy (OH) species can result in the formation of water (Equation 1.29), as does the dissociation of H₂O₂ where cleavage of the O-O bond forms OH (Equation 1.31) and the hydrogenation of

H_2O_2 which results in the cleavage of the O-O bond to form water and OH (Equation 1.32) all of which therefore decreases selectivity towards H_2O_2 .

J. Li *et al.*⁹⁵ discuss the mechanism of direct synthesis of H_2O_2 over (monometallic) Pd-only and the more selective (bimetallic) AuPd surfaces. It is proposed that H_2 adsorption and dissociation occur at the Pd sites, and O_2 adsorption on the Au@Pd(111) can occur (1) at the top-bridge-top site on two Pd atoms that are not adjacent to the Au atom, (2) on two Pd atoms that are adjacent to the Au atom or (3) on one Pd atom and one Au atom.

The selectivity difference of the catalysts was explained by the activation energy of H_2O_2 dissociation on the Pd surface being less than the energy change of H_2O_2 desorption from the Pd surface (resulting in cleavage of the O-O bond and formation of H_2O), whereas on an AuPd surface the activation energy for H_2O_2 dissociation is higher than the energy change of H_2O_2 desorption, hence increasing the stability of H_2O_2 and hence selectivity.⁹⁵ This is due to the Au atoms causing a weaker interaction between the metal and the surface species (O-M) than the O-O bond of the H_2O_2 and OOH species. Additionally, the weaker interactions between the metal and surface species (O-M) facilitates the desorption of H_2O_2 .⁹⁵

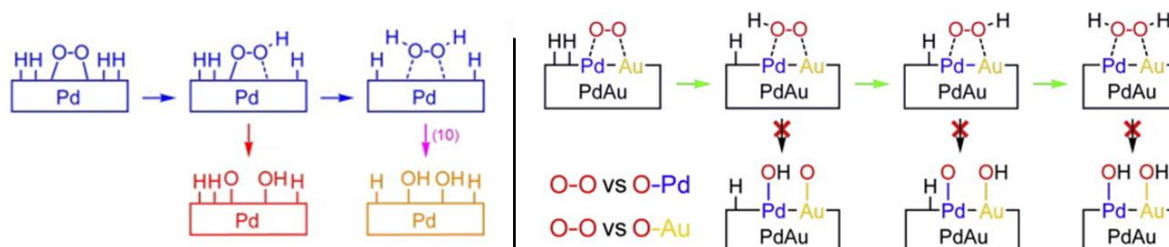


Figure 1.15: Cleavage of the O-O bond over a Pd surface (left) compared to the preferential formation of H_2O_2 and subsequent dissociation over an AuPd surface (right).⁹⁵

1.3.5 Solvents and Gas Dilutants for Direct H_2O_2 Synthesis

There are two important considerations for the reaction mixture in the direct synthesis of H_2O_2 . The first is the gas diluent, this is required as the reactants H_2 and O_2 must be diluted to keep the reaction parameters outside of the explosive region, this gas must be inert so as not to interfere with the reaction. The second consideration is liquid solvent, this must aid H_2O_2 stability and needs to enable high solubility of the gas mixture.

Water has many advantages as a solvent, it does not produce waste, and it is safe to use as it is non-toxic and non-flammable. It is also highly miscible with H₂O₂ and is commonly used as a solvent for storing and stabilising H₂O₂. Unfortunately, the disadvantage of water is the low solubility of both H₂ and O₂ which restricts the H₂O₂ production. Therefore, use of a secondary solvent can be employed to overcome this drawback.⁶⁹

Biphasic solvent mixtures have been employed with the view of overcoming the issue of gas solubility in water, for example water and a fluorinated solvent.⁹⁶ In this system the reactant gases are highly soluble in the fluorinated solvent where the reaction can take place, and the produced H₂O₂ will be present in the aqueous (water) phase.

Organic solvents such as alcohols have a higher solubility of H₂ and O₂ gases and can be used in combination with water.^{97,98} A number of organic solvents: methanol, ethanol, 2-propanol, dioxane, and acetone have been used for the direct synthesis of H₂O₂ combined with water in the liquid phase of the reaction.⁹⁷⁻⁹⁹ In tests using Pd supported catalysts methanol was found to be the superior solvent, giving the greatest rate of reaction.⁹⁹

Aprotic inorganic solvents acetonitrile and dimethyl sulfoxide have also been tested for the direct synthesis reaction and no H₂O₂ was detected, indicating the need for protic solvents such as methanol for proton-electron transfer.⁹²

Common gas diluents used for the reactants (H₂ and O₂) are N₂ and CO₂, both of which have good solubilities in methanol (and other alcohols) compared to water.⁶⁹ One of the advantages of using CO₂ (compared to N₂) is the formation of a carbonic acid solution produced by the CO₂ in water which promotes and the synthesis of, and stabilises the H₂O₂, and as the gas is easily removed at the end of the reaction with no contamination. Hence the CO₂ is a reversible, green in-situ acid promoter. Edwards *et al*⁸⁷ found that when using N₂ as a gas diluent, that by acidifying (with HNO₃) to pH 4 (which comparable to the solvent solution with CO₂), that an enhanced yield of H₂O₂ was achieved, comparable to that achieved with the CO₂ dilutant, demonstrating the importance of the acidified solution. However, the disadvantage to this method is the cost of separation, making CO₂ the preferable choice.

The gas diluent must not react under the conditions of the reaction and H₂/CO₂ will not react to produce CO over a Pd catalyst below 100 °C and temperatures that high would not be conducive to H₂O₂ formation.^{100,101} Another advantage to CO₂ is that it has low solubility with

H₂O₂, this means that once the peroxide is produced it is immediately expelled from the gas solvent and into the aqueous phase.⁶⁹

1.3.6 Catalyst Preparation Methods

There are a variety of established methods for heterogeneous catalyst synthesis, each with many parameters that can be modified in order to synthesise highly active and selective catalysts for a range of catalytic reactions. Bimetallic AuPd catalysts are often prepared via co-impregnation and sol-immobilisation synthesis techniques and these methods have been used extensively for catalysts used in the direct synthesis of H₂O₂.¹⁰²

1.3.6.1 Impregnation

Catalyst synthesis by impregnation was used by Bond *et al*¹⁰³ to produce the first Au nanoparticle supported catalyst. This method is widely used in industrial catalyst preparations due to its simplistic methodology. For impregnation methods, a metal precursor solution is added to a support to form a slurry, whereby the solution fills the pores in the support by capillary action.^{104–107} The slurry is then dried to form a powder which can undergo further heat treatments such as calcinations or reductions.

The volume of the precursor solution used in the impregnation method can have an important effect on the catalyst produced. For dry impregnation, also referred to as incipient-wetness impregnation, the volume of the metal precursor solution corresponds with the pore volume of the support, which ensures that there is no excess solution outside of the pores and results in a good particle dispersion.^{105–107} The concentration of metals that are possible to use will be limited by the solubility of the precursor in the chosen solvent, as the volume that can be used in the catalyst preparation is limited by the pore volume of the support.^{106,107} Hence, for metal precursors that are not very soluble, only lower weight loadings will be possible by this catalyst preparation method.¹⁰⁶ For wet impregnation an excess of solvent is used so that the volume of the precursor is greater than the total volume of the pores, this results in diffusion of the precursor into the pores of the support via a concentration gradient.¹⁰⁶

Heat treatments (such as high temperature calcinations and/or reductions) are required following the impregnation methodology to activate the catalysts active sites, however these

heat treatments can result in changes of morphology.¹⁰⁵ For example, at high heat treatments for AuPd catalysts formation of core(Au)-shell(Pd) nanoparticles are observed.¹⁰⁸ At high temperatures sintering can also occur which results in larger particle sizes, also interactions between the metal and the support can be altered for example SMSI (strong metal-support interactions), oxidation states of the metal will be altered, plus the removal of ligands, and the surface structure of the catalyst can change.¹⁰⁵

Sankar *et al*,¹⁰⁹ developed a modified impregnation method for AuPd catalysts in which an excess of chloride ions was used by addition of HCl into the PdCl₂ precursor solution prior to addition to the support. This is particularly important to ensure formation of PdCl₄²⁻ species, which due to the low solubility of the Pd precursor in water can otherwise result in the formation of insoluble salts which result in large metallic particles (that are catalytically inactive) which can be present in catalysts produced by conventional impregnation methods. This methodology resulted in a more homogeneous mixture for impregnation which resulted in enhanced metal dispersion and a more homogeneous alloy composition as demonstrated by the 5 nm AuPd supported nanoparticles these authors produced.

1.3.6.2 Sol-Immobilisation

Sol-immobilisation differs from impregnation techniques largely due to the reduction of the metal precursor prior to immobilisation onto the support.^{105,106} In this method the metal precursors are reduced, often with a strong reducing agent such as NaBH₄, to produce a colloid.¹⁰⁵ The presence of a stabilising group is used to surround the metal nanoparticles that are formed and protect against agglomeration, resulting in smaller nanoparticle sizes.¹¹⁰ There are two types of stabilisations that can be used, electrostatic and steric stabilisation, and this will be dependent on what protective group is used. Electrostatic stabilisation occurs when an ionic species is adsorbed onto the metal nanoparticles, this species has a high charge density which stabilise the colloid by repulsive Coulomb forces, whereas steric stabilisation occurs from long chain polymers such as PVA (polyvinyl alcohol) or PVP (polyvinyl pyrrolidone), the adsorption of which around the metal nanoparticles forms a separating layer which reduces the attractive van der Waals interactions between the nanoparticles.¹⁰⁶ This method therefore allows good control over the size of the metal nanoparticles formed.^{105,111} However, it is important to note that use of a stabilising group can also reduce

a catalysts activity if it prevents access of the reactant species (either sterically or electrostatically) to the active site of the catalyst.¹¹¹

Additionally, use of a strong reducing agent in excess is important so the metal nanoparticles are formed quickly, favouring the rate of nucleation of the nanoparticle formation, not the growth rate, resulting in smaller particle size. Sol-immobilisation allows for tuning of the catalyst morphology, for example bimetallic catalysts can be produced in which the alloys are either homogeneously dispersed or in a core-shell formation (by sequential reduction of the metal precursors).^{102,112} This is achieved by reducing one metal precursor prior to the second, allowing the second metal to form a shell around the first metal, hence forming core-shell metal particles.

The prepared colloid can be used for catalytic reactions; however, this has disadvantages such as difficulty of separation from the reaction medium (solid catalysts can easily be filtered out) this would also cause difficulty in reusability of the catalyst if it cannot be separated easily. Also, agglomeration can occur to the nanoparticles in a liquid medium over time, which immobilisation onto a support will prevent.

The colloid (or 'sol') is therefore immobilised onto a support. There are two factors important for the immobilisation step, the first is the stabilising agent used, as this cannot have a repulsive interaction with the chosen support. Also, the IEP (isoelectric point) of the support is an important factor in order to maximise the immobilisation of the metal onto the support. The IEP is the pH at which a molecule or substance has a zero net electric charge (different to PZC (point of zero charge) which is the absence of any surface charge).¹⁰⁵ At a pH below the IEP the molecule will act as an acid and above the IEP it will act as a base, this is important as the pH used in the catalyst immobilisation step will affect the properties of the support.⁵

1.3.7 AuPd Bimetallic Catalysts for Direct H₂O₂ Synthesis

It is well documented that AuPd bimetallic catalysts, are much more active towards the direct synthesis of H₂O₂ than their monometallic counterparts. Hutchings and co-workers have investigated AuPd bimetallic catalysts extensively on a variety of supports, and their work indicates a synergistic effect between the metals when combined, with catalysts showing improved activity, selectivity and stability.^{87,88,113–117} Figure 1.16 demonstrates the synergistic

effect of AuPd bimetallic alloyed catalysts for the direct synthesis of H_2O_2 .⁸⁸ What is clearly observed is not only an increase in activity of the bimetallic compared to the corresponding monometallic, but also a much higher selectivity seen for the AuPd bimetallic compared to Pd.

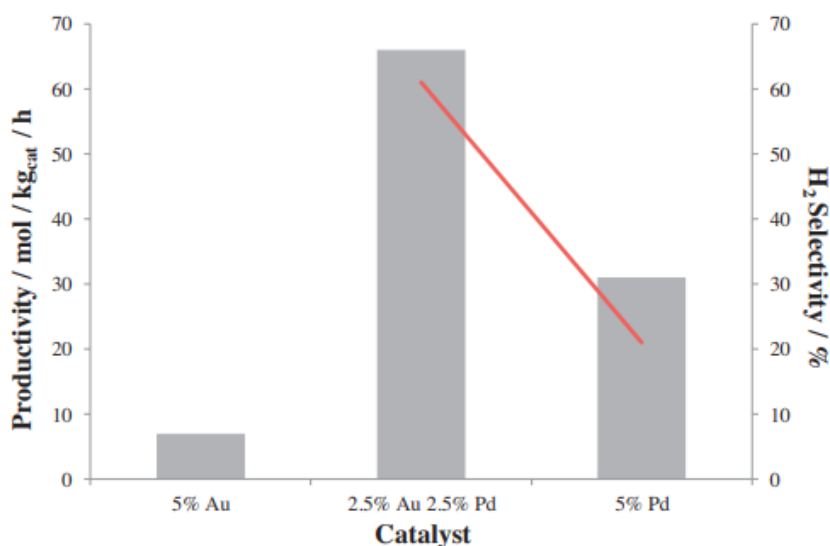


Figure 1.16: Synergistic effect of AuPd alloys for the direct synthesis of H_2O_2 using TiO_2 as the support. Bars: productivity; red line: H_2 selectivity, catalysts calcined at 400°C (the selectivity of 5% Au/ TiO_2 was not determined). Rate of hydrogen peroxide production determined using reaction conditions: 5% H_2/CO_2 (2.9 MPa) and 25% O_2/CO_2 (1.1 MPa), 8.5 g solvent (34% HPLC water 66% MeOH) 0.01 g catalyst, 2°C , 1200 rpm, 30 min).⁸⁸

In studies by Prichard et al.¹¹⁵ in the Hutchings group, characterisation on the bimetallic AuPd catalyst were performed to understand the nature of the supported bimetallic alloys. XPS analysis on catalysts (calcined at 400°C) showed a high surface Pd/Au ratio, indicating the development of core(Au)-shell(Pd) morphologies on TiO_2 , Fe_2O_3 and Al_2O_3 supports. Further characterisation by scanning transmission electron microscopy (STEM) showed bimodal particle size distribution (2-10 nm and 35-80 nm) Au particles present were in the larger size category and Pd in the smaller. It was proposed that this was due to increased surface mobility of Au (compared to Pd) leading to sintering at high temperatures.

A key importance of the studies this group performed was the lack of acid and halide promoters that are often used, not only making this a greener reaction process, but also

eliminating the need to purify the produced H₂O₂ both of which are important factors for large-scale industrial applications.⁸⁸

The primary issue with many of these catalysts is the ability to also catalyse the subsequent decomposition of the product, H₂O₂. Edwards *et al.*¹¹⁷ developed AuPd alloyed catalysts (prepared by impregnation) on an acid-pretreated activated carbon support, which was found to switch off the decomposition reaction. With this catalyst H₂O₂ selectivities of > 95% were achieved at high yields. It was observed that for the acid-treated carbon support (compared to the water-treated support) there was a higher number of smaller Pd rich nanoparticles (2-6 nm) on the catalyst surface. The ratio of Pd⁰/Pd²⁺ sites was shown to be of importance acid pre-treated catalyst primarily having Pd²⁺ (oxidised) species. It was proposed that these Pd nanoparticles decorated and hence inhibited the sites active for H₂O₂ decomposition which resulted in the higher activity and selectivity that this catalyst exhibited. Again, this study showed that a calcination temperature of 400°C was required for stability and reusability.

Edwards *et al.*⁸⁷ further investigated the role of various supports, heat treatments and promoters for AuPd catalysts prepared by co-impregnation. A catalyst series of 5wt% Au, Pd and AuPd (1:1 wt) supported on carbon, SiO₂, TiO₂ and Al₂O₃ (calcined 400°C) were tested for the direct synthesis of H₂O₂ (0.01g catalyst, 2.9 g water, 5.6 g methanol, P(5% H₂/CO₂) = 2.9 MPa P(25% O₂/CO₂) = 4 MPa, 2°C, 0.5 h). For all supports monometallic Au gave the lowest activities, with the highest being 7 mol kg_{cat}⁻¹ h⁻¹ for 5wt% Au/TiO₂. The most active monometallic Pd catalyst was 5wt% Au/SiO₂ with an activity of 80 mol kg_{cat}⁻¹ h⁻¹. However, the bimetallic catalysts are more active than both monometallics on the same support, giving the order of activity for bimetallic support of carbon (110 mol kg_{cat}⁻¹ h⁻¹) ~ silica (108 mol kg_{cat}⁻¹ h⁻¹) > TiO₂ (64 mol kg_{cat}⁻¹ h⁻¹) > Al₂O₃ (15 mol kg_{cat}⁻¹ h⁻¹). Characterisation of these bimetallics showed the presence of core(Au)-shell(Pd) structures on the TiO₂, Al₂O₃ and SiO₂ supports, whereas the AuPd nanoparticles on the carbon supported catalyst were observed to be homogeneous alloys. However, it was also found that the SiO₂ support contained carbon impurities which AuPd alloys preferentially interacted with, resulting in a similar activity seen for the carbon supported bimetallic catalyst. It was proposed that the higher activities were due to surface composition and distribution which enhanced the catalysts selectivity towards H₂O₂.

Heat treatment studies on these catalysts observed that catalysts calcined at <400 °C were more active upon first use than their counterparts calcined at 400 °C possibly due to sintering occurring at the higher temperature. However, the 400 °C catalysts were stable as they could be reused multiple times without loss of metal (Au & Pd) from the catalyst, comparatively for lower calcination temperatures (100, 200 & 300 °C) the catalysts were unstable and did not perform well upon reuse. These results show the same trends as the aforementioned studies for AuPd supported catalysts.⁸⁷

The same study also investigated promoters to enhance the activity of the bimetallic AuPd supported catalysts. It was found that contrary to the positive effect that Br⁻ (NaBr) and PO₄³⁻ (H₃PO₄) were found to have on monometallic Pd catalysts, for the bimetallic catalysts this had a detrimental effect. Additionally, the presence of CO₂ in the gas mixture (compared to using N₂ as the gas diluent) enhances activity due to the formation of an acid solution formed by the CO₂ in water, which is easily removed upon depressurisation at the end of the reaction. Hence the CO₂ acted as a reversible, green in-situ acid promoter.⁸⁷

The importance of isoelectric point of the support used for AuPd catalysts has also been investigated with results showing that this can have a huge impact on the stabilisation of the produced H₂O₂.¹¹³ Figure 1.17 shows that lower isoelectric points such as those seen for carbon supports are much less active towards the undesired degradation of H₂O₂, whereas higher isoelectric points, such as those seen for magnesium oxide result in higher levels of degradation.¹¹³ This again highlights the importance of the characteristics of the support selected for these catalysts.

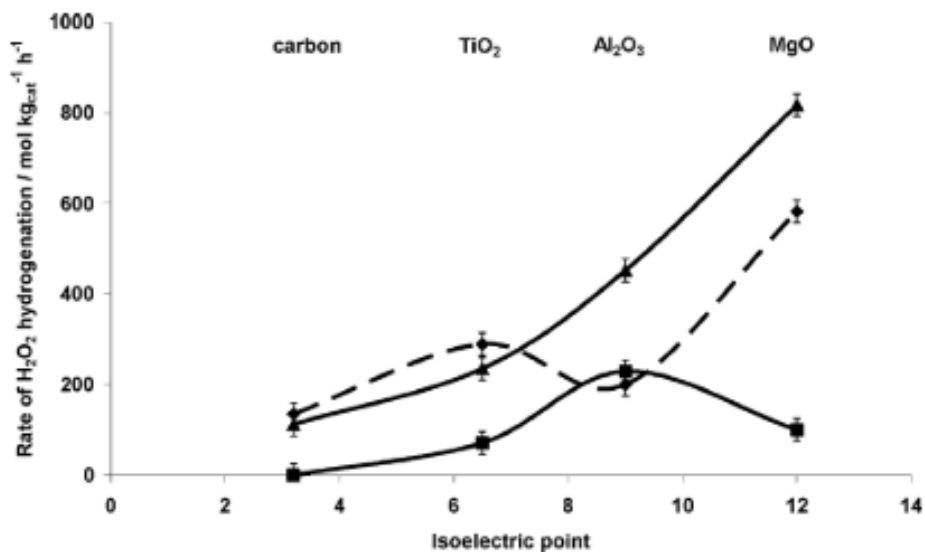


Figure 1.17: H_2O_2 hydrogenation as a function of isoelectric point for Pd-only, Au-only and bimetallic Au-Pd catalysts. Key: Diamonds Pd-only, Squares Au-only, Triangles Au-Pd.¹¹³

The importance of the catalyst preparation procedure was investigated by Pritchard *et al.*¹¹⁵ where the impregnation method was reviewed for a 5wt% AuPd/TiO₂ catalyst (calcined 400°C). The amount of water added during the impregnation step of the catalyst was altered and it was found that as the concentration of the metal salts increased (less water) the activity of the final catalyst towards H₂O₂ increased also. Additionally, by increasing the scale of the catalyst produced (larger batch) also enhanced activity towards H₂O₂. When water was added to the catalyst after the impregnation step (re-wetting and then re-drying) this was found to have minimal effect on the catalyst.

1.3.8 Incorporation of Non-Precious Metals into Pd Catalysts

There have been extensive studies into the use of AuPd bimetallic alloys for the direct synthesis of H₂O₂. However, there have also been numerous investigations into enhancing the catalytic activity of Pd with other metals for the direct synthesis of H₂O₂ and in-situ production of H₂O₂ for oxidation reactions. It has been found that the addition of a range of non-precious metals are able to similarly enhance the activity of a Pd catalyst. Additionally, the incorporation of these secondary metals can reduce or eliminate the need for liquid-

phase promoters in the synthesis of H₂O₂ such as mineral acids (e.g. H₂SO₄, HCl, HBr & H₃PO₄) and halide salts (e.g. KCl & NaBr).¹¹⁸

Crombie *et al.*¹¹⁹ prepared a series of bimetallic 1wt% Pd-X/TiO₂ catalysts (where Pd:X = 1:1 and X = Au, Mn, Fe, Co, Cu, Ni, Ce) by excess chloride impregnation. In this work the authors were testing the catalysts for direct hydrogen peroxide synthesis (0.01g catalyst, 2.9 g water, 5.6 g methanol, P(5% H₂/CO₂) = 2.9 MPa P(25% O₂/CO₂) = 4 MPa, 20°C, 0.5 h) with an aim to use these formulations for the oxidation of benzyl alcohol using in-situ made H₂O₂. Of the PdX combinations tested for the direct synthesis of H₂O₂, 1wt% AuPd/TiO₂ gave the greatest activity (68 mol kg_{cat}⁻¹ h⁻¹) and 1wt% PdCu/TiO₂ gave the lowest activity (2 mol kg_{cat}⁻¹ h⁻¹). 1wt% AuPd/TiO₂ also gave the highest degradation activity (711 mol kg_{cat}⁻¹ h⁻¹) and 1wt% PdNi/TiO₂ gave the lowest (4 mol kg_{cat}⁻¹ h⁻¹). This could potentially suggest that the Ni in the catalyst is responsible for stabilising the H₂O₂ by inhibiting the degradation pathway. The high degradation seen for the AuPd catalyst is exaggerated by the set of reaction conditions at room temperature, rather than 2°C as previous studies have used. It is notable that all monometallic versions of these catalysts showed negligible activity towards H₂O₂ synthesis with the obvious exception of Pd, and to a lesser extent Au. Additionally, for PdMn, PdFe and PdCo bimetallics the synthesis activities were higher than seen for the Pd monometallic, and had lower degradation activities also, demonstrating that there is a positive synergistic effect between the metals in these bimetallics. This work produced a 1wt%PdFe/TiO₂ catalyst that was highly active for benzyl alcohol oxidation using in-situ produced H₂O₂ and the study showed that it was the ability of the catalyst to not only catalyse the oxidation but also synthesise H₂O₂ in-situ which made this catalyst so successful.

Santos *et al.*¹²⁰ produced a series of bimetallic 1wt% Pd-X/TiO₂ catalysts (where Pd:X = 1:1 wt and X = Au, Cu, Co, Fe) by an excess chloride impregnation procedure, for the oxidative degradation of phenol via the in situ production of H₂O₂. For the direct synthesis of H₂O₂ (0.01g catalyst, 2.9 g water, 5.6 g methanol, P(5% H₂/CO₂) = 2.9 MPa P(25% O₂/CO₂) = 4 MPa, 2°C, 0.5 h) it was found that alloying Pd with Au, Co and Fe enhanced activity from 30 mol kg_{cat}⁻¹ h⁻¹ to 97, 42, and 38 mol kg_{cat}⁻¹ h⁻¹ respectively, demonstrating that there is a synergistic effect between the metals. Again, this study showed that the presence of Cu deactivated the catalyst and gave an activity of only 11 mol kg_{cat}⁻¹ h⁻¹. Notably, with the exception of AuPd, the other bimetallics were less active towards the degradation reaction than Pd-only. XPS

analysis of these catalysts showed that the presence of base metals Fe, Co and Cu increased the Pd²⁺ content of the catalysts. Similarly to the previous study, the PdFe catalyst this group synthesised was extremely effective when applied to oxidations by in-situ direct H₂O₂ synthesis.

As seen in these studies, the incorporation of Cu into the Pd catalysts for H₂O₂ synthesis results in a clear inhibition of the catalytic activity. Additionally, computational studies performed by Joshi *et al.*¹²¹ determined that for Cu-containing precious metal nanoparticle catalysts, the formation of the hydroperoxy (OOH*) species, (which is formed by the addition of hydrogen to molecular O₂) is thermodynamically unfavourable. These computational studies are widely supported by numerous results of PdCu catalysts used for this reaction.

Freakley *et al.*¹²² investigated the addition of Sn into Pd catalysts on TiO₂ and SiO₂ supports prepared by co-impregnation. They were able to produce bimetallic SnPd catalysts that were able to switch off the sequential hydrogenation and decomposition reactions, which resulted in selectivities >95% toward H₂O₂ for the direct synthesis. It was proposed that these results were due to tin oxide surface layer that encapsulated the small Pd-rich particles on the catalyst, while leaving larger Pd-Sn alloy particles exposed.

Li *et al.*¹²³ also developed SnPd nanocrystals with a hollow structure, on a range of supports (TiO₂, ZrO₂, ZnO, Al₂O₃, SiO₂ & C). By using rapid thermal treatment (at 140°C), hollow Pd-Sn/TiO₂ catalysts were synthesised that completely inhibited the sequential hydrogenation and decomposition reactions and hence resulted in a substantial increase in the activity towards direct H₂O₂ synthesis. The high performance of these catalysts was attributed to a number of factors, (1) the presence of PdO, (2) the synergistic effect between Pd and Sn, and (3) the interface effect between Pd/SnOx and PdO/SnOx.

Maity *et al.*¹²⁴ prepared Pd-only, Ni_{0.4}Pd_{0.6} (Ni : Pd wt ratio 40 : 60) and Au_{0.5}Pd_{0.5} (Au : Pd wt ratio 50 : 50) nanostructures by a borohydride reduction method, utilising HCl and Br⁻ promoters to stabilise H₂O₂ in the direct synthesis reaction. The incorporation of Ni resulted in an extremely active catalyst, with 3 times the production of H₂O₂ compared to the Pd catalyst over a 72 h reaction. Not only was the PdNi catalyst highly active but extremely high selectivity was observed with a maximum value of 95% selectivity towards H₂O₂ at 0.4% H₂

conversion. Comparatively the AuPd nanostructures only increases the activity by 25% compared to Pd-only.

Wang *et al.*¹²⁵ investigated metal ratios for PdGa/TiO₂ and PdIn/TiO₂ catalysts prepared by an acid-washed sol-immobilisation procedure, this method was employed due to the good control of particle size that this technique provides. They found that addition of Ga and In respectively to the Pd supported catalysts reduced the rate of the degradation reaction. In particular the (3.2wt%) Pd₂Ga/TiO₂ (Pd:Ga 2:1) catalyst improved activity towards the direct synthesis of H₂O₂ while also decreasing the degradation rate (compared to 5.6wt% Pd/TiO₂). It was observed that for these catalysts, lower levels of Ga incorporation resulted in the more active and selective catalysts by inhibiting the subsequent degradation reaction. Similarly, for In incorporation the (5.0wt%) Pd₂In/TiO₂ (Pd:In 2:1) was found to have a similar synthesis rate (compared to 5.6wt% Pd/TiO₂) and a lower degradation. For catalysts with larger In loadings it was found that the degradation activity drops substantially. XPS analysis showed that introduction of Ga and In to the catalysts resulted in an increase of PdO content, whereas the Pd only catalysts contained predominantly metallic species which was responsible for the high degradation rates seen for this catalyst

Wilson *et al.*¹¹⁸ prepared a series of stable and selective PdZn_x/SiO₂ catalysts (where x = 1.5, 6, 30) for the direct synthesis of H₂O₂ without using liquid-phase promoters. They found that by increasing the ratio of Zn/Pd that this effected the catalyst by increasing the number of intermetallic β₁-Pd₁Zn₁ nanoparticles and reducing the number of FCC (face-centred cubic) Pd nanoparticles. Experimental results showed that as the Zn content increases, so did the H₂ selectivity towards H₂O₂, with the Pd catalyst giving 26% selectivity as opposed to PdZn₃₀ which gave 69% selectivity and had negligible levels of FCC Pd nanoparticles on the catalyst. It was concluded that by optimising the catalyst synthesis to produce catalysts with uniform β₁-Pd₁Zn₁ nanoparticles, can enhance selectivity of these catalysts for the reaction.

1.3.9 Trimetallic Catalysts for Direct H₂O₂ Synthesis

Use of bimetallic AuPd catalysts have been well documented for catalysing the direct synthesis of H₂O₂. However, the use of trimetallic catalysts is not a well-studied field for this reaction. Despite this, it has been found that addition of a third noble metal Ru (ruthenium)

or Pt (platinum) to PdAu nanoalloys form a trimetallic catalyst, can enhance the activity.^{108,126-129}

Ntainjua *et al*¹²⁹ prepared a catalyst series of bimetallic 5wt% {AuRu} and 5wt% {PdRu} and trimetallic 5wt% {AuPdRu} supported on TiO₂ synthesised by impregnation, with variations in the metal ratios for each metal composition. It was found that addition of Ru to the catalysts could enhance activity towards the direct synthesis of H₂O₂ with the effect dependant on the amount of Ru introduced into the catalysts. Bimetallic studies over the range of metal composition ratio shows that the optimal loading for a 5wt% {PdRu}/TiO₂ bimetallic was at 4.5wt%-Pd 0.5wt% Ru/TiO₂ which gave an activity of 143 mol kg_{cat}⁻¹ h⁻¹ towards H₂O₂ synthesis (0.01 g catalyst, 2.9 g water, 5.6 g methanol, P(5% H₂/CO₂) = 2.9 MPa P(25% O₂/CO₂) = 4 MPa, 2°C, 0.5 h). It was also observed that metal ratios either side of this point gave decreased activity in the reaction. A similar trend was seen for the AuRu/TiO₂ bimetallic where an optimum composition of 4.25wt%-Au 0.75wt%-Ru/TiO₂ gave an activity of 69 mol kg_{cat}⁻¹ h⁻¹ which although far less active than seen for the PdRu series, was still the highest activity when AuRu was used. As with the PdRu series the activity of the catalyst towards H₂O₂ synthesis decreases either side of this composition ratio. However, what is most interesting is that when Au, Pd and Ru are used to make a 5wt% {AuPdRu}/TiO₂ trimetallic catalyst, the activities far supersede that seen for both the AuRu bimetallic composition series, an AuPd bimetallic (2.5wt%-Au 2.5wt%-Pd/TiO₂ = 64 mol kg_{cat}⁻¹ h⁻¹) and the majority of the PdRu series. In fact, a composition of 4.5wt%-Pd 0.45wt%-Ru 0.05wt%-Au/TiO₂ gave an H₂O₂ synthesis activity of 153 mol kg_{cat}⁻¹ h⁻¹ which exceeds that of even the optimal PdRu bimetallic catalyst.

Edwards *et al*¹²⁷ prepared a series of trimetallic 5wt% AuPdPt/TiO₂ catalysts in which the weight ratio of Au/Pd = 1 and the Pt loadings were in the range of 0.05 – 0.45 wt% (catalysts calcined in static air at 400 °C, 3 h). In this study it was found that incorporation of very small concentrations of Pt were able to enhance the activity towards of H₂O₂ synthesis whilst also increasing the selectivity of the catalyst by suppressing the undesired degradation reaction. For 2.5wt%-Au 2.5wt%-Pd/TiO₂ a H₂O₂ synthesis activity of 64 mol kg_{cat}⁻¹ h⁻¹ and H₂O₂ degradation activity of 235 mol kg_{cat}⁻¹ h⁻¹ were observed. Comparatively 2.45wt%-Au 2.45wt%-Pd 0.05wt%-Pt/TiO₂ gave synthesis and degradation activities of 154 and 135 mol kg_{cat}⁻¹ h⁻¹ respectively. This shows both a large increase in the activity towards the desired synthesis reaction and decrease towards the degradation, increasing selectivity of the catalyst towards

H₂O₂. It was also observed that Pt loadings of 0.1wt% and 0.2wt% in the trimetallics, although showing similar synthesis activities (159 and 156 mol kg_{cat}⁻¹ h⁻¹ respectively) had much higher degradation activities (283 and 318 mol kg_{cat}⁻¹ h⁻¹ respectively) even compared to the AuPd bimetallic catalyst. This demonstrates the importance of finely tuning the Pt loading in the trimetallic as even small differences can have large effects on the selectivity of the catalyst even if the activity is improved. Following the same trend as the previously discussed AuPdRu trimetallic work, as the Pt concentration was increased further the synthesis activity began to decrease. This work also produced a catalyst that was composed primarily of Pd with small concentrations of both Au and Pt added as dopants, this catalyst was 4.6wt%-Pd 0.2wt%-Au 0.2wt%-Pt/TiO₂ and was found to have synthesis and degradation activities of 184 and 382 mol kg_{cat}⁻¹ h⁻¹ respectively. The synthesis activity of this catalyst is substantially higher than the previous trimetallics, however, the decrease in Au of this catalyst appears to correlate with the decreased selectivity seen in the much more active degradation reaction. It could be reasoned that the higher loading of Au is important in these trimetallic catalysts for selectivity purposes. Through characterisation studies of the trimetallic catalysts it was observed that doping with Pt resulted in a suppression of Pd(shell) Au(core) particles that are observed in the bimetallic 2.5wt%-Au 2.5wt%-Pd/TiO₂ catalyst.

Further studies by Edwards *et al*¹⁰⁸ investigated similar series of 5wt% AuPdPt trimetallic impregnation catalysts however using a CeO₂ support, weight ratio of Au/Pd = 1 and the Pt loadings were in the range of 0.05 – 1wt% (catalysts calcined in static air at 400 °C, 3 h), for the direct synthesis of H₂O₂ under the same conditions. In a similar way to the previous studies, the trend of the synthesis data against Pt doping appears like a volcano plot, in this case the optimum catalyst for the synthesis reaction was 2.4wt%-Au 2.4wt%-Pd 0.2wt%-Pt/CeO₂ with an activity of 170 mol kg_{cat}⁻¹ h⁻¹ (degradation 145 mol kg_{cat}⁻¹ h⁻¹). In comparison, the 2.5wt%-Au 2.5wt%-Pd/CeO₂ a H₂O₂ catalyst has a far lower synthesis activity of 68 mol kg_{cat}⁻¹ h⁻¹ but the same degradation at 145 mol kg_{cat}⁻¹ h⁻¹ showing that the presence of Pt in the catalyst in that amount has not only increased the activity, but the selectivity has not been diminished. It is notable that for the Pt loadings greater than 0.2wt%, lower synthesis activities were observed which corresponded with higher degradation activities, a trend that was also seen for the TiO₂ supported trimetallics. From these results it is evident that low levels of Pt doping can enhance the activity without compromising on selectivity. XPS analysis

of the various trimetallic catalysts showed a large increase in the Pd/Au ratio detected on the catalyst surface, for the 2.4wt%-Au 2.4wt%-Pd 0.2wt%-Pt/CeO₂ catalyst Pd/Au = 58 compared to 2.5wt%-Au 2.5wt%-Pd/CeO₂ where Pd/Au = 7.1 is detected. There were two theories as to the cause of this, the first being that the core(Au)-shell(Pd) effect was enhanced due to the presence of the Pt, alternatively the Pt could be inducing redispersion of the Pd species on the catalyst surface. It was further observed that the core-shell effect was enhanced further by increasing the temperature of the calcination step in the catalyst preparation.

The group further investigated the effect of metal compositions in the 5wt% AuPdPt/CeO₂ for the synthesis and degradation of H₂O₂. An extensive selection of catalysts were prepared all with a total metal loading of 5wt% and a variety of metal ratio compositions. It was found that there were three regions of interest in the results from these compositions (1) primarily Pd with small levels of Au and Pt added, (2) primarily Pd with more Au than Pt and, (3) Au/Pd = 1 with small quantities of Pt added.¹⁰⁸

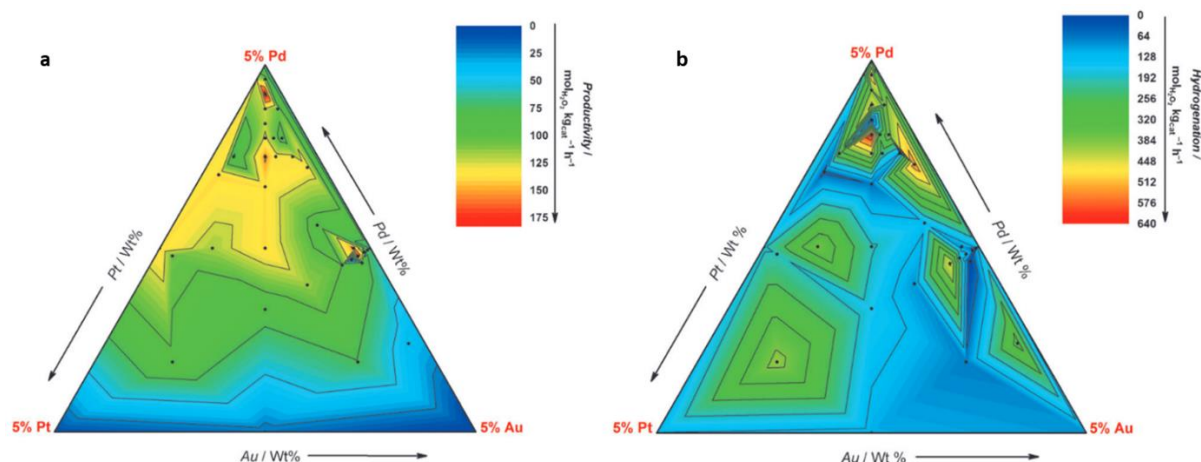


Figure 1.2: Rates of H₂O₂ synthesis and hydrogenation/decomposition for CeO₂ -supported 5 wt % Au/Pd/Pt catalysts presented as a contour diagram. (a) Productivity (b) hydrogenation/decomposition.¹⁰⁸

Work by Gong *et al*¹²⁸ has developed upon earlier works by scaling down the metal loadings. They prepared a series of 1wt% AuPdPt/TiO₂ (Au/Pd = 1 (mol/mol)) with a range of Pt loadings (up to 33 molar % Pt), catalysts were prepared by sol-immobilisation (calcined 400°C, 3 h). While very low levels of Pt doping (approx. 1-5 molar % Pt) were found to greatly increase the

activity towards H₂O₂ synthesis, further addition of Pt content in the catalyst (from approx. 10 molar % Pt) was shown to dramatically decrease the rate of H₂O₂ synthesis to below that of a bimetallic 1wt% AuPd/TiO₂ catalyst.

The optimum catalyst towards the synthesis of H₂O₂ in this series was found to be 1wt% Au₁Pd₁Pt_{0.1}/TiO₂ with an activity of 112 mol kg_{cat}⁻¹ h⁻¹ and a degradation of 245 mol kg_{cat}⁻¹ h⁻¹. This is a substantial improvement upon 1wt% Au₁Pd₁/TiO₂ which gave a synthesis activity of 81 mol kg_{cat}⁻¹ h⁻¹ and a slightly higher degradation of 257 mol kg_{cat}⁻¹ h⁻¹, giving the Pt catalyst not only improved activity but improved selectivity towards the desired reaction pathway. This was further supported by gas analysis at (close to) iso-conversion of H₂ which showed that the bimetallic catalyst gave a H₂O₂ selectivity of 31% at 39% H₂ conversion, while the optimised trimetallic catalyst gave a higher H₂O₂ selectivity of 37% at 43% H₂ conversion. To compare, 1wt% Au₁Pd₁Pt₁/TiO₂ had a very low synthesis activity of 30 mol kg_{cat}⁻¹ h⁻¹ and a higher activity towards the undesired degradation 271 mol kg_{cat}⁻¹ h⁻¹, the low selectivity of this catalyst is further demonstrated from gas analysis showing 15% selectivity towards H₂O₂ at 44% H₂ conversion. This work again highlights the critical importance of tuning the loading of the dopant Pt, with favourable results in low loadings. Through characterisation of these catalysts the authors proposed that the modification of the Pd oxidation states with the introduction of low levels of Pt dopant resulted in mixed Pd²⁺-Pd⁰ domains which enhance selectivity towards H₂O₂ (compared to Pd⁰ or Pd²⁺ rich analogues). However, by increasing the Pt loading Pd⁰ content was increased dramatically which corresponded with the observed loss in selectivity.¹²⁸

It is evident that introduction of small levels of dopant metals can have a remarkable effect on both the activity and selectivity of AuPd supported catalysts towards H₂O₂ synthesis. It has been proposed that electronic modification of the Pd oxidation states by the dopant metal plays a large role in the selectivity of the catalysts. Additionally, the presence of the dopant metal can have effects on the morphology of the catalyst by enhancing core-shell effects and increasing dispersion of the Pd species. By further investigating the use of dopant metals in established structures such as supported AuPd catalysts it is possible to finely tune these catalysts to enhance their performance to a larger degree.¹²⁸

Other work on AuPdPt trimetallics include Nguyen *et al*¹²⁶ who produced Pd@AuPt core-shell nanoparticles with a Pd nanocube core, synthesised by a centrifugal microfluidic device. For

the direct synthesis of H_2O_2 by flow, it was found that the activity of the Pd@AuPt catalysts increased gradually as the Au/Pt ratio was increased (from 0.05 to 0.5). However, when the ratio of Au/Pt exceeded 0.5 the activity started to increase, therefore giving an optimal ratio of Au/Pt = 0.5 for the catalyst.

1.4 References

- 1 J. Wisniak, *Educ. Quim.*, 2010, **21**, 60–69.
- 2 C. H. Bartholomew and R. J. Farruto, in *Introduction and Fundamental Catalytic Phenomena*, John Wiley & Sons, Inc., 2nd edn., 2006, pp. 4–59.
- 3 G. Rothenberg, *Catalysis: Concepts and Green Applications*, Wiley-VCH Verlag GmbH & Co. KGaA, 2008.
- 4 C. Stegelmann, A. Andreasen and C. T. Campbell, *J. Am. Chem. Soc.*, 2009, **131**, 13563.
- 5 J. Daintith, Ed., *A Dictionary of Chemistry*, Oxford University Press, 6th edn., 2008.
- 6 P. Anastas and N. Eghbali, *Chem. Soc. Rev.*, 2010, **39**, 301–312.
- 7 J. R. H. Ross, in *Contemporary Catalysis*, 2019, pp. 161–186.
- 8 Z. N. Hu, J. Liang, K. Ding, Y. Ai, Q. Liang and H. bin Sun, *Appl. Catal. A Gen.*, 2021, **626**, 118339.
- 9 F. Li, B. Frett and H. . Li, *Synlett.*, 2014, **25**, 1403–1408.
- 10 H.-U. Blaser, *Science (80-.)*, 2006, **313**, 312–313.
- 11 Z. Zhao, H. Yang, Y. Li and X. Guo, *Green Chem.*, 2014, **16**, 1274–1281.
- 12 J. Li, L. Zhong, L. Tong, Y. Yu, Q. Liu, S. Zhang, C. Yin, L. Qiao, S. Li, R. Si and J. Zhang, *Adv. Funct. Mater.*, 2019, **29**, 1–9.
- 13 A. Corma, P. Concepción and P. Serna, *Angew. Chemie - Int. Ed.*, 2007, **46**, 7266–7269.
- 14 R. Nie, J. Wang, L. Wang, Y. Qin, P. Chen and Z. Hou, *Carbon N. Y.*, 2012, **50**, 586–596.
- 15 T. Sheng, Y. J. Qi, X. Lin, P. Hu, S. G. Sun and W. F. Lin, *Chem. Eng. J.*, 2016, **293**, 337–344.
- 16 W. C. Cheong, W. Yang, J. Zhang, Y. Li, D. Zhao, S. Liu, K. Wu, Q. Liu, C. Zhang, D. Wang, Q. Peng, C. Chen and Y. Li, *ACS Appl. Mater. Interfaces*, 2019, **11**, 33819–33824.
- 17 H. Bao, Y. Li, L. Liu, Y. Ai, J. Zhou, L. Qi, R. Jiang, Z. Hu, J. Wang, H. Sun and Q. Liang, *Chem. - A Eur. J.*, 2018, **24**, 14418–14424.
- 18 J. Song, Z. F. Huang, L. Pan, K. Li, X. Zhang, L. Wang and J. J. Zou, *Appl. Catal. B Environ.*, 2018, **227**, 386–408.
- 19 S. Furukawa, Y. Yoshida and T. Komatsu, *ACS Catal.*, 2014, **4**, 1441–1450.
- 20 G. D. Frey, V. Lavallo, B. Donnadiou, W. W. Schoeller and G. Bertrand, *Science (80-.)*, 2007, **316**, 439–441.

- 21 L. Zhang, M. Zhou, A. Wang and T. Zhang, *Chem. Rev.*, 2020, **120**, 683–733.
- 22 O. Eisenstein and R. H. Crabtree, *New J. Chem.*, 2013, **37**, 21–27.
- 23 Y. Ren, C. Hao, Q. Chang, N. Li, J. Yang and S. Hu, *Green Chem.*, 2021, **23**, 2938–2943.
- 24 H. Ma and C. Na, *ACS Catal.*, 2015, **5**, 1726–1735.
- 25 H. Göksu, S. F. Ho, Ö. Metin, K. Korkmaz, A. Mendoza Garcia, M. S. Gültekin and S. Sun, *ACS Catal.*, 2014, **4**, 1777–1782.
- 26 M. J. Gilkey and B. Xu, *ACS Catal.*, 2016, **6**, 1420–1436.
- 27 R. Nie, Y. Tao, Y. Nie, T. Lu, J. Wang, Y. Zhang, X. Lu and C. C. Xu, *ACS Catal.*, 2021, **11**, 1071–1095.
- 28 H. S. Kakati and D. C. Deka, *Indian J. Chem. Technol.*, 2003, **10**, 60–62.
- 29 Z. Hu, J. Zhou, Y. Ai, L. Liu, L. Qi, R. Jiang, H. Bao, J. Wang, J. Hu, H. bin Sun and Q. Liang, *J. Catal.*, 2018, **368**, 20–30.
- 30 Y. Sheng, X. Wang, Z. Xing, X. Chen, X. Zou and X. Lu, *ACS Sustain. Chem. Eng.*, 2019, **7**, 8908–8916.
- 31 C. Zhang, J. Lu, M. Li, Y. Wang, Z. Zhang, H. Chen and F. Wang, *Green Chem.*, 2016, **18**, 2435–2442.
- 32 H. bin Sun, Y. Ai, D. Li, Z. Tang, Z. Shao and Q. Liang, *Chem. Eng. J.*, 2017, **314**, 328–335.
- 33 J. Zhou, Y. Li, H. bin Sun, Z. Tang, L. Qi, L. Liu, Y. Ai, Z. Shao and Q. Liang, *Green Chem.*, 2017, **19**, 3400–3407.
- 34 M. Boronat, P. Concepción, A. Corma, S. González, F. Illas and P. Serna, *J. Am. Chem. Soc.*, 2007, **129**, 16230–16237.
- 35 H. Wei, X. Liu, A. Wang, L. Zhang, B. Qiao, X. Yang, Y. Huang, S. Miao, J. Liu and T. Zhang, *Nat. Commun.*, 2014, **5**, 1–8.
- 36 R. Gao, L. Pan, H. Wang, X. Zhang, L. Wang and J. J. Zou, *ACS Catal.*, 2018, **8**, 8420–8429.
- 37 Y. Tan, X. Y. Liu, L. Zhang, A. Wang, L. Li, X. Pan, S. Miao, M. Haruta, H. Wei, H. Wang, F. Wang, X. Wang and T. Zhang, *Angew. Chemie - Int. Ed.*, 2017, **56**, 2709–2713.
- 38 A. Corma, P. Serna, P. Conception and J. J. Calvino, *J. Am. Chem. Soc.*, 2008, **130**, 8748–8758.
- 39 Y. Matsushima, R. Nishiyabu, N. Takanashi, M. Haruta, H. Kimura and Y. Kubo, *J. Mater. Chem.*, 2012, **22**, 24124–24131.
- 40 M. Tamura, N. Yuasa, Y. Nakagawa and K. Tomishige, *Chem. Commun.*, 2017, **53**, 3377–3380.

- 41 M. J. Beier, J. M. Andanson and A. Baiker, *ACS Catal.*, 2012, **2**, 2587–2595.
- 42 M. Makosch, W. I. Lin, V. Bumbálek, J. Sá, J. W. Medlin, K. Hungerbühler and J. A. Van Bokhoven, *ACS Catal.*, 2012, **2**, 2079–2081.
- 43 Q. Wu, B. Zhang, C. Zhang, X. Meng, X. Su, S. Jiang, R. Shi, Y. Li, W. Lin, M. Arai, H. Cheng and F. Zhao, *J. Catal.*, 2018, **364**, 297–307.
- 44 T. Schwob and R. Kempe, *Angew. Chemie - Int. Ed.*, 2016, **55**, 15175–15179.
- 45 D. Formenti, F. Ferretti, F. K. Scharnagl and M. Beller, *Chem. Rev.*, 2019, **119**, 2611–2680.
- 46 L. Zhang, A. Wang, W. Wang, Y. Huang, X. Liu, S. Miao, J. Liu and T. Zhang, *ACS Catal.*, 2015, **5**, 6563–6572.
- 47 Z. L. Wang, X. F. Hao, Z. Jiang, X. P. Sun, D. Xu, J. Wang, H. X. Zhong, F. L. Meng and X. B. Zhang, *J. Am. Chem. Soc.*, 2015, **137**, 15070–15073.
- 48 X. Wei, M. Zhou, X. Zhang, X. Wang and Z. Wu, *ACS Appl. Mater. Interfaces*, 2019, **11**, 39116–39124.
- 49 X. Wang and Y. Li, *J. Mol. Catal. A Chem.*, 2016, **420**, 56–65.
- 50 Y. Sun, A. J. Darling, Y. Li, K. Fujisawa, C. F. Holder, H. Liu, M. J. Janik, M. Terrones and R. E. Schaak, *Chem. Sci.*, 2019, **10**, 10310–10317.
- 51 J. Mao, W. Chen, W. Sun, Z. Chen, J. Pei, D. He, C. Lv, D. Wang and Y. Li, *Angew. Chemie - Int. Ed.*, 2017, **56**, 11971–11975.
- 52 S. Furukawa, K. Takahashi and T. Komatsu, *Chem. Sci.*, 2016, **7**, 4476–4484.
- 53 A. Yarulin, C. Berguerand, I. Yuranov, F. Cárdenas-Lizana, I. Prokopyeva and L. Kiwi-Minsker, *J. Catal.*, 2015, **321**, 7–12.
- 54 A. Yarulin, C. Berguerand, A. O. Alonso, I. Yuranov and L. Kiwi-Minsker, *Catal. Today*, 2015, **256**, 241–249.
- 55 W. Qifan, C. Zhang, W. Lin, H. Cheng, M. Arai and F. Zhao, *Catalysts*, 2019, **9**, 1–14.
- 56 M. Lan, B. Zhang, H. Cheng, X. Li, Q. Wu, Z. Ying, Y. Zhu, Y. Li, X. Meng and F. Zhao, *Mol. Catal.*, 2017, **432**, 23–30.
- 57 Y. Pei, Z. Qi, T. W. Goh, L. L. Wang, R. V. Maligal-Ganesh, H. L. MacMurdo, S. Zhang, C. Xiao, X. Li, F. (Feng) Tao, D. D. Johnson and W. Huang, *J. Catal.*, 2017, **356**, 307–314.
- 58 Y. Shu, H. C. Chan, L. Xie, Z. Shi, Y. Tang and Q. Gao, *ChemCatChem*, 2017, **9**, 4199–4205.
- 59 T. Lu, J. Lin, X. Liu, X. Wang and T. Zhang, *Langmuir*, 2016, **32**, 2771–2779.

- 60 H. Wei, X. Wei, X. Yang, G. Yin, A. Wang, X. Liu, Y. Huang and T. Zhang, *Cuihua Xuebao/Chinese J. Catal.*, 2015, **36**, 160–167.
- 61 N. Yamanaka, T. Hara, N. Ichikuni and S. Shimazu, *Chem. Lett.*, 2018, **47**, 971–974.
- 62 L. Zhang, H. Su, M. Sun, Y. Wang, W. Wu, T. Yu and J. Zeng, *Nano Res.*, 2015, **8**, 2415–2430.
- 63 W. Wu, S. Zhao, Y. E. Cui, W. Chen, Y. Liu, H. Wang, J. Li, Z. Li and J. Zeng, *ChemCatChem*, 2019, **11**, 2793–2798.
- 64 H. Wei, Y. Ren, A. Wang, X. Liu, X. Liu, L. Zhang, S. Miao, L. Li, J. Liu, J. Wang, G. Wang, D. Su and T. Zhang, *Chem. Sci.*, 2017, **8**, 5126–5131.
- 65 Y. Peng, Z. Geng, S. Zhao, L. Wang, H. Li, X. Wang, X. Zheng, J. Zhu, Z. Li, R. Si and J. Zeng, *Nano Lett.*, 2018, **18**, 3785–3791.
- 66 Y. Tan, X. Y. Liu, L. Li, L. Kang, A. Wang and T. Zhang, *J. Catal.*, 2018, **364**, 174–182.
- 67 K. ichi Shimizu, Y. Miyamoto and A. Satsuma, *J. Catal.*, 2010, **270**, 86–94.
- 68 C. Berguerand, A. Yarulin, F. Cárdenas-Lizana, J. Wärnå, E. Sulman, D. Y. Murzin and L. Kiwi-Minsker, *Ind. Eng. Chem. Res.*, 2015, **54**, 8659–8669.
- 69 J. M. Campos-Martin, G. Blanco-Brieva and J. L. G. Fierro, *Angew. Chemie - Int. Ed.*, 2006, **45**, 6962–6984.
- 70 Y. Yi, L. Wang, G. Li and H. Guo, *Catal. Sci. Technol.*, 2016, **6**, 1593–1610.
- 71 R. J. Lewis and G. J. Hutchings, *ChemCatChem*, 2019, **11**, 298–308.
- 72 J. K. Edwards, A. Thomas, B. E. Solsona, P. Landon, A. F. Carley and G. J. Hutchings, *Catal. Today*, 2007, **122**, 397–402.
- 73 B. E. Solsona, J. K. Edwards, P. Landon, A. F. Carley, A. Herzing, C. J. Kiely and G. J. Hutchings, *Chem. Mater.*, 2006, **18**, 2689–2695.
- 74 J. K. Edwards, B. Solsona, E. N. N, A. F. Carley, A. a Herzing, C. J. Kiely and G. J. Hutchings, *Science (80-.)*, 2009, **323**, 1037–1041.
- 75 R. Burch and P. R. Ellis, *Appl. Catal. B Environ.*, 2003, **42**, 203–211.
- 76 J. M. Campos-Martin, G. Blanco-Brieva and J. L. G. Fierro, *Angew. Chemie - Int. Ed.*, 2006, **45**, 6962–6984.
- 77 H. M. Riedl and G. Pfeleiderer, I. G. Farbenindustrie AG, 1939.
- 78 C. W. Jones, in *Applications of Hydrogen Peroxide and Derivatives*, eds. J. H. Clark and M. J. Braithwaite, RSC, 1999, pp. 1–34.
- 79 Y. Hou, Y. Wang, F. He, S. Han, Z. Mi, W. Wu and E. Min, *Mater. Lett.*, 2004, **58**, 1267–

- 1271.
- 80 R. E. Albers, M. Nyström, M. Siverström, A. Sellin, A. C. Dellve, U. Andersson, W. Herrmann and T. Berglin, *Catal. Today*, 2001, **69**, 247–252.
- 81 R. A. Sheldon, *Metal-Catalyzed Oxidations of Organic Compounds*, Academic Press, 1981.
- 82 C. R. Harris, US2479111, *United States Pat. Off.*, 1945.
- 83 D. W. Leyshon, R. J. Jones, R. N. Cochran (ARCO Chemical Technology), US5254326, 1993.
- 84 P. C. Foller and R. T. Bombard, *J. Appl. Electrochem.*, 1995, **25**, 613–627.
- 85 H. Henkel, W. Weber, (Henkel AG and Co KGaA), US 1108752, *Specif. Lett. Pat.*, 1914.
- 86 J. K. Edwards, A. F. Carley, A. A. Herzing, C. J. Kiely and G. J. Hutchings, *Faraday Discuss.*, 2008, **138**, 225–239.
- 87 J. K. Edwards, A. Thomas, A. F. Carley, A. A. Herzing, C. J. Kiely and G. J. Hutchings, *Green Chem.*, 2008, **10**, 388–39.
- 88 J. K. Edwards, S. J. Freakley, R. J. Lewis, J. C. Pritchard and G. J. Hutchings, *Catal. Today*, 2015, **248**, 3–9.
- 89 R. Todorovic and R. J. Meyer, *Catal. Today*, 2011, **160**, 242–248.
- 90 D. C. Ford, A. U. Nilekar, Y. Xu and M. Mavrikakis, *Surf. Sci.*, 2010, **604**, 1565–1575.
- 91 Y. Voloshin, R. Halder and A. Lawal, *Catal. Today*, 2007, **125**, 40–47.
- 92 N. M. Wilson and D. W. Flaherty, *J. Am. Chem. Soc.*, 2016, **138**, 574–586.
- 93 A. Staykov, T. Kamachi, T. Ishihara and K. Yoshizawa, *J. Phys. Chem. C*, 2008, **112**, 19501–19505.
- 94 H. C. Ham, J. A. Stephens, G. S. Hwang, J. Han, S. W. Nam and T. H. Lim, *Catal. Today*, 2011, **165**, 138–144.
- 95 J. Li and K. Yoshizawa, *Catal. Today*, 2015, **248**, 142–148.
- 96 I. T. Horváth, *Acc. Chem. Res.*, 1998, **31**, 641–650.
- 97 N. C. Patel, V. Abovsky and S. Watanasiri, *Fluid Phase Equilib.*, 2001, **185**, 397–405.
- 98 G. H. Graaf, H. J. Smit, E. J. Stamhuis and A. A. C. M. Beenackers, *J. Chem. Eng. Data*, 1992, **37**, 146–158.
- 99 V. V. Krishnan, A. G. Dokoutchaev and M. E. Thompson, *J. Catal.*, 2000, **196**, 366–374.
- 100 F. Solymosi, A. Erdöhelyi and M. Lancz, *J. Catal.*, 1985, **95**, 567–577.

- 101 A. Erdöhelyi, M. Pásztor and F. Solymosi, *J. Catal.*, 1986, **98**, 166–177.
- 102 Q. He, P. J. Miedziak, L. Kesavan, N. Dimitratos, M. Sankar, J. A. Lopez-Sanchez, M. M. Forde, J. K. Edwards, D. W. Knight, S. H. Taylor, C. J. Kiely and G. J. Hutchings, *Faraday Discuss.*, 2013, **162**, 365–378.
- 103 G. C. Bond and P. A. Sermon, *Gold Bull.*, 1973, **6**, 102–105.
- 104 E. Marceau, X. Carrier, M. Che, O. Clause and C. Marcilly, in *Handbook of Heterogeneous Catalysis*, eds. G. Ertl, H. Knozinger, F. Schuth and J. Weitkamp, Wiley-VCH Verlag GmbH & Co. KGaA., 2018.
- 105 B. A. T. Mehrabadi, S. Eskandari, U. Khan, R. D. White and J. R. Regalbuto, *A Review of Preparation Methods for Supported Metal Catalysts*, Elsevier Inc., 1st edn., 2017, vol. 61.
- 106 S. Cattaneo, PhD thesis, Cardiff University, 2018.
- 107 J. A. Moulijn, P. W. N. M. van Leeuwen and R. A. van Santen, Eds., in *Studies in Surface Science and Catalysis*, Elsevier, 1993, vol. 79, pp. 335–360.
- 108 J. K. Edwards, J. Pritchard, L. Lu, M. Piccinini, G. Shaw, A. F. Carley, D. J. Morgan, C. J. Kiely and G. J. Hutchings, *Angew. Chemie - Int. Ed.*, 2014, **53**, 2381–2384.
- 109 M. Sankar, Q. He, M. Morad, J. Pritchard, S. J. Freakley, J. K. Edwards, S. H. Taylor, D. J. Morgan, A. F. Carley, D. W. Knight, C. J. Kiely and G. J. Hutchings, *ACS Nano*, 2012, **6**, 6600–6613.
- 110 I. Gandarias, P. J. Miedziak, E. Nowicka, M. Douthwaite, D. J. Morgan, G. J. Hutchings and S. H. Taylor, *ChemSusChem*, 2015, **8**, 473–480.
- 111 A. Villa, D. Wang, C. E. Chan-Thaw, S. Campisi, G. M. Veith and L. Prati, *Catal. Sci. Technol.*, 2016, **6**, 598–601.
- 112 R. C. Tiruvalam, J. C. Pritchard, N. Dimitratos, J. A. Lopez-Sanchez, J. K. Edwards, A. F. Carley, G. J. Hutchings and C. J. Kiely, *Faraday Discuss.*, 2011, **152**, 63.
- 113 E. N. Ntainjua, J. K. Edwards, A. F. Carley, J. A. Lopez-Sanchez, J. A. Moulijn, A. A. Herzing, C. J. Kiely and G. J. Hutchings, *Green Chem.*, 2008, **10**, 1162–1169.
- 114 J. K. Edwards, S. F. Parker, J. Pritchard, M. Piccinini, S. J. Freakley, Q. He, A. F. Carley, C. J. Kiely and G. J. Hutchings, *Catal. Sci. Technol.*, 2013, **3**, 812–818.
- 115 J. C. Pritchard, Q. He, E. N. Ntainjua, M. Piccinini, J. K. Edwards, A. A. Herzing, A. F. Carley, J. A. Moulijn, C. J. Kiely and G. J. Hutchings, *Green Chem.*, 2010, **12**, 915–92.
- 116 P. Landon, P. Collier, A. Papworth, C. Kieley and G. J. Hutchings, *ChemComm*, 2002, 2058–2029.

- 117 J. K. Edwards, J. Pritchard, M. Piccinini, G. Shaw, Q. He, A. F. Carley, C. J. Kiely and G. J. Hutchings, *J. Catal.*, 2012, **292**, 227–238.
- 118 N. M. Wilson, J. Schröder, P. Priyadarshini, D. T. Bregante, S. Kunz and D. W. Flaherty, *J. Catal.*, 2018, **368**, 261–274.
- 119 C. M. Crombie, R. J. Lewis, R. L. Taylor, D. J. Morgan, T. E. Davies, A. Folli, D. M. Murphy, J. K. Edwards, J. Qi, H. Jiang, C. J. Kiely, X. Liu, M. S. Skjøth-Rasmussen and G. J. Hutchings, *ACS Catal.*, 2021, **11**, 2701–2714.
- 120 A. Santos, R. J. Lewis, D. J. Morgan, T. E. Davies, E. Hampton, P. Gaskin and G. J. Hutchings, *Catal. Sci. Technol.*, 2021, **11**, 7866–7874.
- 121 A. M. Joshi, W. N. Delgass and K. T. Thomson, *J. Phys. Chem. C*, 2007, **111**, 7841–7844.
- 122 S. Freakley, Q. He, J. Harrhy, L. Lu, D. Crole, D. Morgan, E. Ntainjua, J. Edwards, A. Carley, A. Borisevich, C. Kieley and H. Graham, *Science (80-.)*, 2016, **351**, 965–968.
- 123 F. Li, Q. Shao, M. Hu, Y. Chen and X. Huang, *ACS Catal.*, 2018, **8**, 3418–3423.
- 124 S. Maity and M. Eswaramoorthy, *J. Mater. Chem. A*, 2016, **4**, 3233–3237.
- 125 S. Wang, R. J. Lewis, D. E. Doronkin, D. J. Morgan, J. D. Grunwaldt, G. J. Hutchings and S. Behrens, *Catal. Sci. Technol.*, 2020, **10**, 1925–1932.
- 126 H. Van Nguyen, K. Y. Kim, H. Nam, S. Y. Lee, T. Yu and T. S. Seo, *Lab Chip*, 2020, **20**, 3293–3301.
- 127 J. K. Edwards, J. Pritchard, P. J. Miedziak, M. Piccinini, A. F. Carley, Q. He, C. J. Kiely and G. J. Hutchings, *Catal. Sci. Technol.*, 2014, **4**, 3244–3250.
- 128 X. Gong, R. J. Lewis, S. Zhou, D. J. Morgan, T. E. Davies, X. Liu, C. J. Kiely, B. Zong and G. J. Hutchings, *Catal. Sci. Technol.*, 2020, **10**, 4635–4644.
- 129 E. N. Ntainjua, S. J. Freakley and G. J. Hutchings, *Top. Catal.*, 2012, **55**, 718–722.

Chapter 2: Experimental

2.1 Reagents

The following is a list of all chemicals and reagents used in the experimental work of this thesis.

Sigma Aldrich

PdCl_2 (99.995 %)

NiCl_2 (anhydrous, powder, 99.99 % trace metals basis)

CuCl_2 (anhydrous, powder, ≥ 99.995 % trace metals basis)

$\text{Zn}(\text{NO}_3)_2 \cdot 6\text{H}_2\text{O}$ (reagent grade, 98 %)

$\text{CoCl}_2 \cdot 6\text{H}_2\text{O}$ (ACS reagent, 98 %)

InCl_3 (99.999 % trace metals basis)

$\text{Ga}(\text{NO}_3)_3 \cdot x\text{H}_2\text{O}$ (crystals and lumps, 99.999 % trace metals basis)

SnCl_2 (anhydrous, powder, ≥ 99.99 % trace metals basis)

PVA (polyvinyl alcohol, MW 9,000-10,000, 80 % hydrolysed)

NaBH_4 (granular, 99.99 % trace metals basis)

3-nitrostyrene (96 %)

3-vinylaniline (contains KOH as inhibitor, 97 %)

3-ethylaniline (98 %)

3-ethylnitrobenzene (95%)

Toluene anhydrous (99.8 %)

ortho-xylene (analytical standard)

H_2O_2 (50 wt. % in H_2O , stabilised)

$\text{Ce}(\text{SO}_4)_2$ (39.6 - 44.7 % Ce)

D₂O (99 atom % D)

Formic acid (ACS reagent, ≥ 96 %)

Strem Chemicals

H₂AuCl₄·3H₂O (99.9985 %)

Johnson Matthey

H₂PtCl₆·6H₂O (assay 30.21 %)

Alfa Aesar

Zeolite ZSM-5 ammonium (Powder, S.A. 400 m²/g, 30:1 mole ratio SiO₂:Al₂O₃)

Degussa

TiO₂ (P25, Rutile/Anatase: 85:15, 99.9 %, 20 nm)

Fischer Scientific

H₂O (HPLC grade)

MeOH (HPLC grade)

HCl (37 %, Certified AR for Analysis, d=1.18)

H₂SO₄ (98 %)

BOC

5 % H₂/CO₂ (5 % balance)

25 % O₂/CO₂ (25 % balance)

2.2 Catalyst Preparation

2.2.1 Wet Impregnation

For 0.5wt% Pt/TiO₂ 1 g:^{1,2} Aqueous metal precursor solution H₂PtCl₆·H₂O (Au = 9.50 mg/mL) was prepared. A 50 mL round-bottom flask was equipped with a magnetic stirrer and filled with distilled water (16 mL minus the precursor volume) and the desired amount of precursor was added. The flask was placed in an oil bath set to 60 °C and stirred. When the solution reached a steady 60 °C the support was added (0.995 g) over 10 minutes, then left to stir for a further 10 minutes. The temperature of the oil bath was increased to 95 °C and left stirring for 16 h (until catalyst was fully dry). The catalyst was then ground into a fine powder using a pestle and mortar. The catalyst then underwent the heat treatments, calcination (flowing air, ramp 10 °C min⁻¹, 450 °C, 4 h) and/or reduction (H₂/Ar, ramp 10 °C min⁻¹, 450 °C, 4h).

2.2.2 Sol-Immobilisation

For 1wt% AuPd/TiO₂ 1 g:¹ Aqueous metal precursor solutions of H₂AuCl₄·3H₂O (Au = 12.25 mg/mL) and PdCl₂ (Pd = 6.00 mg/mL, 0.58 M HCl) were prepared. A beaker was equipped with a magnetic stirrer and filled with distilled water (400 mL per 1 g of catalyst), the solution was stirred, and the desired amount of precursor(s) was added. Polyvinyl alcohol solution (1 wt%) was added (PVA/metal (wt) = 1.2) followed by a freshly prepared NaBH₄ solution (0.1 M) (NaBH₄/metal (mol/mol) = 5). This produced a red sol for monometallic Au and a dark brown sol for bimetallic AuPd, which was stirred for 30 minutes. TiO₂ P25 support (0.99 g) was added to the solution to immobilise the colloid and the solution was acidified to pH 2 by concentrated sulfuric acid (2-3 drops), vigorous stirring was continued for 1 hour. The mixture was filtered using a Buchner funnel and the catalyst was washed thoroughly with distilled water (1 L) to remove the chloride present from the precursors. The catalyst was dried in a vacuum oven at 30 °C for 16 h and then ground into a fine powder using a pestle and mortar. The catalyst was calcined (static air, ramp 10 °C min⁻¹, 400 °C, 3 h) prior to use.

2.2.3 Excess Chloride Wet Co-Impregnation

This procedure was based on research by Sankar *et al.*²

For 1wt% AuPd/ZSM-5 1 g: Prior to catalyst synthesis NH₄-ZSM-5 (SiO₂:Al₂O₃ = 30:1) was calcined (static air, ramp 20 °C min⁻¹, 550 °C, 3 h) to produce H-ZSM-5. Aqueous metal precursor solutions of HAuCl₄·3H₂O (Au = 12.25 mg/mL) and PdCl₂ (Pd = 6.00 mg/mL, 0.58 M HCl) were prepared. A 50 mL round-bottom flask was equipped with a magnetic stirrer and filled with distilled water (16 mL minus precursor volumes) and the desired amount of precursors were added. The flask was placed in an oil bath set to 60 °C and stirred. When the solution reached a steady 60 °C the support was added (0.99 g) over 10 minutes, then left to stir for a further 10 minutes. The temperature of the oil bath was increased to 95 °C and left stirring for 16 h (until catalyst was fully dry). The catalyst was then ground into a fine powder using a pestle and mortar. The catalyst then underwent reductive heat treatment (H₂/Ar, ramp 10 °C min⁻¹, 400 °C, 4h) prior to use.

2.2.4 Catalyst Precursors

Table 2.1: Metal precursors and corresponding metal concentrations used in catalyst preparation.

| Precursor | Metal Concentration (mg/mL) |
|--|-----------------------------|
| HAuCl ₄ ·3H ₂ O | 12.25 |
| PdCl ₂ (0.58 M HCl) | 6.00 |
| H ₂ PtCl ₆ ·6H ₂ O | 9.50 |
| NiCl ₂ | 2.18 |
| CuCl ₂ | 2.36 |
| Zn(NO ₃) ₂ ·6H ₂ O | 5.43 |
| CoCl ₂ ·6H ₂ O | 5.10 |
| InCl ₃ | 5.11 |
| Ga(NO ₃) ₃ ·xH ₂ O | 5.50 |
| SnCl ₂ | 4.84 |

2.3 Catalyst Testing

2.3.1 3-Nitrostyrene Hydrogenation

The liquid phase chemoselective hydrogenation of 3-nitrostyrene³ was performed in a 50 ml round-bottomed glass Colaver flask. 3-Nitrostyrene (0.2 mL), toluene (8 mL) and catalyst (0.05 g) were charged to the reactor and purged with N₂ to remove air contamination. The reactor was placed into an oil bath, ensuring all reactants were below the oil level, and heated to 40 °C. The Colaver flask was purged with H₂ (0.3 MPa) 3 times while stirring (800 rpm). The reaction was then started under the conditions P(H₂) = 0.3 MPa, 40 °C. After a pre-determined reaction time, the reactor was cooled to < 5 °C in an ice bath, after which the reaction mixture was filtered to remove the catalyst. Gas chromatography analysis (Varian 450-GC gas chromatograph equipped with a HP-5 boiling-point column, a flame ionisation detector and a CP8400 autosampler) was performed on the final reaction solution (1 mL) and *o*-xylene (0.1 mL) was added as an external standard. Conversion of the substrate and product selectivity were calculated using suitable GC calibration plots and response factors using Equations 2.1-2.6.

$$\text{Normalised GC Peak Area}_{3-NS} = \frac{\text{Peak area}_{3-NS}}{\text{Peak Area}_{o\text{-xylene}}} \quad (2.1)$$

$$\text{moles}_{3-NS} (\text{mol}) = \frac{\text{Normalised GC Area}_{3-NS} \times \text{moles}_{o\text{-xylene}}}{\text{Calibration factor}} \quad (2.2)$$

$$\text{Conversion}_{3-NS} (\%) = \frac{\text{Initial moles}_{3-NS} - \text{moles}_{3-NS}}{\text{Initial moles}_{3-NS}} \times 100 \quad (2.3)$$

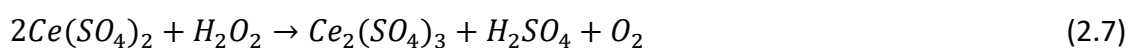
$$\text{Selectivity}_{3-VA} (\%) = \frac{\text{moles}_{3-VA}}{\text{Initial moles}_{3-NS} - \text{moles}_{3-NS}} \times 100 \quad (2.4)$$

$$\text{Initial Rate} (\text{mol}_{3-NS} \text{ kg}^{-1} \text{ min}^{-1}) = \frac{\text{moles}_{3-NS}}{\text{mass}_{\text{catalyst}}(\text{kg}) \times \text{time}(\text{min})} \quad (2.5)$$

$$\text{Turnover Frequency} (\text{h}^{-1}) = \frac{\text{moles}_{3-NS}}{\text{moles}_{Pt} \times \text{time} (\text{h})} \quad (2.6)$$

2.3.2 Direct Hydrogen Peroxide Synthesis

Direct hydrogen peroxide synthesis^{4,5} was evaluated using a Parr Instruments stainless steel autoclave with a nominal volume of 100 ml and a maximum working pressure of 14 MPa. Supported catalyst (0.01 g), and solvents HPLC grade water (2.9 g) and methanol (5.6 g) were charged to a 100 mL glass liner. The liner was fitted into an autoclave and purged with 5% H₂/CO₂ (0.7 MPa) 3 times. The reaction was run under the test conditions: 0.5 h, 2°C, P(5% H₂/CO₂) = 2.9 MPa P(25% O₂/CO₂) = 1.1 MPa, 1200 rpm. The aforementioned reaction parameters represent the optimum conditions and solvents that we have previously used for the synthesis of H₂O₂ with a higher solubility of H₂ in MeOH compared to H₂O being a key factor in achieving enhanced yields of H₂O₂. The end reaction solution was filtered and then assayed by acidified Ce⁴⁺ (aq) (0.01 M) titration in the presence of ferroin indicator to calculate hydrogen peroxide concentration. Catalyst productivities are reported as mol_{H₂O₂} kg_{cat}⁻¹ h⁻¹. A gas bag was collected from the end gas mixture and analysed by gas chromatography (Agilent CP7658 system fitted with an Agilent CP-Wax 52CB column) to determine hydrogen conversion and the hydrogen selectivity towards hydrogen peroxide (an initial gas bag was also taken at 2 °C from a charged and pressurised liner). Equation 2.7-2.12 were used to give the results in this work.



$$Moles_{H_2O_2}(mol) = \frac{Moles_{Ce(SO_4)_2}(mol)}{2} \quad (2.8)$$

$$Productivity (mol_{H_2O_2} kg_{cat}^{-1} h^{-1}) = \frac{Moles_{H_2O_2}(mol)}{Catalyst\ Mass\ (kg) \times Reaction\ Time\ (h)} \quad (2.9)$$

$$H_2O_2\ (wt\%) = \frac{Moles_{H_2O_2}(mol) \times Molecular\ Mass_{H_2O_2}(g\ mol^{-1})}{Mass_{solvent}\ (g)} \times 100 \quad (2.10)$$

$$H_2\ Conversion\ (\%) = \frac{mmol_{H_2}(t_0) - mmol_{H_2}(t_1)}{(mmol_{H_2}(t_0))} \times 100 \quad (2.11)$$

$$H_2O_2\ Selectivity\ (\%) = \frac{moles_{H_2O_2}\ produced\ (mmol)}{moles_{H_2}\ consumed\ (mmol)} \times 100 \quad (2.12)$$

2.3.3 Time-on-Line Experiments for the Direct Hydrogen Peroxide Synthesis

For time-on-line experiments, the synthesis reaction protocol was followed for various reaction times (0.08, 0.17, 0.25, 0.5 and 1 h). Initial rates were calculated from 0.08 – 0.17 h reaction time data points as concentration Vs. time was linear.

2.3.4 Gas Replacement Experiments for the Direct Synthesis of H₂O₂

For top-up experiments, the synthesis reaction protocol was followed, with the exception that for each consecutive 0.5 h reaction, gases were vented and replenished. (Reaction times 0.5, 1, 1.5, 2, 2.5 h).

2.3.5 Catalyst Reusability in the Direct Synthesis and Degradation of H₂O₂

For reuse reactions, the synthesis reaction protocol was followed, with the exception that up to 0.1 g of catalyst was added, then filtered and dried under vacuum (30 °C, 16 h). Then retested for hydrogen peroxide synthesis under the above protocol for 0.08 and 0.5 h, or for hydrogen peroxide degradation (see below).

2.3.6 Hydrogen Peroxide Degradation

Hydrogen peroxide degradation (H₂O₂ hydrogenation and decomposition pathways) was evaluated using a Parr Instruments stainless steel autoclave with a nominal volume of 100 ml and a maximum working pressure of 14 MPa. Hydrogen peroxide (0.68 g, 50 wt%), HPLC grade water (2.22 g) and methanol (5.6 g) were charged to a 100 mL glass liner. A small aliquot of initial reaction solution was assayed by acidified Ce⁴⁺ (aq) (0.01 M) titration in the presence of ferroin indicator to calculate initial hydrogen peroxide concentration (4 wt% H₂O₂). Supported catalyst (0.01 g) was then added to the reaction mixture. The liner was fitted into an autoclave and purged with 5% H₂/CO₂ (0.7 Mpa) 3 times. The reaction was run under the test conditions: 0.5 h, 2 °C, P(5% H₂/CO₂) = 2.9 Mpa, 1200 rpm. The end reaction solution was filtered and then assayed by acidified Ce⁴⁺ (aq) (0.01 M) titration in the presence of ferroin indicator to calculate final hydrogen peroxide concentration. Catalyst degradation is reported as activities ($\text{mol}_{\text{H}_2\text{O}_2} \text{kg}_{\text{cat}}^{-1} \text{h}^{-1}$) and wt% H₂O₂.

2.4 Characterisation Techniques

2.4.1 GC (Gas Chromatography)

There are two types of gas chromatography, these are gas-liquid, and gas-solid, however gas-liquid chromatography is predominantly used and as such will be discussed further.⁶ A liquid sample is injected and vapourised (alternatively a gas bag can be injected if the analyte is a gaseous mixture, no vaporisation is therefore required). For liquid injections an oxygen trap is utilised to remove any oxygen present before heating, to prevent oxidation from occurring.⁷ The gaseous sample flows through the column by the inert carrier gas (mobile phase) and the separation of the analytes is dependent on the interaction with the stationary phase that coats the inside of the GC column. By adjusting the temperature (and ramp time) in the column (in the oven), the analytes can be separated more efficiently. The effluent exiting the column is then analysed by the detector.⁸⁻¹⁰ Figure 2.1 shows the schematic of a GC.

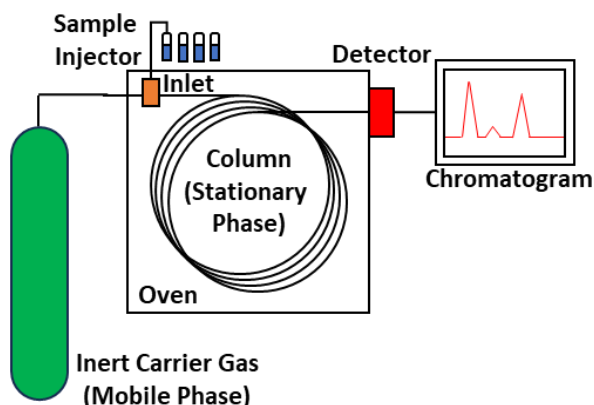


Figure 2.1: Gas Chromatography (GC) schematic.

It is important to consider how each part of the instrument will affect the analysis. When the liquid sample is injected and vaporised, it is important that the entire injected sample undergoes vaporisation so that the proportion of compounds remains the same as in the original solution, and that there is no decomposition of any compounds (analytes) in this process.⁸⁻¹⁰

The mobile phase is an inert gas that pushes the vapourised sample through the column. Typical choices include hydrogen, helium, nitrogen, and argon (Ar) which will be unreactive

under the GC conditions.^{6,8} In this work some of the GC analysis was performed for gaseous H₂, O₂ and CO₂ mixtures, so the mobile phase could be either He or Ar.

With regards to the column, a packed column is 1-5 m long with an internal diameter (i.d.) of 1-5 mm, (or micro-packed columns i.d. < 1 mm). The column is filled with spherical particles coated in a liquid or elastomeric (polymer) stationary phase. The resolution produced from this system is limited due to the column length. Comparatively, capillary columns can be as long as 100 m. In capillary columns the stationary phase can be deposited as a thin film coating the inner wall, this is called wall-coated open tubular, or the stationary phase can be impregnated into a porous layer on the inner wall, known as support-coated open tubular. The advantages of these over packed columns are increased separation and resolution, and that lower temperatures are required. One consideration is that the thinner capillary column must not be overloaded as this would result in peak broadening and poor separation.⁹

There are a variety of detectors that can be used in conjunction with a GC, however in this work an FID (flame ionisation detector) was used for the detection of organic compounds such as 3-nitrostyrene, and a TCD (thermal conductivity detector) was used to detect gases including H₂, O₂ and CO₂.

In an FID a hydrogen flame is used to pyrolyse organic (carbon containing) molecules, generating ions and electrons that produces a current dependent upon the volume of effluent per unit time.^{6,8,9} This current is measured on a pico-ammeter and has a very low detection limit (only a couple of picograms per second) of effluent.⁸ The response is proportional to the number of reduced carbons and therefore the sensitivity of this technique is referred to as mass rather than concentration. This detector is obviously not compatible for detecting compounds with no (or very few) carbon atoms. As this is a destructive detector (the effluent is destroyed) it cannot be used in conjunction with other detection methods.⁹

A TCD compares the thermal conductivity of the sample flow (in a carrier gas), to a reference of the pure carrier gas.⁶ Therefore, it is important that the thermal conductivity of the carrier gas is different to that of the analytes in the sample. Both helium and hydrogen have high thermal conductivities (six to ten times greater compared to many organic compounds), and therefore any changes in the effluent will be more noticeable due to a large change in thermal conductivity, whereas nitrogen and argon have similar thermal conductivities to organic

compounds and will therefore be less sensitive.⁶ The set-up of a TCD often uses two detectors, with a Wheatstone bridge circuit.¹⁰ The sample gas (in carrier gas) flows over one arm, and the pure carrier gas flows over another. The different signals from the two created an out-of-balance signal which is then detected. TCD is a non-destructive detector and can therefore be combined with other detectors and can be used for inorganic compounds in addition to organic compounds unlike the FID.^{6,9}

Instrument Specification

For the analysis of the 3-nitrostyrene hydrogenation reaction solution a Varian 450-GC gas chromatograph equipped with a HP-5 boiling-point column, a flame ionisation detector and a CP8400 autosampler was utilised.³

For the analysis of H₂O₂ synthesis gas composition a Varian 3800 GC fitted with TCD and equipped with a Porapak Q column was utilised.

2.4.2 UV-Vis (Ultraviolet-Visible Spectroscopy)

UV-Vis spectroscopy is an analytical tool that measures the amount of UV and visible light absorbed by a sample, this can be used to identify the concentration of a known material in an aqueous sample. The scheme for an UV-Vis spectrophotometer is shown in Figure 2.2.

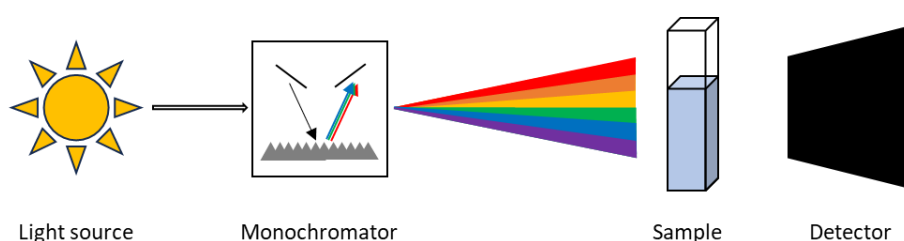


Figure 2.2: UV-vis spectrometer schematic.¹¹

The light source must maintain a constant intensity for the range of wavelengths, a deuterium arc lamp provides a good, constant intensity in the UV region (to 185 nm) and useful intensity for the visible spectrum. Comparatively, the tungsten-halogen lamp gives a good intensity for the entire visible range but just the higher wavelengths in the UV spectrum (350 – 3000 nm).

The xenon flash lamp is more commonly used with a range of 185 – 2500 nm. This lamp is more efficient and longer lasting than the other two as it only emits light during the sample measurement, this also has benefits such as light-sensitive solutions will not experience photobleaching. Additionally, this lamp does not require warm up time like the previous two.¹¹

The monochromator separates white light with a diffraction grating into its constituent wavelengths *e.g.* red (650 nm) and violet (380 nm) and using rotation in the mechanism each wavelength can be passed through the sample individually. The intensity (*I*) of the beam detected with the original intensity (*I*₀) then gives a measured absorbance. To increase accuracy two monochromators can be used in conjunction, reducing stray light and increasing spectral accuracy.¹¹

It is important to consider the material of the cuvette used as this will affect readings at various absorbances. When choosing a cuvette, it must be considered at what absorbance the sample will require to take measurements and a material with a suitable range can be selected. Table 2.2 shows the wavelength range for common cuvette materials. A UV quartz cuvette has been used for all UV-vis measurements in this thesis. Another consideration is solvent, the chosen solvent must have an absorbance different to that of the sample.¹¹

Table 2.2: Common cuvette materials and corresponding wavelength range¹¹

| Cuvette Material | Operational Wavelength Range / nm |
|-------------------------|--|
| Plastic (Polystyrene) | 340 – 800 |
| Optical Glass | 334 - 2500 |
| UV Quartz | 170 - 2700 |
| NIR Quartz | 220 - 3800 |

The Beer-Lambert Law states that the amount of light absorbed by the sample is proportional to the number of absorbing molecules in the sample which the light passes through. However, there is a limitation to the Beer-Lambert Law where samples that are too concentrated do not linearly correlate with the absorptivity due to electrostatic interactions between the

molecules in close proximity. Therefore, the calibration must extend beyond the most concentrated sample to analysis to ensure the correlation is still linear.¹¹ The Beer-Lambert Law is given in Equation 2.13.

$$A = \epsilon cl = \log\left(\frac{I_0}{I}\right) \quad (2.13)$$

Where A = Absorption

ϵ = Molar absorption co-efficient / L mol⁻¹ cm⁻¹

c = Concentration / M

l = Path length /cm (usually 1 cm for standard cuvette)

I₀ = Initial intensity

I = Intensity

UV-vis can be a powerful tool in the analysis gold of nanoparticles as they have a distinct optical feature in that they exhibit a localised surface plasmon resonance (LSPR), whereby the collective oscillation of electrons in the conduction band resonates with a specific wavelength. This results in an absorption band at 500-600nm. The position of this peak is dependant of the size and shape of the gold nanoparticles, with increased particle size, a red-shift is seen (increased wavelength). A red-shift is also seen for unevenly shaped nanoparticles compared to uniform spherical nanoparticles.¹² Figure 2.3 demonstrates how gold nanoparticle size affects absorption wavelength.

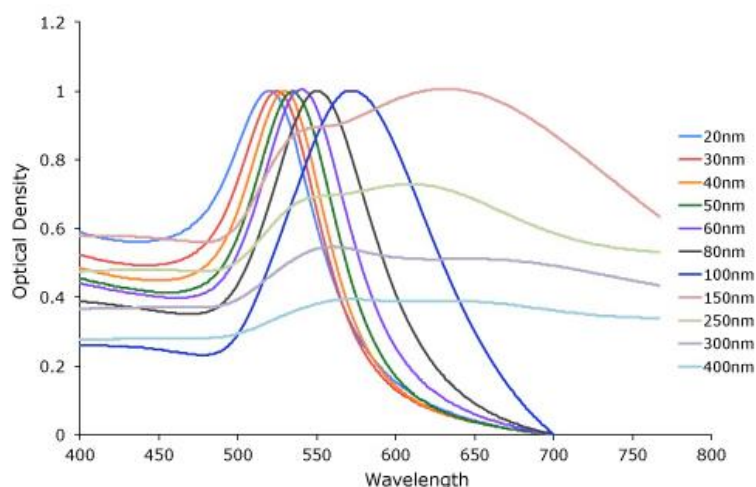


Figure 2.3: Increase in absorption wavelength for increasing Au nanoparticle size.¹²

Instrument Specification

To observe the Au plasmonic peak in colloidal catalyst solutions the as-prepared aqueous sols, contained in a quartz cuvette, were optically characterised using an Agilent Cary 60 UV-vis spectrometer (V-570, JASCO) operating over the 200 to 800 nm wavelength range.⁵

2.4.3 FT-IR (Fourier Transform Infra-Red Spectroscopy)

In an FTIR spectrometer IR radiation is emitted from a source (such as mid-IR and tungsten-halogen lamps) and passes through an aperture. The IR beam is directed at a beam splitter which has the ability to both transmit and reflect the IR. Mirrors are used to focus and collimate the IR radiation and are made from materials with a low coefficient of thermal expansion (e.g. Pyrex), with the front surfaces are coated with a thin film of metal (e.g. Al/Ag/ Au). The beam is directed at the sample and the sample will absorb specific frequencies. When the IR beam reaches the detector, the measurements are recorded. Figure 2.4 shows a schematic of an FT-IR.¹³

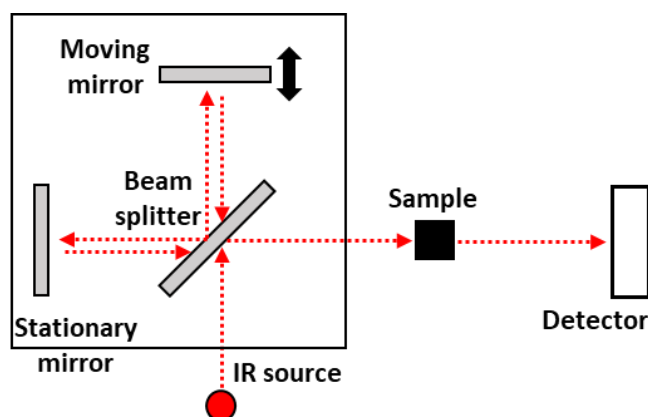


Figure 2.4: FT-IR schematic

There are three main regions in IR spectroscopy, these are near-IR ($400\text{--}10\text{ cm}^{-1}$), mid-IR ($4000\text{--}400\text{ cm}^{-1}$) and far-IR ($14000\text{--}4000\text{ cm}^{-1}$). When a sample is exposed to IR radiation, the chemical bonds absorb it at frequencies that match their vibration modes, this causes the bonds to vibrate at a specific frequency. There are two modes of vibration, which are stretching (the bond between atoms is stretched) and bending (the angle of the bond between the atoms is altered).¹³

There are two types of stretching mode, symmetrical (two atoms move simultaneously to and away from the central atom) and asymmetrical stretching (one atom moves towards the central atom which one moves away). There are four types of bending vibrations, scissoring (both atoms moving away of towards each other in-plane), rocking (both atoms moving clockwise or anticlockwise in-plane), wagging (both atoms move back and form simultaneously out-of-plane), and twisting (one atom moving forward and one backward out-of-plane).¹³ This is demonstrated in Figure 2.5.

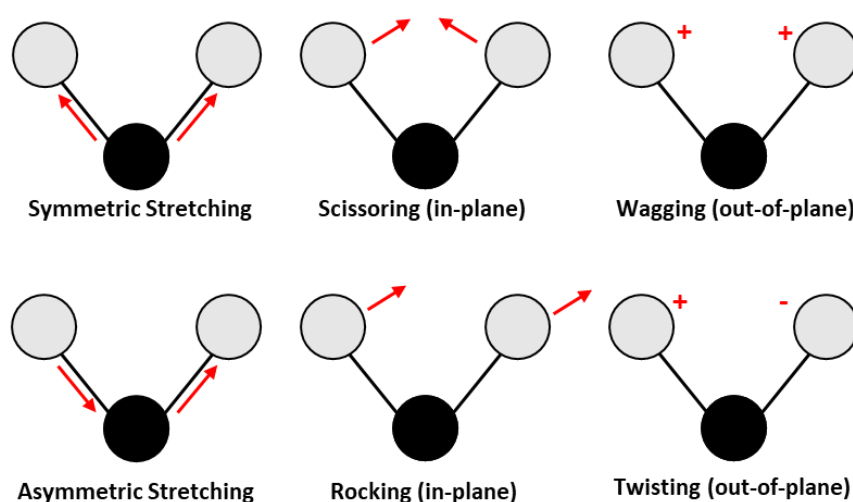


Figure 2.5: Vibrational stretching and bending modes.

Instrument Specification

Performed using a Bruker (Hanau, Germany) Tensor 27 spectrometer fitted with a HgCdTe (MCT) detector, operated with OPUS software (Ettinger, Germany).⁴

2.4.4 CO-DRIFTS (Diffuse Reflectance Infrared Fourier Transform Spectroscopy)

DRIFTS is applied to powders as the technique requires scattering of radiation within the sample. The sample is packed inside a chamber with two IR transparent windows. IR radiation is directed onto the sample and the IR radiation that has been reflected by diffuse scattering (from the sample) is detected. If an incident beam on the sample results in only a single reflection from the surface this is known as specular reflectance spectroscopy (SRS). However, DRIFTS measurements rely on a combination of internal and external reflections, giving diffusely scattered light over a wide area. Collection optics in DRIFTS are designed to only

collect the diffuse reflected radiation. Factors affecting the DRIFTS spectrum include refractive index (of the sample), particle size and size distribution, packing density, and sample homogeneity.^{14,15} A schematic for CO-DRIFTS is given in Figure 2.6.

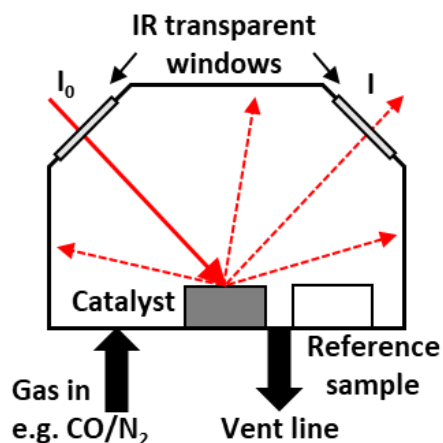


Figure 2.6: CO-DRIFTS schematic.

In this thesis, CO was passed over the sample so it could be adsorbed onto the metal catalyst until saturation was reached. The different adsorption bands of the CO onto the metal (in this case Pt and Pd) were analysed by the IR. Absorption bands corresponding to bridging CO and linear CO amongst others were found and these correspond with the metal environments of the catalyst surface.

Instrument Specification

Measurements were conducted on a Bruker Tensor 27 spectrometer combined with a mercury telluride (MCT) detector. Samples were loaded into the Praying Mantis high temperature (HVC-DRP-4) in-situ cell before exposure to N₂ and then 20% CO/Ar (or 5% CO/N₂) at a flow rate of 50 cm³ min⁻¹. A background spectrum using KBr was obtained prior to loading with the desired analyte, with measurement recorded every 1 minute at room temperature. Once the size of CO adsorption bands in the DRIFTS spectra were consistent, the gas flow was replaced to N₂, and measurement was repeated until no change in subsequent spectra was observed.³⁻⁵

2.4.5 Chemisorption

Selective gas chemisorption is a technique whereby a catalyst (of known mass and metal loading) is exposed to a known quantity of probe molecules, and from these assumptions can be made to give information such as number of surface atoms/ active sites, metal dispersion, and (surface weighted) average particle size.¹⁶

In this thesis a pulse-flow method was adopted and shown schematically in Figure 2.7. A catalyst sample (mass recorded) is fixed in a quartz U-tube between quartz wool. A reductive pretreatment must be performed as metal nanoparticles that are exposed to air often have a thin oxide layer. This involved heating the sample under reductive conditions (e.g. flowing H_2/Ar), the length of time and temperature of the reduction will be dependant of sample size, metal loading and metal type.

For the actual chemisorption measurements, the temperature should remain constant, therefore a set temperature (e.g. 30 °C) should be selected. The pulse-flow method involves injecting a known quantity of a probe gas (in an inert carrier gas of differing thermal conductivity e.g. He) to flow over the sample (e.g. catalyst) until the surface is saturated. By injecting small quantities of the adsorbate, it will take multiple injections until saturation is complete but over time (with more pulses) less gas will be adsorbed and more will reach the detector. The detector will record a constant value once saturation has been achieved (see Figure 2.7). A few more injections are done once saturation is achieved to provide a calibration.

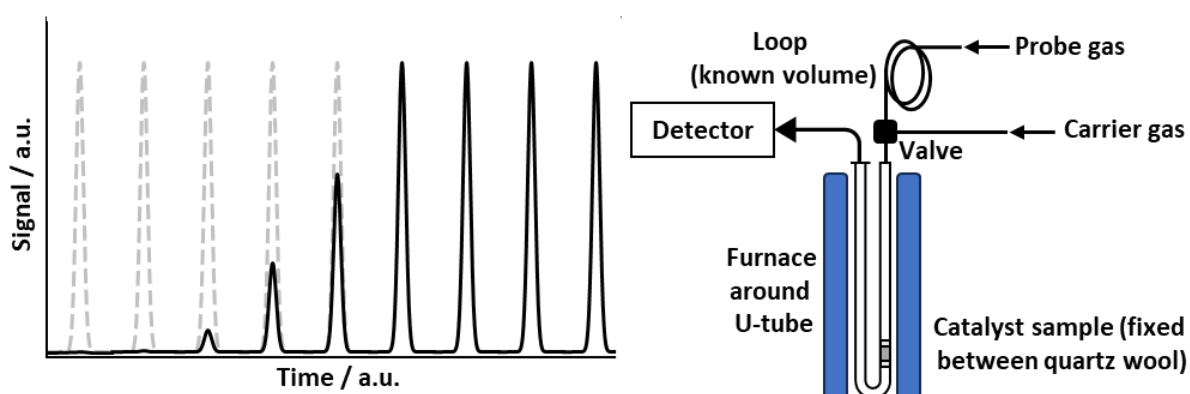


Figure 2.7: (Left) example chemisorption measurements as detected (Right) chemisorption schematic.

There are various adsorbate gases that can be utilised for chemisorption experiments including H₂, CO, and O₂,¹⁷⁻¹⁹ with CO being the selected adsorbate for this thesis. When considering the adsorption of the adsorbate gas onto a metal, stoichiometry issues must be considered. For CO the adsorption can be associative, resulting in linear (CO/M = 1), bridged (CO/M = 2), capped (CO/M = 3) or dissociative (CO/M = 2) forms. For numerous metals a CO/M value of 1–2 is typically assumed. For metals such as Pt, Ir and Rh it is assumed CO/M = 1 and for metals such as Pd and Ni it is assumed CO/M = 2.²⁰⁻²⁴

Using the stoichiometric assumptions fraction exposed/ dispersion (D) of the metal nanoparticles can be calculated using Equation 2.14:²⁵

$$D = \frac{N_{ms}}{N_{mt}} = \frac{N_{aa}}{f N_{mt}} \quad (2.14)$$

Where N_{ms} = total surface metal atoms

N_{mt} = total metal atoms

N_{aa} = number of molecules adsorbed

f = stoichiometry factor

From the calculation of dispersion, the specific surface area (S_{sp}) of the metal nanoparticles can be calculated using Equation 2.15:²⁵

$$S_{sp} = a_m \left(\frac{N_A}{Mw} \right) D \quad (2.15)$$

Where a_m = surface per unit area

N_A = Avogadro's number

Mw = molecular weight (of metal)

The value of a_m for Pt is assumed to equal 8.07 Å² based on and fcc unit cell with equal amounts of (111), (110) and (100) planes.²⁵ Assumptions of uniform monolayer coverage and hemi-spherical particles are made for these calculations.

Instrument Specification

Quantachrome Instruments ChemBET Pulsar TPR /TPD Chemisorption Analyser equipped with a (thermal conductivity detector) TCD. Pt/TiO₂ catalyst (0.05–0.1 g) was fixed between two pieces of quartz wool in a quartz u-tube. The sample was reduced (flowing 10% H₂/Ar, 150 °C, 0.5 h). The sample was then purged in He for 1 h (or until a stabilised signal was achieved) and the sample was cooled to 30 °C. The analysis was performed with 10% CO/He. Pulses were introduced into the sample cell with a calibrated injection loop at a controlled temperature (30°C) until the detected CO peak area remained constant.³

2.4.6 N₂ Physisorption Isotherms (N₂ adsorption/ desorption Isotherms)

Catalysts supports such as zeolites are porous and have a large surface area, these attributes can be analysed by physisorption techniques. By comparing the catalyst support to the analogous catalyst (*e.g.* with immobilised metal species), it is possible to determine how pore volume and surface area are affected. For example, metal particles can block pores and catalyst heat treatments could also cause changes to the physical structure.

To perform physisorption experiments a sample (of known mass) is degassed (under vacuum and high temperature) to remove any species that are physisorbed on the surface. The sample must be cooled (in liquid nitrogen) to the boiling point of the absorbate (in this case N₂) and an adsorption isotherm is recorded. This is done by volumetrically measuring the amount of probe molecule removed from the gas phase. The adsorption isotherm is measured by increasing volumes the volume of gas until saturation is achieved and then reversing the process for the desorption isotherm. The data collected from the adsorption (and desorption) isotherm be input into the BET equation, displayed as Equation 2.16.²⁶

$$\frac{1}{X[(P_0/P)-1]} = \frac{1}{X_m C} + \frac{C-1}{X_m C} \left(\frac{P}{P_0}\right) \quad (2.16)$$

Where X = mass of N₂ adsorbed (at a given relative pressure)

(P/P₀) = relative pressure

X_m = monolayer capacity

C = BET constant

Instrument Specification

N₂ physisorption isotherms were performed by Dr Richard Lewis.

Performed using a Micromeritics 3-Flex. Samples (approx. 0.070 g) were degassed (350 °C, 9 h) prior to analysis. Analysis was carried out at 77 K, with P₀ measured continuously. Free space was measured post-analysis with He. Data analyses were carried out using the Micromeritics 3-Flex software with the non-local density functional theory (NLDFT), Tarazona model.⁴

2.4.7 TEM and STEM (Transmission Electron Microscopy and Scanning Transmission Electron Microscopy)

Electron microscopes have the ability to produce images of far greater magnification and resolution than light microscopes due to the electron wavelengths being 10000 times shorter than visible light, and if lens aberration is minimised resolution can be in the order of 0.1 nm.²⁷

Figure 2.8 shows the schematics for both a TEM and STEM.²⁸

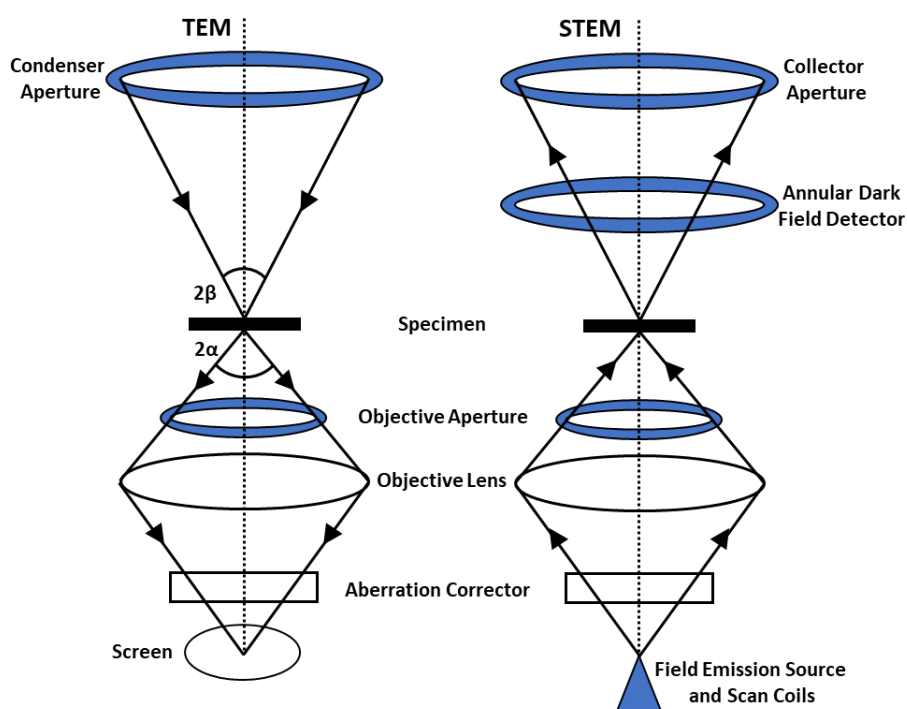


Figure 2.8: TEM and STEM schematics.

The main components of a TEM (Transition Electron Microscope) include an electron source, stacked electromagnetic lenses including, condenser lens, objective and projector lenses, and a specimen stage. The environment inside the TEM is under vacuum, to prevent collisions between electrons and air molecules that would absorb electron.²⁷

In a standard TEM, an electron acceleration voltage of 200 keV is used, higher voltage typically equates to higher resolution. The electron gun is comprised of three parts, a cathode (electron source) a Wehnelt electrode and an anode.²⁷ The electrons are emitted from the cathode and accelerated by the electric field towards the anode. Two types of electron gun include thermionic emission and field emission, with the former method being more common.^{27,29,30} Thermionic emission can be achieved with either a tungsten filament or a lanthanum hexaboride (LaB₆) gun. The tungsten filament (cathode) is heated to approximately 2800 K to release electrons from the surface. Lanthanum hexaboride (LaB₆) is often preferable as the electrons need less kinetic energy to escape the surface, resulting in a lower temperature for the cathode. With a field emission electron gun a high voltage / electric field is applied to a metal surface (e.g. a tungsten crystal) creating a tunnelling effect, which releases electrons from the conducting band of the metal. Field emission generates an electron beam over 100 times more intense than the thermionic emission guns.^{27,30}

The objective aperture in a TEM can be found between the poles of the electromagnetic lens. It is a small hole that limits light scattering. Electromagnetic lenses throughout the TEM are used to focus the electron beam. Firstly, two (or more) condenser lenses demagnify the electron beam emitted from the electron gun, controlling the beam diameter and convergence angles of the incident beam on the sample. An intermediate lens is used to switch the TEM between an image mode (lens is focused on the image plane of the objective lens) and a diffraction mode (lens is focused on the back-focal plane of the objective lens where the diffraction pattern forms). The projector lens is used to again magnify the image (or diffraction pattern) and projects the image onto the fluorescent screen where it can be observed. The aberration correctors are added at the end to correct any aberrations from the objective lens.²⁷

To obtain a TEM image, the sample is bombarded with electrons and the electrons are elastically or inelastically scattered as they interact with the sample. If the transmitted

electrons are imaged this is called dark field imaging and if the scattered electrons are imaged it is called light-field imaging.^{27,31,32}

To generate a high quality image the contrast (difference in brightness between two points) must be good. In TEM imaging, contrast is generated there is a difference in the number of electrons being scattered away from the transmitted beam. Electron scattering can create images by mass-density and diffraction contrast.^{27,30,32,33} Mass-density contrast is caused by increase of scattering due to an increase in atomic number and sample thickness. Diffraction contrast is caused by electron deflection (Bragg's law) and is therefore dependant on crystal structure).²⁷ TEM can also utilise phase difference, known as phase contrast. Here, the interaction of the deflected beams (from the sample) with the transmitted beams, give high-resolution images (HR-TEM) which can be used to determine crystal structure.^{27,30,32,33}

In STEM (Scanning Transmission Electron Spectroscopy) the electron beam is instead focussed (converged) into a small probe and scanned (in a raster pattern) across the sample.³³ In a STEM setup, it is important to note that the aberration corrector is placed before the sample (unlike TEM) to correct aberrations in the objective lens, as the lens is used to for the electron probe.³²

In STEM elastic scattering is the main source of image contrast, with the angle of the electron scattering of importance but not the direction of propagation. Various detectors can be used in a STEM, one of which being a bright-field detector.²⁸ This is a small angle detector (electron scattering > 50 mrad) positioned on the axis and in this imaging holes appear bright. An annular dark field (ADF) detector detects scattered electrons (10-50 mrad). With this detector the signal increases with increasing scattering cross section and increase in specimen thickness. In this imaging holes appear dark. A high-angle annular dark-field (HAADF) detectors detect scattered electron angles > 50 mrad. This detector shows the most contrast due to incoherent scattering.³³ The image contrast given can be interpreted as mass-thickness contrast, also known as (atomic) Z-contrast images, where the contrast is proportional to Z^2 .^{28,32} This is useful when analysing catalysts with small metal particles. For example, heavier elements such as Pt produces a higher number of scattered electrons when compared to Pd and therefore Pt will appear brighter.

Instrument Specification

EM for Pt/TiO₂ catalysts (for the chemoselective reduction of 3-nitrostyrene) were performed by Dr Sultan Althahban, Dr Xiang Gao, Dr Qian He and Prof. Christopher Kiely:

High-Angle Annular Dark-Field Scanning Transmission Electron Microscopy (HAADF-STEM) was performed for Pt/TiO₂ samples: Samples were prepared by dry dispersion of the catalyst powder onto a holey carbon film with a 300 mesh copper TEM grid. Bright-field and HAADF-STEM images were taken using an aberration-corrected JEM-ARM-200CF microscope operating at 200 kV, equipped with a Centurio silicon drift detector for X-ray energy-dispersive spectroscopy (JEOL). The particle size distribution analysis was performed from analysis of HAADF electron micrographs using ImageJ v.1.52i software.³

EM for AuPdX/TiO₂ and AuPdX/ZSM-5 (for direct H₂O₂ synthesis) were performed by Dr Thomas Davies:

Transmission electron microscopy (TEM) was performed on a JEOL JEM-2100 operating at 200 kV. Samples were prepared by dry dispersion of the catalyst powder on 300 mesh copper grids coated with holey carbon film. Energy dispersive X-ray spectroscopy (XEDS) was performed using an Oxford Instruments (Abingdon, UK) X-Max^N 80 detector, and the data analysed used Aztec software.^{4,5}

Aberration Corrected Scanning Transmission Electron Microscopy (AC-STEM) was performed for H₂O₂ catalyst samples: Aberration-corrected scanning transmission electron microscopy (AC-STEM) was performed using a probe-corrected Hitachi HF5000 S/TEM, operating at 200 kV. The instrument was equipped with bright field (BF), high angle annular dark field (HAADF) and secondary electron (SE) detectors for high spatial resolution STEM imaging experiments. This microscope was also equipped with a secondary electron detector and dual Oxford Instruments XEDS detectors (2 × 100 mm²) having a total collection angle of 2.02 sr.^{4,5}

2.4.8 ICP-MS (Inductively Coupled Plasma Mass Spectrometry)

ICP-MS analysis is a technique used to measure and identify elements in a sample matrix by ionisation of the sample. Figure 2.9 shows a schematic for an ICP-MS.

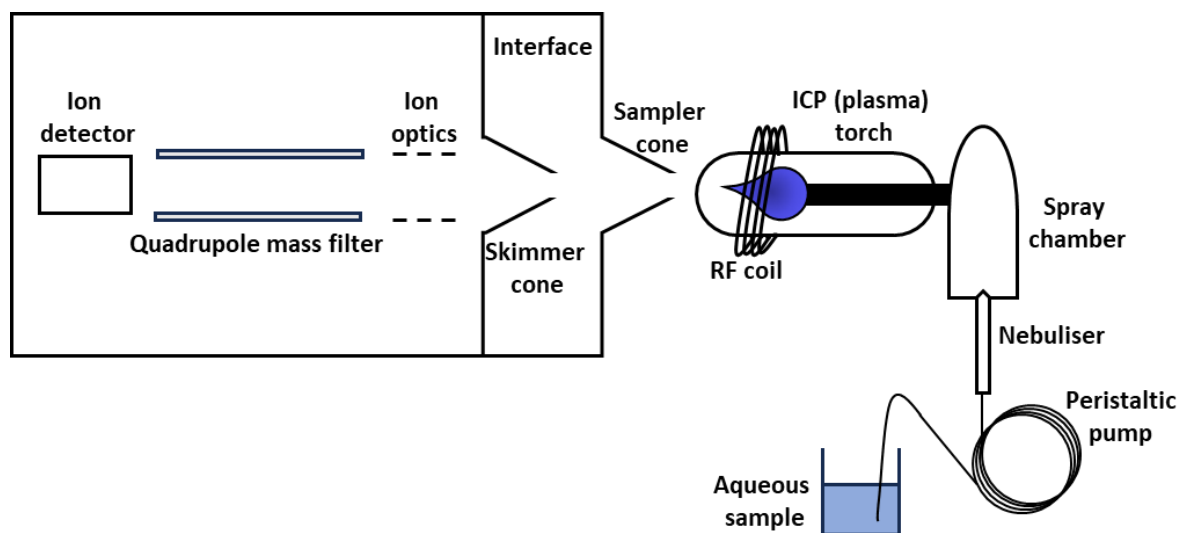


Figure 2.9: ICP-MS schematic.³⁴

In an argon ICP a plasma is produced by a magnetic field from the RF (radiofrequency) coil, which is coiled around the quartz torch with Ar gas flowing. Electrons are produced using a high voltage, which collide with Ar causing ionisation and plasma ignition. This is called inductive coupling, (as no electrodes are used in the energy transfer).³⁴

The sampler and skimmer cone as seen in Figure 2.9 are (water-cooled) metal cones make up a differentially pumped interface, which provides passage for the sample ions from the ICP at atmospheric pressure, to the mass spectrometer that operates under a vacuum of 2 torr (2.6×10^{-3} atm). The temperature difference (between the cones and the plasma) creates a boundary layer where the analytes form oxides.³⁴

In the mass spectrometer the analytes are separated from the other ions and analysed. There are various mass spectrometers that can be attached to the ICP ion source. A quadrupole (Q) mass spectrometer allows ions with a specific m/z (mass/charge ratio) to be detected, with any other ions ejected. A sector instrument mass spectrometer focuses a beam of dispersed ions using magnetic and electric fields so that only ions with a specific m/z reach the detector through a slit. Time-of-flight (TOF) mass spectroscopy instruments, here ions travel at

velocities dependant on their m/z through a tube, the lighter ions will therefore reach the end of the tube (and be detected) before heavier ions, and all ions are therefore detected.³⁴

Instrument Specification

To quantify total metal leaching from the supported catalysts during H_2O_2 synthesis:

Samples were analysed by Mr Simon Waller.

Post-reaction solutions were analysed using an Agilent 7900 ICP-MS equipped with I-AS auto-sampler. All samples were diluted by a factor of 10 using HPLC grade H_2O (1% HNO_3 and 0.5% HCl matrix). All calibrants were matrix matched and measured against a five-point calibration using certified reference materials purchased from Perkin Elmer and certified internal standards acquired from Agilent. Detection limits can vary from PPB to PPT levels depending on the element(s) used and between runs.^{4,5}

To quantify total metal loading of $AuPdX/TiO_2$ catalysts:

Analysis was performed by Exeter Analytical LTD (EAI). Samples were digested *via* a HF assisted microwave digestion method using a Milestone Connect Ethos UP microwave with an SK15 sample rotor. Digested samples were analysed by inductively coupled plasma-optical emission spectroscopy (ICP-OES). All calibrants were matrix matched and measured against a five-point calibration using certified reference materials purchased from Perkin Elmer and certified internal standards acquired from Agilent.⁵

2.4.9 XRD (X-Ray Diffraction)

XRD is a non-destructive characterisation technique that provides information on the bulk structure of a crystalline material. A monochromatic X-ray beam is focused onto a sample and scattered at specific angles from the lattice planes in the sample, which gives a diffraction pattern. The distribution of atoms within the lattice affects peak intensity.³⁵

XRD occurs by the diffraction of X-rays by the electron cloud (of an atom) in a periodic lattice. Bragg's law explains the conditions of diffraction needed for detection and is given in Equation

2.17. Some of the X-rays that are diffracted are out of phase, these cancel out. However, if the beams have the same wavelength and are in-phase constructive interference occurs and the wavelength is amplified.³⁵

Bragg's Law:

$$n\lambda = 2d \sin\theta \quad (2.17)$$

Where n = an integer

λ = wavelength of X-ray

d = path difference (spacing between the crystal layers)

θ = incident angle (angle between the incident ray and the scatter plane)

Figure 2.10 shows the Bragg-Brentano diffractometer set-up. The sample must be spun as the powdered catalyst sample is tightly packed and the crystals will be randomly orientated. In order to satisfy the Bragg equation, the sample spins to maximise the likelihood of the Bragg condition being satisfied. This will also decrease signal-to-noise ratio.³⁵

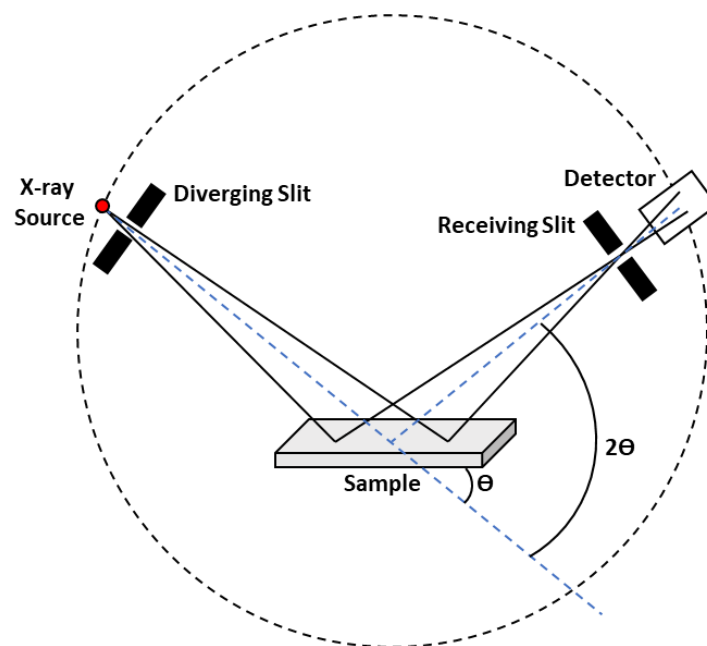


Figure 2.10: XRD schematic - the Bragg-Brentano diffractometer³⁶

Instrument Specification

The bulk structure of the catalysts was determined by powder X-ray diffraction using a (θ - θ) PANalytical X'pert Pro powder diffractometer using a Cu K_{α} radiation source (Ni filtered), operating at 40 keV and 40 mA. Standard analysis was carried out using a 40 min run with a back filled sample, between 2θ values of 5–80°. Phase identification was carried out using the International Centre for Diffraction Data (ICDD) database.^{4,5}

2.4.10 XPS (X-Ray Photoelectron Spectroscopy)

An X-ray photoelectron spectrometer (Figure 2.11) has a series of pumps that are capable of creating an ultra-high vacuum (UHV) of 10^{-10} mbar. Photons are produced by electron bombardment of a metal anode target. Common anode metals include aluminium ($h\nu = 1486.6$ eV) and magnesium ($h\nu = 1253.6$ eV). They are held at a high potential (15 kV) resulting in the emission of the $K_{1,2}$ radiation line. A switchable Al/Mg dual anode is used to distinguish between photoemission and Auger peaks (kinetic energy of Auger electrons is independent of $h\nu$). Monochromatic sources such as aluminium and silver can be employed to reduce the inherent linewidth of the exciting radiation and remove secondary X-ray emission lines such as the $K_{\alpha_{3,4}}$ line, which improved resolution. An electrostatic concentric hemispherical analyser (CHA) is used for the detection of photoelectrons. Photoelectrons are retarded at the analyser entrance to the pass energy (PE) in order to enhance the resolution. This is called the constant analyser energy (CAE) mode of operation, and the energy resolution is independent of the analyser transmission. Electron detection is accomplished through a bank of channeltron electron multipliers or a channel plate array.³⁷

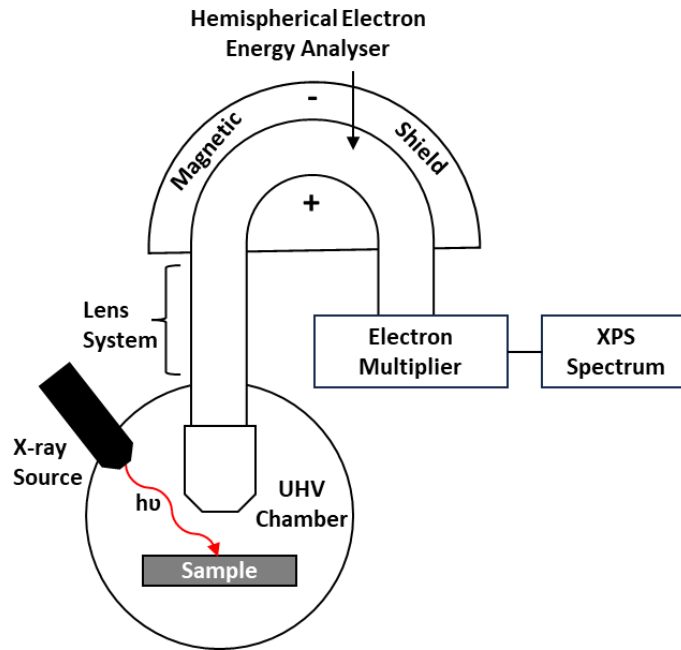


Figure 2.11: XPS schematic.³⁸

XPS is based upon Einsteins photoelectric effect as given in Equation 2.18.

$$E_K = h\nu - E_B \quad (2.18)$$

Where E_K = Kinetic energy (of the emitted electron)

$h\nu$ = Energy of the incident radiation

E_B = Binding energy (of the electron for a particular energy level)

This states that when photons (with sufficient energy) interact with a material, photoelectrons will be emitted, this is known as photoemission. In XPS the energy of the incident photon is >1200 eV, to ensure sufficient energy to eject an electron from one of the atoms core energy levels.³⁷

Information on the environment of the atoms that emit the photoelectron is provided by chemical shift, and this is called an initial state effect. Essentially, the binding energy of an emitted photoelectron is dependent upon the localised charge of the atom it is emitted from, and by extension the ligands it is bound to. This is an initial state effect because the energy is dependent on the ground state of the atom prior to effects caused by the photoionisation³⁷

Photoemissions result in core-hole formation which must be rapidly neutralised by electrons that originate from higher energy levels, this results in quantum energy released as either Auger emission or fluorescence.³⁷ The atomic number (Z) of the species will affect this, with the Auger emission (Figure 2.12) switching to fluorescence at approximately $Z = 30$ and above.^{37,39} When an inner-shell electron is ejected due to photon excitation, an electron from an outer shell fills the core-hole, releasing energy. This energy causes the emission of a second electron, known as an Auger electron. Auger signals are also observed in the photoelectron spectrum and can therefore assist in identifying various species and oxidation states, particularly for metals do not show measurable chemical shifts from photoemission (e.g. Zn) because it is not sensitive to a change in oxidation state. For such examples the Auger emissions give a larger chemical shift.³⁷

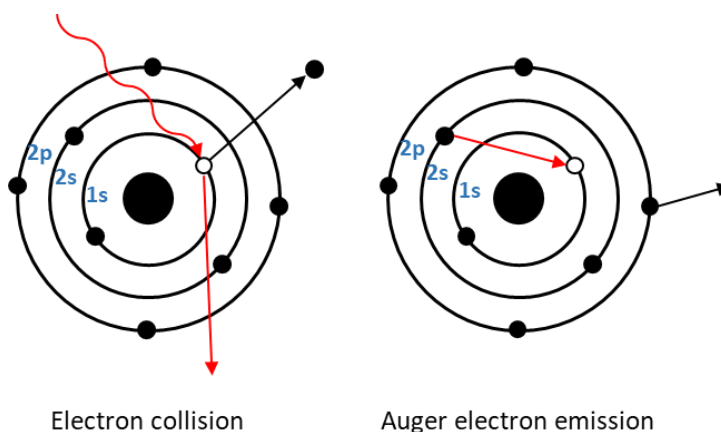


Figure 2.12: (Left) Electron collision followed by (right) Auger emission.

Fluorescence (Figure 2.13) is caused by a photon exciting an electron into a higher energy level, the electron then returns to its original energy level and emits a photon with energy equal to the difference in energy levels. This photoemission is called fluorescence. The heavier the element, the greater the fluorescence as the difference in energy levels will be greater.³⁷

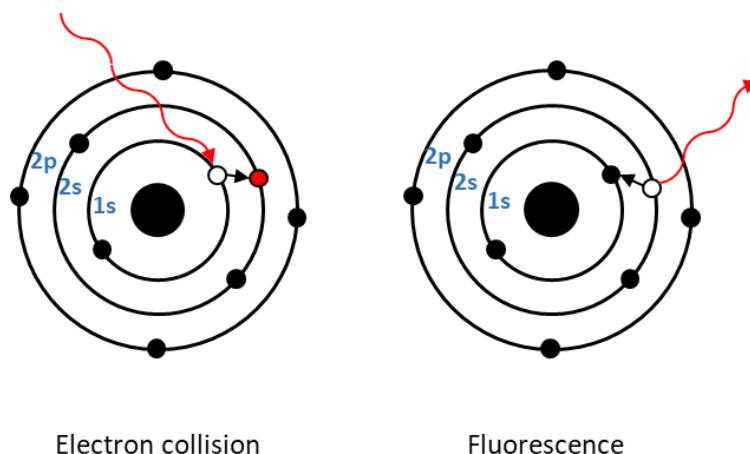


Figure 2.13: (Left) Electron collision followed by (right) Fluorescence

Final state effects are those that occur after the photoionisation and involve any effects that occur as a result of the perturbation to the electronic structure. Electrons present in the ionised species undergo reorganisation to minimise the increased energy as a result of the photoionisation and this results in final state effects, each with their own energies and which give extra peaks in the spectrum.³⁷

Instrument Specification

XPS analysis was performed by Dr David Morgan.

Thermo Scientific K-Alpha⁺ photoelectron spectrometer utilising a micro-focused monochromatic Al K_α X-ray source operating at 72 W. Samples were pressed into a copper holder and analysed using the 400 μm spot mode at pass energies of 40 and 150 eV for high-resolution and survey spectra respectively. Charge compensation was performed using a combination of low energy electrons and argon ions, which resulted in a C(1s) binding energy of 284.8 eV for the adventitious carbon present on all samples and all samples also showed a constant Ti(2p_{3/2}) of 458.5 eV. All data was processed using CasaXPS v2.3.24 using a Shirley background, Scofield sensitivity factors and an electron energy dependence of -0.6 as recommended by the manufacturer. Peak fits were performed using a combination of Voigt-type functions and models derived from bulk reference samples where appropriate. Analysis

of catalytic samples, after use in the direct synthesis of H_2O_2 was conducted after the sample was dried under vacuum (30 °C, 16 h).³⁻⁵

2.4.11 XAS (X-Ray Absorption Spectroscopy)

XAS is composed of two different types of absorption processes, EXAFS (Extended X-ray Absorption Fine Structure) and XANES (X-ray Absorption Near Edge Structure). EXAFS provides information on interatomic distances, near neighbour coordination numbers and lattice dynamics, and is a result of an interference effect between the electrons ejected from the inner core shell levels and backscattered electrons from neighbouring atoms. XANES provides information on valence state, energy bandwidth and bond angles, and is a result of excitation of an inner shell electron by an incident photon to a higher energy level.⁴⁰

Figure 2.14 highlights the XANES and EXAFS absorption sites for a La_2CuO_4 perovskite structure.⁴⁰

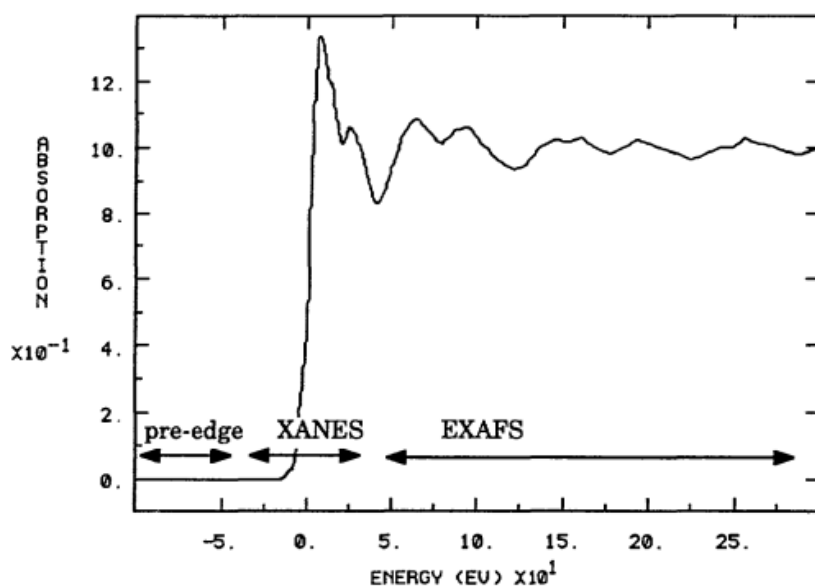


Figure 2.14: Absorption sites for a La_2CuO_4 perovskite structure.⁴⁰

EXAFS data can be collected in multiple ways as seen schematically in Figure 2.15. These include transmission, fluorescence, energy dispersion and reflectance. The most common of

these methods is transmission whereby the sample must be in the form of a foil, a thin single crystal, or a homogeneous powder.⁴⁰

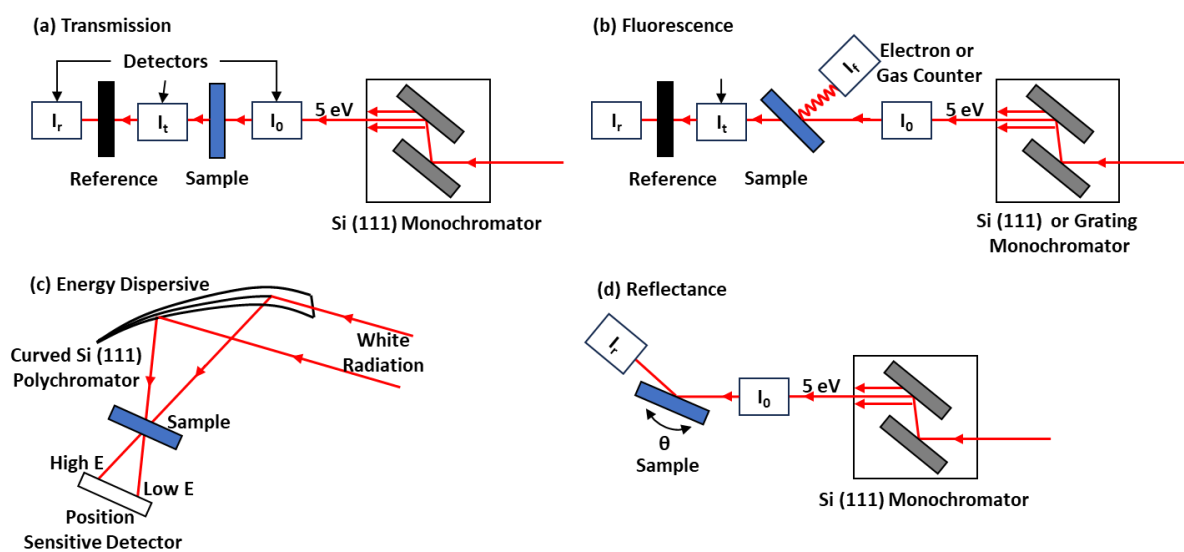


Figure 2.15: Experimental set-ups for XAS analysis⁴⁰

In XANES the x-ray absorption is a result of an incident photon causing excitation of an inner level electron to a higher energy level. For example, if in an atom a 1s energy level electron is excited, the lowest lying empty p-state will be occupied, this is called K-edge absorption.⁴⁰

For XANES experiments transmission and fluorescence experimental configurations are used to detect X-rays and ‘total electron yield count’ mode is used for detecting secondary electrons. Transmission mode can be advantageous due to the good signal-to-noise ratio and the fact that the measurements from this technique are representative of the bulk material. Fluorescence is used for dilute samples, the degree of which will depend on factors such as detection angle and photon flux. For samples that are extremely thin, total electron yield count is used, for these measurements an ultra-high vacuum is required due to surface sensitivity.⁴⁰

Analysing the XANES spectrum, the relative location of the absorption edge gives information on the effective charge on the absorbing atom, the location and intensity of the resolvable features provides information on the relative width and occupancy of the final states, and the polarised nature of the synchrotron radiation provides information on the final electronic states.⁴⁰

Instrument Specification

EXAS analysis was performed by Dr Emma Gibson and Prof. Andrew Beale.

The following method is taken from *Nat. Catal.*, 2019, **2**, 873–881.

XAFS spectroscopy measurements were performed on stations B18 and I20 at the Diamond Light Source (Oxon), operating at 3 GeV in multibunch mode with a current of 200 mA. Both stations are equipped with a Si(111) double-crystal monochromator, ion chambers for measuring incident and transmitted beam intensities and/or a multi-element Ge (fluorescence) detector for recording X-ray absorption spectra. The measurements were carried out in air on self-supporting wafers (approximately 0.1 g) at the Pt L₃-edge, and a 10- μ m-thick Pt foil was used as a calibration sample for the monochromator. The measurements were performed at room temperature. To improve the signal-to-noise ratio, multiple scans were taken. All data were subjected to background correction using Athena51 (that is, an IFEFFIT software package for pre- and post-edge background subtraction and data normalization). The XAFS spectra were normalized from 30 to 150 eV above the edge energy, although the EXAFS spectra were normalized from 150 eV to the last data point using the Autobk algorithm. Normalization was performed between $\mu(E)$ and $\mu_0(E)$ by a line regression through the data in the region below the edge and subtracted from the data. A quadratic polynomial was then regressed to the data above the edge and extrapolated back to the threshold energy (E_0). The extrapolated value of the post-edge polynomial at E_0 was used as the normalization constant; E_0 is normally determined using either the maximum in the first derivative (approximately 50% of the rising absorption edge) or immediately after any pre-edge or shoulder features. The isolated EXAFS spectra were analysed using the DL-EXCURV. The data were analysed using a least-squares single- or dual shell-EXAFS fitting analysis that was performed on data that had been phase corrected using muffin-tin potentials. An amplitude reduction factor (S_0^2) of 0.94 (obtained from fitting a Pt metal foil) was also used in the analysis.³

2.5 References

- 1 G. J. Hutchings and C. J. Kiely, *Acc. Chem. Res.*, 2013, **46**, 1759–1772.
- 2 M. Sankar, Q. He, M. Morad, J. Pritchard, S. J. Freakley, J. K. Edwards, S. H. Taylor, D. J. Morgan, A. F. Carley, D. W. Knight, C. J. Kiely and G. J. Hutchings, *ACS Nano*, 2012, **6**, 6600–6613.
- 3 M. Macino, A. J. Barnes, S. M. Althahban, R. Qu, E. K. Gibson, D. J. Morgan, S. J. Freakley, N. Dimitratos, C. J. Kiely, X. Gao, A. M. Beale, D. Bethell, Q. He, M. Sankar and G. J. Hutchings, *Nat. Catal.*, 2019, **2**, 873–881.
- 4 A. Barnes, R. J. Lewis, D. J. Morgan, T. E. Davies and G. J. Hutchings, *Catalysts*, 2022, **12**, 1–15.
- 5 A. Barnes, R. J. Lewis, D. J. Morgan, T. E. Davies and G. J. Hutchings, *Catal. Sci. Technol.*, 2022, **12**, 1986–1995.
- 6 D. A. Skoog, J. F. Holler and S. R. Crouch, in *Principles of Instrumental Analysis*, Cengage Learning, 7th edn. 2016, ch. 27 pp. 720–745.
- 7 M. H. Gordon, *Principles of Gas Chromatography*, Springer, Boston, MA, 1990.
- 8 D. S. Gawale, R. S. Jaiswal, R. P. Chavhan, D. J. Chaudhari, N. Jaiswal and D. Patil, *Int. J. Pharm. Res. Appl.*, 2022, **7**, 615–620.
- 9 K. D. Bartle and P. Myers, *Trends Anal. Chem.*, 2002, **21**, 547–557.
- 10 V. G. Berezkin, V. R. Alishoyev and I. B. Memirovskaya, in *Gas Chromatography of Polymers*, Elsevier, Amsterdam, 1977, pp. 1–31.
- 11 The Basics of UV-Vis Spectrophotometry - A Primer, www.agilent.com/cs/library/primers/public/primer-uv-vis-basics-5980-1397en-agilent.pdf, (accessed June 2024).
- 12 Cyto Diagnostics, <https://www.cytodiagnosics.com/pages/introduction-to-gold-nanoparticle-characterization>, (accessed June 2024).
- 13 A. Dutta, in *Spectroscopic Methods for Nanomaterials Characterization*, eds. T. Sabu, R. Thomas, A. K. Zachariah and R. K. Mishra, Elsevier Inc., 2017, ch. 4, pp. 73–93.
- 14 J. A. Lercher and A. Jentys, in *Studies in Surface Science and Catalysis*, eds. J. Čejka, H. van Bekkum, C. Avelino and F. Schüth, Elsevier B.V., Germany, 2007, vol. 168, pp. 435–476.
- 15 P. Larkin, in *Infrared and Raman Spectroscopy*, Elsevier, Amsterdam; Boston, 2011, ch. 3, pp. 27–54.
- 16 H. L. Gruber, *Anal. Chem.*, 1962, **34**, 1828–1831.
- 17 H. Berndt and U. Müller, *Appl. Catal. A Gen.*, 1999, **180**, 63–69.
- 18 T. J. Osinga, B. G. Linsen and W. P. van Beek, *J. Catal.*, 1967, **7**, 277–279.
- 19 R. M. Dell, F. S. Stone and P. F. Tiley, *Trans. Faraday Soc.*, 1953, **49**, 195–201.

- 20 P. Canton, G. Fagherazzi, M. Battagliarin, F. Menegazzo, F. Pinna and N. Pernicone, *Langmuir*, 2002, **18**, 6530–6535.
- 21 P. Canton, F. Menegazzo, S. Polizzi, F. Pinna, N. Pernicone, P. Riello and G. Fagherazzi, *Catal. Letters*, 2003, **88**, 141–146.
- 22 G. Fagherazzi, P. Canton, P. Riello, N. Pernicone, F. Pinna and M. Battagliarin, *Langmuir*, 2000, **16**, 4539–4546.
- 23 A. Le Valant, C. Comminges, F. Can, K. Thomas, M. Houalla and F. Epron, *J. Phys. Chem. C*, 2016, **120**, 26374–26385.
- 24 F. Drault, C. Comminges, F. Can, L. Pirault-Roy, F. Epron and A. Le Valant, *Materials*, 2018, **11**, 1–13.
- 25 M. B. Conway, PhD Thesis, Cardiff University, 2021.
- 26 S. Brunauer, P. H. Emmett and E. Teller, *J. Am. Chem. Soc.*, 1938, **60**, 309–319.
- 27 Y. Leng, in *Materials Characterization: Introduction to Microscopic and Spectroscopic Methods*, Wiley-VCH Verlag GmbH & Co. KGaA, 2nd edn., 2013, ch. 3, pp. 83–126.
- 28 Y. Wen, T. Shang and L. Gu, *Microscopy*, 2017, **66**, 25–38.
- 29 Y. Leng, in *Materials Characterization: Introduction to Microscopic and Spectroscopic Methods*, Wiley-VCH Verlag GmbH & Co. KGaA, 2nd edn., 2013, ch. 4, pp. 127–161.
- 30 L. E. Franken, K. Grünewald, E. J. Boekema and M. C. A. Stuart, *Small*, 2020, **16**, 1–15.
- 31 P. Sciau, in *Advances in Imaging and Electron Physics*, ed. P. W. Hawkes, Elsevier Inc., 1st edn., 2016, vol. 198, ch. 2, pp. 43–67.
- 32 S. J. Pennycook, in *Encyclopedia of Condensed Matter Physics*, ed. P. W. Franco Bassani, Gerald L. Liedl, Elsevier Ltd, 2005, pp. 240–247.
- 33 A. K. Datye, P. L. Hansen and S. Helvey, *Handbook of Heterogeneous Catalysis*, Wiley, 2008, ch. 3, pp. 803–833.
- 34 F. Cubadda, in *Food Toxicants Analysis: Techniques, Strategies and Developments*, ed. Y. Picó, Elsevier B.V., 1st edn., 2007, ch. 19, pp. 697–751.
- 35 A. A. Bunaciu, E. gabriela Udriștioiu and H. Y. Aboul-Enein, *Crit. Rev. Anal. Chem.*, 2015, **45**, 289–299.
- 36 A. Koçak, *Materials Science and Engineering: Thin Film Preparation, Particle Size and Thickness Analysis*, 2018.
- 37 D. J. Morgan, *X-Ray Photoelectron Spectroscopy (XPS): An Introduction*, 2012.
- 38 D. Regonini, University of Bath, 2008.
- 39 M. I. Babencov, B. V. Bobykin and V. K. Petukhov, *Phys. Lett. A*, 1972, **40**, 347–348.
- 40 E. E. Alp, S. M. Mini and M. Ramanathan, *EXAFS and XANES - A Versatile Tool to Study the Atomic and Electronic Structure of Materials*, (ANL/APS/TM--7), United States, 1990.

Chapter 3: Tuning of Catalytic Sites in Pt/TiO₂ Catalysts for the Chemoselective Hydrogenation of 3-Nitrostyrene

3.1 Introduction

The chemoselective hydrogenation of 3-nitrostyrene to 3-vinylaniline is a challenging reaction due to the presence of an olefin group that competes with the nitro functional group to be reduced. Synthesis of functional anilines such as 3-vinylaniline are important in the production of pharmaceuticals, agrochemicals, dyes, and fine chemicals. Figure 3.1 shows the main products resulting from 3-nitrostyrene reduction, there is the desired product 3-vinylaniline, plus the over reduction product 3-ethylaniline where both the nitro and olefin group are reduced, and 3-ethylnitrobenzene where only the olefin is reduced.

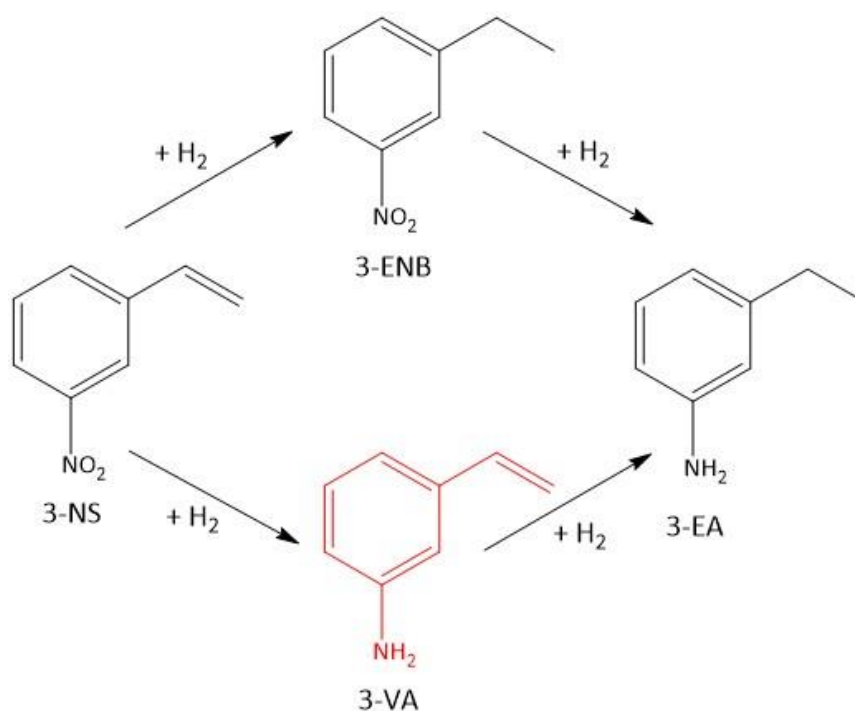


Figure 3.1: Reaction scheme for the chemoselective hydrogenation of 3-nitrostyrene (3-NS) to 3-vinylaniline (3-VA), including side product 3-ethylnitrobenzene (3-ENB) and the over hydrogenation side product 3-ethylaniline (3-EA).

Using H₂ as a hydrogen source is beneficial for a number of reasons, economically, it is highly available, and it is a green reductant as it doesn't produce hazardous by-products. Unfortunately, when using H₂ as the hydrogen donor high selectivity is not naturally achieved compared to hydrazine for example. Therefore, it is imperative to use a catalyst that is selective towards the hydrogenation of the nitro group, this can be achieved by the catalyst having intrinsic activity towards the nitro group reduction and/or by the preferential absorption of the nitro (-NO₂) group onto the catalyst rather than the olefin (-C=C) group.

It is often accepted that precious metal catalysts, while active can lack selectivity, therefore many methods have been implemented to increase the selectivity of such catalysts. Platinum has been widely used for this reaction due to its inherent activity in many catalytic reactions including nitrostyrene reduction. Various heat treatments can be employed to affect catalysts, typically hydrogenation catalysts undergo calcinations to decompose metal precursors present on the catalyst support, and gas-phase reductions are used to reduce metal ions. In work by Corma et al.¹ Pt nanoparticle size and morphology was tuned by selecting an activation temperature that resulted in a highly chemoselective 0.2wt% Pt/TiO₂ catalyst for the selective reduction of 3-nitrostyrene.

This work aims to utilise various heat treatments through use of a calcination step prior to the reduction step in order to tune Pt sites on low loading Pt/TiO₂ catalysts. It is important to see how the loading and subsequent treatment of these catalyst is able to affect the properties of the catalysts through factors such as nanoparticle size and strong metal-support interactions (SMSI) and how this in turn alters both activity and selectivity of the catalysts.

3.2 Results and Discussion

3.2.1 Hydrogenation of 3-Nitrostyrene

A series of Pt/TiO₂ (P25) catalysts (0.05, 0.08, 0.2 & 0.5 wt%) were prepared by wet impregnation and heat treated, then tested for the liquid phase chemoselective hydrogenation of 3-NS (3-nitrostyrene) to 3-VA (3-vinylaniline) at 40 °C under 3 bar H₂ pressure with toluene as the solvent. Initially, a 0.2wt% Pt/TiO₂ catalyst reduced (5% H₂/Ar, 450 °C, 4 hrs, 10°C/min) (termed 0.2wt% Pt/TiO₂ 'red') was synthesised and found to convert 3-NS to 3-VA rapidly and selectively. A 3-NS concentration versus time plot was found to be linear for the initial reaction which was measured up to 10 minutes (see Figure 3.2), giving an initial rate of conversion of $2.5 \times 10^{-1} \text{ mol}_{3\text{NS}} \text{ kg}_{\text{cat}}^{-1} \text{ min}^{-1}$. For extended reaction times, this catalyst was shown to give greater than 99% selectivity towards 3-VA up to at least 40% conversion of 3-NS, with only a small decrease to 97% selectivity at 75% conversion.

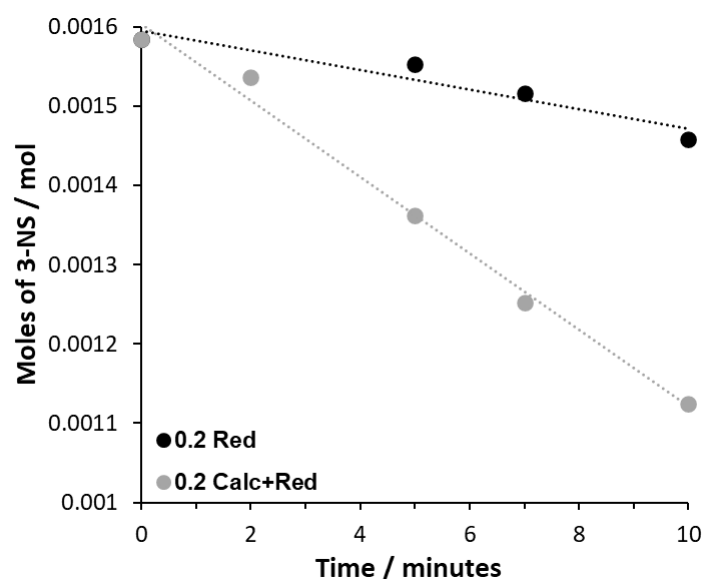


Figure 3.2: Moles of 3-NS in the reaction medium versus reaction time using 0.2wt% Pt/TiO₂ 'red' and 0.2wt% Pt/TiO₂ 'calc+red' catalysts. Reaction conditions: 3-NS (0.2 mL, toluene (8 mL), $p(\text{H}_2)$: 3 bar, catalyst (50 mg), temperature: 40 °C, stirring throughout.

Inspired by the work of Corma *et al.*¹ where heat treatment was used to effect activation of a Pt catalyst, a portion of the dried-only 0.2wt% Pt/TiO₂ sample was calcined (static air, 450 °C, 4 hrs) (termed 0.2wt% Pt/TiO₂ 'calc') and another portion was calcined (static air, 450 °C 4 hrs)

followed by reduction (5% H₂/Ar, 450 °C, 4 hrs) (termed 0.2wt% Pt/TiO₂ 'calc+red'). These catalysts were then tested for the hydrogenation of 3-NS. The 0.2wt% Pt/TiO₂ 'calc+red' catalyst ($9.7 \times 10^{-1} \text{ mol}_{3\text{NS}} \text{ kg}_{\text{cat}}^{-1} \text{ min}^{-1}$) was observed to have a much higher initial rate than the 'red' counterpart ($2.5 \times 10^{-1} \text{ mol}_{3\text{NS}} \text{ kg}_{\text{cat}}^{-1} \text{ min}^{-1}$). Comparatively, the 'calc' only analogue showed no activity towards the reaction and has therefore not been included in the figure.

As shown in Table 3.1, Corma *et al.*¹ have previously reported that a 0.2 wt% Pt/TiO₂ catalyst reduced at 450 °C displayed growth of a TiO_x layer over the Pt nanoparticles, resulting in SMSI which was attributed to the resulting high selectivity towards the desired 3-VA (~90%), due to the preferential adsorption of the nitro functional group. However, reduction at 200 °C did not show evidence of TiO_x overgrowth on the Pt nanoparticles and hence displayed a much lower selectivity towards 3-VA (~ 42%), with 3-EA (~52%) being the main product. In this study, the 0.2% Pt/TiO₂ 'red.' and 0.2% Pt/TiO₂ 'calc+red' materials (heat treated at 450 °C) only showed a difference in their catalytic activities not in their selectivities (at iso-conversion).

Table 3.1: Comparison of this works 0.2wt% Pt/TiO₂ catalysts and those synthesised by Corma et al.¹ for the chemoselective reduction of 3-nitrostyrene to 3-vinylaniline.

| Catalyst (Heat Treatment) | Reaction Conditions | 3-NS Conversion / % (3-VA Selectivity / %) | TOF / h ⁻¹ [mol _{3NS} mol _{Pt} ⁻¹ h ⁻¹] |
|---|--|---|--|
| 0.2wt% Pt/TiO₂ (Calc+Red 450°C) This work | 3-NS/Pt = 1000 Temp = 40°C Pressure = 3 bar Time = 60 min | 99 (90) | 5650* |
| 0.2wt% Pt/TiO₂ (Red 450°C) This work | 3-NS/Pt = 1000 Temp = 40°C Pressure = 3 bar Time = 60 min | 74 (97) | 1450* |
| 0.2wt% Pt/TiO₂ (Red 450°C) Corma et al. ¹ | 3-NS/Pt = 323 Temp = 40°C Pressure = 3 bar Time = 390 min | 95.1 (93.1) | 47 |
| 0.2wt% Pt/TiO₂ (Red 200°C) Corma et al. ¹ | 3-NS/Pt = 323 Temp = 40°C Pressure = 3 bar | 89.3 (41.5) | N/A |

*TOF calculated from 10 minute reaction.

To further investigate these observations, a series of Pt/TiO₂ catalysts with Pt loadings 0.05, 0.08, 0.5wt% were synthesised and portions underwent the ‘calc’, ‘calc+red’ and ‘red’ heat treatments previously investigated (Figure 3.2) for the 0.2wt% Pt/TiO₂ catalyst. Initial rates of 3-NS conversion for the catalyst series are shown in Figure 3.3. However, for clarity, as all the ‘calc’ samples were inactive for each Pt loading, these results have not been presented.

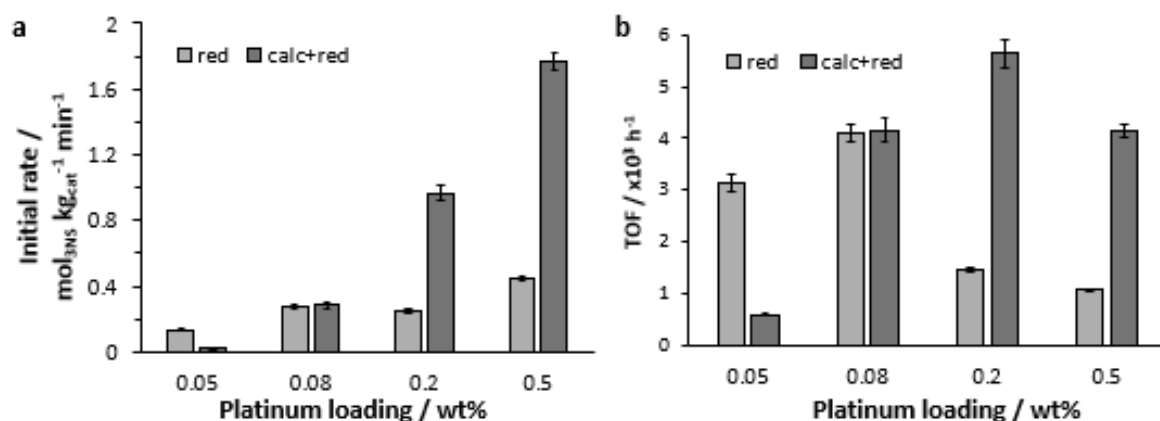


Figure 3.3: Effect of heat treatments (reduced versus calcined + reduced) on the activity of Pt/TiO₂ catalysts (where Pt loading = 0.05, 0.08, 0.2, 0.5wt%). (a) Initial 3-NS conversion rates - all initial rates are calculated from reaction measurements up to 10 minutes, with the exception of the 0.5 C+R catalyst which used measured up to 7 minutes. (b) Turnover frequencies (TOF) based on the initial rate obtained during the selective hydrogenation of 3-NS. Reaction conditions: 3-NS (0.2 mL), toluene (8 mL), p(H₂): 3 bar, catalyst (50 mg), temperature: 40 °C, stirring throughout.

It was observed that for the higher Pt loadings (0.2 and 0.5 wt%) the activity of the reduced-only samples ($2.5 \times 10^{-1} \text{ mol}_{3\text{NS}} \text{ kg}_{\text{cat}}^{-1} \text{ min}^{-1}$ and $4.5 \times 10^{-1} \text{ mol}_{3\text{NS}} \text{ kg}_{\text{cat}}^{-1} \text{ min}^{-1}$ for 0.2wt% Pt/TiO₂ 'red' and 0.5wt% Pt/TiO₂ 'red' respectively) was much lower than for the calcined + reduced samples ($9.7 \times 10^{-1} \text{ mol}_{3\text{NS}} \text{ kg}_{\text{cat}}^{-1} \text{ min}^{-1}$ and $1.8 \text{ mol}_{3\text{NS}} \text{ kg}_{\text{cat}}^{-1} \text{ min}^{-1}$ 0.2wt% Pt/TiO₂ 'calc+red' and 0.5wt% Pt/TiO₂ 'calc+red' respectively). The opposite activity trend can be observed for the lowest Pt loaded catalysts (0.05 wt%), where the reduced catalyst ($1.3 \times 10^{-1} \text{ mol}_{3\text{NS}} \text{ kg}_{\text{cat}}^{-1} \text{ min}^{-1}$) was shown to be more reactive compared to its calcined + reduced counterpart ($2.5 \times 10^{-2} \text{ mol}_{3\text{NS}} \text{ kg}_{\text{cat}}^{-1} \text{ min}^{-1}$). This shift in higher activity from the reduced catalysts to the calcined + reduced catalysts appears to occur at a Pt loading of 0.08wt% where the reduced catalyst ($2.8 \times 10^{-1} \text{ mol}_{3\text{NS}} \text{ kg}^{-1} \text{ min}^{-1}$) and calcined + reduced catalyst ($2.8 \times 10^{-1} \text{ mol}_{3\text{NS}} \text{ kg}_{\text{cat}}^{-1} \text{ min}^{-1}$) are almost identical in activity. However, to determine the exact cut off for this shift more catalysts at similar loadings (to 0.08wt%) would need to be tested.

The general trend seen is that as the Pt loading increases, so does the initial rate of conversion of 3-NS. However, by TOF values, the activity of the catalyst at a normalised Pt concentration can be analysed. In this case it can be seen that 0.2wt% Pt/TiO₂ 'calc+red' has substantially the highest TOF ($5.7 \times 10^3 \text{ hr}^{-1}$) making this the favourable catalyst. There are almost identical

TOF seen for the 0.08wt% Pt/TiO₂ 'red' ($4.1 \times 10^3 \text{ hr}^{-1}$), 0.08wt% Pt/TiO₂ 'calc+red' ($4.2 \times 10^3 \text{ hr}^{-1}$) and 0.5wt% Pt/TiO₂ 'calc+red' ($4.1 \times 10^3 \text{ hr}^{-1}$) catalysts. Possible explanations for this are described in the TEM section with regards to particle size and distribution.

It is notable that for all catalyst samples, regardless of loading or heat treatment, the selectivity towards 3-VA, corresponding to the initial rates, remains high (>99%). The only products detected in the GC analysis of all post-reaction solutions for each catalyst, were the primary product 3-VA, and in the cases where less than 100% selectivity was seen, small quantities of (3-EA) which is formed by the complete hydrogenation of both the nitro and C=C groups. Another potential product is 3-ethylnitrobenzene (3-ENB), which is formed by the selective hydrogenation of C=C branch present in 3-NS however this was not detected or only in trace quantities in the GC analysis. In line with other reports concerning this reaction,¹ the fully hydrogenated 3-ethyl-1-cyclohexylamine product was not detected under our reaction conditions as the aromatic ring is stable against reduction, and therefore will not be included in the discussion.

Table 3.2 shows the conversion and selectivity data for various times intervals of the reaction. It can be seen for the lower loading catalysts (0.05 & 0.08 wt%) that have undergone both heat treatments selectivity to 3-vinylaniline is maintained at >99% for reaction times extending to 120 minutes, however, the conversion for these four catalysts remains low, with the highest being 60% conversion for the 0.08wt% Pt/TiO₂ catalyst achieved over 120 minutes. Selectivities below >99% are only observed for the 0.2 and 0.5 wt% catalysts, however this is only observed at much higher conversions.

Table 3.2: Conversion and selectivity data for the chemoselective reduction of 3-nitrostyrene to 3-vinylaniline at various reaction times over 0.05, 0.08, 0.2 & 0.5wt% Pt/TiO₂ catalysts 'reduced' and 'calcined + reduced'. Reaction conditions: 3-NS (0.2 mL), toluene (8 mL), p(H₂): 3 bar, catalyst (50 mg), temperature: 40 °C, stirring throughout.

| Catalyst Loading | Heat Treatment | Time / min | 3-NS Conversion / % | 3-VA Selectivity / % |
|------------------|--------------------|------------|---------------------|----------------------|
| 0.05wt% Pt | Reduced | 30 | 13 | >99 |
| | | 60 | 24 | >99 |
| | | 120 | 35 | >99 |
| | Calcined + Reduced | 30 | 5 | >99 |
| | | 120 | 10 | >99 |
| | | | | |
| 0.08wt% Pt | Reduced | 15 | 10 | >99 |
| | | 30 | 27 | >99 |
| | | 60 | 37 | >99 |
| | | 120 | 60 | >99 |
| | Calcined + Reduced | 15 | 15 | >99 |
| | | 30 | 27 | >99 |
| | | 60 | 31 | >99 |
| | | 120 | 48 | >99 |
| | | | | |
| | | | | |
| 0.2wt% Pt | Reduced | 15 | 23 | >99 |
| | | 30 | 41 | >99 |
| | | 60 | 74 | 97 |
| | Calcined + Reduced | 15 | 40 | >99 |
| | | 30 | 68 | 96 |
| | | 60 | 99 | 90 |
| | | | | |
| | | | | |
| 0.5wt% Pt | Reduced | 15 | 34 | >99 |
| | | 30 | 70 | 97 |
| | | 60 | 86 | 96 |
| | Calcined + Reduced | 15 | 55 | 97 |
| | | 30 | 99 | 76 |
| | | 60 | 100 | 38 |
| | | | | |
| | | | | |

By plotting the conversion and selectivity data as seen in Figure 3.4, it can more clearly be seen that for the catalysts achieving higher conversions (0.2wt% Pt/TiO₂ 'red' & 'calc+red', and 0.5wt% Pt/TiO₂ 'red' & 'calc+red') the selectivity drops off at around 70% conversion. Catalysts with higher Pt loading will have a higher conversion at a shorter reaction length, therefore it is important to compare selectivities not at the same reaction times but instead at iso-conversion. It appears that for the different catalysts, when comparing iso-conversions, very similar selectivities are observed. Although not all catalysts have been run to >99% conversion it could be inferred from the correlation between lower conversions and their corresponding selectivities that the lower loading catalysts could follow the same trend and lose selectivity at higher conversions due to over hydrogenation resulting in the reduction of the olefin group and hence production of 3-ethylaniline. However, all catalysts would have to be run to 100% conversion to confirm this. However, it is notable that at 99% conversion the 0.5wt% catalyst selectivity drops rapidly to 76% due to the formation of the over hydrogenated product 3-ethylaniline which can occur at high conversion when there is no preferential adsorption of the nitro group.

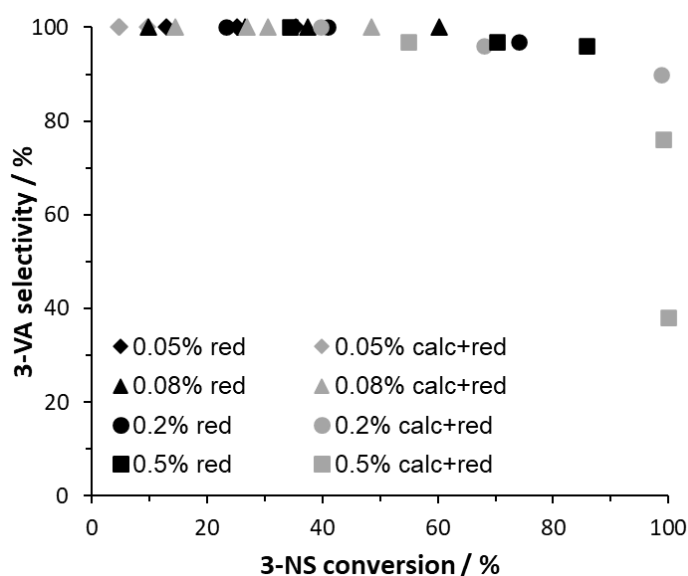


Figure 3.4: Product selectivity versus. reactant conversion for a variety of Pt/TiO₂ catalysts (where Pt loading = 0.05, 0.08, 0.2, 0.5 wt.%) in the chemoselective hydrogenation of 3-nitrostyrene. Reaction conditions: 3-NS (0.2 mL), toluene (8 mL), p(H₂): 3 bar, catalyst (50 mg), temperature: 40 °C, stirring throughout.

Additionally, the standard reaction was performed with different initial starting concentrations of 3-NS to determine the order of the reaction. These experiments were performed for both 0.2 wt% Pt/TiO₂ 'red' at initial 3-NS volumes: 100 μL (4×10^{-3} mol cm⁻³), 150 μL (6×10^{-3} mol cm⁻³) & 200 μL (8×10^{-3} mol cm⁻³), and for 0.08 wt% Pt/TiO₂ 'calc+red' at initial 3-NS volumes: 100 μL (4×10^{-3} mol cm⁻³), 200 μL (8×10^{-3} mol cm⁻³), 300 μL (1.2×10^{-2} mol cm⁻³) & 400 μL (1.6×10^{-2} mol cm⁻³). As shown in Figure 3.5 there is no change in initial rate for the different initial 3-NS volumes (and therefore concentrations), hence the order of reaction is confirmed to be zero order with respect to 3-NS concentration. This means that the sites responsible for the adsorption of the nitro group in 3-nitrostyrene are all saturated.

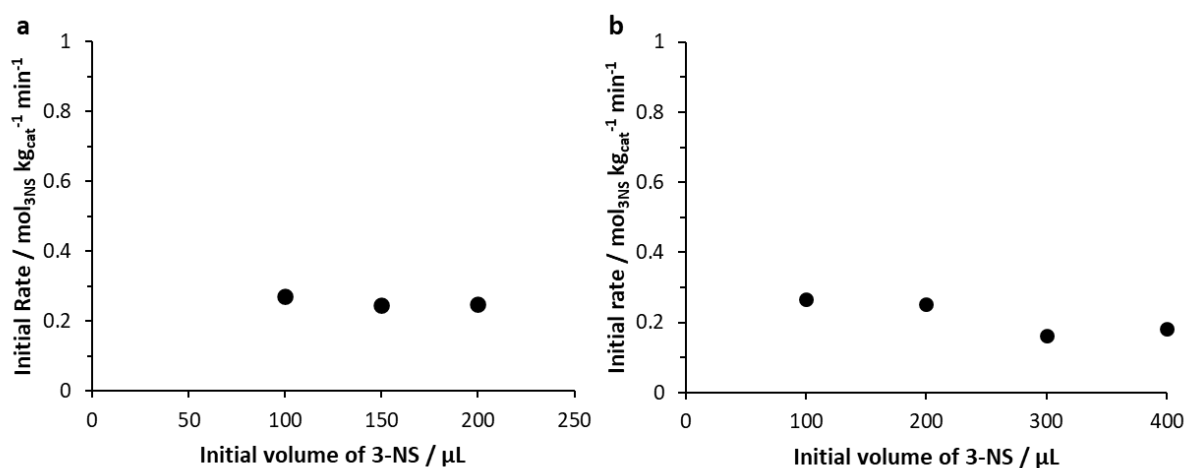


Figure 3.5: Initial rate for different 3-NS starting concentrations using (a) 0.2wt% Pt/TiO₂ 'red' and (b) 0.08wt% Pt/TiO₂ 'calc+red'. Reaction conditions: 3-NS (various volumes), toluene (8 mL), $p(H_2)$: 3 bar, catalyst (50 mg), temperature: 40 °C, stirring throughout.

3.2.2 Electron Microscopy Studies

Microscopy studies allow investigation as to how the size, structure and distribution of metal nanoparticles can affect activity. Images of the catalysts were recorded by HAADF-STEM (high-angle annular dark-field scanning transmission electron microscope) to investigate how the various heat treatments ('calc' 'calc+red' and 'red') and Pt loadings (0.05, 0.08, 0.2 & 0.5wt%) have affected metal dispersion. In the calcined-only samples, the Pt species consisted mostly of sub-nm clusters and highly dispersed single Pt atoms distributed over the support, as seen in Figure 3.6.

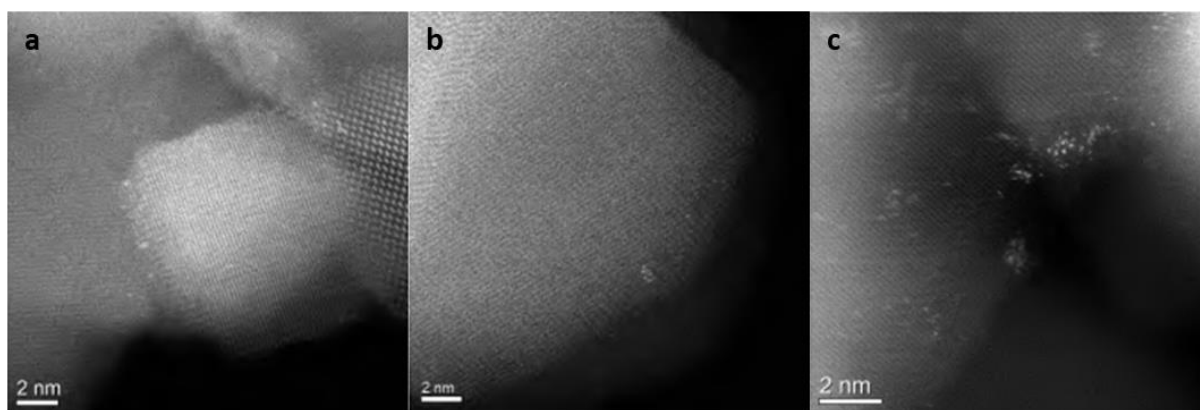


Figure 3.6: Representative HAADF-STEM images of (calcined-only) catalyst samples (a) 0.08 wt% Pt/TiO₂ 'calc' (b) 0.2 wt% Pt/TiO₂ 'calc' (c) 0.5 wt% Pt/TiO₂ 'calc'.² All microscopy imaging and analysis provided by Dr Qian He (Cardiff Catalysis Institute), Dr Sultan Althahban & Prof. Christopher Kiely (Lehigh University).

HAADF-STEM analysis of the 'red' and 'calc+red' catalysts showed larger particle sizes than the 'calc' samples, with small clusters primarily in the 1-2 nm range. As seen in Figure 3.7 (a & b) for the 0.05wt% Pt/TiO₂ catalysts (both 'red' and 'calc+red') ultra-small clusters (<1 nm) were detected, with no single Pt atoms observed, as in the 'calc' samples. The 'calc+red' catalyst had less uniform particle size (skewness 0.03) compared to the 'red' analogue (skewness - 0.06) which correlated with the higher activity seen for the 0.05 wt% 'red' ($1.3 \times 10^{-1} \text{ mol}_{3\text{NS}} \text{ kg}_{\text{cat}}^{-1} \text{ min}^{-1}$) catalyst compared to the 'calc+red' ($2.5 \times 10^{-2} \text{ mol}_{3\text{NS}} \text{ kg}_{\text{cat}}^{-1} \text{ min}^{-1}$) as seen in Table 3.3.

Figure 3.7 (c & d) show the STEM analysis of 0.08wt% 'red' and 'calc+red' catalysts. Both catalysts were observed to have the same mean particle size (1.2 nm) and similar size distributions. This similarity in Pt nanostructure coincides with the similar reaction activities seen for both the 0.08wt% 'red' and 'calc+red' catalysts (2.8×10^{-1} and $1.75 \times 10^{-3} \text{ mol}_{3\text{NS}} \text{ kg}_{\text{cat}}^{-1} \text{ min}^{-1}$).

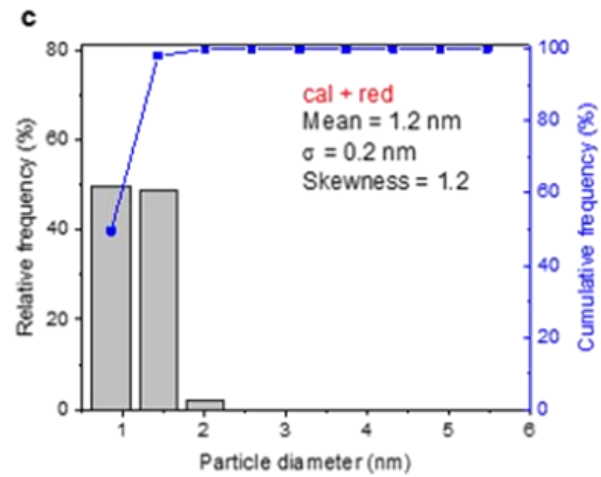
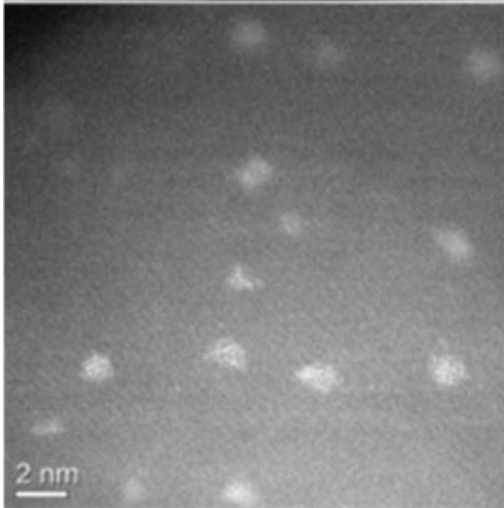
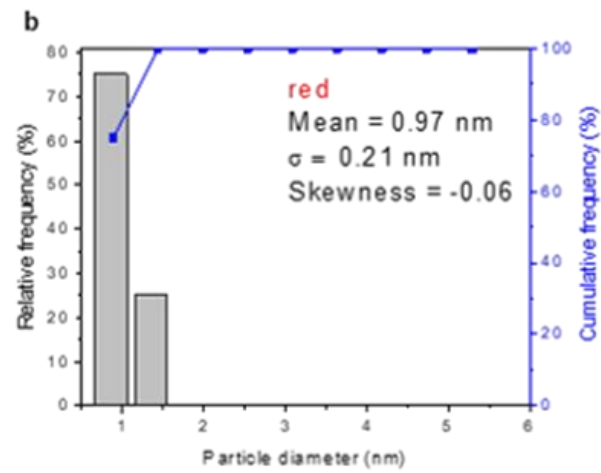
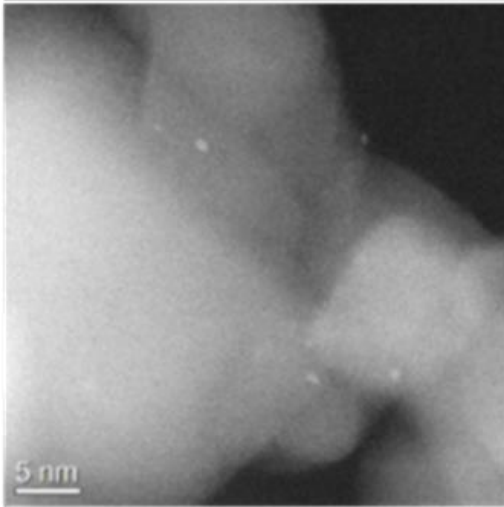
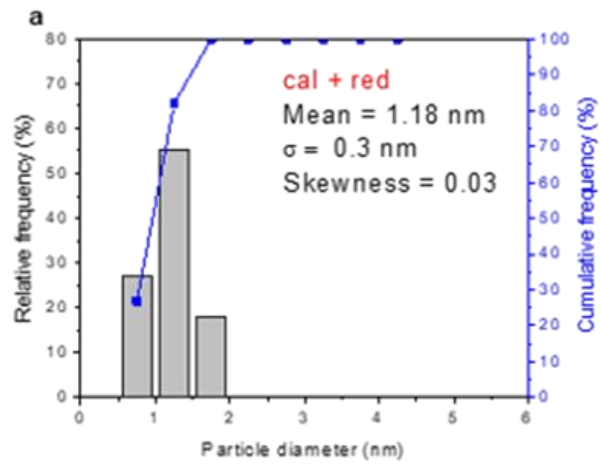
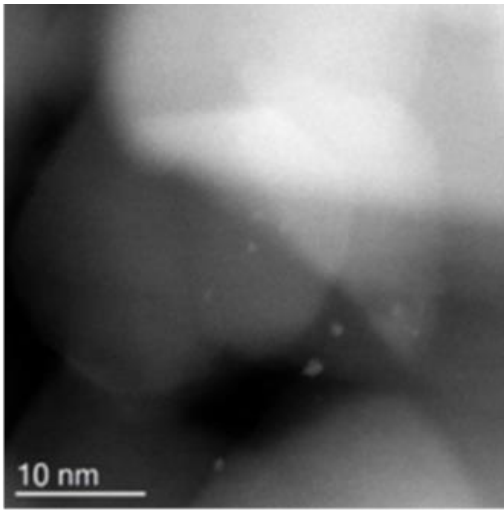
For the 0.2wt% Pt/TiO₂ catalysts it is seen in Figure 3.7 (e & f) that there is a much larger particle size distribution for the 'red' analogue (1-4 nm) compared to the more uniform distribution of nanoparticles seen for the 'calc+red' (1-2 nm). With the corresponding mean particle sizes of 1.6 nm and 1.1 nm respectively. This substantial difference in particle size is reflected in the activities, with a much greater catalytic activity seen for the 'calc+red' catalyst ($9.7 \times 10^{-1} \text{ mol}_{3\text{NS}} \text{ kg}_{\text{cat}}^{-1} \text{ min}^{-1}$) compared to the 'red' ($2.5 \times 10^{-1} \text{ mol}_{3\text{NS}} \text{ kg}_{\text{cat}}^{-1} \text{ min}^{-1}$).

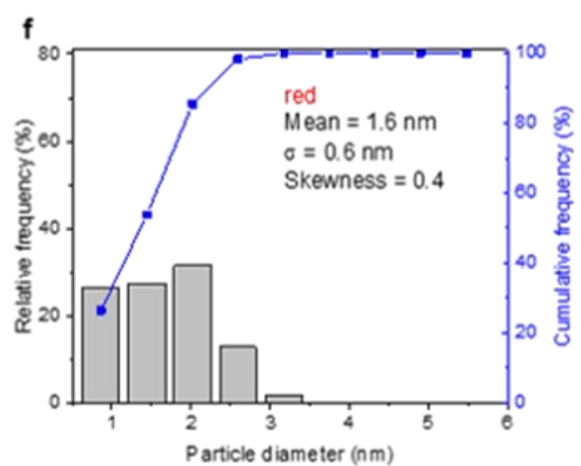
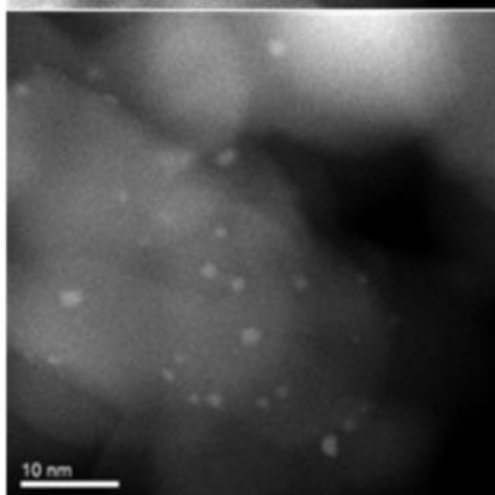
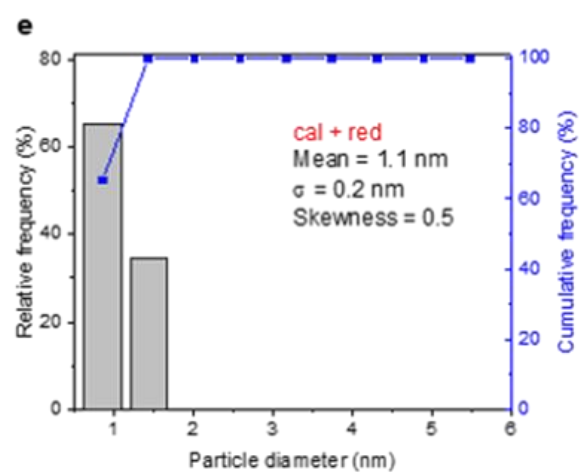
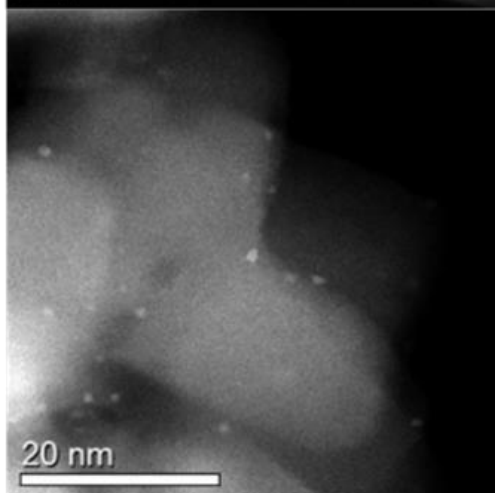
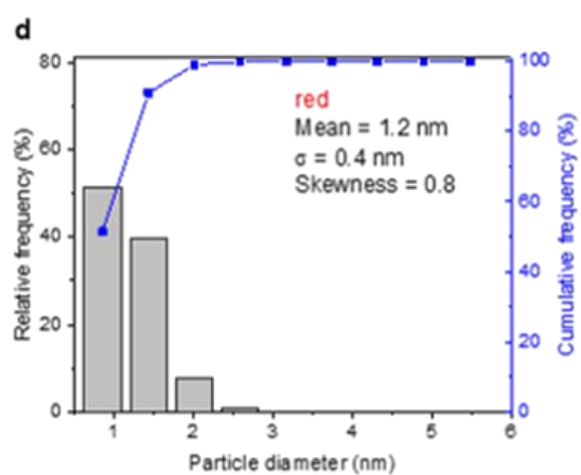
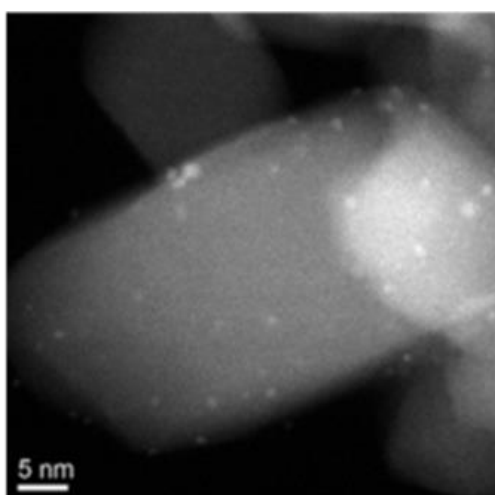
This same trend is again seen for the 0.5wt% Pt/TiO₂ catalysts. The uniform distribution of the 'calc+red' sample was not seen for the 'red' sample, which contained some particles larger than 5 nm in addition to the more abundant particles in the 1-2 nm range. As with the 0.2wt% samples, 'the calc+red' catalyst with the smaller size distribution, and smaller nanoparticle sizes was much more active ($1.8 \text{ mol}_{3\text{NS}} \text{ kg}_{\text{cat}}^{-1} \text{ min}^{-1}$ 'calc+red' compared to $4.5 \times 10^{-1} \text{ mol}_{3\text{NS}} \text{ kg}_{\text{cat}}^{-1} \text{ min}^{-1}$ 'red').

Calcination followed by reduction treatments as seen above can improve particle uniformity and distribution and is a phenomenon that has been observed previously.^{3,4} It is thought that this calcination step enhances anchoring of the Pt titania support which limits mobility of the particles during the following reduction step, preventing Pt agglomeration. It was seen that 0.2wt% & 0.5wt% Pt/TiO₂ 'red' catalysts had Pt particles over 2-3 nm, and these catalysts do not undergo the calcination step to aid stability and hence prevent agglomeration. The observations that have been made from the STEM images (Figure 3.7) and subsequent particle measurements coincide with the higher catalytic activities that were seen for the narrower particle size distributions and greater dispersion. It is notable than when considering the catalysts with the greatest TOF values 0.08 'red' ($4.1 \times 10^3 \text{ mol}_{3\text{NS}} \text{ mol}_{\text{Pt}}^{-1} \text{ hr}^{-1}$), 0.08 'calc+red' ($4.2 \times 10^3 \text{ mol}_{3\text{NS}} \text{ mol}_{\text{Pt}}^{-1} \text{ hr}^{-1}$), 0.2 'calc+red' ($5.7 \times 10^3 \text{ mol}_{3\text{NS}} \text{ mol}_{\text{Pt}}^{-1} \text{ hr}^{-1}$) and 0.5 'calc+red' ($4.1 \times 10^3 \text{ mol}_{3\text{NS}} \text{ mol}_{\text{Pt}}^{-1} \text{ hr}^{-1}$) that these catalysts had the largest population of ~1 nm particles and narrowest size distributions, shown in Table 3.3.

Table 3.3: Summary of prepared catalyst initial rates, TOF values, and mean particle sizes as determined by HAADF-STEM analysis.

| Catalyst Loading | Heat Treatment | Initial Rate / $\text{mol}_{\text{3NS}} \text{kg}_{\text{cat}}^{-1} \text{min}^{-1}$ | TOF / $\times 10^3 \text{hr}^{-1}$ | Mean Particle Size / nm |
|-------------------------|-----------------------|--|--|--------------------------------|
| 0.05 | Calc+Red | 0.025 | 0.596 | 1.8 |
| | Red | 0.13 | 3.12 | 0.97 |
| 0.08 | Calc+Red | 0.28 | 4.16 | 1.2 |
| | Red | 0.28 | 4.10 | 1.2 |
| 0.2 | Calc+Red | 0.97 | 5.65 | 1.1 |
| | Red | 0.25 | 1.45 | 1.6 |
| 0.5 | Calc+Red | 1.8 | 4.14 | 1.4 |
| | Red | 0.45 | 1.06 | 1.6 |





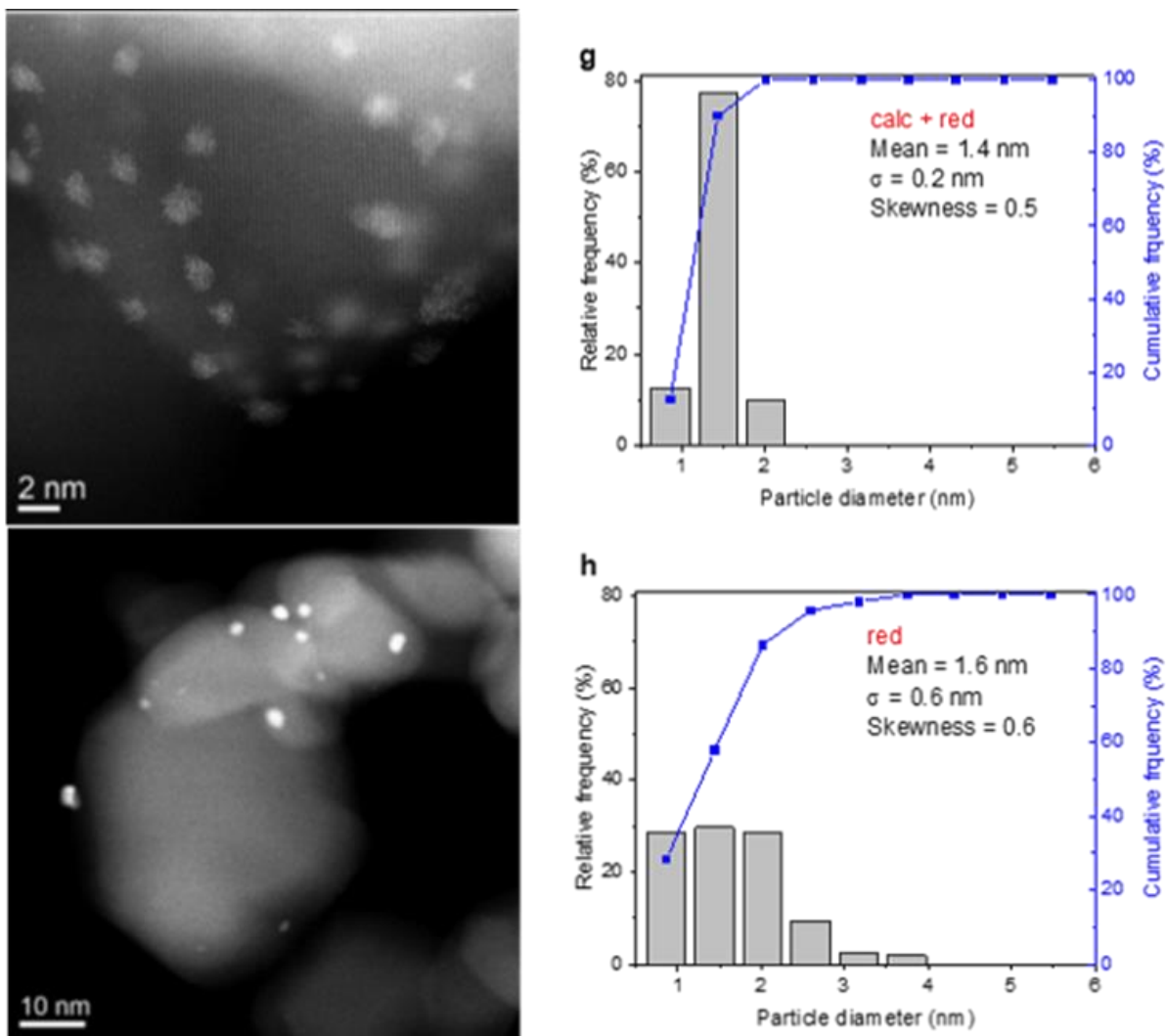


Figure 3.7: Representative HAADF-STEM images and the derived particle size distributions of the unused Pt/TiO₂ catalysts (a) 0.05wt% Pt/TiO₂ 'calc+red' (b) 0.05wt% Pt/TiO₂ 'red', (c) 0.08wt% Pt/TiO₂ 'calc+red' (d) 0.08wt% Pt/TiO₂ 'red' (e) 0.2wt% Pt/TiO₂ 'calc+red' (f) 0.2wt% Pt/TiO₂ 'red', (g) 0.5wt% Pt/TiO₂ 'calc+red' (h) 0.5wt% Pt/TiO₂ 'red'.² All microscopy imaging and analysis provided by Dr Qian He, Dr Sultan Althabhan & Prof. Christopher Kiely (Lehigh University).

3.2.3 X-ray Photoelectron Spectroscopy Studies

XPS analysis was performed on the Pt/TiO₂ catalyst series (0.05, 0.08, 0.2 & 0.5wt% Pt) for the fresh, 'calc', 'red' and 'calc+red' catalysts and is shown in Figure 3.8. The XPS data showed similar peaks (same binding energies) throughout for the different Pt loadings in the series and therefore can be analysed in much the same way. However, as expected, catalyst samples with very low loadings (0.05 & 0.08 wt% Pt), gave noisy spectra even after a large number of scans (>100). An overlapping Ti loss peak at ~75 eV made quantification of these spectra particularly challenging.⁵

XPS analysis for each Pt loading was consistent, as such for simplicity the 0.5wt% Pt/TiO₂ catalysts will be discussed primarily. A Pt(4f_{7/2}) binding energy of 72.2 eV was measured for all of the fresh (dried-only) catalyst samples. This indicates the presence of a Pt(II) species, this could be due to the residual chlorine from the Pt precursor that was also detected in the XPS analysis (see Table 3.4), additionally the presence of Pt oxides could also be responsible for this peak.⁵

0.5wt% Pt/TiO₂ 'calc' showed two Pt environments, the first had a binding energy again of 72.2 eV, in the dried-only sample this had been due to the presence of the Pt(II) species by residual chlorine. However, the calcination at 450 °C removed the majority of the Cl content (from 2.32 at% down to 0.39 at%, see Table 3.4) therefore this peak is most likely due to a PtO_x phase for the calcined sample. The Cl content present in the catalysts has come from the PtCl₆ precursor used in the catalyst preparation and the decrease of Cl after heat treatment is evident for all the catalysts at the different Pt loadings (Table 3.4). The second binding energy was seen at 74.4 eV which can be assigned to PtO₂ or Pt hydroxide.⁶

XPS of the 0.5wt% Pt/TiO₂ 'red' and 'calc+red' catalysts show Pt(0), which is indicated by an asymmetric peak shape and a binding energy between 70.6 and 70.8 eV.⁷ STEM imaging also indicated the presence of metallic Pt(0) structure in larger particles of the 0.5wt% Pt/TiO₂ 'red' catalyst, which agrees with the XPS findings.

XPS of the 0.08 and 0.05wt% lower Pt loading showed a weak signal for the Pt(4f), particularly for the 'red' and 'calc+red' samples, could be attributed to changes in particle size.

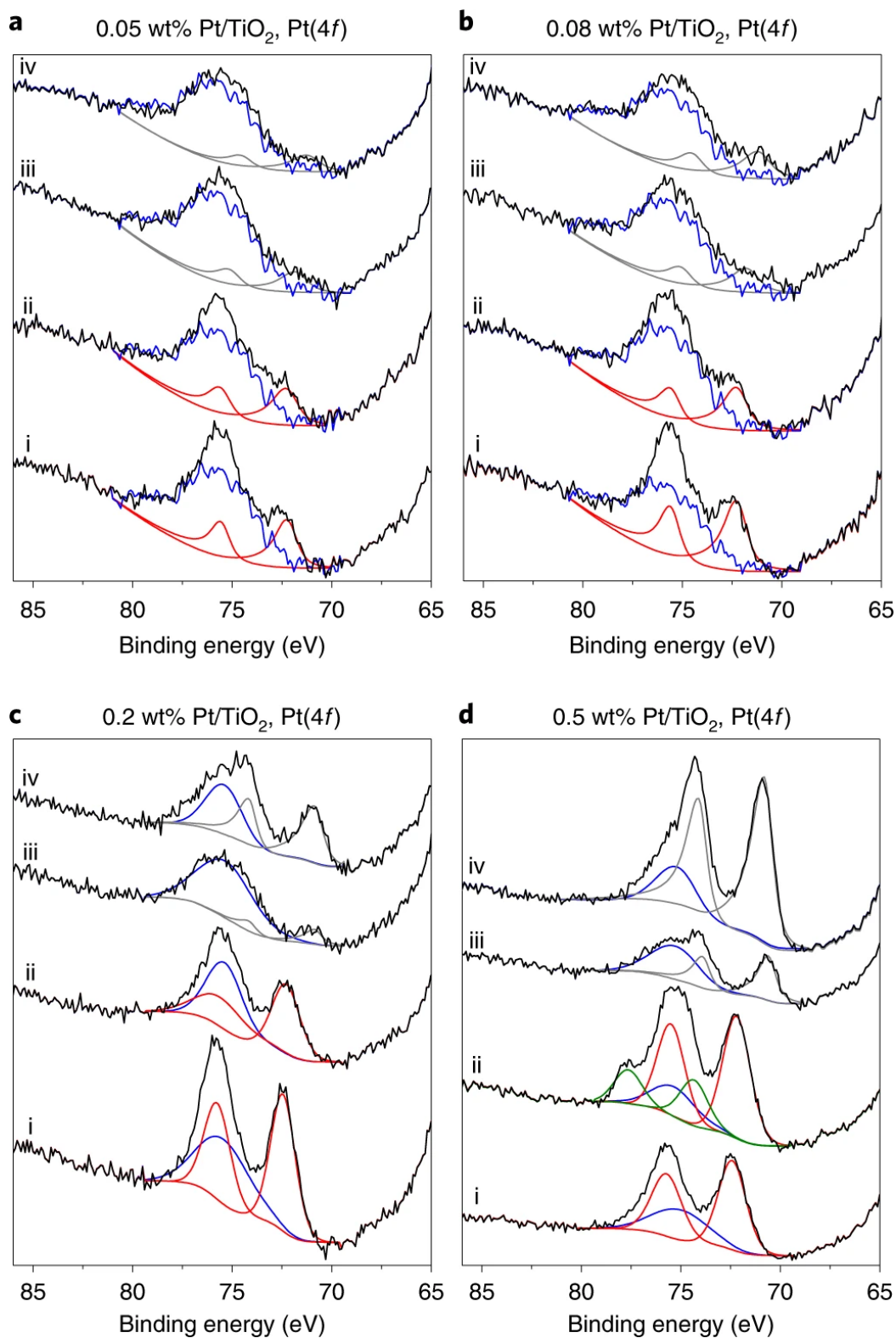


Figure 3.8: XPS data (a) 0.05wt% Pt/TiO₂ (b) 0.08wt% Pt/TiO₂ (c) 0.2wt% Pt/TiO₂ and (d) 0.5wt% Pt/TiO₂ catalysts with heat treatments: (i) dried only (ii) calcined-only (iii) reduced-only (iv) calcined+reduced.² All XPS fittings provided by Dr David Morgan.

Table 3.4: Atom % derivations from XPS analysis.

| Catalyst | Heat Treatment | Pt / atom % | Cl / atom % | Ti / atom % | O / atom % |
|-----------------------------------|----------------|-------------|-------------|-------------|------------|
| 0.05wt% Pt/TiO₂ | Fresh | 0.05 | 1.14 | 33.34 | 65.47 |
| | Calc | 0.04 | 0.53 | 33.93 | 65.51 |
| | Red | 0.03 | 0.54 | 33.77 | 65.66 |
| | Calc+Red | 0.03 | 0.56 | 33.67 | 65.74 |
| 0.08wt% Pt/TiO₂ | Fresh | 0.05 | 0.73 | 33.22 | 66.00 |
| | Calc | 0.04 | 0.53 | 33.21 | 66.22 |
| | Red | 0.03 | 0.43 | 33.36 | 66.19 |
| | Calc+Red | 0.03 | 0.55 | 32.83 | 66.58 |
| 0.2wt% Pt/TiO₂ | Fresh | 0.01 | 1.58 | 30.22 | 68.19 |
| | Calc | 0.01 | n/d | 30.56 | 69.43 |
| | Red | 0.02 | n/d | 30.77 | 69.21 |
| | Calc+Red | 0.09 | n/d | 30.27 | 69.64 |
| 0.5wt% Pt/TiO₂ | Fresh | 0.02 | 2.32 | 30.21 | 67.45 |
| | Calc | 0.03 | 0.39 | 30.28 | 69.30 |
| | Red | 0.07 | 0.25 | 30.24 | 69.44 |
| | Calc+Red | 0.03 | 0.21 | 30.36 | 69.40 |

3.2.4 X-ray Absorption Spectroscopy Studies

XAFS (x-ray absorption fine structure) measurements were performed for the 0.05, 0.08, 0.2 and 0.5 wt% Pt/TiO₂ ‘red’ and ‘calc+red’ catalysts. Analysis of this data included interpretation of XANES (x-ray absorption near edge structure) and EXAFS-FT (extended X-ray absorption fine structure – fourier transform) and is displayed in Figure 3.9. It is observed that the Pt L₃ edge XANES spectrum is dominated by the dipole allowed 2p_{3/2} → 5d_{5/2} transition of a core electron, this is due to sensitivity towards the oxidation and co-ordination state of Pt.⁸⁻¹¹

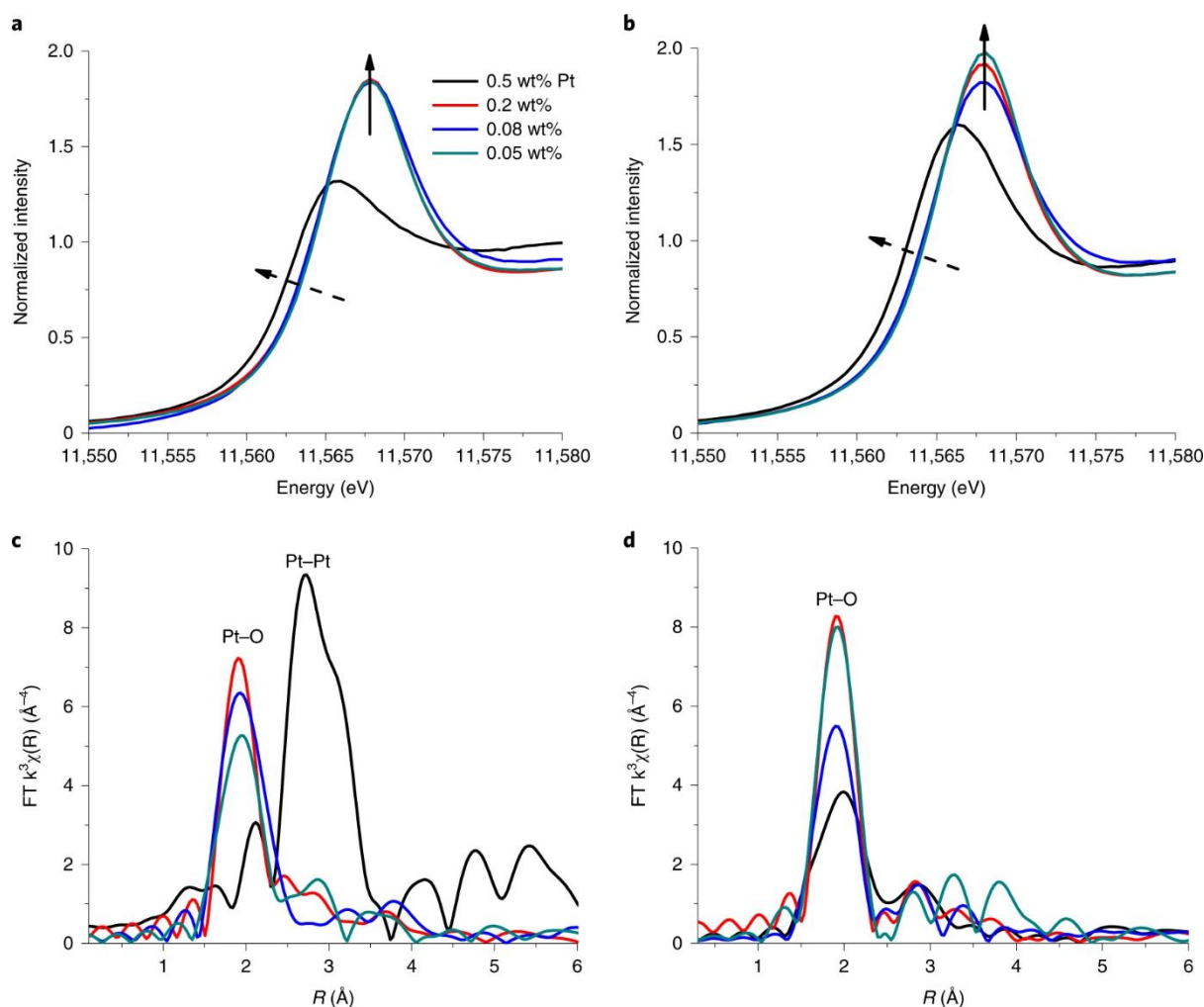


Figure 3.9: XANES spectra (a, b) Pt L3-edge XANES and (c, d) k3 EXAFS FT data recorded on Pt/TiO₂ samples after (a, c) reduction-only and (b, d) calcination + reduction.² Note: dashed arrow indicates the decrease in edge position with increased loading. The solid arrow indicates the increased rising absorption edge. Labels above the peaks indicate the scattering pairs that give rise to that contribution. All XAS measurements and analysis provided by Dr Emma Gibson (University of Glasgow) and Prof. Andrew Beale (UK Catalysis Hub).

The XANES spectra for the reduced-only catalysts, are almost identical for the three lowest Pt loadings (0.05, 0.08 and 0.2 wt%) with a maximum in the $\mu(E)$ trace seen at $\sim 11,568$ eV. However, it is important to note that the maximum of the rising absorption edge of the samples and the edge position is lower ('red'-shifted) compared to that of the reference PtO₂ phase in Figure 3.10. The 0.5wt% Pt/TiO₂ 'red' sample is particularly red-shifted, and its rising absorption edge possesses the lowest overall intensity at 11,568 eV. Previous reports have shown that these changes are affected by oxidation state and are indicative of the extent of

reduction and oxidation with all samples possessing an average Pt oxidation state $< +4$. The 0.5wt% Pt/TiO₂ catalyst was more reduced than the lower loadings (0.05, 0.08, 0.2 wt%), which the most oxidised.¹² These observations coincide with the findings of the XPS and HAADF-STEM data. This is also seen for the 'calc+red' samples however, by looking at the rising absorption edge intensity, all samples except 0.08wt% Pt/TiO₂ appear more oxidised than the reduced-only counterparts.

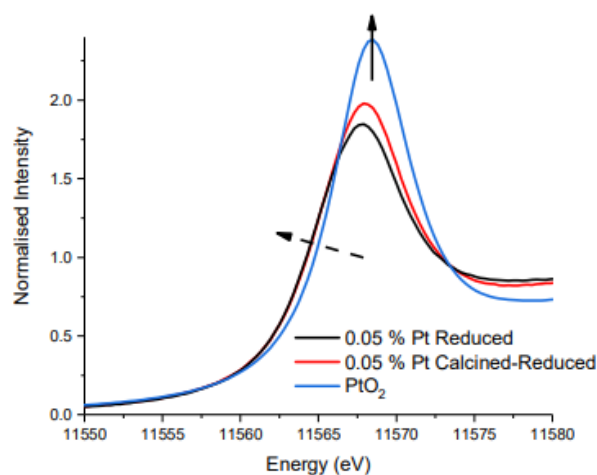


Figure 3.10: XANES spectra of the low loading 0.05wt.% Pt/TiO₂ 'red' and 'calc+red', compared to the reference spectra PtO₂.² All XAS measurements and analysis provided by Dr Emma Gibson (University of Glasgow) and Prof. Andrew Beale (UK Catalysis Hub).

The EXAFS data (Figure 3.9) for the reduced-only samples, (except 0.5wt% Pt/TiO₂ 'red') shows a strong peak at ~ 2.0 Å which can be assigned to a Pt-O distance typical of PtO₂ species (Figure 3.11) which illustrates the similarities of the Pt-O distances in these samples compared to that of PtO₂. It is notable that in comparison to the reference sample in Figure 3.11a, that the Pt-O intensity is less intense for the catalyst samples indicating that the Pt-O environments in the samples are more disordered. This is due to static disorder caused by the high dispersion of PtO₂ species across the titania support and also, as already determined by XANES analysis, a partial reduction of the Pt⁴⁺ to Pt²⁺. As a PtO reference was not available for this analysis the presence or absence of this species cannot be confirmed from this technique.

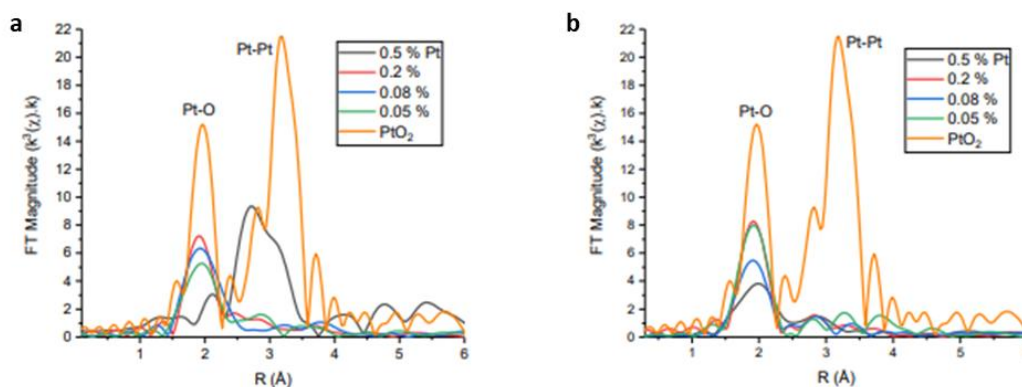


Figure 3.11: *k*₃ EXAFS FT data of Pt/TiO₂ (a) ‘red’ and (b) ‘calc + red’ catalysts, compared to the reference spectra PtO₂ (orange).² All XAS measurements and analysis provided by Dr Emma Gibson (University of Glasgow) and Dr Andrew Beale (UK Catalysis Hub).

For the 0.5 wt% Pt/TiO₂ ‘red’ sample, a broad peak at ~2.73 Å was observed, corresponding to a Pt-Pt metal bond. Further analysis of the EXAFS data for this sample suggests the existence of Pt nanoparticles ~ 1 nm in diameter,¹³ as seen in Table 3.5. 0.05 and 0.2 wt.% Pt/TiO₂ ‘red’ samples also showed weak peaks at 2.87 and 2.81 Å, which may suggest the presence of a small amount of Pt metal in these samples, in addition to the more prevalent Pt-O environment.

Table 3.5: EXAFS parameters for 0.5wt% Pt/TiO₂ ‘red’ and a Pt foil standard as determined from Pt L₃, K-edge data.² All XAS measurements and analysis provided by Dr Emma Gibson (University of Glasgow) and Prof. Andrew Beale (UK Catalysis Hub).

| Sample | Pt-Pt / Å | N | 2σ ² / Å ² | R-factor |
|-------------|-----------|-----|----------------------------------|----------|
| Pt foil | 2.76 | 12 | 0.009 | 33.33 |
| Pt (0.5wt%) | 2.76 | 7.8 | 0.009 | 41.38 |

EXAFS of the calcined+reduced samples, like the majority of the reduced samples, shows a strong peak at ~2.0 Å representing the Pt-O contribution. With the exception of the 0.2wt% Pt ‘calc+red’ sample, the intensity of this peak is inversely proportional to the Pt content. Again, this correlated with the XANES analysis which indicated more of the oxidised Pt⁴⁺ species was present with the ‘calc+red’ treatment. For the 0.05wt% Pt/TiO₂ ‘calc+red’ catalyst

the Pt-Pt scattering contributions were consistent with those seen in the PtO₂ reference sample, suggesting that some PtO₂ nanocrystallites may have evolved in this catalyst. The 0.5 wt% Pt/TiO₂ 'calc+red' sample Pt-O peak shows a noticeable skew and kurtosis towards higher Pt-O distances, this in combination with the weaker absorption edge intensity, suggests the presence of more Pt²⁺ for this catalyst. However, there was no real evidence for metallic Pt species visual inspection or when the data was fitted.

3.2.5 CO-DRIFTS (CO Diffuse Reflectance Infrared Fourier Transform Spectroscopy) and Chemisorption Analysis

CO-DRIFTS was performed on all the catalyst samples to understand the Pt metal exposure on the catalyst. By passing gaseous CO over the samples and observing the IR reflections it is possible to determine how the CO is bonding with the surface Pt and hence the properties of the Pt itself. CO-DRIFTS of the catalysts can be seen in Figure 3.12 with each loading (0.05, 0.08, 0.2 & 0.5wt% Pt) for samples exposed to 'red and 'calc+red' heat treatments.

All catalysts show a broad asymmetrical peak between 2050 – 2060 cm⁻¹ which is representative of CO linearly adsorbed on low coordination Pt edge and corner sites.^{14–18} This band is reported to be sensitive to factors such as Pt dispersion, Pt microstructure (e.g., steps, crystal face) and charge transfer in the vicinity of the Pt adsorption site. A sharp peak at ~2089 cm⁻¹, was most prominently seen for the 'calc+red' samples, however, a small peak in this vicinity (~2089 cm⁻¹) can also be observed in the majority of the 'red' catalyst samples (except for 0.5 wt% Pt/TiO₂ 'red'). This band is representative of CO adsorbed onto Pt (111) terrace sites with a coordination number of 9.^{14,16,18,19}

It is noticeable in the CO DRIFTS spectra for the Pt catalysts, that there is much lower CO adsorption in the 'red' samples compared to their 'calc+red' counterparts, in particular for the 0.2 & 0.5wt% Pt catalysts. This suggests the presence of SMSI (strong-metal-support-interaction) present in these 'red' samples.²⁰ The Pt/TiO₂ system has been reported to display this phenomenon when reduced at temperatures over 400 °C (these catalysts were reduced at 450 °C). The SMSI effect can be attributed to formation of bonds between Pt metal and cationic and atomic titania species and by coverage of the Pt particles by a layer of TiO_x which is a result of hydrogen spill-over. Supporting this, are the findings by Corma *et al.*¹ where TiO_x

coverage of Pt particles in a 0.2 wt% Pt/TiO₂ catalyst reduced at 450 °C was seen. It can therefore be deduced that the 0.2 & 0.5 ‘red’ catalysts contain Pt nanoparticles covered by a TiO_x layer. Although SMSI can be beneficial for this reaction by increasing chemoselectivity, it can also block the Pt catalytic sites causing a decrease in catalytic activity. This is reflected in the lower TOF (Figure 3.3) seen for the 0.2wt% Pt/TiO₂ ‘red’ ($1.45 \times 10^3 \text{ hr}^{-1}$) and 0.5wt% Pt/TiO₂ ‘red’ ($1.06 \times 10^3 \text{ hr}^{-1}$) compared to the other catalyst samples, including the ‘calc+red’ analogues of the higher loadings. It could therefore be suggested that the SMSI effects can be eliminated by using a sequential calcination step followed by a reduction step for these catalysts.

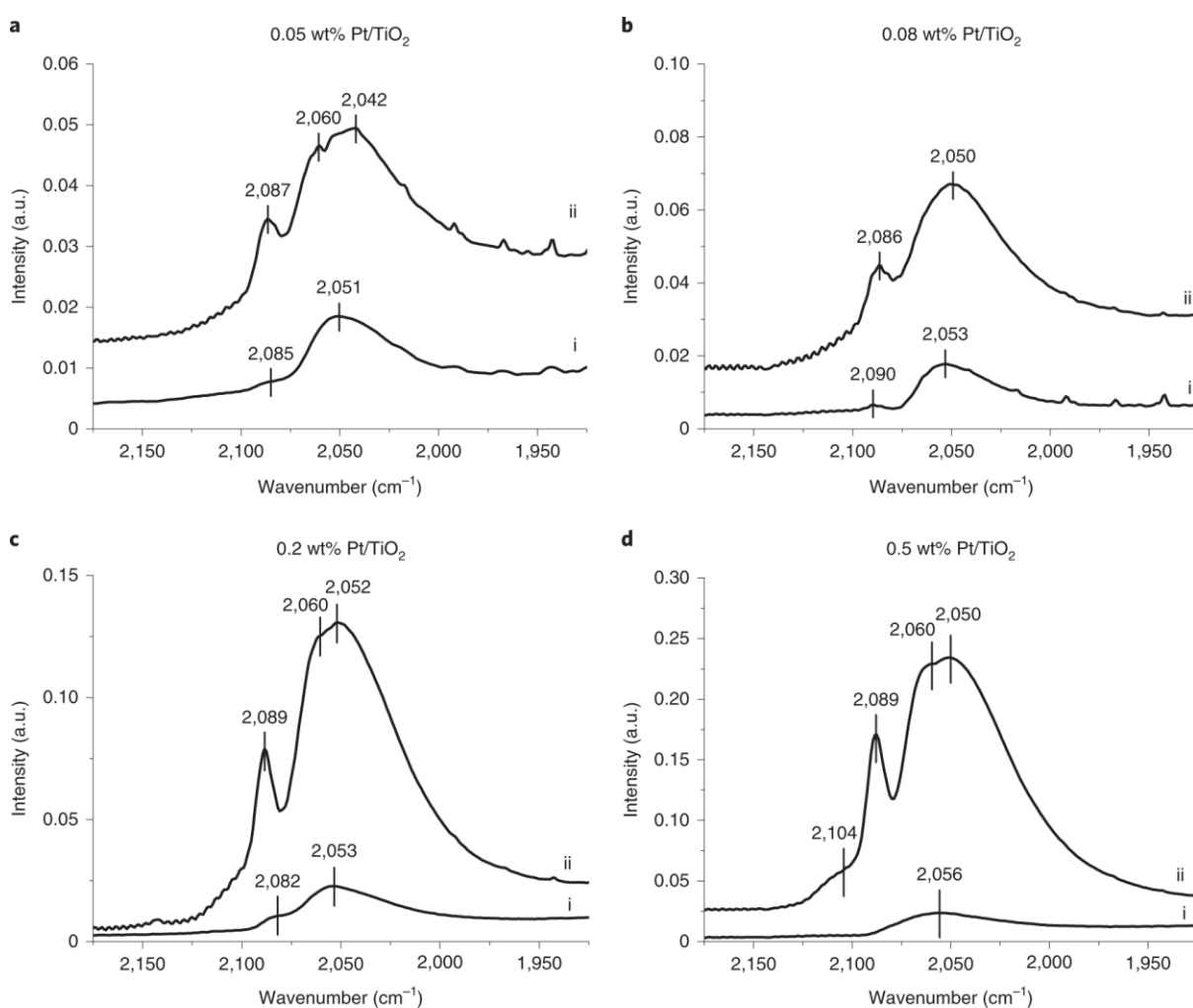


Figure 3.12: CO DRIFTS spectra (a) 0.05wt% (b) 0.08wt% (c) 0.2wt% (d) 0.5wt% Pt/TiO₂ catalysts in (i) the reduced only and (ii) calcined+reduced states.²

To visualise the Pt nanoparticles on the various Pt/TiO₂ catalysts the Mackay icosahedral model has been employed.²¹ By using the STEM images, and assuming each Pt nanoparticle is a ‘half-sphere- Mackay icosahedron with various shell numbers, it is possible to estimate the number of surface and peripheral atoms in the Pt clusters. Table 3.6 shows the values associated with the Mackay icosahedron model.

Table 3.6: The Mackay Icosahedral model.²

| Shell number | Cluster size / nm | Number of atoms in the cluster / half sphere | Number of atoms on the surface / half sphere | Number of atoms at the perimeter / half sphere |
|---------------------|------------------------------|---|---|---|
| 1 | 0.84 | 13 | 6 | 6 |
| 2 | 1.43 | 55 | 21 | 10 |
| 3 | 2.01 | 147 | 46 | 14 |
| 4 | 2.59 | 309 | 81 | 18 |

The particle size distributions from the HAADF-STEM data and the shell numbers that corresponded to the measured particles allowed cluster diameters of the Pt particles to be estimated. Based on this the proportion of peripheral sites to total numbers of Pt atoms was calculated. This was then converted to the absolute number of atoms on the surface and perimeter (peripheral sites) and in Figure 3.13 the total peripheral and total surface Pt atoms have been expressed as a weight percentage of the total catalyst mass, for the Pt/TiO₂ catalyst series.

Previous reports have demonstrated that peripheral sites at the Pt/TiO₂ interface enhance selectivity towards various selective hydrogenation reactions including the hydrogenation of crotonaldehyde and furfuraldehyde.^{22,23} Therefore, the using the calculations from the Mackay model and plotting against rate of 3-NS conversion it is possible to look for correlations between the rate and peripheral sites for this reaction also (Figure 3.13).

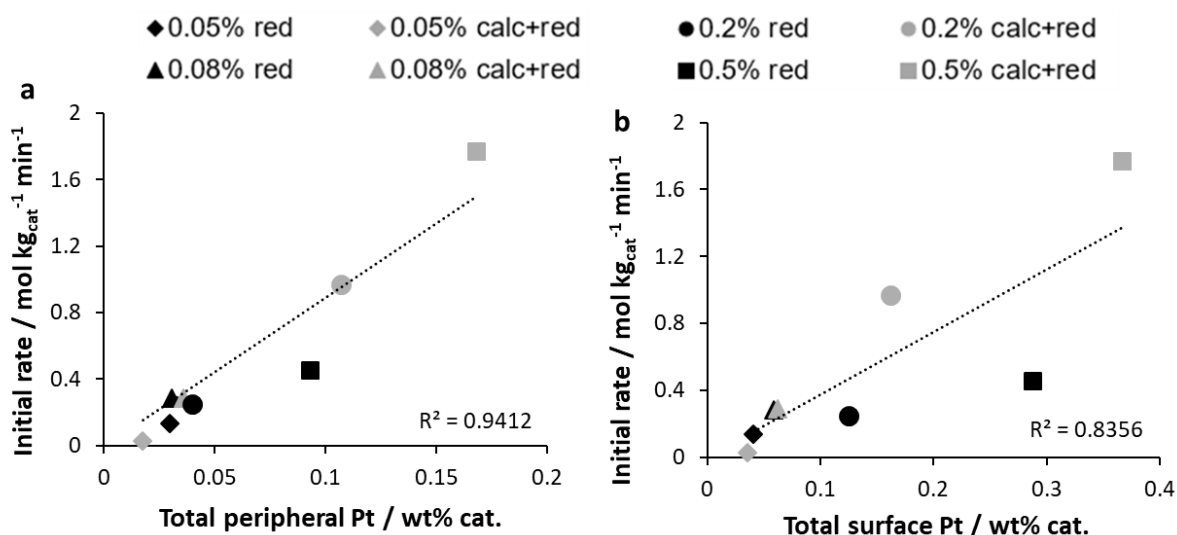


Figure 3.13: The correlation between the 3-NS initial conversion rate and Pt present in (a) peripheral sites and (b) as exposed surface atoms for the Pt/TiO₂ catalysts (where Pt loading = 0.05, 0.08, 0.2, 0.5 wt.%) as estimated from analysis of HAADF-STEM images. Courtesy of project collaborators.

It is evident that there is a significant correlation between the number of peripheral sites and the rate of 3-NS conversion ($R^2 = 0.94$), this correlation is much weaker when comparing total number of surface atoms ($R^2 = 0.79$). Clearly this suggests that the active site of the Pt nanoparticles is primarily the peripheral sites, and hence the catalysts with more peripheral sites show the higher catalytic activity. Supporting these results are the findings by Boronat *et al.*²⁴ which have shown that the peripheral sites created where Pt nanoparticles contact the TiO₂ support are integral for the selective hydrogenation of nitro-groups. This data, combined with the previous findings indicate that it is the peripheral sites rather than the Pt surface atoms that are the active site for this reaction.

It is also important to note that in catalysts where there is SMSI effect and a layer of TiO_x is covering the Pt sites (0.2wt% & 0.5wt% Pt/TiO₂ 'red'), the calculated peripheral sites do not fit as well with the general trend seen in Figure 3.13 compared with the other catalysts, this is possibly due to the TiO_x layer covering the peripheral active sites, which have been assumed to be available in the calculations done from STEM analysis.

CO chemisorption titrations were also performed on the catalysts to determine the exposed Pt metal surface area of the catalysts, as seen in Figure 3.14. Interestingly, there is a noticeable difference in the measured Pt surface area for the 0.2wt% Pt/TiO₂ 'red' and 0.5wt% Pt/TiO₂ 'red' when compared to the calculated surface Pt using the STEM data and the Mackay icosahedral model. This is likely because the Mackay model does not account for the surface Pt that is being covered by a layer of TiO_x in the catalysts affected by SMSI, whereas any overlayers present would prevent adsorption of CO therefore altering dispersion. Therefore, the surface area will be more accurate as calculated from the CO titrations. However, it would not be comparable to the peripheral site calculations (Figure 3.13) as the Mackay model does not take the SMSI factor into consideration.

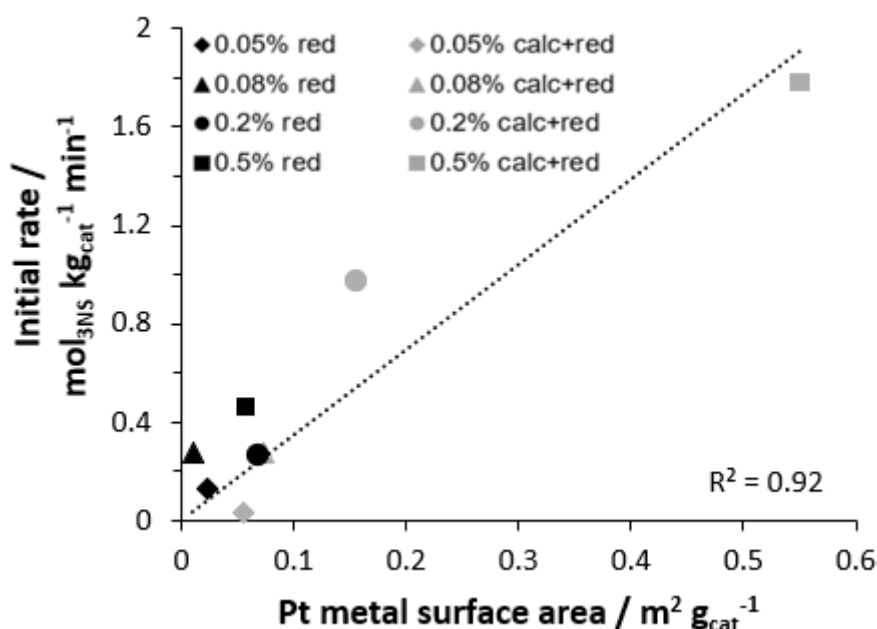


Figure 3.14: Initial rates vs platinum metal surface area determined by CO titration. Reaction conditions: 3-NS (0.2 mL), toluene (8 mL), p(H₂): 3 bar, catalyst (50 mg), temperature: 40 °C, stirring throughout.

3.3 Conclusions

These results demonstrate the importance of heat treatment regime in determining activity of Pt-based catalysts towards the chemoselective reduction of 3-nitrostyrene. A high temperature (450 °C) reductive heat treatment has been shown to induce an SMSI effect, which causes the TiO_x support to cover the Pt nanoparticles and hence the catalytic sites. However, the detrimental effects of SMSI on the activity are not seen for the corresponding 'calcined+reduced' catalyst samples, where the catalyst undergoes a high temperature calcination (450 °C) prior to the reduction step. It is suggested that this calcination step enhances anchoring of the Pt titania support and hence limits mobility of the particles during the following reduction step. This would further explain why the 0.2wt% & 0.5wt% Pt/TiO₂ 'red' catalysts had Pt particles over 2-3 nm, as for these catalysts lack of the calcination step to aid stability, has allowed Pt particles to move and agglomerate during the reduction step. Furthermore, as these catalysts (0.2wt% & 0.5wt% Pt/TiO₂ 'red') are the only catalysts that were seen to have SMSI, as implied by CO-DRIFTS analysis, the larger Pt particle size could influence a size-dependant TiO_x coverage phenomenon.

However, it can be ascertained from the results that for the higher Pt loadings (0.2 & 0.5wt%), a 'calcined+reduced' heat treatment results in more active catalysts compared to its reduced-only analogues. For the lower Pt loadings (0.05 & 0.08wt%), even in the reduced-only heat treatment STEM analysis showed a high dispersion and relative scarcity of nearby Pt neighbours, and little agglomeration of the Pt nanoparticles despite Pt mobility, rendering the calcination step unnecessary. It can be surmised from the data that those catalysts with Pt particles around 1 nm and those without SMSI effects causing TiO_x surface coverage, demonstrated enhanced catalytic performance towards this reaction. This resulted in a highly active 0.2wt% Pt/TiO₂ 'calc+red' catalyst.

3.4 References

- 1 A. Corma, P. Serna, P. Concepción and J. J. Calvino, *J. Am. Chem. Soc.*, 2008, **130**, 8748–8758.
- 2 M. Macino, A. J. Barnes, S. M. Althahban, R. Qu, E. K. Gibson, D. J. Morgan, S. J. Freakley, N. Dimitratos, C. J. Kiely, X. Gao, A. M. Beale, D. Bethell, Q. He, M. Sankar and G. J. Hutchings, *Nat. Catal.*, 2019, **2**, 873–881.
- 3 G. J. Kim, D. W. Kwon and S. C. Hong, *J. Phys. Chem. C*, 2016, **120**, 17996–18004.
- 4 J. Matos, L. K. Ono, F. Behafarid, J. R. Croy, S. Mostafa, A. T. Delariva, A. K. Datye, A. I. Frenkel and B. Roldan Cuenya, *Phys. Chem. Chem. Phys.*, 2012, **14**, 11457–11467.
- 5 R. Zimmermann, P. Steiner, R. Claessen, F. Reinert, S. Hufner, P. Blaha and P. Dufek, *J. Phys. Condens. Matter*, 1999, **11**, 1657.
- 6 A. V Naumkin, A. Kraut-Vass, S. W. Gaarenstroom and C. . Powell, *NIST X-ray Photoelectron Spectrosc. Database 20, Version 4.1(National Inst. Stand. Technol. 2017)*.
- 7 E. Janin, M. Björkqvist, T. M. Grehk, M. Göthelid, C. M. Pradier, U. O. Karlsson and A. Rosengren, *Appl. Surf. Sci.*, 1996, **99**, 371–378.
- 8 J. E. Penner-Hahn, *Coord. Chem. Rev.*, 1999, **190–192**, 1101–1123.
- 9 M. Brown, R. E. Peierls and E. A. Stern, *Phys. Rev. B*, 1977, **15**, 738–744.
- 10 F. De Groot, *Chem. Rev.*, 2001, **101**, 1779–1808.
- 11 D. . Koningsberger and R. Prins, *X-Ray Absorption: Principles, Applications, Techniques of EXAFS, SEXAFS and XANES*, Wiley, 1988.
- 12 H. Yoshida, S. Nonoyama, Y. Yawawa and T. Hattori, *Physi. Scr.*, 2005, **2005**, 813.
- 13 A. M. Beale and B. M. Weckhuysen, *Phys. Chem. Chem. Phys.*, 2010, **12**, 5562–5574.
- 14 A. Corma, P. Serna, P. Concepción and J. J. Calvino, *J. Am. Chem. Soc.*, 2008, **130**, 8748–8753.
- 15 J. Raskó, *J. Catal.*, 2003, **217**, 478–486.
- 16 S. Zafeiratos, G. Papakonstantinou, M. M. Jacksic and S. G. Neophytides, *J. Catal.*, 2005, **232**, 127–136.
- 17 L. DeRita, S. Dai, K. Lopez-Zepeda, N. Pham, G. W. Graham, X. Pan and P. Christopher, *J. Am. Chem. Soc.*, 2017, **139**, 14150–14165.
- 18 H. V. Thang, G. Pacchioni, L. DeRita and P. Christopher, *J. Catal.*, 2018, **367**, 104–114.
- 19 A. Y. Stakheev, E. S. Shpiro, O. P. Tkachenko, N. I. Jaeger and G. Schulz-Ekloff, *J. Catal.*,

- 1997, **169**, 382–388.
- 20 S. J. Tauster, S. C. Fung and R. L. Garten, *J. Am. Chem. Soc.*, 1978, **100**, 170–175.
- 21 E. Macia, J.-M. Dubois and P. A. Thiel, *Ullmann 's Encyclopedia of Industrial Chemistry: Quasicrystals*, Wiley-VCH Verlag GmbH & Co. KGaA, 2008.
- 22 M. A. Vannice and B. Sen, *J. Catal.*, 1989, **115**, 65–78.
- 23 L. R. Baker, G. Kennedy, M. Van Spronsen, A. Hervier, X. Cai, S. Chen, L. W. Wang and G. A. Somorjai, *J. Am. Chem. Soc.*, 2012, **134**, 14208–14216.
- 24 M. Boronat and A. Corma, *Langmuir*, 2010, **26**, 16607–16614.

Chapter 4: Enhancing catalytic performance of AuPd catalysts towards the direct synthesis of H₂O₂ through incorporation of base metals.

4.1 Introduction

The direct synthesis of H₂O₂ is an important reaction in the pursuit of green chemistry. H₂O₂ has many applications as a green oxidant as its only by-product is water.^{1,2} The largest industrial production of H₂O₂ is made by the anthraquinone process, which has environmental and economic concerns.¹⁻³ Direct synthesis from its constituent gases, H₂ and O₂ is therefore an attractive process as it overcomes many of the concerns from alternative methods. Figure 4.1 shows the direct synthesis of H₂O₂ and side reactions with their respective enthalpies of reaction.¹

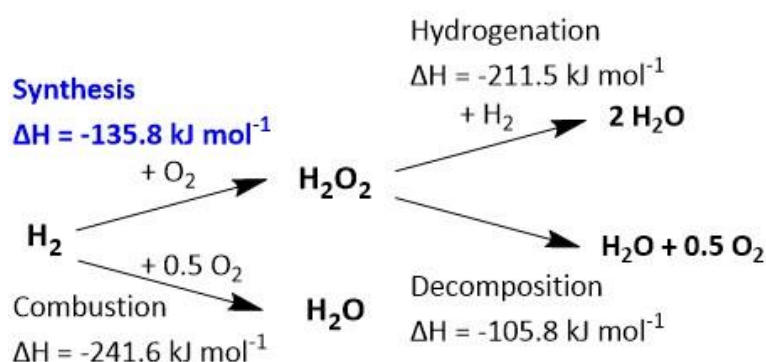


Figure 4.1: The direct synthesis of hydrogen peroxide and subsequent hydrogenation and degradation reactions, including the enthalpies of each reaction.

The use of supported monometallic Pd and bimetallic AuPd catalysts for the direct synthesis of H₂O₂ are well documented, with the AuPd catalyst showing that the alloying of these metals results in a synergistic effect that far improves the activity, selectivity and stability of the respective monometallics.^{2,4-9} There have also been studies using a number of non-precious transition metals (such as Ni, Zn, Cu, In, Co, Ga and Sn)¹⁰⁻¹⁶ and precious metals (including Pt, Ag and Ru)¹⁷⁻¹⁹ as a secondary metal alloyed with Pd which in many cases can show enhanced catalytic effects from the Pd-only analogue. It has been proposed that the enhancement of catalyst performance for many of these catalysts, especially in the case of AuPd, is due to

electronic modification of Pd species and the isolation and coverage of neighbouring Pd sites that promote O-O bond cleavage that result in the formation of H₂O.²⁰ Notably, in the cases where Cu was used in conjunction with Pd there was a clear inhibition of activity towards H₂O₂ synthesis,^{10,11} and computational studies suggested that this was due to the thermodynamically unfavourable formation of the hydroperoxy (OOH*) species over this metal composition.²¹

There has been more recent work on the incorporation of a third metal into AuPd supported catalysts, namely the noble metals Pt and Ru.^{17,22-24} Of particular interest is the work by Gong *et al*²⁴ who found that incorporation of very low levels of Pt (1wt% Au₁Pd₁Pt_{0.1}/TiO₂) substantially enhanced the activity towards the synthesis of H₂O₂, and as the Pt doping increased (1wt% Au₁Pd₁Pt₁/TiO₂) the activity decreased. These authors also employed a sol-immobilisation catalyst preparation methodology, this method enables enhanced control of nanoparticle size and uniformity when compared to other commonly used preparation techniques such as impregnation.^{25,26}

The aim of this chapter is to develop upon the incorporation of low level doping of a third metal into AuPd titania supported catalysts to enhance the direct synthesis of H₂O₂, with the focus on non-precious transition metals due to their abundance and low cost.

4.2 Results and Discussion

4.2.1 Investigating the effect of tertiary metal incorporation on the direct synthesis of H₂O₂.

An initial testing of monometallic 1wt% Au/TiO₂ and 1wt% Pd/TiO₂ catalysts for both H₂O₂ direct synthesis and degradation was performed to investigate the effect of forming metallic alloys, and how this enhances catalytic activity (compared to the low activity of the monometallic analogues). Catalysts were prepared by sol-immobilisation and then calcined in order to increase anchoring of the nanoparticles to the support to prevent leaching of the metals into the reaction solution. Table 4.1 shows the results of the mono- and bi-metallic catalyst testing for reference.

Table 4.1: Direct synthesis and degradation of H₂O₂ by monometallic 1wt% Au/TiO₂ and 1wt% Pd/TiO₂.

| Catalyst | Synthesis | Degradation |
|----------------------------|--|-------------|
| | moles _{H₂O₂} kg _{cat} ⁻¹ hr ⁻¹ | |
| 1wt% Au/TiO ₂ | 3 | 3 |
| 1wt% Pd/TiO ₂ | 42 | 41 |
| 1wt% AuPd/TiO ₂ | 61 | 215 |

H₂O₂ direct synthesis conditions: 0.5 h, 2 °C, P(5% H₂/CO₂) = 420 psi, P(25% O₂/CO₂) = 160 psi, 0.01 g catalyst, 2.9 g water, 5.6 g methanol, 1200 rpm. Degradation conditions: 0.5 h, 2 °C, P(5% H₂/CO₂) = 420 psi, 0.01 g catalyst, 0.68 g H₂O₂ (50 wt%), 2.22 g water, 5.6 g methanol, 1200 rpm. Catalysts prepared by sol-immobilisation and calcined (static air, ramp 10 °C min⁻¹, 400 °C, 3 h).

As reported in Table 4.1, there is little activity seen over a monometallic Au catalyst, for both the direct synthesis and degradation of H₂O₂ (3 mol_{H₂O₂}kg_{cat}⁻¹h⁻¹ for both reactions). The monometallic Pd catalyst shows improved activity compared to the monometallic Au catalyst (synthesis activity 42 and 3 moles_{H₂O₂} kg_{cat}⁻¹ hr⁻¹ respectively). The alloying of Au and Pd and resulting formation of bimetallic alloys improved activity compared to the monometallics, with a synthesis rate of 61 moles_{H₂O₂} kg_{cat}⁻¹ hr⁻¹ observed. This enhanced activity of the bimetallic towards H₂O₂ synthesis has been well reported and is due to a synergistic effect

between the alloying of the Au and Pd in the bimetallic.⁶ Presence of the Au results in electronic modification of the Pd species and improved dispersion.²⁰

Developing on previous work which identified that the incorporation of small quantities of Pt into a AuPd catalyst can enhance catalytic activity towards the direct synthesis of H₂O₂, within this work a series of transition metals (X = Ni, Zn, Cu, In, Co, Ga, Sn, Pt) have been incorporated in an AuPd/TiO₂ catalyst by a sol-immobilisation methodology.²⁴ These transition metals have been selected due to their previous utilisation as a secondary metal modifier for Pd-based catalysts in the direct synthesis of H₂O₂¹⁰⁻¹⁶ and the results are shown in Figure 4.2.

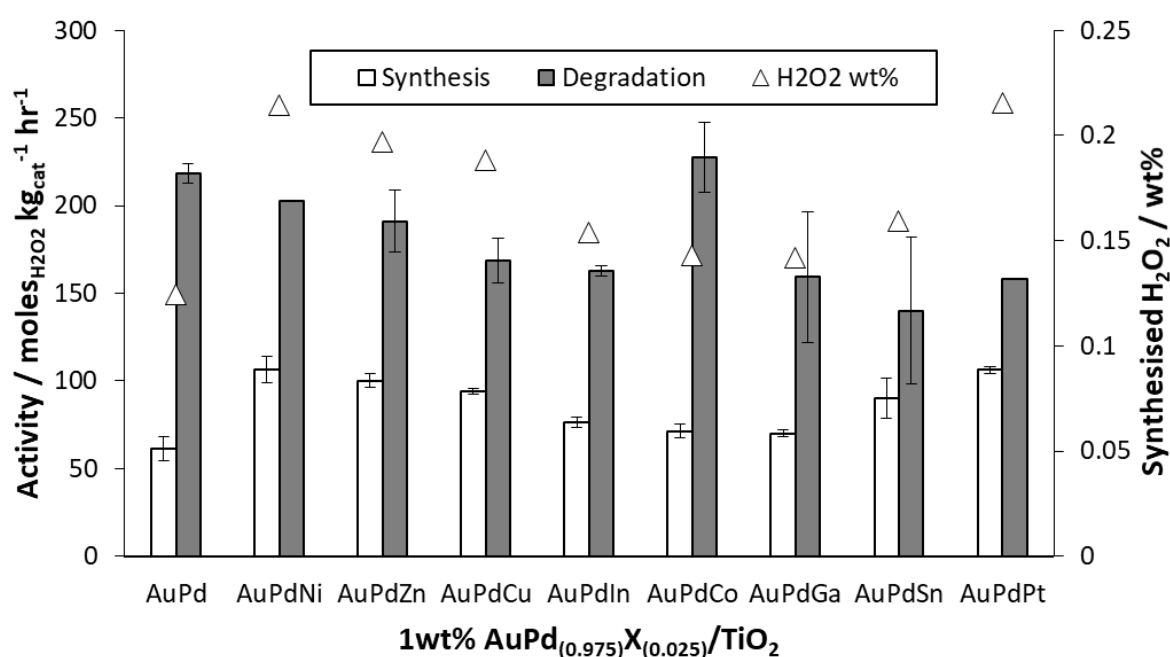


Figure 4.2: Incorporation of different tertiary metals (Ni, Zn Cu, In, Co, Ga, Sn or Pt) to a 1wt% AuPd/TiO₂ catalyst for the direct hydrogen peroxide synthesis and degradation. Concentration of H₂O₂ (wt %) synthesised is calculated from the directs synthesis reaction. H₂O₂ direct synthesis conditions: 0.5 h, 2 °C, P(5% H₂/CO₂) = 420 psi, P(25% O₂/CO₂) = 160 psi, 0.01 g catalyst, 2.9 g water, 5.6 g methanol, 1200 rpm. Degradation conditions: 0.5 h, 2 °C, P(5% H₂/CO₂) = 420 psi, 0.01 g catalyst, 0.68 g H₂O₂ (50 wt%), 2.22 g water, 5.6 g methanol, 1200 rpm. Catalysts tested are 1wt% AuPd_(0.975)X_(0.025)/TiO₂ prepared by sol-immobilisation and calcined (static air, ramp 10 °C min⁻¹, 400 °C, 3 h).

Table 4.2: Incorporation of tertiary metals (Ni, Zn Cu, In, Co, Ga, Sn or Pt) to a 1wt% AuPd/TiO₂ catalyst for the direct hydrogen peroxide synthesis. H₂O₂ direct synthesis conditions: 0.5 h, 2 °C, P(5% H₂/CO₂) = 420 psi, P(25% O₂/CO₂) = 160 psi, 0.01 g catalyst, 2.9 g water, 5.6 g methanol, 1200 rpm.

| Catalyst 1wt% AuPd _(0.975) X _(0.025) /TiO ₂ | H ₂ O ₂ / wt% | H ₂ O ₂ / x10 ⁻⁴ mol |
|---|-------------------------------------|---|
| AuPd | 0.125 | 3.11 |
| AuPdNi | 0.215 | 5.36 |
| AuPdZn | 0.197 | 4.92 |
| AuPdCu | 0.188 | 4.69 |
| AuPdIn | 0.154 | 3.85 |
| AuPdCo | 0.143 | 3.57 |
| AuPdGa | 0.142 | 3.54 |
| AuPdSn | 0.159 | 3.97 |
| AuPdPt | 0.216 | 5.39 |

In keeping with previous observations of low level Pt doping enhancing catalytic activity, the H₂O₂ synthesis activity of the 1wt% AuPd_(0.975)Pt_(0.025)/TiO₂ catalyst (106 mol_{H₂O₂} kg_{cat}⁻¹ h⁻¹), is significantly improved compared to the bimetallic analogue (61 mol_{H₂O₂} kg_{cat}⁻¹ h⁻¹). By incorporating into the catalysts various transition metals, that are known to alloy with Pd and Au, it was found that similar improvements in activity comparable to those offered by a trimetallic AuPdPt catalyst can be achieved. All trimetallic catalysts studied improved on the synthesis activity of the AuPd bimetallic, however, of the trimetallics AuPdGa and AuPdCo catalysts gave the lowest activities (70 and 71 mol_{H₂O₂} kg_{cat}⁻¹ h⁻¹ respectively) and AuPdPt and AuPdNi trimetallics gave the highest activities (106 and 107 mol_{H₂O₂} kg_{cat}⁻¹ h⁻¹ respectively). Additionally, (with the exception of 1wt% AuPd_(0.975)Co_(0.025)/TiO₂) all trimetallic catalysts gave lower rates of H₂O₂ degradation compared to the bimetallic analogue (1wt% AuPd/TiO₂). This suggests that the addition of the dopant metal may favour H₂O₂ synthesis and is hence resulting in more selective catalysts.

Notably, there are three trimetallic catalysts: 1wt% AuPd_(0.975)Ni_(0.025)/TiO₂ (107 mol_{H₂O₂} kg_{cat}⁻¹ h⁻¹), 1wt% AuPd_(0.975)Zn_(0.025)/TiO₂ (100 mol_{H₂O₂} kg_{cat}⁻¹ h⁻¹) and 1wt% AuPd_(0.975)Cu_(0.025)/TiO₂ (94 mol_{H₂O₂} kg_{cat}⁻¹ h⁻¹) that have activities in the same range as the AuPdPt (106 mol_{H₂O₂} kg_{cat}⁻¹ h⁻¹).

h^{-1}) trimetallic catalyst. There have been studies successfully demonstrating the efficacy of alloying both Ni and Zn with Pd for H_2O_2 synthesis, however, it has previously been shown that Cu in combination with AuPd and Pd has inhibited H_2O_2 synthesis activity.^{10,11} In particular, Joshi *et al.*²¹ have performed DFT studies indicating that the formation of the intermediate hydroperoxy (OOH^*) species and H_2O_2 , are thermodynamically unfavourable over Cu-containing supported catalysts. However, these previous studies were conducted with much higher concentrations of Cu to that used in this work.

By measuring the leaching of the metals into the reaction solution of H_2O_2 synthesis, we can determine the stability of the metals onto the TiO_2 support (Table 4.3). It has been shown that the presence of colloidal Pd in a reaction system can contribute to the reaction.^{27,28} This would result in potential changes in activity for those catalysts that had higher leaching. Additionally, if the leached metal is contributing to the activity of the catalyst, its loss upon reuse will affect the reusability of the catalyst. The Au on the catalyst is particularly stable with no observed leaching and Pd only shows relatively low levels of leaching, with a maximum of 4.55% seen from 1wt% $\text{AuPd}_{(0.975)}\text{Co}_{(0.025)}/\text{TiO}_2$. The higher leaching of the Co catalyst corresponds with this catalyst having the lowest synthesis activity ($71 \text{ mol}_{\text{H}_2\text{O}_2} \text{ kg}_{\text{cat}}^{-1} \text{ h}^{-1}$) of the trimetallic series, and the highest rate of H_2O_2 degradation ($228 \text{ mol}_{\text{H}_2\text{O}_2} \text{ kg}_{\text{cat}}^{-1} \text{ h}^{-1}$). Interestingly the 1wt% $\text{AuPd}_{(0.975)}\text{Pt}_{(0.025)}/\text{TiO}_2$ catalyst is the only one to show any Au leaching, one explanation could be because of the formation of non-alloyed particles that are due to Pt not being completely miscible with Au. However, to know if any colloidal system is contributing to the reaction further tests of the filtered post reaction solutions would need to be performed to see if any further reaction is caused from the levels of leaching detected from these catalysts. Due to the low levels of the tertiary metal incorporated into the catalyst, any leaching is below the detection limits of the instrument.

Table 4.3: Metal leaching and metal speciation of 1wt% AuPd_(0.975)X_(0.025)/TiO₂ (where X = Ni, Zn, Cu, In, Co, Ga, Sn, Pt) catalysts. Leaching was measured by filtering the reaction solution from the direct synthesis of H₂O₂ (0.5 h) and analysing by ICP-MS. Metal speciation is analysed by XPS of fresh (unused) catalyst samples calculated using fittings by Dr David Morgan.

| Catalyst (AuPdX) for: 1wt% AuPd _(0.975) X _(0.025) /TiO ₂ | Metal leaching / % (ppb) | | Metal Speciation | |
|--|-----------------------------|-------------|------------------|-----------------------------------|
| | Au | Pd | Au:Pd | Pd ²⁺ :Pd ⁰ |
| AuPd | 0 | 1.90 (4.8) | 1 : 1.8 | 1 : 0.7 |
| AuPdNi | 0 | 2.52 (6.3) | 1 : 1.5 | 1 : 1.2 |
| AuPdZn | 0 | 1.74 (4.4) | 1 : 2.4 | 1 : 1.2 |
| AuPdCu | 0 | 0.42 (1.1) | 1 : 2.2 | 1 : 1.6 |
| AuPdIn | 0 | 2.52 (6.3) | 1 : 1.8 | 1 : 1.2 |
| AuPdCo | 0 | 4.55 (11.4) | 1 : 2.3 | 1 : 1.5 |
| AuPdGa | 0 | 2.00 (5.0) | 1 : 1.9 | 1 : 1.1 |
| AuPdSn | 0 | 0.00 (0.0) | - | - |
| AuPdPt | 0.25 | 0.46 (1.2) | - | - |

H₂O₂ direct synthesis conditions: 2 °C, P(5% H₂/CO₂) = 420 psi, P(25% O₂/CO₂) = 160 psi, 0.01 g catalyst, 2.9 g water, 5.6 g methanol, 1200 rpm. Catalysts prepared by sol-immobilisation and calcined (static air, ramp 10 °C min⁻¹, 400 °C, 3 h). Leaching of dopant metal X is BDL (below detection limit).

For all catalysts synthesised the theoretical Au: Pd ratio is 1:1 (mol/mol), however XPS analysis (Table 4.3) shows a higher abundance of Pd on the surface of all catalysts. This could potentially indicate coverage of some Au sites by Pd in a surface enriched Pd surface, probably an effect of the thermal treatment of the catalyst. With the exception of the bimetallic 1wt% AuPd/TiO₂ catalyst, all trimetallic catalysts have larger quantities of the Pd⁰ species on the catalyst surface. Hence, the addition of even small concentrations of the tertiary metal results in a substantial shift of Pd to the reduced species (Pd⁰).

The abundance of the reduced Pd in the trimetallic catalysts (compared to the bimetallic) may be surprising, since all catalysts underwent an oxidative heat treatment (400 °C, 3 h, static air) prior to use. However, this is in line with previous studies into AuPdPt supported trimetallics where again, the addition of Pt was found to be a key modifier of Pd oxidation state.²⁴ It is well established that the Pd oxidation state is a key factor in H₂O₂ synthesis reactions. Mixed

Pd^{2+} and Pd^0 species are known to offer enhanced performance compared to those with a majority of either Pd oxidation state.^{24,29} From these results, it is evident that there is a correlation between catalytic activity and the shift in Pd speciation towards the reduced species. To highlight this, both AuPd and AuPdGa have low catalytic activities (61 and 70 $\text{mol}_{\text{H}_2\text{O}_2} \text{kg}_{\text{cat}}^{-1} \text{h}^{-1}$ respectively) and also have the smallest Pd^0 content of the catalyst series.

In order to determine the formation of alloys in the catalysts, bimetallic colloids of all the dopant metals with Au were analysed by UV-vis. Gold monometallic and bimetallic colloids were produced (prior to immobilisation on a support) and analysed by UV-vis before and after reduction with NaBH_4 . AuCl_4^- has a LSPR (localised surface plasmon resonance) peak that appears at around 300 nm on a UV-vis spectrum, whereas reduced Au has a peak at around 520 nm, indicating the presence of Au nanoparticles. However, if an alloy is formed with another metal during the reduction step, the plasmonic peak for Au will not be present, hence when this peak is absent an alloy has been formed. All colloids prior to reduction were analysed (in the presence of the PVA (polyvinyl alcohol) stabiliser as in the sol-immobilisation methodology) by UV-vis and all samples showed the LSPR AuCl_4^- peak.

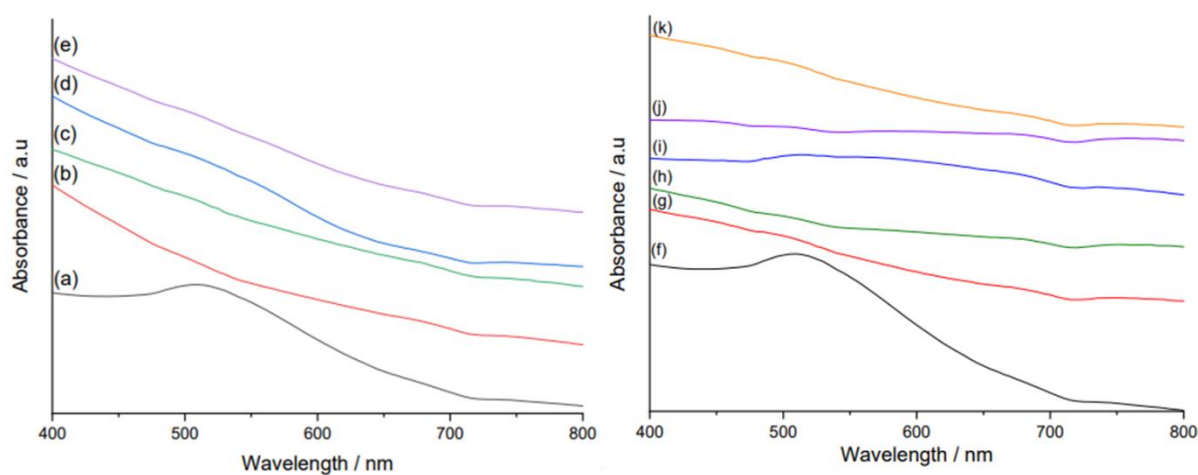


Figure 4.3: Representative UV-vis spectra from aqueous sol-immobilisation prepared bi-metallic Au based reduced colloids. (a) Au (b) AuPd (c) AuCu (d) AuZn (e) AuNi (f) Au (g) AuCo (h) AuPt (i) AuGa (j) AuIn (k) AuSn.³⁰ The absence of the Au plasmon peak (approx. 520 nm) in the bimetallic colloids is indicative of alloy formation.

Figure 4.3 shows that upon reduction with NaBH₄ no (or small) plasmonic peak was visible for the bimetallic solutions and we can therefore deduce that a bimetallic alloy can be formed with Au. Pd alloys readily with Au (Figure 4.3) and has been documented in previous work.^{2,4-9}

Unfortunately, it is not possible to prove the formation of a trimetallic alloy by this method as the plasmonic peak would not be present if only bimetallic alloys were formed between AuPd and AuX (where X = Ni, Zn, Cu, In, Co, Ga, Sn, Pt). However, the metals that have been chosen as dopants in this catalyst series have been widely reported to form a bimetallic alloy with Pd.¹⁰⁻¹⁶ In future work EDX analysis could be employed to prove the formation of trimetallic alloys, however for the catalysts in this work the third metal was not detected by the microscopy studies due to the low loading, a similar issue was had by Gong *et al*²⁴ with the low loading Pt doping in their 1wt% Au₁Pd₁Pt_{0.1}/TiO₂ trimetallic catalyst.

4.2.2 Optimising the tertiary metal loading in AuPdNi, AuPdZn and AuPdCu supported catalysts

By selecting the three most promising transition metal incorporated trimetallic catalysts, the effect of the tertiary metal loading was investigated. A series of AuPdNi, AuPdZn and AuPdCu catalysts supported on titania(P25) were synthesised, a range of loadings (0.0125 – 0.1 wt%) were chosen for the dopant metal, with a total metal loading (including Au: Pd with a ratio of 1:1) of 1wt%. The activities for H₂O₂ synthesis and degradation are shown for each loading in Figure 4.4.

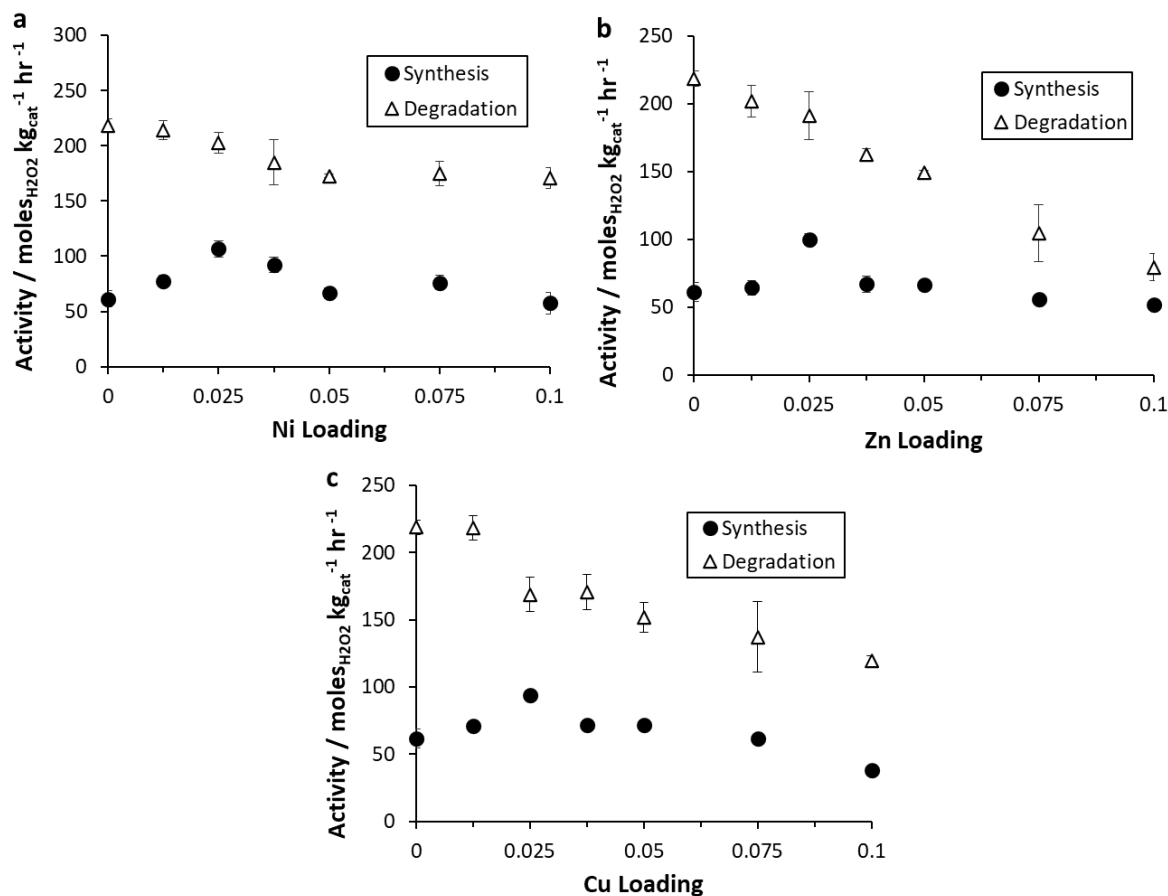


Figure 4.4: Effect of incorporating different volumes of a tertiary metals (Ni, Zn or Cu) to a 1wt% AuPd/TiO₂ catalyst on the direct hydrogen peroxide synthesis and degradation (a) 1wt% AuPd_{(1-x)Ni_(x)}/TiO₂ (b) 1wt% AuPd_{(1-x)Zn_(x)}/TiO₂ (c) 1wt% AuPd_{(1-x)Cu_(x)}/TiO₂ (where $x = 0, 0.0125, 0.025, 0.0375, 0.05, 0.075, 0.1$ wt%). H₂O₂ direct synthesis conditions: 0.5 h, 2 °C, P(5% H₂/CO₂) = 420 psi, P(25% O₂/CO₂) = 160 psi, 0.01 g catalyst, 2.9 g water, 5.6 g methanol, 1200 rpm. Degradation conditions: 0.5 h, 2 °C, P(5% H₂/CO₂) = 420 psi, 0.01 g catalyst, 0.68 g H₂O₂ (50 wt%), 2.22 g water, 5.6 g methanol, 1200 rpm. Peroxide concentration measured by titration with Ce⁴⁺. Catalysts tested are 1wt% AuPd_{(0.975)X_(0.025)}/TiO₂ prepared by sol-immobilisation and calcined (static air, ramp 10 °C min⁻¹, 400 °C, 3 h).

In the case of all three (Ni, Cu and Zn) catalyst series, optimum metal doping of the tertiary metal was found to be 0.025 wt% as this most greatly enhanced the catalytic activity of the synthesis of H₂O₂. Although that small addition of the dopant metal until this point increased the synthesis activity, it was observed that over 0.025wt% of Ni, Cu and Zn, further addition of the tertiary metals caused a decrease in activity. At a dopant metal loading of 0.1 wt% all three catalyst compositions (1wt% AuPd_{(0.9)Ni_(0.1)}/TiO₂, 1wt% AuPd_{(0.9)Zn_(0.1)}/TiO₂ and 1wt%

AuPd_(0.9)Cu_(0.1)/TiO₂) gave activities (57, 52 and 38 mol_{H₂O₂} kg_{cat}⁻¹ h⁻¹ respectively) lower than that seen for the bimetallic catalyst (61 mol_{H₂O₂} kg_{cat}⁻¹ h⁻¹). And of these catalysts series the most noticeable drop in activity is seen for Cu. This is not surprising as previous studies with much higher levels of Cu in the catalyst have shown Cu inhibiting activity towards this reaction.^{10,11} What this work has therefore shown is that there is clearly a very small range over which Cu incorporation may enhance catalytic activity towards H₂O₂ synthesis, before the activity is hindered, as it has previously been found to do at the higher quantities that have been tested. It is also notable that for all catalyst series studied as the level of the tertiary dopant metal increases, the rate of degradation decreases.

Analysis of the trimetallic catalysts series was performed by XPS to determine how the loading of the tertiary metal is affecting Pd speciation and how this correlates with catalytic activity. As seen in Figure 4.5 for the 1wt% AuPd_(x)Ni_(1-x)/TiO₂, 1wt% AuPd_(x)Zn_(1-x)/TiO₂ and 1wt% AuPd_(x)Cu_(1-x)/TiO₂ catalyst series, the Pd species in all catalysts are comprised of a mixture of Pd⁰ and Pd²⁺.

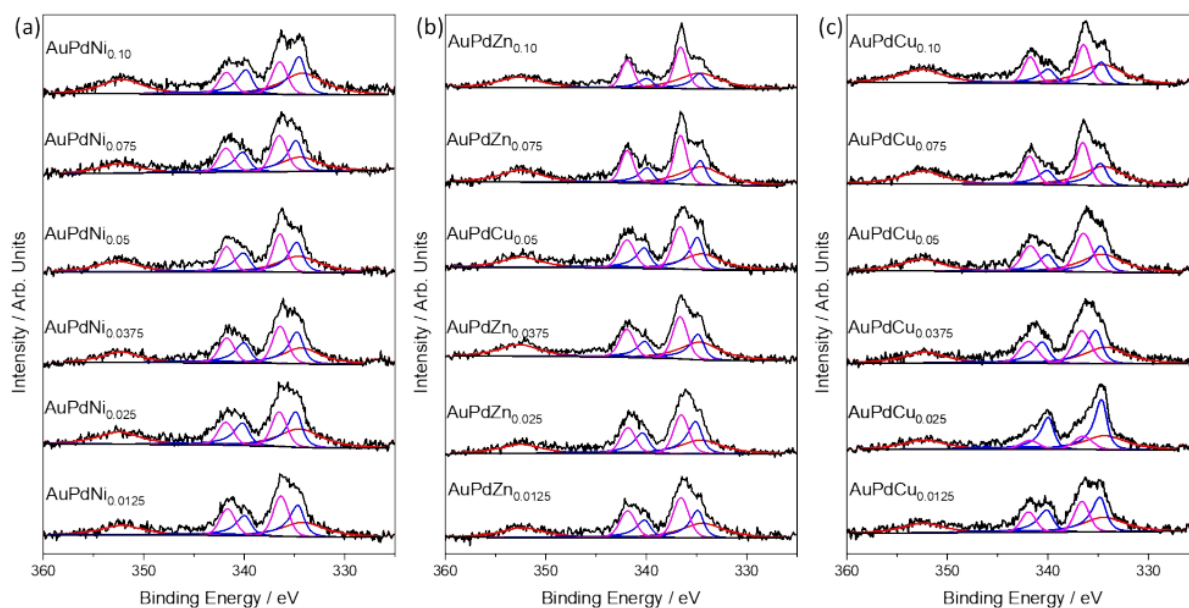


Figure 4.5: XPS spectra of Pd(3d) regions for as-prepared (a) 1wt% AuPd_(x)Ni_(1-x)/TiO₂ (b) 1wt% AuPd_(x)Zn_(1-x)/TiO₂ and (c) 1wt% AuPd_(x)Cu_(1-x)/TiO₂ catalysts as a function of tertiary metal concentration.³⁰ Key: Au(4d) (red), Pd⁰ (blue), Pd²⁺ (magenta). Catalysts prepared by sol-immobilisation and calcined (static air, ramp 10 °C min⁻¹, 400 °C, 3 h).

XPS analysis (Table 4.4) showed that the addition of minute concentrations of the tertiary metal has resulted in a substantial shift of the Pd species towards Pd²⁺, which is known to offer lower rates of H₂O₂ synthesis than the Pd⁰ species.³¹ This shift is particularly noticeable for the AuPdZn and AuPdCu series. This correlates well with the results showing H₂O₂ synthesis activity decreasing with an increased concentration of the tertiary metal.

Table 4.4: Metal speciation from XPS analysis of the freshly prepared 1wt% AuPd_(x)Ni_(1-x)/TiO₂, 1wt% AuPd_(x)Zn_(1-x)/TiO₂ and 1wt% AuPd_(x)Cu_(1-x)/TiO₂ catalysts. Catalysts prepared by sol-immobilisation and calcined (static air, ramp 10 °C min⁻¹, 400 °C, 3 h). Calculated using fittings by Dr David Morgan.

| Ni, Zn, Cu loading / wt% | AuPdNi | | AuPdZn | | AuPdCu | |
|-----------------------------|---------|-----------------------------------|---------|-----------------------------------|---------|-----------------------------------|
| | Au:Pd | Pd ²⁺ :Pd ⁰ | Au:Pd | Pd ²⁺ :Pd ⁰ | Au:Pd | Pd ²⁺ :Pd ⁰ |
| 0.0125 | 1 : 2.2 | 1 : 1.0 | 1 : 2.1 | 1 : 0.9 | 1 : 2.2 | 1 : 2.0 |
| 0.025 | 1 : 1.5 | 1 : 1.2 | 1 : 2.4 | 1 : 1.2 | 1 : 2.2 | 1 : 1.6 |
| 0.0375 | 1 : 2.1 | 1 : 0.9 | 1 : 1.6 | 1 : 1.0 | 1 : 1.8 | 1 : 1.4 |
| 0.05 | 1 : 1.6 | 1 : 0.9 | 1 : 2.0 | 1 : 1.0 | 1 : 1.8 | 1 : 0.9 |
| 0.075 | 1 : 1.8 | 1 : 0.8 | 1 : 1.6 | 1 : 0.9 | 1 : 1.4 | 1 : 0.9 |
| 0.1 | 1 : 1.3 | 1 : 1.3 | 1 : 1.3 | 1 : 0.6 | 1 : 1.4 | 1 : 1.0 |

4.2.3 Further Study and Characterisation of the optimised 1wt% AuPd_(0.975)X_(0.025)/TiO₂ catalysts.

As it was established that 1wt% AuPd_(0.975)X_(0.025)/TiO₂ was the optimal loading of the trimetallic Ni, Zn and Cu series due to the improved synthesis activities, these three catalysts were investigated further. Hydrogen conversion and H₂O₂ selectivity over a standard 30 minute H₂O₂ synthesis reaction was assessed for these catalysts, in addition to the 1wt% AuPd/TiO₂ analogue, with the data reported in Table 4.5. Over a 30 minute reaction hydrogen conversion is substantially greater for the trimetallic catalysts, compared to the bimetallic analogue (12%), particularly when Cu and Ni are added as the dopant metal (31 and 32% H₂ conversion respectively). The increased hydrogen conversion correlates with an increased activity towards H₂O₂ synthesis. However, as the hydrogen conversion increased, the selectivity towards H₂O₂ decreased, with the bimetallic catalyst having a hydrogen selectivity

of 59% compared to the Cu and Ni trimetallics at 40 and 41% respectively. In previous studies investigating Pt doping²⁴ selectivity was seen to increase through the incorporation of the dopant metal, which is not observed in this study, albeit with different dopant metals. However, to be able to fully see how the selectivity differs over the various catalysts it is important to look at the catalysts at equivalent hydrogen conversions.

Table 4.5: Comparison of catalytic selectivity of H₂O₂ at 30 minute reaction and at iso-conversion of H₂ for the 1wt% AuPd_{(0.975)X_(0.025)/TiO₂ (where X = Ni Cu Zn) series.}

| Catalyst | Reaction Time / min | H ₂ Conversion / % | H ₂ O ₂ Selectivity / % | Productivity / mol _{H₂O₂} kg _{cat} ⁻¹ h ⁻¹ | H ₂ O ₂ Conc. / wt% |
|---------------|---------------------|-------------------------------|---|--|---|
| AuPd | 30 | 12 | 59 | 61 | 0.125 |
| | 60 | 22 | 55 | 51 | 0.207 |
| | 75 | 32 | 47 | 51 | 0.258 |
| AuPdNi | 30 | 32 | 41 | 107 | 0.215 |
| AuPdCu | 30 | 31 | 40 | 94 | 0.188 |
| AuPdZn | 30 | 24 | 50 | 100 | 0.197 |

H₂O₂ direct synthesis conditions: 2 °C, P(5% H₂/CO₂) = 420 psi, P(25% O₂/CO₂) = 160 psi, 0.01 g catalyst, 2.9 g water, 5.6 g methanol, 1200 rpm. Catalysts prepared by sol-immobilisation and calcined (static air, ramp 10 °C min⁻¹, 400 °C, 3 h).

By comparing H₂O₂ selectivity at iso-conversion (~30% H₂ conversion) the H₂O₂ selectivity of the bimetallic catalyst (47%) is seen to be comparable to the trimetallic analogues. The introduction of the dopant metal decreases the selectivity e.g. AuPdNi (41%), AuPdCu (40%) and AuPdZn (50%). However, the decrease in selectivity is not as large as it would originally appear when compared to the 30 minute conversion of AuPd.

In Figure 4.6 the differences between the selectivities of AuPd and the trimetallics can be seen more clearly. There is a linear trend (between 12 and 32% H₂ conversion) seen for the selectivity and conversion for the AuPd catalyst, the comparative selectivities of the trimetallics fall below this trend, giving lower selectivity at the same conversion. It does appear that the AuPdZn catalyst has a smaller decrease in selectivity when compared to the

AuPd at iso-conversion, than the decrease seen for AuPdNi and AuPdCu. However, more selectivity data is needed to draw more accurate conclusions about how the selectivity is affected over different H₂ conversions for the trimetallics.

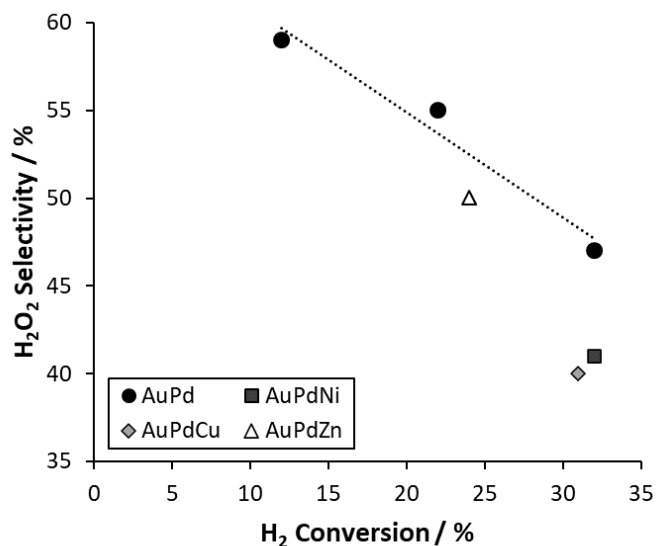


Figure 4.6: Conversion Vs. selectivity for 1wt% AuPd_(0.975)X_(0.025)/TiO₂ (where X = Ni, Cu, Zn) H₂O₂ synthesis. H₂O₂ direct synthesis conditions: 2 °C, P(5% H₂/CO₂) = 420 psi, P(25% O₂/CO₂) = 160 psi, 0.01 g catalyst, 2.9 g water, 5.6 g methanol, 1200 rpm. Catalysts prepared by sol-immobilisation and calcined (static air, ramp 10 °C min⁻¹, 400 °C, 3 h).

As previously mentioned, XPS analysis of these catalysts shows that quantities of 0.025wt% of the tertiary metals (Ni, Cu, Zn) result in a significant shift in the Pd oxidation state, towards the reduced species Pd⁰. Further analysis of the XPS data reported in Table 4.3 reveals an inverse correlation between Pd⁰ content and H₂O₂ selectivity. The bimetallic catalyst, that shows the highest H₂O₂ selectivity (47%) at H₂ conversion of 32% has a Pd²⁺ : Pd⁰ = 1: 0.7 whereas, 1wt% AuPd_(0.975)Cu_(0.025)/TiO₂ has the lowest H₂O₂ selectivity (40%) at H₂ conversion 31% and has a Pd²⁺ : Pd⁰ = 1: 1.6 which is the highest Pd⁰ content of the 4 catalysts.

Building on the XPS results, where it was observed that incorporation of the dopant metal resulted in a Pd oxidation state shift, the catalysts were characterised further by CO-DRIFTS analysis shown in Figure 4.7. The DRIFTS spectra for this series of catalysts are dominated by Pd–CO adsorption bands. The peak at 1990 cm⁻¹ corresponds to Pd–CO, where CO is linearly

bonded to low co-ordination Pd, which are edge or corner Pd sites, the broad peak around 1940 cm^{-1} represents the 2- and 3-fold adsorption of bridging CO on Pd.³² Both of these peaks (linear and bridging CO) show a small red-shift upon the addition of the dopant metal. There are a number of explanations that could explain this red shift, for example coverage by the dopant metal or due to a chemical or vibrational shift. Coupling effects of neighbours could also be responsible for this phenomenon. It could however be a result of increased charge-transfer to Pd d-orbitals, resulting in enhanced back donation to 2π CO molecular orbitals.³² Ouyang *et al.*²⁹ previously reported a similar transfer of electron density that resulted from alloying Au and Pd, with an associated suppression of O–O bond scission. This is in line with the decreased H_2O_2 degradation seen from the incorporation of small quantities of tertiary base metals Ni, Zn and Cu.

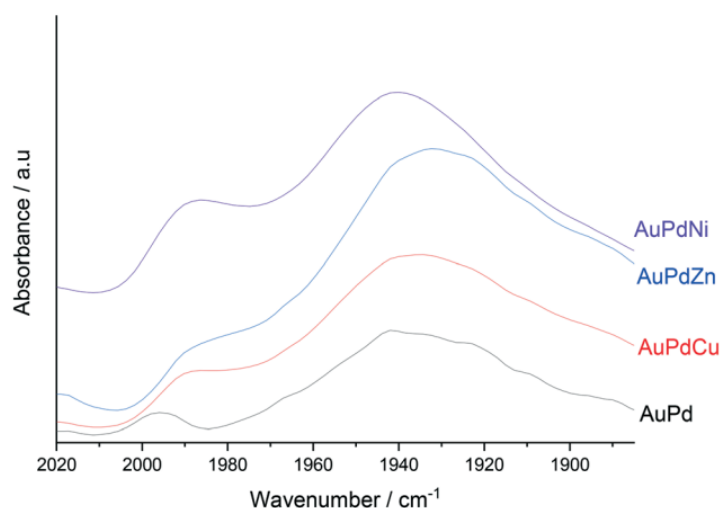


Figure 4.7: CO-DRIFTS spectra for 1% $\text{AuPd}_{(0.975)}\text{X}_{(0.025)}/\text{TiO}_2$ catalysts (where $X = \text{Ni, Zn, Cu}$).³⁰ Catalysts prepared by sol-immobilisation and calcined (static air, ramp $10\text{ }^\circ\text{C min}^{-1}$, $400\text{ }^\circ\text{C}$, 3 h).

It is important to consider the structure of a support material as this can have an important influence of the properties of the catalyst, and this can be altered by factors such as incorporation of metals, catalyst preparation methods and heat treatments. XRD analysis was performed for the 1wt% $\text{AuPd}_{(0.975)}\text{X}_{(0.025)}/\text{TiO}_2$ (where $X = \text{Ni, Cu, Zn}$) catalyst series along with the untreated TiO_2 (P25) support to determine how the structure may be effected. The XRD diffractogram (Figure 4.8) for the TiO_2 support (untreated) shows the reflections ($2\theta = 25, 27, 37, 38, 39, 48, 54, 55, 63, 69, 70, 75^\circ$). The catalysts show no observable difference in the XRD patterns, displaying the same reflections as the that observed for the bare TiO_2 (P25) support.

From these observations, it is possible to deduce that the metal particles are small, and the support is a stable material, which is good for use in catalyst material as the main bulk structure does not undergo noticeable changes during catalyst preparation, namely the heat treatment.

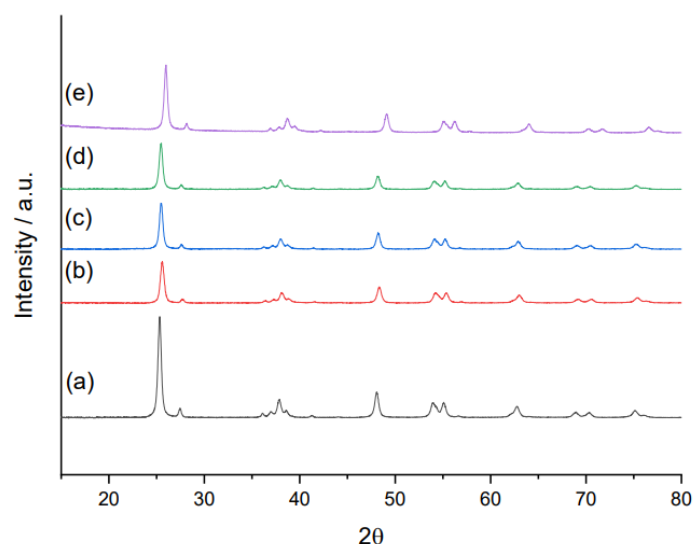


Figure 4.8: X-ray diffractograms of 1% $\text{AuPd}_{(0.975)}\text{X}_{(0.025)}/\text{TiO}_2$ catalysts, prepared by sol-immobilisation and calcined (400 °C, 3 h, static air, ramp rate = 10 °C min^{-1}). (a) TiO_2 , (b) 1wt% AuPd/TiO_2 , (c) 1wt% $\text{AuPd}_{(0.975)}\text{Ni}_{(0.025)}/\text{TiO}_2$, (d) 1wt% $\text{AuPd}_{(0.975)}\text{Cu}_{(0.025)}/\text{TiO}_2$ and (e) 1wt% $\text{AuPd}_{(0.975)}\text{Zn}_{(0.025)}/\text{TiO}_2$.³⁰ Catalysts prepared by sol-immobilisation and calcined (static air, ramp 10 °C min^{-1} , 400 °C, 3 h). Note: No reflections associated with immobilised metal species are observed in any of the as-prepared catalysts. ICDD patterns for reference: (TiO_2 anatase ICDD: 01-089-4921, TiO_2 rutile ICDD:07-089-0555).

There is difficulty in characterising such small quantities of the dopant metal on the catalyst, as the levels used in this series have been below the detection level of many of the techniques typically used to investigate and characterise heterogeneous catalytic materials. Therefore, samples of the 4 catalysts underwent digestion by HF and subsequent ICP analysis, with the quantified metal loadings reported in Table 4.6. The concentration of the Au and Pd was found to be consistent with the theoretical loading, across the catalyst series. However, only a very small percentage of the dopant metals were detected (compared to theoretical quantity), of the Ni (4.0%), Zn (7.6%) and Cu (5.6%). Due to the sol-immobilisation synthesis methodology, it could be assumed that any of the dopant metal that is not immobilised onto the support was likely lost during the filtration step of the catalyst preparation, and this can be investigated in future work by ICP analysis of the post-synthesis solutions of the catalyst

preparation. Loss of the third metal could also indicate that it is not alloying with the Au and Pd as this would likely prevent its loss, if this is the case then rather than these being trimetallic catalysts they could instead be doped bimetallics. However, it is not clear why the dopant metal hasn't fully alloyed and immobilised to the support as expected. Regardless, despite the inordinately low concentrations of dopant metal measured, there is clearly a profound effect on the activity, and selectivity of the catalysts, when compared to the bimetallic analogue.

Table 4.6: Fresh samples of each catalyst (200 mg) were digested by HF and analysed by ICP. The table shows the theoretical wt% of each metal in the catalysts, compared with the actual wt% values that were collected from the ICP data. Catalysts analysed were 1wt% AuPd_(0.975)X_(0.025)/TiO₂ (where X = Ni, Zn, Cu) prepared by sol-immobilisation and calcined (static air, ramp 10 °C min⁻¹, 400 °C, 3 h).

| Catalyst | Theoretical / wt% | | | | Actual / wt% | | | |
|---------------|-------------------|-------|-------|-------|--------------|-------|--------|-------|
| | Au | Pd | X | Total | Au | Pd | X | Total |
| AuPd | 0.649 | 0.351 | - | 1 | 0.645 | 0.437 | - | 1.082 |
| AuPdNi | 0.633 | 0.342 | 0.025 | 1 | 0.640 | 0.416 | 0.0010 | 1.057 |
| AuPdZn | 0.633 | 0.34 | 0.025 | 1 | 0.644 | 0.415 | 0.0019 | 1.061 |
| AuPdCu | 0.633 | 0.342 | 0.025 | 1 | 0.637 | 0.405 | 0.0014 | 1.043 |

Analysis by Exeter Analytical LTD (EAI)

Numerous studies have shown strong correlation between nanoparticle size and catalytic activity towards H₂O₂ synthesis.^{33,34} Studies by Tian *et al.*^{35,36} have shown that a sub-nanometre particle range is optimal for achieving high catalytic performance for H₂O₂ synthesis, with larger nanoparticles favouring the competing H₂O₂ degradation pathways. Bright field transmission electron microscopy of the 1wt% AuPd_(0.975)X_(0.025)/TiO₂ (X = Ni, Cu, Zn) catalysts, was used to determine mean particle size for the catalysts and are presented in Figure 4.9. There was minimal variation observed across the subset of catalysts, hence it is reasonable to suggest that the enhanced catalytic activity that was achieved through incorporation of tertiary base metals cannot be associated with increased nanoparticle dispersion.

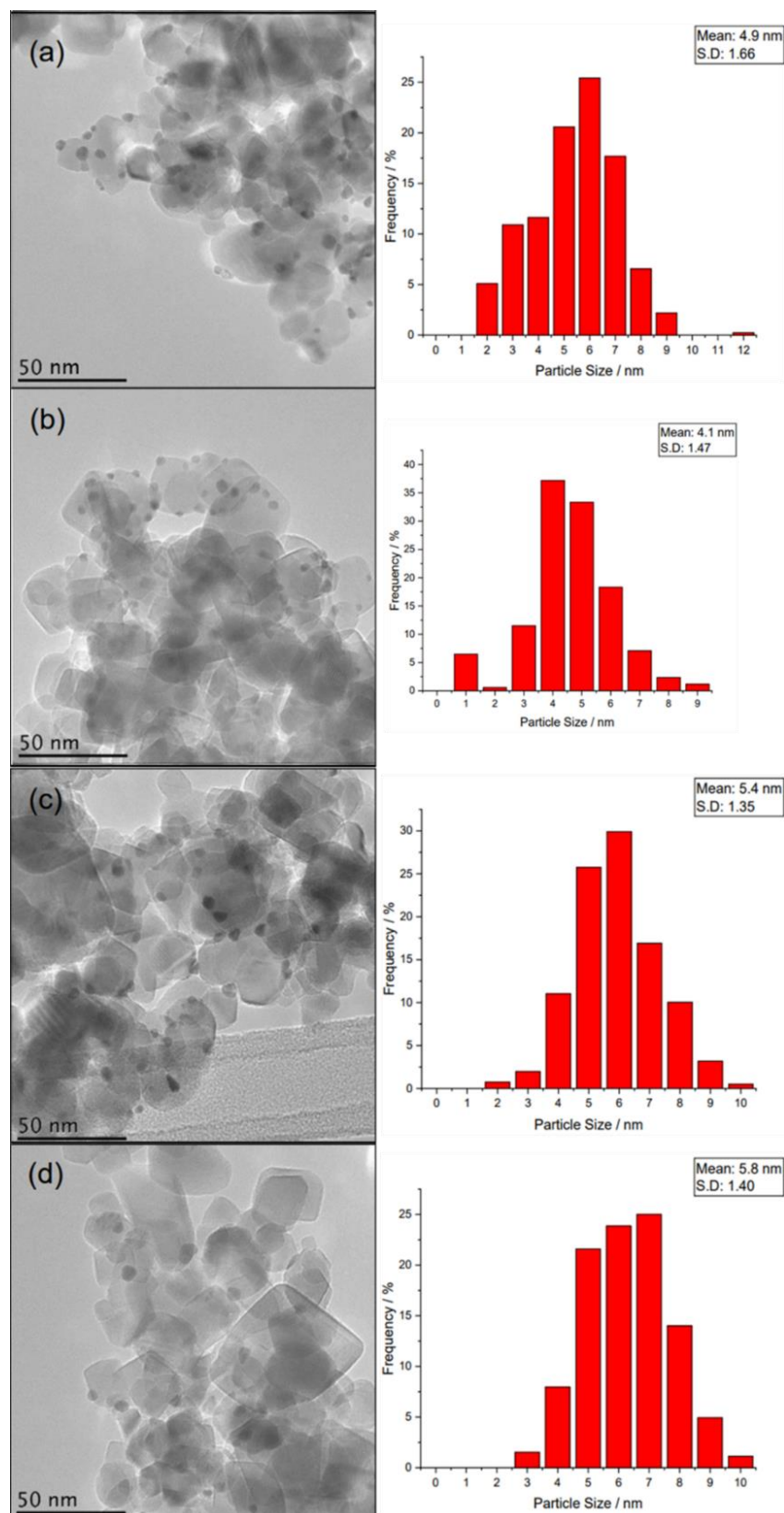


Figure 4.9: Representative bright field transmission electron micrographs and corresponding particle size histograms of TiO₂ supported tri-metallic catalysts, prepared by a sol-immobilisation and calcined (400 °C, 3 h, static air, ramp rate = 10 °C min⁻¹). (a) 1wt% AuPd/TiO₂ (b) 1wt% AuPd_(0.975)Ni_(0.025)/TiO₂ (c) 1wt% AuPd_(0.975)Cu_(0.025)/TiO₂ (d) 1wt% AuPd_(0.975)Zn_(0.025)/TiO₂.³⁰

From the combined experimental and characterisation observations of the 1wt% AuPd_(0.975)X_(0.025)/TiO₂ (X = Ni, Cu, Zn) catalyst series, the formation of tri-metallic alloyed nanoparticles can be supported and the promotive effect of the dopant metal is proposed to be due to the resulting electronic modification of the Pd species.

4.2.4 Investigating 1wt% AuPd_(0.975)X_(0.025)/TiO₂ Over Prolonged Reaction Times

Time-on-line and gas replacement reactions were performed to compare the rate of reaction over time, to see if the improved activity of the tertiary catalysts is retained at longer reaction times. The results are shown in Figure 4.10, and time-on-line studies show a clearly enhanced activity of the 1wt% AuPd_(0.975)X_(0.025)/TiO₂ catalysts, with the trimetallic catalysts achieving H₂O₂ concentrations (0.22–0.26 wt%), far greater than that of the bimetallic AuPd analogue (0.17 wt%). Furthermore, the net concentrations of H₂O₂ achieved over the trimetallic catalysts were comparable to an optimised 1wt% Au₁Pd₁Pt_{0.1}/TiO₂ catalyst that had previously been reported, prepared via a similar methodology, under identical reaction conditions.²⁴

Further evaluation of catalytic activity over multiple sequential H₂O synthesis reactions, where gaseous reagents were replenished every 0.5 h, also demonstrated an enhancement in H₂O₂ concentration for the trimetallic catalysts, compared to the bimetallic analogue. Five consecutive reactions (2.5 h), produced H₂O₂ concentrations of the 1wt% AuPd_(0.975)X_(0.025)/TiO₂ catalysts (0.47–0.58 wt%), far greater (15–33%), than that observed over the AuPd analogue (0.39 wt%). Notably, despite the significantly lower loading of these catalysts, the 1wt% AuPd_(0.975)Ni_(0.025)/TiO₂ achieved H₂O₂ concentrations comparable to those previously reported by S. Freakley et al.¹⁵ using a near 100% selective 3% Pd–2% Sn/TiO₂ catalyst.

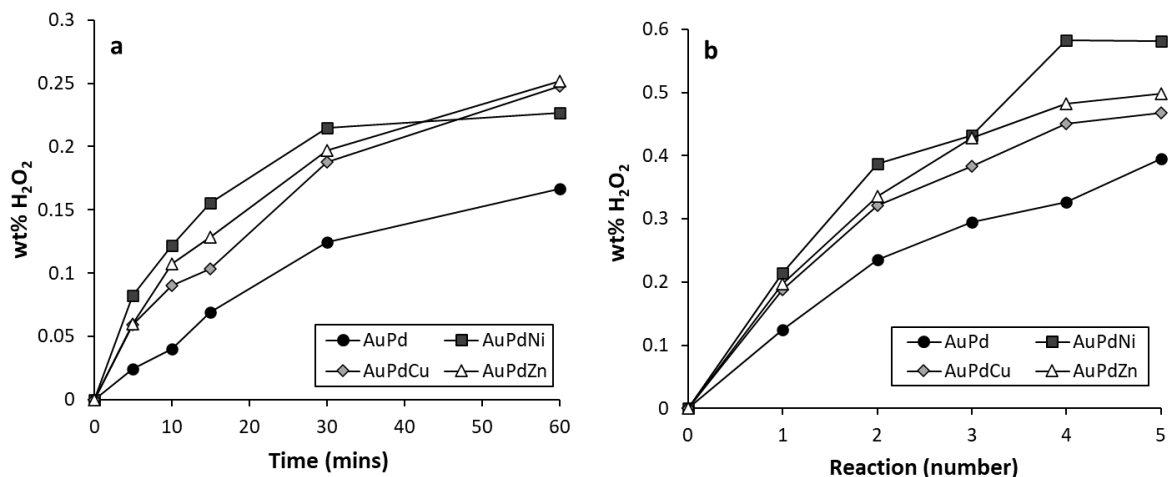


Figure 4.10: (a) Time-on line of direct H₂O₂ synthesis by 1wt% AuPd_(0.975)X_(0.025)/TiO₂ (where X = Ni, Zn, Cu). (b) Gas replacement consecutive reactions for direct H₂O₂ synthesis by 1wt% AuPd_(0.975)X_(0.025)/TiO₂ (where X = Ni, Zn, Cu) for each 0.5 h consecutive reaction, the reactor gas is vented and refilled. H₂O₂ direct synthesis conditions: 2 °C, P(5% H₂/CO₂) = 420 psi, P(25% O₂/CO₂) = 160 psi, 0.01 g catalyst, 2.9 g water, 5.6 g methanol, 1200 rpm. Catalysts prepared by sol-immobilisation and calcined (static air, ramp 10 °C min⁻¹, 400 °C, 3 h).

The enhanced performance of the trimetallic 1wt% AuPd_(0.975)X_(0.025)/TiO₂ catalysts (compared to the bimetallic analogue), is emphasised when comparing the initial rates of the reaction as presented in Table 4.7). Initial rates are measured from a 5 minute reaction time, at this stage of the reaction it is assumed that there is no competing degradation reaction. These experiments further demonstrate how much more active the trimetallic catalysts are, in particular AuPdNi (256 moles_{H₂O₂} kg_{cat}⁻¹ hr⁻¹), compared to the AuPd analogue (76 moles_{H₂O₂} kg_{cat}⁻¹ hr⁻¹).

Table 4.7: Initial rates were calculated from 5 minute direct synthesis of H₂O₂ catalysed by 1wt% AuPd_{(0.975)X_(0.025)/TiO₂ (where X = Ni, Zn, Cu).}

| Catalyst (AuPdX) for: 1wt% AuPd _{(0.975)X_(0.025)/TiO₂} | Initial Rate / moles _{H₂O₂} kg _{cat} ⁻¹ hr ⁻¹ |
|--|--|
| AuPd | 76 |
| AuPdNi | 256 |
| AuPdZn | 181 |
| AuPdCu | 177 |

H₂O₂ direct synthesis conditions: 2 °C, P(5% H₂/CO₂) = 420 psi, P(25% O₂/CO₂) = 160 psi, 0.01 g catalyst, 2.9 g water, 5.6 g methanol, 1200 rpm, 5 min. Catalysts prepared by sol-immobilisation and calcined (static air, ramp 10 °C min⁻¹, 400 °C, 3 h).

Analysis of the catalysts by XPS over the course of the time-on-line H₂O₂ synthesis (Figure 4.11 & Table 4.8) indicates a clear shift towards the Pd⁰ reduced species, which can be expected due to the reductive atmosphere during H₂O₂ synthesis. The Pd⁰ species has been found to enhance the activity towards the competing H₂O₂ degradation reaction^{37,38} and therefore could be contributing to the reduction in the H₂O₂ synthesis activity over time.

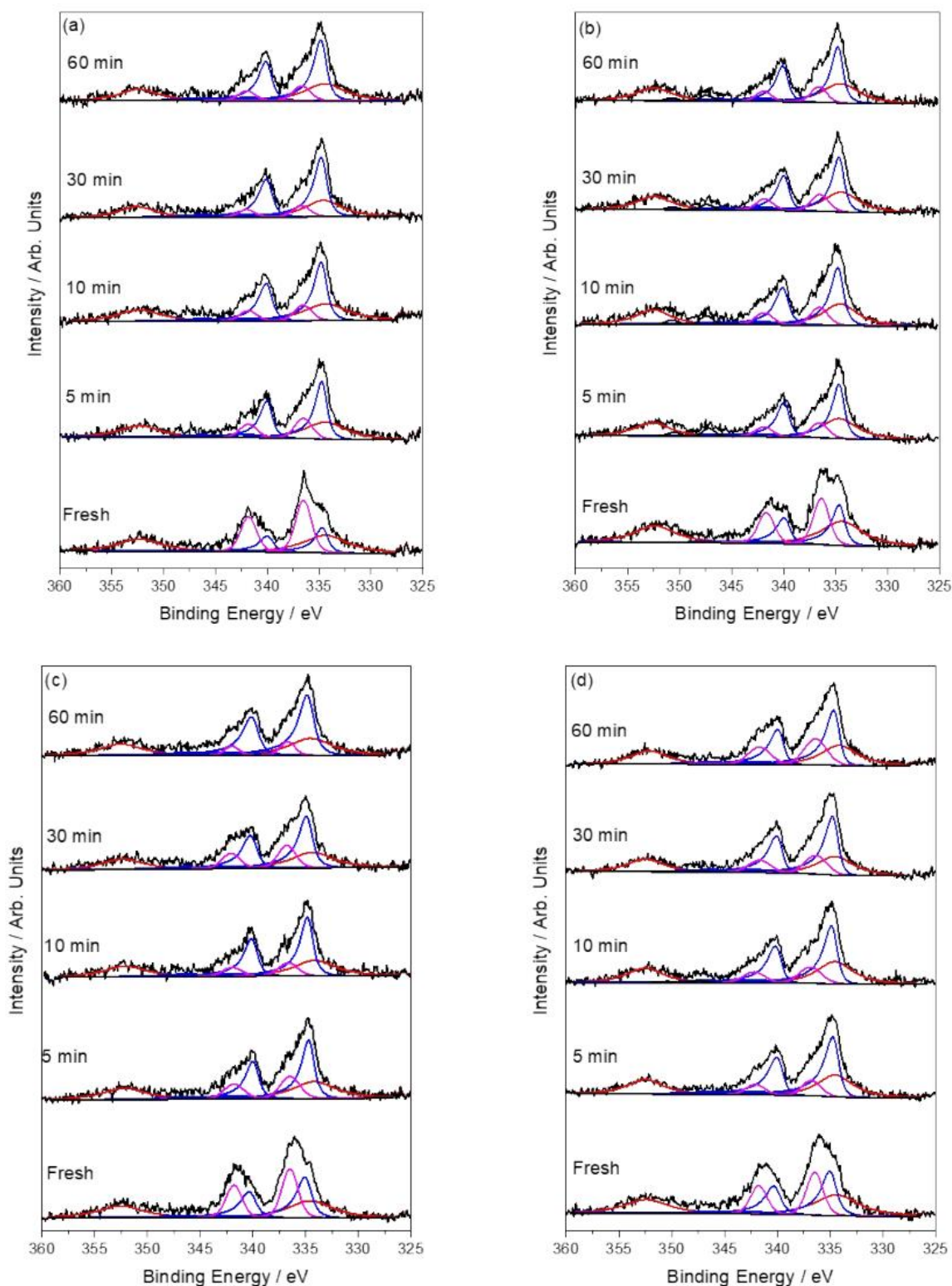


Figure 4.11: XPS spectra of Pd(3d) regions for (a) 1wt% AuPd/TiO₂ (b) 1wt% AuPd_(0.975)Ni_(0.025)/TiO₂ (c) 1wt% AuPd_(0.975)Zn_(0.025)/TiO₂ and (d) 1wt% AuPd_(0.975)Cu_(0.025)/TiO₂ catalysts as a function of reaction time.³⁰ Key: Au(4d) (red), Pd⁰ (blue), Pd²⁺ (magenta). H₂O₂ direct synthesis reaction conditions: Catalyst (0.01 g), H₂O (2.9 g), MeOH (5.6 g), 5% H₂ / CO₂ (420 psi), 25% O₂ / CO₂ (160 psi), 2 °C 1200 rpm. Note: Used catalysts are dried under vacuum (30 °C, 16 h) prior to subsequent utilisation in the direct synthesis of H₂O₂ or XPS analysis.

Table 4.8: Metal speciation of the bimetallic and trimetallic catalysts for time-on-line H₂O₂ synthesis of fresh (0 min) catalyst and used catalyst samples. Calculated using fittings by Dr David Morgan.

| Time (mins) | AuPd | | AuPdNi | | AuPdZn | | AuPdCu | |
|----------------|---------|-----------------------------------|---------|-----------------------------------|---------|-----------------------------------|---------|-----------------------------------|
| | Au:Pd | Pd ²⁺ :Pd ⁰ |
| 0 | 1 : 1.8 | 1 : 0.7 | 1 : 1.5 | 1 : 1.2 | 1 : 2.4 | 1 : 1.2 | 1 : 2.2 | 1 : 1.6 |
| 5 | 1 : 1.8 | 1 : 3.2 | 1 : 1.6 | 1 : 4.0 | 1 : 2.3 | 1 : 3.2 | 1 : 1.9 | 1 : 4.4 |
| 10 | 1 : 1.8 | 1 : 4.5 | 1 : 1.8 | 1 : 3.6 | 1 : 2.2 | 1 : 5.7 | 1 : 1.9 | 1 : 3.6 |
| 15 | 1 : 1.9 | 1 : 5.3 | 1 : 1.8 | 1 : 4.0 | 1 : 2.6 | 1 : 5.0 | 1 : 1.9 | 1 : 2.9 |
| 30 | 1 : 1.2 | 1 : 3.7 | 1 : 1.6 | 1 : 3.6 | 1 : 2.5 | 1 : 9.0 | 1 : 1.7 | 1 : 3.0 |
| 60 | 1 : 2.1 | 1 : 6.0 | 1 : 1.8 | 1 : 4.5 | 1 : 2.4 | 1 : 7.7 | 1 : 2.2 | 1 : 2.25 |

H₂O₂ direct synthesis conditions: 2 °C, P(5% H₂/CO₂) = 420 psi, P(25% O₂/CO₂) = 160 psi, 0.01 g catalyst, 2.9 g water, 5.6 g methanol, 1200 rpm. Catalysts prepared by sol-immobilisation and calcined (static air, ramp 10 °C min⁻¹, 400 °C, 3 h).

4.2.5 Reusability of trimetallic catalysts

Reusability of the catalysts was evaluated by using an excess of catalyst for a standard H₂O₂ direct synthesis, filtering the used catalyst from the post-reaction solution, and drying under vacuum (30°C, 16 h), the now dried catalyst (10 mg) can be retested for H₂O₂ synthesis over a reaction time of 5 minutes and 30 minutes, and tested for the degradation of H₂O₂. Results of this can be seen in Figure 4.12.

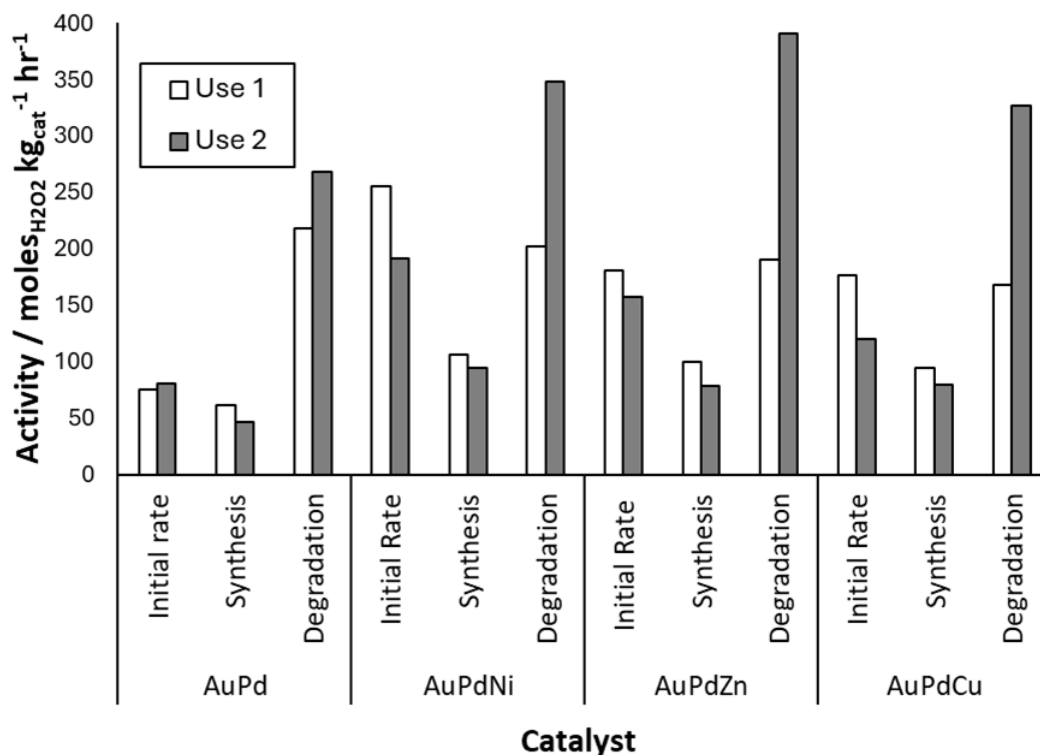


Figure 4.12: Reuse testing for 1wt% $\text{AuPd}_{(0.975)}\text{X}_{(0.025)}/\text{TiO}_2$ (where $X = \text{Ni, Zn, Cu}$). For reuse testing an excess of catalyst was used in a standard H_2O_2 synthesis test, then filtered and dried in a vac oven 30°C , 16 h. Dried catalyst was then tested as follows: H_2O_2 direct synthesis conditions: 0.5 h (0.08 hr for initial rate), 2°C , $P(5\% \text{H}_2/\text{CO}_2) = 420 \text{ psi}$, $P(25\% \text{O}_2/\text{CO}_2) = 160 \text{ psi}$, 10 mg catalyst, 2.9 g water, 5.6 g methanol, 1200 rpm. Degradation conditions: 0.5 h, 2°C , $P(5\% \text{H}_2/\text{CO}_2) = 420 \text{ psi}$, 10 mg catalyst, 0.68 g H_2O_2 (50 wt%), 2.22 g water, 5.6 g methanol, 1200 rpm. Catalysts prepared by sol-immobilisation and calcined (static air, ramp $10^\circ\text{C min}^{-1}$, 400°C , 3 h).

It is evident that the H_2O_2 synthesis activity for all catalyst decreased significantly upon reuse. Correspondingly, the degradation activity increases, showing that upon reuse selectivity towards the synthesis reaction is reduced. However, in future work it would be useful to analyse gas composition post-reaction to determine how the H_2 conversion and H_2O_2 selectivity is affected upon reuse of the catalyst. It should be noted that the observable increases in degradation activities between the fresh and used catalysts is much less pronounced for the bimetallic AuPd catalyst compared to the trimetallics. Regardless, the reuse synthesis activities of the trimetallic catalysts (Ni 95, Zn 79, Cu 80 moles_{H₂O₂} kg_{cat}⁻¹ hr⁻¹ respectively) is still greater than the rate seen for the bimetallic catalyst on first use (61 mol_{H₂O₂} kg_{cat}⁻¹ h⁻¹).

Initial H₂O₂ synthesis rates have also been calculated from 5 minute reaction times, for initial use and reuse of the catalysts, as here it is assumed that there is no contribution from the subsequent degradation reactions, as there is over the course of a standard 30 minute reaction. The enhanced activity of the trimetallic 1wt% AuPd_(0.975)X_(0.025)/TiO₂ (X = Ni, Cu, Zn) catalysts is further demonstrated with initial rates between 2.6 and 3.5 times that of the AuPd bimetallic analogue. What is particularly interesting however, is the increase in initial synthesis activity observed by 1wt% AuPd/TiO₂ (from 76 to 80 mol_{H₂O₂} kg_{cat}⁻¹ h⁻¹), it could be that the increased number of metallic Pd species formed present upon reuse is increasing the activity of this bimetallic catalyst. However, the increase in degradation activity seen for this catalyst upon reuse is likely what has caused the decrease in activity seen for the 30 minute H₂O₂ synthesis reuse. The increased degradation rate has negligible effect upon the initial rate as the H₂O₂ in the reaction medium is too low. A more active but unselective catalyst such as this would be better suited to a flow system so that the formed H₂O₂ is removed from the system before its degradation can occur over the catalyst.

A consideration that must be addressed for any three-phase system using a heterogeneous catalyst, is the potential leaching of the active metals off the catalyst support, which can result in a homogeneous contribution to the observed catalytic activity. This is a known issue for this reaction as the homogeneous Pd species can catalyse the direct synthesis of H₂O₂.^{27,28} Therefore, an additional factor in the reusability of the catalyst is the metal stability, the post reaction solution was analysed by ICP-MS to determine the degree of metal leaching for the catalysts and is reiterated in Table 4.9. All catalysts demonstrated high stability of Au, with none detected in the post reaction solution. However, there was some Pd (approx. 1–6 ppb for the 4 catalysts) detected. It is notable that any potential leaching of the tertiary metal was below the detectable limits of ICP-MS. Due to the low level of leaching observed from each catalyst upon use in a 30 minute reaction, it can be assumed that that catalytic contributions from homogeneous Pd species are negligible.

This work provides leaching data from a standard 30 minute reaction, however, what is not clear is at what time in the reaction this occurs. It is possible that leaching occurs in the initial stages of the reaction (5 minutes or less), or it could be continuous, in which case for extended reaction times and further reuses of the result in loss of much larger quantities of the Pd and

this could have serious consequences for reusability. To determine this, leaching studies for the duration of the time-on-line studies and the reuse reactions must be performed.

Table 4.9: Metal leaching was measured by filtering the reaction solution of the direct synthesis of H₂O₂ and analysing using ICP-MS. Leaching of dopant metal X is BDL (below detection limit).

| Catalyst (AuPdX) for: 1wt% AuPd _(0.975) X _(0.025) /TiO ₂ | Metal leaching / % (ppb) | |
|--|--------------------------|------------|
| | Au | Pd |
| AuPd | 0 | 1.90 (4.8) |
| AuPdNi | 0 | 2.52 (6.3) |
| AuPdZn | 0 | 1.74 (4.4) |
| AuPdCu | 0 | 0.42 (1.1) |

H₂O₂ direct synthesis conditions: 2 °C, P(5% H₂/CO₂) = 420 psi, P(25% O₂/CO₂) = 160 psi, 0.01 g catalyst, 2.9 g water, 5.6 g methanol, 1200 rpm. Catalysts prepared by sol-immobilisation and calcined (static air, ramp 10 °C min⁻¹, 400 °C, 3 h). Leaching of dopant metal X is BDL (below detection limit).

It is evidenced by the XPS analysis (Figure 4.13, Table 4.10) that upon use of each catalyst the Pd species shifts clearly towards the reduced Pd⁰ species, this is observed to a greater extent upon the second use of each of the catalysts. It is well established that the Pd⁰ species enhances activity towards the competing H₂O₂ degradation reaction^{37,38}, and this is also evidenced in the increased degradation (and hence the decreased synthesis) activities seen upon reuse, which at least to some degree, the in-situ reduction of Pd²⁺ to Pd⁰ may be considered responsible for.

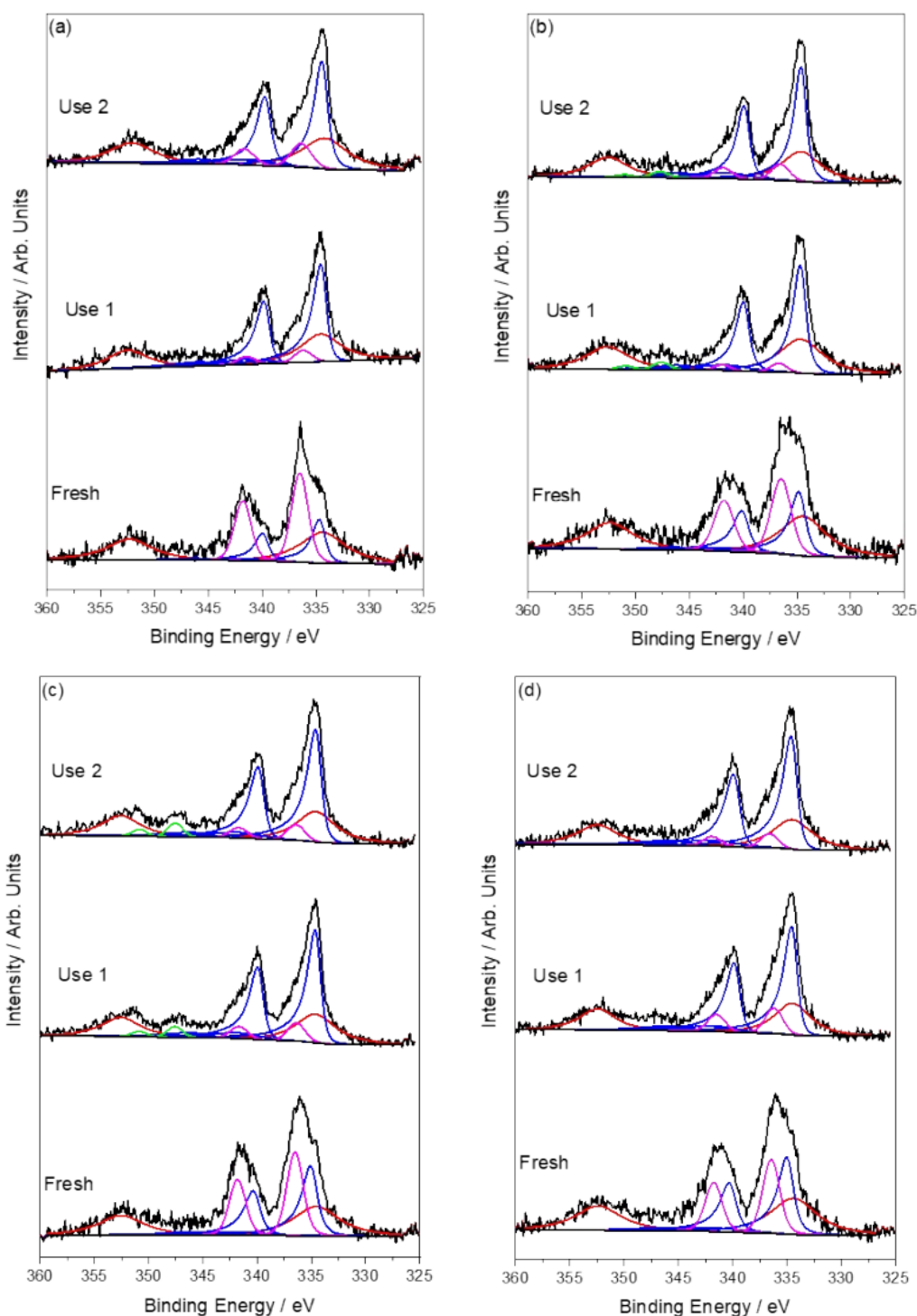


Figure 4.13: XPS spectra of Pd(3d) regions for the as-prepared (a) 1wt% AuPd/TiO₂ (b) 1wt% AuPd_(0.975)Ni_(0.025)/TiO₂ (c) 1wt% AuPd_(0.975)Zn_(0.025)/TiO₂ and (d) 1wt% AuPd_(0.975)Cu_(0.025)/TiO₂ catalysts in addition to corresponding spectra after one and two uses in the direct synthesis of H₂O₂.³⁰ Key: Au(4d) (red), Pd⁰ (blue), Pd²⁺ (magenta), Ca²⁺ (green). The presence of Ca²⁺ is considered to originate from the reaction mixture. H₂O₂ direct synthesis reaction conditions: Catalyst (0.01 g), H₂O (2.9 g), MeOH (5.6 g), 5% H₂ / CO₂ (420 psi), 25% O₂ / CO₂ (160 psi), 0.5 h, 2 °C 1200 rpm. Catalysts prepared by sol-immobilisation and calcined (static air, ramp 10 °C min⁻¹, 400 °C, 3 h). Note: Used catalysts are dried under vacuum (30 °C, 16 h) prior to subsequent utilisation in the direct synthesis of H₂O₂ or XPS analysis.

Table 4.10: Metal speciation of fresh catalyst (reaction number 0) and used catalyst samples (reaction number 1 & 2). Calculated using fittings by Dave Morgan. For used samples, catalyst was filtered and dried after direct H₂O₂ synthesis for XPS analysis.

| Reaction Number | AuPd | | AuPdNi | | AuPdZn | | AuPdCu | |
|-----------------|---------|-----------------------------------|---------|-----------------------------------|---------|-----------------------------------|---------|-----------------------------------|
| | Au:Pd | Pd ²⁺ :Pd ⁰ |
| 0 | 1 : 1.8 | 1 : 0.7 | 1 : 1.5 | 1 : 1.2 | 1 : 2.4 | 1 : 1.2 | 1 : 2.2 | 1 : 1.6 |
| Use 1 | 1 : 1.2 | 1 : 3.7 | 1 : 1.6 | 1 : 3.6 | 1 : 2.5 | 1 : 9.0 | 1 : 1.7 | 1 : 3.0 |
| Use 2 | 1 : 1.8 | 1 : 7.3 | 1 : 1.5 | 1 : 21 | 1 : 2.6 | 1 : 9.3 | 1 : 2.9 | 1 : 13.5 |

H₂O₂ direct synthesis conditions: 2 °C, P(5% H₂/CO₂) = 420 psi, P(25% O₂/CO₂) = 160 psi, 0.01 g catalyst, 2.9 g water, 5.6 g methanol, 1200 rpm. Catalysts prepared by sol-immobilisation and calcined (static air, ramp 10 °C min⁻¹, 400 °C, 3 h).

Interestingly the Zn catalyst has a much larger increase of Pd⁰ content (Pd²⁺:Pd⁰ = 1 : 9.0) upon first use for H₂O₂ synthesis and this corresponds with this catalysts greater degradation activity upon reuse (compared to the other catalysts). However, after the second use of the AuPdZn catalyst the Pd species does not change to the same degree as the other catalysts (AuPd, AuPdNi and AuPdCu) which have a much larger increase in Pd⁰ species upon the second use in the synthesis of H₂O₂. This could suggest that if the catalysts were tested a third time the rate of the H₂O₂ degradation reaction for the other catalysts would increase to a greater extent than the AuPdZn corresponding to the larger Pd⁰ content. However, confirming this is an area for future work.

4.3 Conclusions

This study has clearly shown how the addition of exceedingly low quantities of earth abundant transition metals, namely Ni, Zn and Cu into supported AuPd nanoparticles can vastly enhance catalytic activity towards H_2O_2 synthesis. The optimal quantity of the dopant metal in each case was found to be 0.025wt% with these catalysts having 1.5–1.8 times the activity compared to the bimetallic analogue.

Performing gas analysis, determined that the enhancement in synthesis activity of these catalysts was largely due to the increase in H_2 conversion, rather than an increase in H_2O_2 selectivity, despite the lower degradation rates seen for the trimetallic catalysts. This was contrary to previous findings with a AuPdPt trimetallic where enhancement in catalytic performance was found to correlate with improvements in selectivity towards H_2O_2 .²⁴

XPS and DRIFTS analysis suggests that the improved activity is due to electronic modification of Pd, with the addition of low concentrations of tertiary metals found to promote the formation of Pd^{2+} – Pd^0 domains. It is evident that introduction and alloying of the tertiary metal has a prominent effect of the Pd oxidation state, however further investigation is needed to fully deconvolute the effect of electronic modification from the restructuring of the alloyed nanoparticles.

The in-situ reduction of the Pd sites upon use is of concern when considering the stability and reusability of the catalysts, however it is notable that in terms of leaching these catalysts were very stable. It can therefore be considered that the catalysts presented in this study represent a promising basis for further exploration for the direct synthesis of H_2O_2 .

4.4 References

- 1 J. M. Campos-Martin, G. Blanco-Brieva and J. L. G. Fierro, *Angew. Chemie - Int. Ed.*, 2006, **45**, 6962–6984.
- 2 R. J. Lewis and G. J. Hutchings, *ChemCatChem*, 2019, **11**, 298–308.
- 3 C. W. Jones, in *Applications of Hydrogen Peroxide and Derivatives*, eds. J. H. Clark and M. J. Braithwaite, RSC, 1999, pp. 1–34.
- 4 J. K. Edwards, A. Thomas, A. F. Carley, A. A. Herzing, C. J. Kiely and G. J. Hutchings, *Green Chem.*, 2008, **10**, 388–39.
- 5 J. K. Edwards, J. Pritchard, M. Piccinini, G. Shaw, Q. He, A. F. Carley, C. J. Kiely and G. J. Hutchings, *J. Catal.*, 2012, **292**, 227–238.
- 6 J. K. Edwards, S. J. Freakley, R. J. Lewis, J. C. Pritchard and G. J. Hutchings, *Catal. Today*, 2015, **248**, 3–9.
- 7 P. Landon, P. Collier, A. Papworth, C. Kieley and G. J. Hutchings, *ChemComm*, 2002, 2058–2029.
- 8 J. K. Edwards, S. F. Parker, J. Pritchard, M. Piccinini, S. J. Freakley, Q. He, A. F. Carley, C. J. Kiely and G. J. Hutchings, *Catal. Sci. Technol.*, 2013, **3**, 812–818.
- 9 J. C. Pritchard, Q. He, E. N. Ntainjua, M. Piccinini, J. K. Edwards, A. A. Herzing, A. F. Carley, J. A. Moulijn, C. J. Kiely and G. J. Hutchings, *Green Chem.*, 2010, **12**, 915–92.
- 10 C. M. Crombie, R. J. Lewis, R. L. Taylor, D. J. Morgan, T. E. Davies, A. Folli, D. M. Murphy, J. K. Edwards, J. Qi, H. Jiang, C. J. Kiely, X. Liu, M. S. Skjøth-Rasmussen and G. J. Hutchings, *ACS Catal.*, 2021, **11**, 2701–2714.
- 11 A. Santos, R. J. Lewis, D. J. Morgan, T. E. Davies, E. Hampton, P. Gaskin and G. J. Hutchings, *Catal. Sci. Technol.*, 2021, **11**, 7866–7874.
- 12 N. M. Wilson, J. Schröder, P. Priyadarshini, D. T. Bregante, S. Kunz and D. W. Flaherty, *J. Catal.*, 2018, **368**, 261–274.
- 13 S. Maity and M. Eswaramoorthy, *J. Mater. Chem. A*, 2016, **4**, 3233–3237.
- 14 S. Wang, R. J. Lewis, D. E. Doronkin, D. J. Morgan, J. D. Grunwaldt, G. J. Hutchings and S. Behrens, *Catal. Sci. Technol.*, 2020, **10**, 1925–1932.
- 15 S. Freakley, Q. He, J. Harrhy, L. Lu, D. Crole, D. Morgan, E. Ntainjua, J. Edwards, A. Carley, A. Borisevich, C. Kieley and H. Graham, *Science (80-.)*, 2016, **351**, 965–968.
- 16 F. Li, Q. Shao, M. Hu, Y. Chen and X. Huang, *ACS Catal.*, 2018, **8**, 3418–3423.
- 17 E. N. Ntainjua, S. J. Freakley and G. J. Hutchings, *Top. Catal.*, 2012, **55**, 718–722.
- 18 J. Gu, S. Wang, Z. He, Y. Han and J. Zhang, *Catal. Sci. Technol.*, 2016, **6**, 809–817.
- 19 G. Bernardotto, F. Menegazzo, F. Pinna, M. Signoretto, G. Cruciani and G. Strukul, *Appl. Catal. A Gen.*, 2009, **358**, 129–135.

- 20 J. Li, T. Ishihara and K. Yoshizawa, *J. Phys. Chem. C*, 2011, **115**, 25359–25367.
- 21 A. M. Joshi, W. N. Delgass and K. T. Thomson, *J. Phys. Chem. C*, 2007, **111**, 7841–7844.
- 22 J. K. Edwards, J. Pritchard, P. J. Miedziak, M. Piccinini, A. F. Carley, Q. He, C. J. Kiely and G. J. Hutchings, *Catal. Sci. Technol.*, 2014, **4**, 3244–3250.
- 23 J. K. Edwards, J. Pritchard, L. Lu, M. Piccinini, G. Shaw, A. F. Carley, D. J. Morgan, C. J. Kiely and G. J. Hutchings, *Angew. Chemie - Int. Ed.*, 2014, **53**, 2381–2384.
- 24 X. Gong, R. J. Lewis, S. Zhou, D. J. Morgan, T. E. Davies, X. Liu, C. J. Kiely, B. Zong and G. J. Hutchings, *Catal. Sci. Technol.*, 2020, **10**, 4635–4644.
- 25 A. Villa, D. Wang, G. M. Veith, F. Vindigni and L. Prati, *Catal. Sci. Technol.*, 2013, **3**, 3036–3041.
- 26 B. A. T. Mehrabadi, S. Eskandari, U. Khan, R. D. White and J. R. Regalbuto, *A Review of Preparation Methods for Supported Metal Catalysts*, Elsevier Inc., 1st edn., 2017, vol. 61.
- 27 D. P. Dissanayake and J. H. Lunsford, *J. Catal.*, 2002, **206**, 173–176.
- 28 S. J. Freakley, N. Agarwal, R. U. McVicker, S. Althahban, R. J. Lewis, D. J. Morgan, N. Dimitratos, C. J. Kiely and G. J. Hutchings, *Catal. Sci. Technol.*, 2020, **10**, 5935–5944.
- 29 L. Ouyang, P. F. Tian, G. J. Da, X. C. Xu, C. Ao, T. Y. Chen, R. Si, J. Xu and Y. F. Han, *J. Catal.*, 2015, **321**, 70–80.
- 30 A. Barnes, R. J. Lewis, D. J. Morgan, T. E. Davies and G. J. Hutchings, *Catal. Sci. Technol.*, 2022, **12**, 1986–1995.
- 31 R. Burch and P. R. Ellis, *Appl. Catal. B Environ.*, 2003, **42**, 203–211.
- 32 K. Duan, Z. Liu, J. Li, L. Yuan, H. Hu and S. I. Woo, *Catal. Commun.*, 2014, **57**, 19–22.
- 33 G. Giorgianni, S. Abate, G. Centi and S. Perathoner, *ChemCatChem*, 2019, **11**, 550–559.
- 34 S. Kim, D. W. Lee, K. Y. Lee and E. A. Cho, *Catal. Letters*, 2014, **144**, 905–911.
- 35 P. Tian, D. Ding, Y. Sun, F. Xuan, X. Xu, J. Xu and Y. F. Han, *J. Catal.*, 2019, **369**, 95–104.
- 36 P. Tian, L. Ouyang, X. Xu, C. Ao, X. Xu, R. Si, X. Shen, M. Lin, J. Xu and Y. F. Han, *J. Catal.*, 2017, **349**, 30–40.
- 37 A. G. Gaikwad, S. D. Sansare and V. R. Choudhary, *J. Mol. Catal. A Chem.*, 2002, **181**, 143–149.
- 38 V. R. Choudhary, A. G. Gaikwad and S. D. Sansare, *Catal. Letters*, 2002, **83**, 235–239.

Chapter 5: Improving Catalytic Activity towards the Direct Synthesis of H₂O₂ through Cu Incorporation into AuPd/ZSM-5 Catalysts

5.1 Introduction

It is well established the importance of H₂O₂ as an oxidant in green chemistry and hence the synthesis of active and selective catalysts for its direct synthesis.^{1,2} The work presented in Chapter 4 of this thesis demonstrated the efficacy of small level doping of transition metals in an AuPd titania (P25) supported catalyst. In particular, base metals Ni, Zn and Cu were particularly effective in enhancing activity towards the direct synthesis of H₂O₂, with an optimum catalyst composition of 1wt% AuPd_(0.975)X_(0.025)/TiO₂ (where X = Ni, Zn, Cu). These catalysts were able to perform comparably to similar Pt doped catalysts reported by Gong *et al*,³ without the additional costs incurred from use of another noble metal dopant. A key discovery from this work was the incorporation of low levels of Cu substantially improving the activity of the catalyst, which has previously been shown to inhibit activity towards H₂O₂ synthesis, albeit in much larger quantities.^{4,5}

Another important factor in catalyst design is the support, and the use of zeolite supports for the direct synthesis of H₂O₂ is a promising area.⁶⁻¹⁰ Zeolite supports can enhance catalyst activity and selectivity compared to other oxide analogues, most likely due to the improved dispersion of the metal nanoparticles on the support, and the acidic nature of the support.¹¹ It has been demonstrated that supports such as ZSM-5, with lower isoelectric points are able to offer improved activities for the synthesis of H₂O₂ as they are less favourable towards the competing degradation reaction..^{11,12} Another zeolite that could be considered based on the success of the previous work using TiO₂, is titanium silicate-1 (TS-1). However, the aluminium present in ZSM-5 makes this a more acidic support compared to TS-1, a factor that has been shown to aid this reaction, therefore ZSM-5 was chosen as the support for this next body of work.

In Chapter 4 the catalyst series was prepared by a sol-immobilisation methodology, however ICP-OES analysis of those catalysts showed that the majority of the desired third metal was not deposited onto the catalyst support, which was thought to be lost during the washing and

filtration step of this technique. Therefore, an impregnation method for catalyst preparation was employed for the following work to reduce metal loss during the catalyst synthesis. Impregnation catalyst preparations are popular due to the ease of scale up for industrial applications, and it has been found that addition of chloride ions to the precursors, especially Pd, can result in improved dispersion and a more homogeneous alloy composition.¹³

The aim of this work was to develop on the observation that low level doping of transition metals into AuPd catalysts was able to enhance catalytic activity towards the direct synthesis of H₂O₂. The objective was to see how support and catalyst preparation would affect the optimum loading of a dopant metal that was found to be successful in the previous work presented in Chapter 4.

In this work the effect of Ni, Zn and Cu on a 1wt% AuPd/ZSM-5 catalyst, prepared by an excess chloride co-impregnation method, is investigated for the direct synthesis of H₂O₂. It was found that 0.025wt% was an optimum dopant level for the tertiary metal on a TiO₂ (P25) support, and loadings greater than this caused a large change in activity. What will be interesting is whether this behaviour will be seen on a different support (ZSM-5) and if the optimum dopant range will be comparable.

5.2 Results and Discussion

5.2.1 Screening the tertiary metal

Inspired by the previous work in Chapter 4, a series of 1wt% AuPd_(0.975)X_(0.025)/ZSM-5 (where X = Cu, Zn, Ni) catalysts were prepared by an excess chloride co-impregnation methodology and reduced (5% H₂/Ar, 400 °C, 4 h, 10 °C min⁻¹). The selected tertiary metal loading was chosen as it was found that these quantities of the dopant metals were optimum for Cu, Zn and Ni on a TiO₂ support. Zeolite supports such as ZSM-5 enable good metal distribution and addition of chloride during impregnation of the metal onto the support results in better dispersion and more uniform particle size.¹³ The ZSM-5 support undergoes a pre calcination step (static air, ramp 20 °C min⁻¹, 550 °C, 3 h) before catalyst preparation to convert NH₄-ZSM-5 (SiO₂:Al₂O₃ = 30:1) to H-ZSM-5. Catalysts were tested for the 30 minute direct synthesis of H₂O₂, the 30 minute degradation of H₂O₂ and initial rates for the synthesis of H₂O₂ were calculated from 5 minute synthesis reactions, as shown in Figure 5.1a. Analysis of post-reaction gas mixtures from a 30 minute synthesis reaction provided H₂ conversion and H₂O₂ selectivity data as seen in Figure 5.1b.

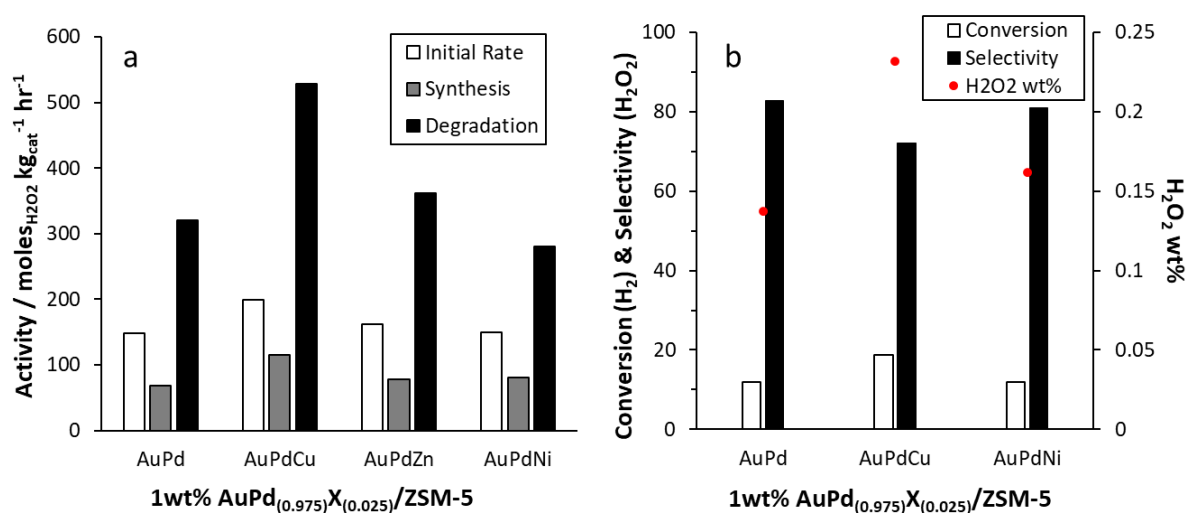


Figure 5.1: (a) Effect of incorporating different tertiary metals (Ni, Zn Cu) to a 1wt% AuPd/ZSM-5 catalyst on the direct hydrogen peroxide synthesis, initial synthesis rate and H₂O₂ degradation. (b) H₂ conversion, H₂O₂ selectivity and H₂O₂ wt% from a 30-minute H₂O₂ synthesis reaction. H₂O₂ synthesis conditions: 0.5 h, 2 °C, P(5% H₂/CO₂) = 420 psi, P(25% O₂/CO₂) = 160 psi, 0.01 g catalyst, 2.9 g water, 5.6 g methanol, 1200 rpm. (Initial rate: 0.08 h). Degradation conditions: 0.5 h, 2 °C, P(5% H₂/CO₂) = 420 psi, 0.01 g catalyst, 0.68 g H₂O₂ (50 wt%), 2.22 g water, 5.6 g methanol, 1200 rpm. Catalysts prepared by excess chloride co-precipitation and reduced (5% H₂/Ar, 400 °C, 4 h, 10 °C min⁻¹).

As seen in Figure 5.1a, the synthesis rate of 1wt% AuPd_(0.975)Cu_(0.025)/ZSM-5 (115 moles_{H₂O₂} kg_{cat}⁻¹ hr⁻¹) is greater than the other trimetallics: 1wt% AuPd_(0.975)Zn_(0.025)/ZSM-5 (77 moles_{H₂O₂} kg_{cat}⁻¹ hr⁻¹) and 1wt% AuPd_(0.975)Ni_(0.025)/ZSM-5 (81 moles_{H₂O₂} kg_{cat}⁻¹ hr⁻¹), and all trimetallics are more active towards the direct synthesis of H₂O₂ than 1wt% AuPd/ZSM-5 (69 moles_{H₂O₂} kg_{cat}⁻¹ hr⁻¹). This supports the findings of Chapter 4, which demonstrated that small levels of these transition metals (Cu, Zn & Ni), can enhance catalytic activity, when compared to the bimetallic analogue.

Initial rates of the synthesis reaction further demonstrate the enhanced activity seen by 1wt% AuPd_(0.975)Cu_(0.025)/ZSM-5 catalyst (199 moles_{H₂O₂} kg_{cat}⁻¹ hr⁻¹), as the contribution of the competitive and undesirable H₂O₂ degradation pathways is considered to be negligible in the initial reaction rate.

When compared to the H₂O₂ synthesis rates of the titania (P25) supported catalysts reported in Chapter 4, the 1wt% AuPd_(0.975)Cu_(0.025)/ZSM-5 (115 moles_{H₂O₂} kg_{cat}⁻¹ hr⁻¹) catalyst supersedes all of the 1wt% AuPd_(0.975)X_(0.025)/TiO₂ (where X = Cu (94 moles_{H₂O₂} kg_{cat}⁻¹ hr⁻¹), Zn (100 moles_{H₂O₂} kg_{cat}⁻¹ hr⁻¹), Ni (moles_{H₂O₂} kg_{cat}⁻¹ hr⁻¹)) catalysts. Notably, the ZSM-5 supported AuPdZn and AuPdNi catalysts are less active than the TiO₂ supported counterparts. However, the reasons for this are not apparent as catalyst preparation method was also different between the catalyst of different supports and therefore to understand what had caused the different trends in activity catalysts would need to be prepared with both supports (TiO₂ and ZSM-5) by both synthesis methods (sol-immobilisation and excess-chloride co-precipitation). Additionally, the activity of 1wt% AuPd_(0.975)Cu_(0.025)/ZSM-5 (115 moles_{H₂O₂} kg_{cat}⁻¹ hr⁻¹) is comparable to that reported in the literature for a 1wt% Au₁Pd₁Pt_{0.1}/TiO₂ (112 moles_{H₂O₂} kg_{cat}⁻¹ hr⁻¹) which was prepared by sol-immobilisation rather than an impregnation method.³

There are studies where it has been shown that Cu incorporated into Pd-only catalysts (using much higher loadings than used here), can inhibit catalytic activity,^{4,5} with DFT studies indicating that the formation of the intermediate hydroperoxyl species (OOH*) and subsequently H₂O₂ is thermodynamically unfavoured over Cu-containing precious metal surfaces.¹⁴ However, contrary to these earlier works, this investigation has again demonstrated that introducing low loadings of Cu (0.025 wt%), into AuPd nanoalloys can promote catalytic activity towards H₂O₂ synthesis, with this study aligning well with the

observations outlined in Chapter 4, further highlighting that the promotive effect is not reliant on catalyst support or the catalyst synthesis method.

The 1wt% $\text{AuPd}_{(0.975)}\text{Cu}_{(0.025)}/\text{ZSM-5}$ catalyst is also observed to have the highest H_2 conversion (19%) compared to AuPd (12%) and AuPdNi (12%), which could contribute to the higher synthesis activity seen for the AuPdCu analogue. The selectivity towards H_2O_2 for the AuPdCu catalyst (72%) is slightly lower than that of AuPd (83%) and AuPdNi (81%), coinciding with the higher rate of degradation seen for the Cu catalyst ($529 \text{ moles}_{\text{H}_2\text{O}_2} \text{ kg}_{\text{cat}}^{-1} \text{ hr}^{-1}$). However, it should be noted that the H_2O_2 selectivity for AuPdCu is not measured at H_2 iso-conversion to the AuPd and AuPdNi catalysts, and the selectivity will generally decrease at a higher conversion for all catalysts. However, even with lower selectivity, the AuPdCu catalyst is still considerably more active towards the production of H_2O_2 and will therefore be the focus of further study.

Interestingly, the rate of degradation over the 1wt% $\text{AuPd}_{(0.975)}\text{Ni}_{(0.025)}/\text{ZSM-5}$ ($281 \text{ moles}_{\text{H}_2\text{O}_2} \text{ kg}_{\text{cat}}^{-1} \text{ hr}^{-1}$) catalyst is lower even than that of the bimetallic 1wt% AuPd/ZSM-5 ($320 \text{ moles}_{\text{H}_2\text{O}_2} \text{ kg}_{\text{cat}}^{-1} \text{ hr}^{-1}$), while showing the same H_2O_2 selectivities ((AuPd (83%) and AuPdNi (81%)) for the synthesis reaction at iso-conversion (12% H_2 conversion). This could indicate that the Ni incorporation is causing the degradation reaction to switch off. The investigation of Ni doping in ZSM-5 catalysts would be an interesting field for future work, with the aim of switching off the subsequent degradation reaction. However, it should be noted that the conditions of the degradation and the synthesis reactions are different which could be responsible for the discrepancies between the H_2O_2 selectivity (in the synthesis reaction) and the degradation activity. The degradation conditions have a much higher concentration of H_2O_2 which can oxidise the metals in the catalyst and therefore alter the activity and selectivities exhibited by the catalyst. Further degradation testing at lower initial H_2O_2 should be performed to see how the rate of degradation is affected, additionally XPS of the used degradation catalysts should be performed to see how the oxidation states of the metal have been altered compared to those in the synthesis.

To determine the stability of the catalysts in the direct synthesis of H₂O₂, analysis of the filtered post-reaction solution was analysed by ICP-MS (Inductively coupled plasma mass spectrometry) to measure the quantity of metal that had leached from the support during the reaction, the data is shown in Table 5.1.

Table 5.1: Metal leaching determined from ICP-MS analysis of the filtered 30 minute reaction solutions from the direct synthesis of hydrogen peroxide, for the 1wt% AuPd_(0.975)X_(0.025)/ZSM-5 (where X = Cu, Zn, Ni) catalyst series. Metal leaching is given as a % of each individual metal loading.

| Catalyst | H ₂ O ₂ Synthesis / moles _{H₂O₂} kg _{cat} ⁻¹ hr ⁻¹ | Metal leached (after 30 min reaction) / % | |
|----------|---|--|------|
| | | Au | Pd |
| AuPd | 69 | 0.34 | 0.71 |
| AuPdCu | 115 | BDL | 0.13 |
| AuPdZn | 77 | BDL | BDL |
| AuPdNi | 81 | BDL | BDL |

H₂O₂ synthesis conditions: 0.5 h, 2 °C, P(5% H₂/CO₂) = 420 psi, P(25% O₂/CO₂) = 160 psi, 0.01 g catalyst, 2.9 g water, 5.6 g methanol, 1200 rpm. Catalysts prepared by excess chloride co-precipitation and reduced (5% H₂/Ar, 400 °C, 4 h, 10 °C min⁻¹). BDL (Below Detection Limit).

During the synthesis with a 1wt% AuPd_(0.975)Cu_(0.025)/ZSM-5 catalyst, very low levels of Pd leaching (0.13%) were observed. However, when compared to the bimetallic 1wt% AuPd/ZSM-5 it is possible that the addition of the third dopant metal may be having a stabilising effect on precious metal species, as leaching was observed for both Au (0.34 %) and Pd (0.71 %) in the case of the bimetallic AuPd catalyst. It was not possible to detect leaching of the dopant metal as any levels were not significant enough for detection. Evidently, the catalysts produced are highly stable with no or negligible leaching detected, especially with the addition of the tertiary metal into the catalyst.

Further evaluation of the fresh 1wt% AuPd_(0.975)X_(0.025)/ZSM-5 catalysts was performed by XPS (X-ray photoelectron spectroscopy) analysis and is shown in Figure 5.2 and Table 5.2. It is important to understand the effect that addition of the dopant metal has on the species of

Pd on the catalyst as this largely influences the activity and selectivity of the catalysts towards H_2O_2 synthesis.

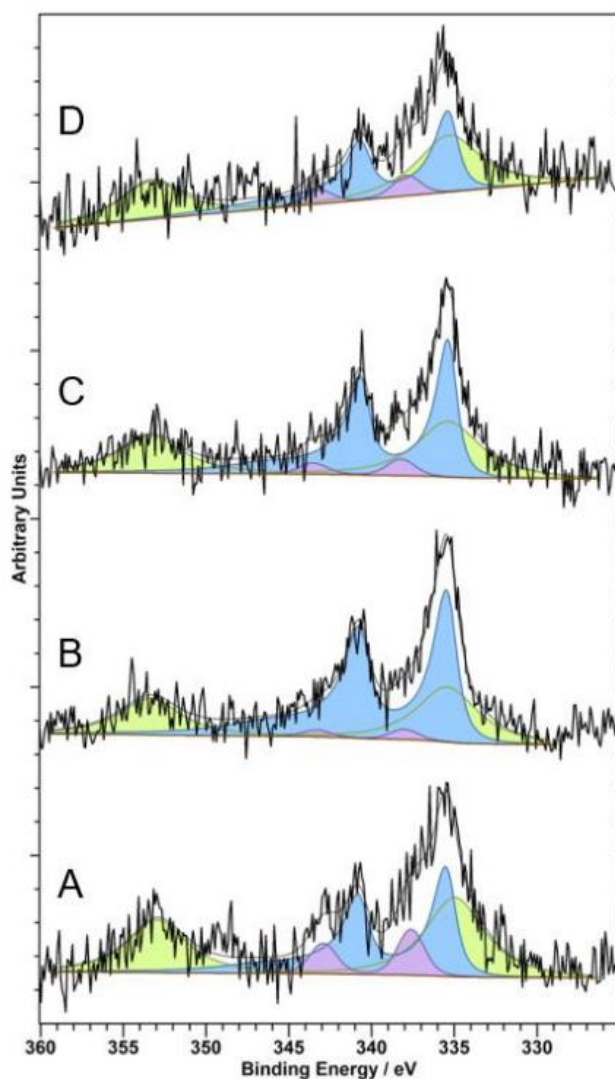


Figure 5.2: XPS spectra of Pd(3d) regions for the as-prepared 1wt% AuPd_(0.975)X_(0.025)/ZSM-5 catalysts as a function of tertiary metal dopant. (A) 1wt% AuPd/ZSM-5; (B) 1wt% AuPd_(0.975)Cu_(0.025)/ZSM-5; (C) 1wt% AuPd_(0.975)Ni_(0.025)/ZSM-5; and (D) 1wt% AuPd_(0.975)Zn_(0.025)/ZSM-5.¹⁵ Key: Au(4d) (green); Pd⁰ (blue); Pd²⁺ (purple). Catalysts prepared by excess chloride co-precipitation and reduced (5% H₂/Ar, 400 °C, 4 h, 10 °C min⁻¹). XPS analysis and images by Dr David Morgan.

Table 5.2: Effect of tertiary metal doping upon surface atomic composition of fresh 1wt% AuPd_{(0.975)X_(0.025)/ZSM-5 (where X = Cu, Ni, Zn) determined by XPS. XPS analysis performed by Dr David Morgan.}

| Catalyst | Au:Pd | Pd ²⁺ :Pd ⁰ |
|---|-------|-----------------------------------|
| 1wt% AuPd/ZSM-5 | 0.78 | 0.30 |
| 1wt% AuPd _(0.975) Cu _(0.025) /ZSM-5 | 0.81 | 1.06 |
| 1wt% AuPd _(0.975) Ni _(0.025) /ZSM-5 | 0.83 | 2.12 |
| 1wt% AuPd _(0.975) Zn _(0.025) /ZSM-5 | 0.28 | 1.13 |

Catalysts prepared by excess chloride co-precipitation and reduced (5% H₂/Ar, 400 °C, 4 h, 10 °C min⁻¹).

The catalysts were all subjected to a reductive heat treatment as part of the catalyst preparation (5% H₂/Ar, 400 °C, 4 h, 10 °C min⁻¹), in spite of this all catalysts contained the Pd²⁺ (PdO) species as well as the Pd⁰ reduced species. The observed Pd speciation in the bimetallic 1wt% AuPd/ZSM-5 (Pd²⁺:Pd⁰ = 0.3) aligns with previous investigations into AuPd systems, whereby the introduction of Au has been shown to modify Pd speciation.¹¹ Low levels of doping with Cu (Pd²⁺:Pd⁰ = 1.06), Zn (Pd²⁺:Pd⁰ = 1.13) and Ni (Pd²⁺:Pd⁰ = 2.12) into the AuPd catalyst resulted in a noticeable shift in Pd speciation and an increase in the proportion of the oxidised species Pd²⁺. It is known that a mixture of the Pd oxidation states in the catalyst improves activity towards direct H₂O₂ synthesis when compared to Pd⁰ or Pd²⁺ rich analogues.^{16,17} It is observed that the trimetallic catalysts, which have an improved mixture of Pd species compared to the bimetallic, have a higher H₂O₂ synthesis activity, which aligns well with earlier works that report the improved performance of catalysts consisting of domains of mixed Pd species.^{16,17} The introduction of Ni into the catalyst shows the largest shift in Pd oxidation state towards Pd²⁺ (Pd²⁺:Pd⁰ = 2.12) which corresponds with the higher H₂O₂ selectivity (and lower degradation) observed for 1wt% AuPd_(0.975)Ni_(0.025)/ZSM-5. However, it is important to note that the Pd species seen in the fresh catalyst samples will not necessarily be consistent with those under the reaction conditions.

It has been reported that AuPd catalysts which are produced by impregnation methods and undergo high heat treatments, as the catalysts reported here have been, form core(Au)-shell(Pd) nanoparticles during the heat treatment. An indication of the core(Au)-shell(Pd) formation is a lower Au:Pd ratio observed in the XPS analysis, which is particularly evident for

the 1wt% AuPd_(0.975)Zn_(0.025)/ZSM-5 (Au:Pd = 0.28) and could suggest that this catalyst has a high number of these. core shell formations. To confirm the presence of core-shell nanoparticle structures microscopy and EDX (energy dispersive spectroscopy) analysis would need to be performed on the catalysts.

It is important to consider the structure of a material and how this may differentiate between catalysts and how the catalyst preparation and heat treatments can affect the characteristics of the support itself. Impregnation techniques result in bimodal particle size distribution and the use of zeolite supports for AuPd has been shown to lead to large nanoparticles, therefore XRD (x-ray diffraction) analysis was conducted to provide information about particle size distribution and to investigate the role of catalyst preparation on the zeolite framework for the 1wt% AuPdX/ZSM-5 catalyst series.

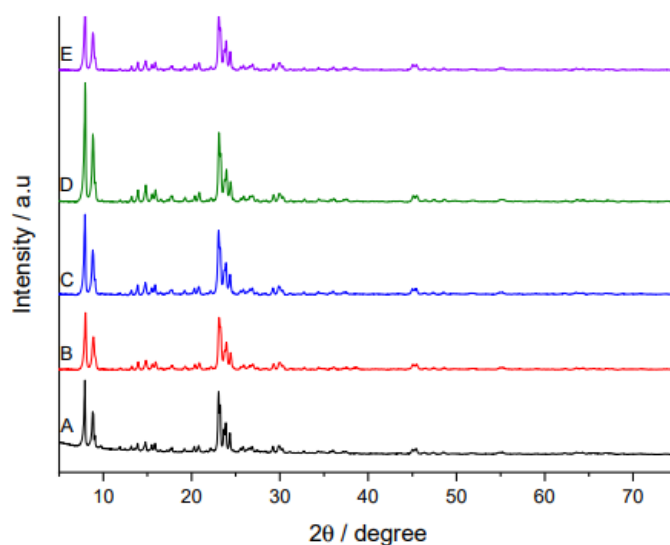


Figure 5.3: X-ray diffractograms of 1wt% AuPd_(0.975)X_(0.025)/ZSM-5 catalysts. (A) ZSM-5, (B) 1wt% AuPd/ZSM-5, (C) 1wt% AuPd_(0.975)Cu_(0.025)/ZSM-5, (D) 1wt% AuPd_(0.975)Ni_(0.025)/ZSM-5 and (E) 1wt% AuPd_(0.975)Zn_(0.025)/ZSM-5.¹⁵ Catalysts prepared by excess chloride co-precipitation and reduced (5% H₂/Ar, 400 °C, 4 h, 10 °C min⁻¹). ICDD patterns for reference: (ZSM-5 ICDD: 00-044-003).

The XRD pattern (Figure 5.3) for ZSM-5 shows the main reflections associated with this material ($2\theta = 7.8, 8.8, 14.8, 23.14, 23.91$ and 24.5°). The ZSM-5 supported catalysts which have undergone metal impregnation via an excess chloride wet co-impregnation procedure, and a subsequent reductive heat treatment (flowing 5% H₂/Ar, 400 °C, 4 h, 10 °C min⁻¹), show

no observable difference in the XRD patterns, displaying the same reflections as the that observed for the bare support. Therefore, it can be deduced that the metal particles are small, and the zeolite appears to have maintained its crystallinity. ZSM-5 is a thermally stable material and is therefore good catalyst material as the main bulk structure does not undergo noticeable changes during catalyst preparation.

Another characterisation technique, FTIR (Fourier-transform infrared) spectroscopy, was employed to determine if the catalyst preparation and subsequent heat treatment degrade the zeolite framework, the analysis is shown in Figure 5.4. As indicated by XRD analysis (Figure 5.3), FTIR indicated no significant changes in the structure of the ZSM-5 support despite undergoing metal impregnation and reductive heat treatment. Three distinct infrared bands can be observed at 800, 1060 and 1220 cm^{-1} which are characteristic of SiO_4 tetrahedron units, the adsorption band at 800 cm^{-1} is assigned to the symmetric stretching of the external linkages of the SiO_4 tetrahedron, the adsorption band at 1060 cm^{-1} is attributed to the internal asymmetric stretching vibration of Si-O linkage, and the adsorption band at 1220 cm^{-1} is assigned to the 5-membered rings present in the structure of the ZSM-5 zeolite.¹⁸ Again, there is no differentiation between the catalysts and the ZSM-5 support, therefore it can be concluded that catalyst preparation does not damage the support.

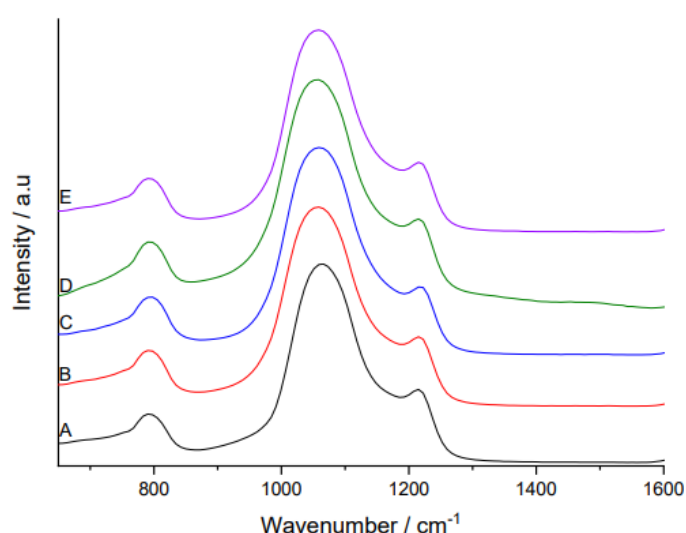


Figure 5.4: Fourier-transform infrared spectroscopy of 1wt% $\text{AuPd}_{(0.975)}\text{X}_{(0.025)}/\text{ZSM-5}$ catalysts. (A) ZSM-5, (B) 1wt% $\text{AuPd}/\text{ZSM-5}$, (C) 1wt% $\text{AuPd}_{(0.975)}\text{Cu}_{(0.025)}/\text{ZSM-5}$, (D) 1wt% $\text{AuPd}_{(0.975)}\text{Ni}_{(0.025)}/\text{ZSM-5}$ and (E) 1wt% $\text{AuPd}_{(0.975)}\text{Zn}_{(0.025)}/\text{ZSM-5}$.¹⁵ Catalysts prepared by excess chloride co-precipitation and reduced (5% H_2/Ar , 400 °C, 4 h, 10 °C min^{-1}).

5.2.2 Optimisation of Cu loading in 1wt% AuPd_(1-x)Cu_(x)/ZSM-5 for the Direct Synthesis of H₂O₂

A clear increase in catalytic activity towards direct H₂O₂ synthesis was observed for the Cu doped catalyst (1wt% AuPd_(0.975)Cu_(0.025)/ZSM-5) when compared to its AuPd bimetallic analogue. This is similar to what was observed in Chapter 4, with the synergistic effect from the addition of 0.025wt% Cu producing a highly active 1wt% AuPd_(0.975)Cu_(0.025)/TiO₂ (94 moles_{H₂O₂} kg_{cat}⁻¹ hr⁻¹) catalyst prepared by sol-immobilisation, for the direct synthesis of H₂O₂. However, this work uses a different support (ZSM-5) and a different catalyst preparation (excess chloride co-impregnation), therefore this study to determine if the optimal Cu loading varies when using a different support and catalyst preparation technique.

To optimise the metal loading of the tertiary metal in the 1wt% AuPd_(1-x)Cu_(x)/ZSM-5 catalyst, and investigate the effect of the Cu doping amount, a catalyst series was produced with a Cu loading from 0.0125 wt% to 0.0375 wt%, all with a total metal loading of 1 wt% and is shown in Figure 5.5.

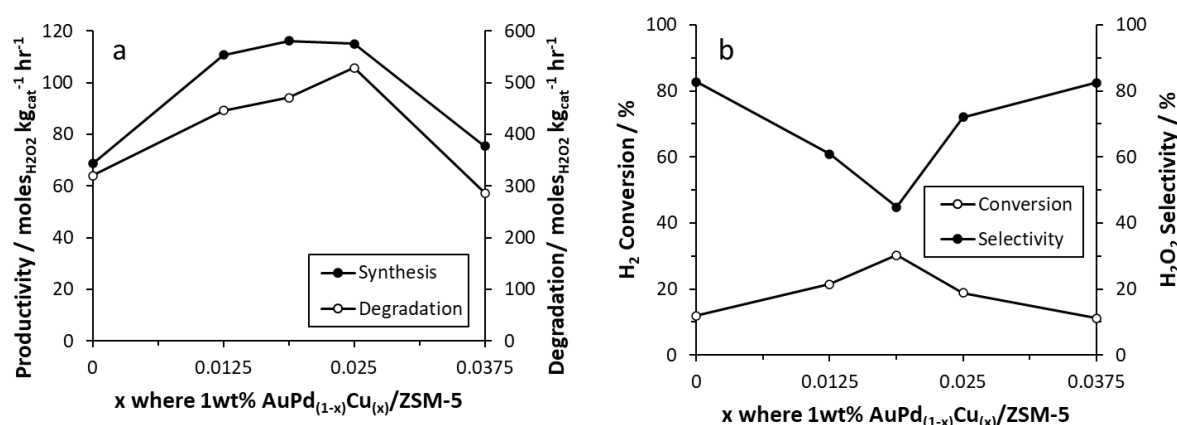


Figure 5.5: (a) The direct hydrogen peroxide synthesis and degradation for 1wt% AuPd_(1-x)Cu_(x)/ZSM-5 (where x = 0, 0.0125, 0.025, 0.0375, 0.05, 0.075, 0.1) (b) Hydrogen conversion and hydrogen peroxide selectivity for the direct synthesis of hydrogen peroxide for 1wt% AuPd_(1-x)Cu_(x)/ZSM-5 (where x = 0, 0.0125, 0.025, 0.0375, 0.05, 0.075, 0.1). Synthesis conditions: 0.5 h, 2 °C, P(5% H₂/CO₂) = 420 psi, P(25% O₂/CO₂) = 160 psi, 0.01 g catalyst, 2.9 g water, 5.6 g methanol, 1200 rpm. Degradation conditions: 0.5 h, 2 °C, P(5% H₂/CO₂) = 420 psi, 0.01 g catalyst, 0.68 g H₂O₂ (50 wt%), 2.22 g water, 5.6 g methanol, 1200 rpm. Catalysts prepared by excess chloride co-precipitation and reduced (5% H₂/Ar, 400 °C, 4 h, 10 °C min⁻¹).

There is an improvement in the synthesis activities for a Cu loading of 0.0125 wt% (111 moles_{H₂O₂} kg_{cat}⁻¹ hr⁻¹), 0.01875 (116 moles_{H₂O₂} kg_{cat}⁻¹ hr⁻¹), 0.025 (115 moles_{H₂O₂} kg_{cat}⁻¹ hr⁻¹).

There is also a similar trend seen in the degradation activities, with increased activity seen for Cu loadings 0.0125 (447 moles_{H₂O₂} kg_{cat}⁻¹ hr⁻¹), 0.01875 (471 moles_{H₂O₂} kg_{cat}⁻¹ hr⁻¹), 0.025 (529 moles_{H₂O₂} kg_{cat}⁻¹ hr⁻¹). The decrease in the synthesis and degradation activities for the 0.0375 Cu loading (75 and 287 moles_{H₂O₂} kg_{cat}⁻¹ hr⁻¹ respectively) aligns with previous research whereby Cu in much higher loadings has been seen to inhibit direct H₂O₂ synthesis activity.^{4,5} What can therefore be deduced is that a small and highly sensitive window of low Cu doping can enhance the activity for this reaction considerably. This trend is similarly seen in Chapter 4 using a TiO₂ support.

However, it is necessary to explore more than just synthesis activities alone when determining the most efficient catalyst. Gas analysis for the reaction shows the H₂ conversion peaks at 30% for a Cu loading 0.01875wt%, however the H₂O₂ selectivity is the lowest for this catalyst at only 45%. In contrast, 0.025wt Cu loading has a much higher H₂O₂ selectivity (72 %). Hence the more favourable catalyst of the two, when looking at the combination of synthesis activity and H₂O₂ selectivity, is 1wt% AuPd_(0.975)Cu_(0.025)/ZSM-5.

The conversion of H₂ is shown to peak correspondingly with the more active Cu catalysts, while H₂O₂ selectivity is observed to decrease as the H₂ conversion increases (and vice versa). The addition of Cu at loadings greater than 0.025 wt%, results in a substantial decrease in H₂ conversion, which correlates with the loss in catalytic activity towards the direct synthesis and subsequent degradation reactions. This observation implies that the enhanced activity of the Cu-containing catalysts is associated with increased reactivity (the rate of H₂ conversion) rather than H₂O₂ selectivity. However, it should be noted that the conclusions drawn from this data have not been made at comparable H₂ conversions, and hence the high H₂O₂ selectivity of 1wt% AuPd/ZSM-5 catalyst (81%) can be related to the low rates of conversion (10%) observed.

Initial rates of the synthesis reaction in Table 5.3 further demonstrate the enhanced activity seen by 1wt% AuPd_(1-x)Cu_(x)/ZSM-5 catalyst (where X = 0.0125, 0.01875, 0.025) with rates of 45.1, 45.7 and 48.5 respectively. As in with the initial rates measurements the contribution of the competitive and undesirable H₂O₂ degradation pathways is considered to be negligible.

Table 5.3: Initial rates for the direct synthesis of H₂O₂ (5 minutes) and metal leaching during the direct synthesis of H₂O₂ (30 minutes) over the 1wt% AuPd_(1-x)Cu_(x)/ZSM-5 catalyst series as determined by ICP-MS.

| Cu Loading / wt% | Initial Rate / mmol _(H₂O₂) mmol _(metal) ⁻¹ min ⁻¹ | Metal leached (after 30 min reaction) / % | | |
|---------------------|--|---|------|-----|
| | | Au | Pd | Cu |
| 0 | 37.6 | 0.34 | 0.71 | - |
| 0.0125 | 45.1 | 0.52 | 1.21 | BDL |
| 0.01875 | 45.7 | BDL | 0.07 | BDL |
| 0.025 | 48.5 | BDL | 0.13 | BDL |
| 0.0375 | 29.7 | 0.07 | 0.14 | BDL |

H₂O₂ synthesis conditions: 0.5 h (initial rate 0.08 h), 2 °C, P(5% H₂/CO₂) = 420 psi, P(25% O₂/CO₂) = 160 psi, 0.01 g catalyst, 2.9 g water, 5.6 g methanol, 1200 rpm. Catalysts prepared by excess chloride co-precipitation and reduced (5% H₂/Ar, 400 °C, 4 h, 10 °C min⁻¹). BDL Below Detection Limit.

Leaching data of the H₂O synthesis post-reaction solution was also measured and shown in Table 5.3. For all catalyst formulations very low leaching is seen, which shows good stability of the metals supported on the catalyst. Due to the negligible leaching demonstrated from the catalyst it can be inferred that there is no substantial amounts of homogeneous Pd in the solution contributing to the reaction.

As the XPS analysis of the AuPdX series (Table 5.2) showed the electronic modification of Pd species as a result of the incorporation of dopant metals, it was subsequently decided to probe the extent of electronic modification as a result of Cu loading. CO-DRIFTS analysis of the 1%AuPd_(1-x)Cu_(x)/ZSM-5 catalytic series was conducted (Figure 5.6), with this technique used widely to probe the surface of supported precious metal catalysts.^{16,19} As seen in Figure 5.6 the spectra was measured in the range 1750–2150 cm⁻¹ as this contains the stretching modes associated with CO adsorbed on Pd and Au surfaces, with the spectra showing primarily Pd–CO IR bands. Au-CO bands are not detected because CO only adsorbs very weakly onto Au at room temperature and hence desorbs quickly, therefore for analysis of Au bands sub-ambient temperatures are needed.

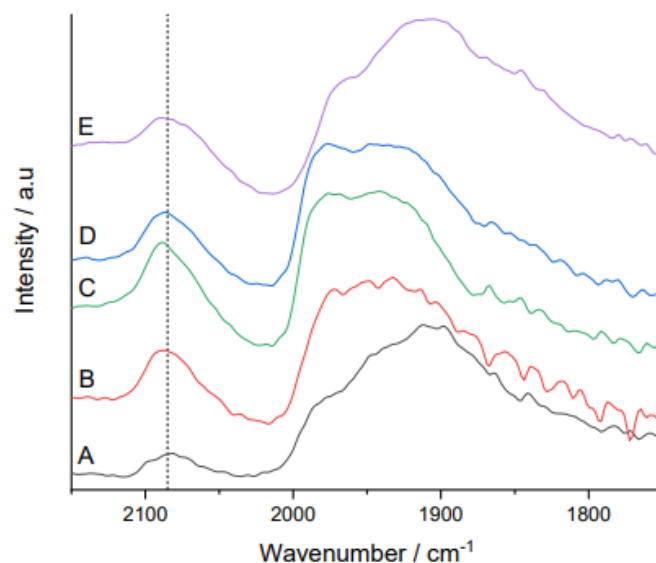


Figure 5.6: CO-DRIFTS spectra showing coverage of CO absorption on 1wt% AuPd_(1-x)Cu_(x)/ZSM-5 catalysts (A) 1wt% AuPd/ZSM-5 (B) 1wt% AuPd_(0.9875)Cu_(0.0125)/ZSM-5 (C) 1wt% AuPd_(0.98125)Cu_(0.01875)/ZSM-5 (D) 1wt% AuPd_(0.975)Cu_(0.025)/ZSM-5 (E) 1wt% AuPd_(0.9625)Cu_(0.0375)/ZSM-5.¹⁵ Catalysts prepared by excess chloride co-precipitation and reduced (5% H₂/Ar, 400 °C, 4 h, 10 °C min⁻¹).

The peak seen at 2080 cm⁻¹ for each of the catalyst samples signifies CO linearly bound to low co-ordination Pd sites (namely, corner and edge sites). The broad peak around 1950 cm⁻¹ represents the bi- and tri-dentate bridging modes of CO with Pd.¹⁹

Notably, with the addition of Cu into the AuPd nanoalloy, a small blue shift is seen in the band which relates to linearly bonded CO on Pd. This aligns well with investigations by Wilson *et al.*¹⁶ into the formation of AuPd alloys, whereby this shift can be ascribed to the segregation of Pd at the nanoparticle surface and a corresponding occupation of lower coordination sites. From these findings it can be proposed that the addition of small quantities of Cu into AuPd nanoalloys results in a similar modification of the nanoparticle composition.

XRD was performed for the 1wt% AuPd_(1-x)Cu_(x)/ZSM-5 (where x = 0, 0.0125, 0.01875, 0.025, 0.0375) series. As shown previously in Figure 5.3 the XRD pattern for ZSM-5 shows the main reflections associated with this material (2θ = 7.8, 8.8, 14.8, 23.14, 23.91 and 24.5°). Figure 5.7 shows XRD of the ZSM-5 supported catalysts which have undergone metal impregnation

and a subsequent reductive heat treatment (flowing 5% H₂/Ar, 400 °C, 4 h, 10 °C min⁻¹). As with the previous set of catalysts, there is no observable difference in the XRD patterns.

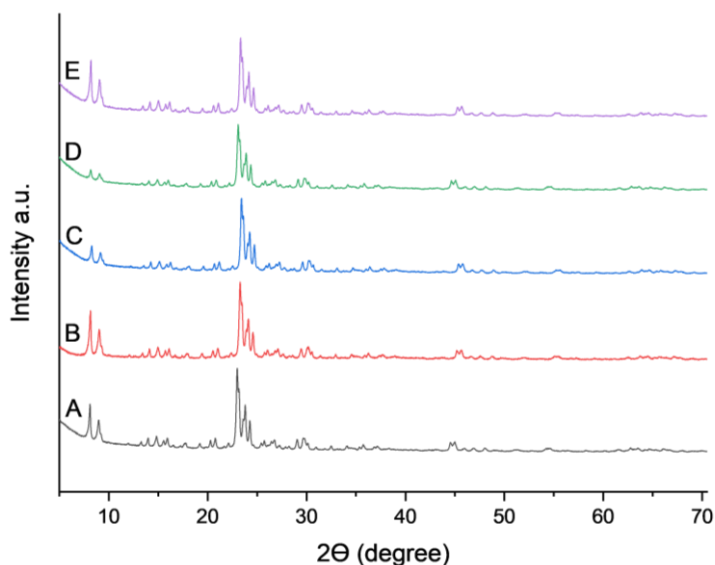


Figure 5.7: X-ray diffractograms of 1wt% AuPd_(1-x)Cu_(x)/ZSM-5 catalysts. (A) 1wt% AuPd/ZSM-5 (B) 1wt% AuPd_(0.9875)Cu_(0.0125)/ZSM-5 (C) 1wt% AuPd_(0.98125)Cu_(0.01875)/ZSM-5 (D) 1wt% AuPd_(0.975)Cu_(0.025)/ZSM-5 (E) 1wt% AuPd_(0.9625)Cu_(0.0375)/ZSM-5.¹⁵ Catalysts prepared by excess chloride co-precipitation and reduced (5% H₂/Ar, 400 °C, 4 h, 10 °C min⁻¹). ICDD patterns for reference: (ZSM-5 ICDD: 00-044-003).

Similarly, FTIR spectroscopy, was employed to look at how the catalysts in the series differ and is shown in Figure 5.8. Again, as seen in the XRD analysis, investigation of the 1wt% AuPd_(1-x)Cu_(x)/ZSM-5 (where x = 0, 0.0125, 0.01875, 0.025, 0.0375) catalyst series by FTIR (Figure 5.8) indicated no significant changes in the structure of the ZSM-5 support despite undergoing metal impregnation and reductive heat treatment.

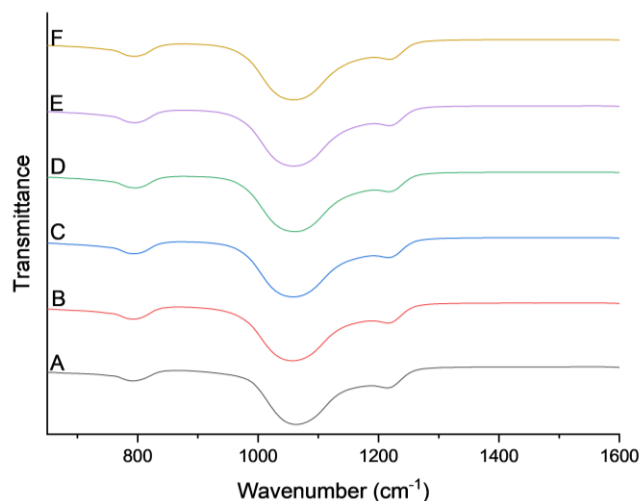


Figure 5.8: Fourier-transform infrared spectroscopy of 1wt% AuPd_(1-x)Cu_(x)/ZSM-5 catalysts. (A) ZSM-5, (B) 1wt% AuPd/ZSM-5 (C) 1wt% AuPd_(0.9875)Cu_(0.0125)/ZSM-5 (D) 1wt% AuPd_(0.98125)Cu_(0.01875)/ZSM-5 (E) 1wt% AuPd_(0.975)Cu_(0.025)/ZSM-5 (F) 1wt% AuPd_(0.9625)Cu_(0.0375)/ZSM-5.¹⁵ Catalysts prepared by excess chloride co-precipitation and reduced (5% H₂/Ar, 400 °C, 4 h, 10 °C min⁻¹).

5.2.3 Further Study and Characterisation of 1wt% AuPd_(0.975)Cu_(0.025)/ZSM-5

Time-on-line studies were run to further investigate the catalytic performance of the Cu incorporated 1wt% AuPd_(0.975)Cu_(0.025)/ZSM-5 catalyst compared to the bimetallic analogue 1wt% AuPd/ZSM-5, and shown in Figure 5.9. It is important to see if the catalyst is able to maintain its enhanced activity over a prolonged reaction time.

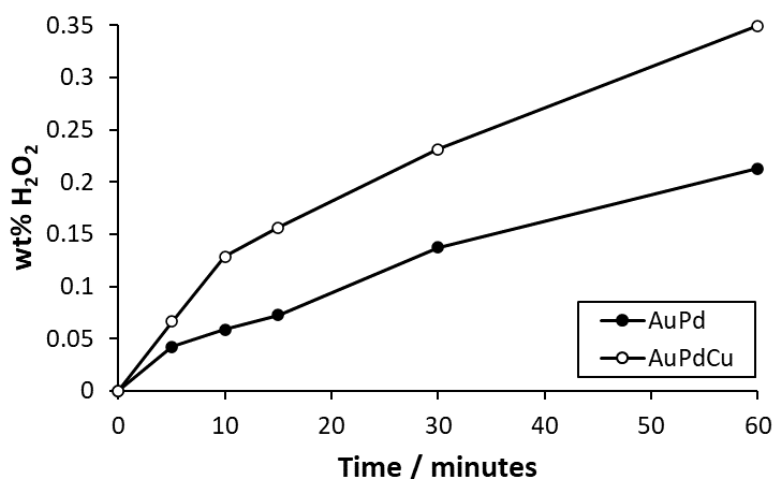


Figure 5.9: Time-on line of direct H₂O₂ synthesis by 1wt% AuPd/ZSM-5 and 1wt% AuPd_(0.975)Cu_(0.025)/ZSM-5. Synthesis conditions: 2 °C, P(5% H₂/CO₂) = 420 psi, P(25% O₂/CO₂) = 160 psi, 0.01 g catalyst, 2.9 g water, 5.6 g methanol, 1200 rpm. Catalysts prepared by excess chloride co-precipitation and reduced (5% H₂/Ar, 400 °C, 4 h, 10 °C min⁻¹).

Initial rates of the direct synthesis of H₂O₂ were measured from the initial 5 minutes of the reaction, where it is assumed that there is no competing H₂O₂ degradation taking place in the reaction. At this initial 5-minute reaction time, the Cu catalyst (0.066 wt%) still produces more H₂O₂ than the bimetallic AuPd (0.042 wt%).

At extended reaction times (60 minutes) the rate of H₂O₂ synthesis seen by 1wt%AuPd_(0.975)Cu_(0.025)/ZSM-5 is still greater than that observed for 1wt%AuPd/ZSM-5. As seen previously the rate of degradation for the Cu catalyst is high, and whilst the competing degradation reaction is not present for the initial 5-10 minutes of the reaction, it will start to compete with the rate of synthesis after 10 mins, and therefore the rate of production of H₂O₂ will decrease. To compete with the high degradation rate, the rate of synthesis for the Cu catalyst must be even greater to maintain the net increase in H₂O₂ production past this point, indicating that the catalyst maintains its enhanced catalytic activity over prolonged periods.

For both catalysts H₂O₂ production has not reached a steady state, meaning that at this point the rate of degradation is not equal to the rate of synthesis over either catalyst in a 60 minute reaction time.

Table 5.4 shows the H₂ conversion and corresponding H₂O₂ selectivity the 30 and 60 minute H₂O₂ direct synthesis over 1wt%AuPd_(0.975)Cu_(0.025)/ZSM-5 and 1wt%AuPd/ZSM-5.

Table 5.4: Hydrogen conversion and hydrogen peroxide selectivity for 30-minute and 60-minute reaction times for direct hydrogen peroxide synthesis, determined by gas analysis.

| Catalyst | H ₂ O ₂ Produced | | H ₂ Conversion | | H ₂ O ₂ Selectivity | |
|--|--|--------|---------------------------|--------|---|--------|
| | / wt% | | / % | | / % | |
| | 30 min | 60 min | 30 min | 60 min | 30 min | 60 min |
| 1wt% AuPd/ZSM-5 | 0.137 | 0.213 | 12 | 16 | 83 | 79 |
| 1wt% AuPd_(0.975)Cu_(0.025)/ZSM-5 | 0.232 | 0.350 | 19 | 57 | 72 | 36 |

H₂O₂ synthesis conditions: 2 °C, P(5% H₂/CO₂) = 420 psi, P(25% O₂/CO₂) = 160 psi, 0.01 g catalyst, 2.9 g water, 5.6 g methanol, 1200 rpm. Catalysts prepared by excess chloride co-precipitation and reduced (5% H₂/Ar, 400 °C, 4 h, 10 °C min⁻¹).

The higher H₂ conversions seen for AuPdCu at 30 and 60 minutes (19% and 57% respectively) are much greater than for AuPd at 30 and 60 minutes (12% and 16% respectively). With the higher H₂ conversion seen for the AuPdCu catalyst, there is naturally an increased synthesis activity observed. The lower H₂O₂ selectivity seen for the AuPdCu catalyst at 60 minutes corresponds with the decreased synthesis rate observed at 60 minutes, that is likely due to the competing degradation reaction.

To properly compare the relative selectivities of the catalysts it is important to look at H₂O₂ selectivities at iso-conversion of H₂. The H₂ conversion of 1wt%AuPd/ZSM-5 at 60 minutes is 16% while the H₂ conversion of 1wt%AuPd_(0.975)Cu_(0.025)/ZSM-5 at 30 minutes is 19%, correspondingly the H₂O₂ selectivities are 79% and 72% respectively. The selectivities of the catalysts are very similar, at near iso-conversion, indicating that while the 1wt%AuPd_(0.975)Cu_(0.025)/ZSM-5 catalyst has a much enhanced activity towards H₂O₂ synthesis, it is not substantially effecting the selectivity of the catalyst compared to the much less active bimetallic analogue.

Further investigation of catalytic performance was performed with gas replacement reactions, as seen in Figure 5.10, to study the activity of the catalyst over prolonged reaction periods. The enhanced H₂O₂ synthesis activity of the 1wt% AuPd_(0.975)Cu_(0.025)/ZSM-5 catalyst, is again clear. It is notable that for 1wt% AuPd_(0.975)Cu_(0.025)/ZSM-5, by reaction 4 the concentration of H₂O₂ in the reaction medium is decreasing, this could be due a number of reasons, the degradation rate becoming greater than rate of synthesis, or it could be due to deactivation of the catalyst. Longer gas replacement studies and reuse studies on the catalyst after this point could indicate if the catalyst has deactivated. Comparably, for 1wt% AuPd/ZSM-5 the amount of H₂O₂ produced appears to be steadily increasing as a constant rate from reaction 2 to 4, however, as it has not yet reached the H₂O₂ concentration that the AuPdCu catalyst has, it is unknown whether a steady state or catalyst deactivation will occur at the same concentration. Longer gas replacement studies are needed to determine if the AuPd catalyst is able to achieve H₂O₂ concentrations comparable to that of the AuPdCu catalyst, and at what concentration a steady state is achieved. Leaching analysis also should be performed for the gas replacement studies (for both catalysts) along with characterisation such as XPS and microscopy of both catalysts after each reaction to see if changes to the

catalyst could be responsible for any potential catalyst deactivation. Additionally, gas analysis for each reaction should be performed, if the catalyst does deactivate then H₂ conversion may cease.

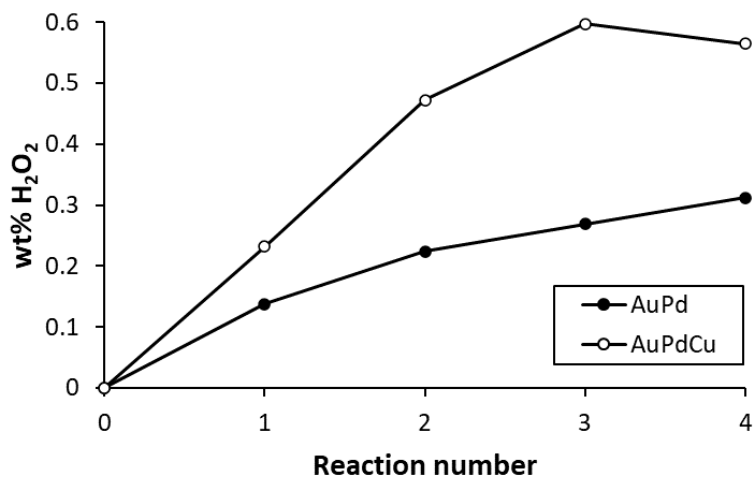


Figure 5.10: Gas replacement reactions for direct H₂O₂ synthesis by 1wt% AuPd/ZSM-5 and 1wt% AuPd_(0.975)Cu_(0.025)/ZSM-5. For each consecutive reaction, the reactor gas is vented and refilled. Synthesis conditions: 0.5 h, 2 °C, P(5% H₂/CO₂) = 420 psi, P(25% O₂/CO₂) = 160 psi, 0.01 g catalyst, 2.9 g water, 5.6 g methanol, 1200 rpm. Catalysts prepared by excess chloride co-precipitation and reduced (5% H₂/Ar, 400 °C, 4 h, 10 °C min⁻¹).

BET analysis as seen in Figure 5.11, was performed to investigate how the ZSM-5 support is affected by metal impregnation and reductive heat treatment. It is important to note that the ZSM-5 support has been calcined before BET analysis as it would be prior to catalyst preparation. As seen from the data in Table 5.5 the surface area of the ZSM-5 support (493 m² g⁻¹) is larger than for the metal impregnated catalysts 1wt% AuPd/ZSM-5 (446 m² g⁻¹) and 1wt% AuPd_(0.975)Cu_(0.025)/ZSM-5 (440 m² g⁻¹). This is likely due to the deposition of metal nanoparticles within the pore-structure of the zeolite, as further indicated by determination of micropore volume with the V_{micropore} of the ZSM-5 support (0.185 cm³ g⁻¹) reduced upon the immobilisation of active metals onto the support; with the V_{micropore} of the 1wt%AuPd/ZSM-5 (0.170 cm³ g⁻¹) and 1wt% AuPd_(0.975)Cu_(0.025)/ZSM-5 (0.171 cm³ g⁻¹) catalysts considerably lower than that of the parent support.

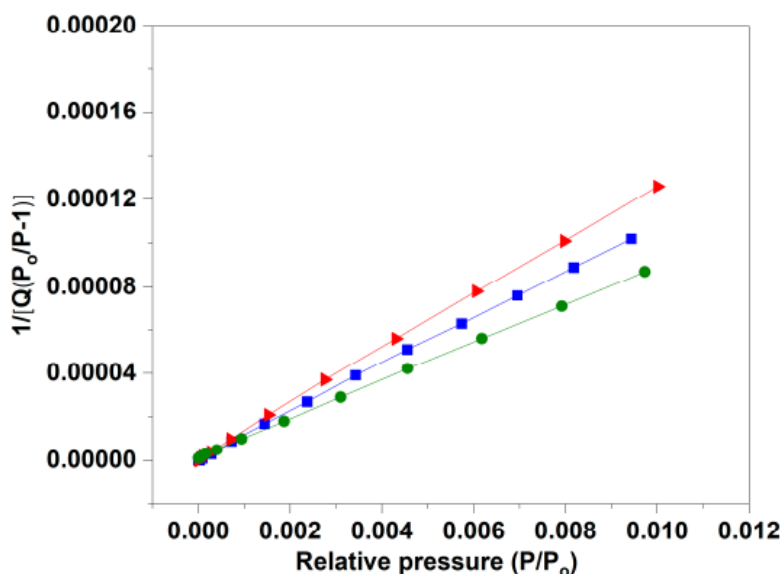


Figure 5.11: BET analysis plots for key 1wt% AuPd_(0.0975)X_(0.025)/ZSM-5 catalysts and HZSM-5(30). Key: ZSM-5(30) (red triangles), 1w% AuPd/ZSM-5 (blue squares), 1wt% AuPd_(0.975)Cu_(0.025)/ZSM-5 (green circles).¹⁵ Note: ZSM-5 support exposed to calcination prior to metal immobilisation (flowing air, 550 °C, 3 h, 20 °C min⁻¹). Catalysts prepared by excess chloride co-precipitation and reduced (5% H₂/Ar, 400 °C, 4 h, 10 °C min⁻¹).

Table 5.5: Porosity and surface area of 1wt % AuPd/ZSM-5 1wt% AuPd_(0.975)Cu_(0.025)/ZSM-5 and the corresponding ZSM-5 support. ZSM-5 support is calcined (flowing air, 550 °C, 3 h, ramp rate 20 °C min⁻¹) prior to catalyst preparation.

| Catalyst | Surface area / m ² g ⁻¹ | V _{micropore} / cm ³ g ⁻¹ |
|---|---|--|
| ZSM-5(30) | 493 | 0.185 |
| 1wt% AuPd/ZSM-5 | 446 | 0.170 |
| 1wt% AuPd _(0.975) Cu _(0.025) /ZSM-5 | 440 | 0.171 |

Catalysts prepared by excess chloride co-precipitation and reduced (5% H₂/Ar, 400 °C, 4 h, 10 °C min⁻¹).

5.2.4 Reusability of trimetallic catalysts

A key aspect of any catalyst is its reusability, as for large scale industrial reactions efficient reusability of a catalyst will be imperative. To conduct reusability experiments 0.05 g of catalyst was first used in a direct H_2O_2 synthesis experiment, then filtered from the reaction solution, and dried under vacuum prior to the testing of a standard mass of catalyst (0.01 g). Figure 5.12 shows initial H_2O_2 synthesis rates (5 minute synthesis), H_2O_2 synthesis and H_2O_2 degradation for the fresh and reused 1wt% AuPd/ZSM-5 and 1wt% AuPd_(0.975)Cu_(0.025)/ZSM-5 catalysts.

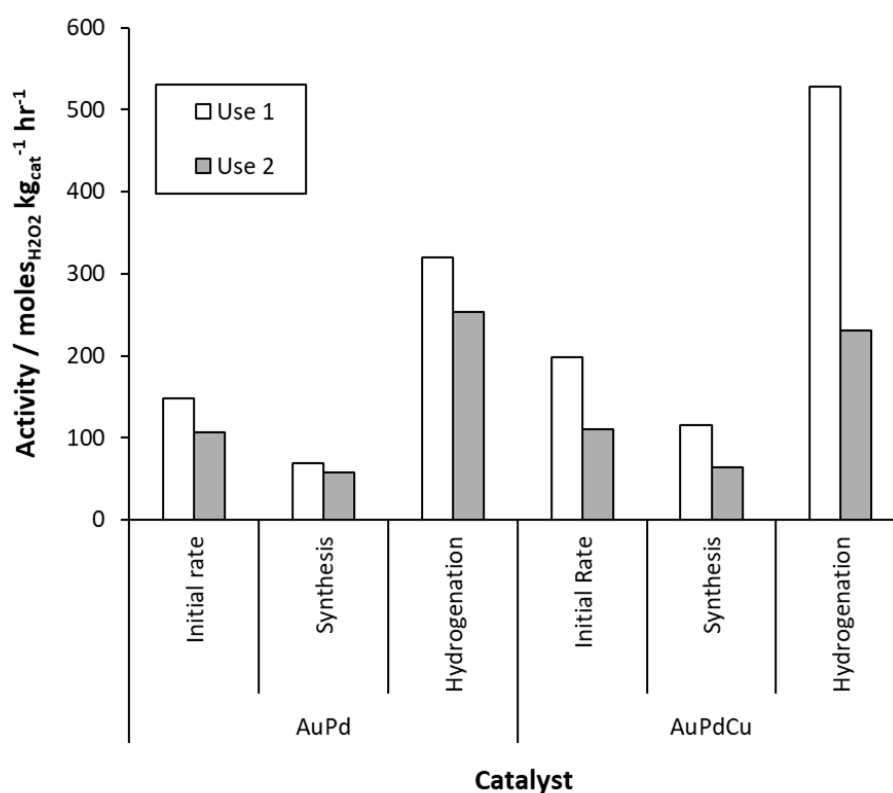


Figure 5.12: For reuse testing an excess of catalyst (1wt% AuPd/ZSM-5 and 1wt% AuPd_(0.975)Cu_(0.025)/ZSM-5) was used in a standard H_2O_2 synthesis test, then filtered and dried in a vacuum oven 30°C, 16hrs. Dried catalyst was then tested as follows: Synthesis conditions: 0.5 h (0.08 hr for initial rate), 2 °C, P(5% H_2/CO_2) = 420 psi, P(25% O_2/CO_2) = 160 psi, 10 mg catalyst, 2.9 g water, 5.6 g methanol, 1200 rpm. Degradation conditions: 0.5 h, 2 °C, P(5% H_2/CO_2) = 420 psi, 10 mg catalyst, 0.68 g H_2O_2 (50 wt%), 2.22 g water, 5.6 g methanol, 1200 rpm. Catalysts prepared by excess chloride coprecipitation and reduced (5% H_2/Ar , 400 °C, 4 h, 10 °C min^{-1}).

Table 5.6: H₂O₂ produced in 5 minute and 30 minute synthesis reactions, initial use and reuse. Synthesis conditions: 0.5 h (or 0.08 hr), 2 °C, P(5% H₂/CO₂) = 420 psi, P(25% O₂/CO₂) = 160 psi, 10 mg catalyst, 2.9 g water, 5.6 g methanol, 1200 rpm.

| Catalyst | Reaction time / min | H ₂ O ₂ synthesised / wt% | | H ₂ O ₂ synthesised / mol | |
|----------|---------------------|---|-------------------------|---|-------------------------|
| | | Use 1 | Use 2 | Use 1 | Use 2 |
| AuPd | 5 | 4.96 x 10 ⁻² | 3.56 x 10 ⁻² | 1.24 x 10 ⁻⁴ | 8.90 x 10 ⁻⁵ |
| | 30 | 1.37 x 10 ⁻¹ | 1.15 x 10 ⁻¹ | 3.43 x 10 ⁻⁴ | 2.86 x 10 ⁻⁴ |
| AuPdCu | 5 | 6.63 x 10 ⁻² | 3.70 x 10 ⁻² | 1.66 x 10 ⁻⁴ | 9.23 x 10 ⁻⁵ |
| | 30 | 2.30 x 10 ⁻¹ | 1.27 x 10 ⁻¹ | 5.75 x 10 ⁻⁴ | 3.18 x 10 ⁻⁴ |

Upon reuse of both the 1wt% AuPd/ZSM-5 and 1wt% AuPd_(0.975)Cu_(0.025)/ZSM-5 catalysts performance towards the synthesis and degradation of H₂O₂ decreased. However, the H₂O₂ synthesis rate upon reuse, of the AuPdCu catalyst (64 mol_{H₂O₂} kg_{cat}⁻¹ hr⁻¹) was found to still be greater than that of the AuPd analogue (57 mol_{H₂O₂} kg_{cat}⁻¹ hr⁻¹). Most notably the rate of degradation for the AuPdCu catalyst decreased from 529 to 231 mol_{H₂O₂} kg_{cat}⁻¹ hr⁻¹ upon reuse, which is almost half the rate of degradation observed upon its first use. The rate of degradation of the AuPd catalyst also decreases, but to a lesser extent, from 320 to 253 mol_{H₂O₂} kg_{cat}⁻¹ hr⁻¹ upon reuse. Notably, the degradation rate upon reuse is higher for the bimetallic AuPd than for the AuPdCu catalyst, suggesting that the AuPdCu reuse catalyst is less selective towards the degradation reaction than the AuPd reuse catalyst. It is notable that although the synthesis activity of the 1wt% AuPd_(0.975)Cu_(0.025)/ZSM-5 decreases substantially upon reuse, it is still more active than synthesis reuse of 1wt% AuPd/ZSM-5.

There are many factors that can affect the reusability of a heterogeneous catalyst in a liquid phase reaction, one being leaching of metals from the catalyst during the reaction. Additionally metal leaching can result in a homogeneous contribution to the observed catalytic activity, which is also a concern as colloidal Pd is active in catalysing the direct synthesis reaction.²⁰ ICP-MS was used to analyse the filtered reaction solution from the H₂O₂ synthesis, and the leaching data is given in Table 5.7. There is only a small quantity of leaching of Pd from the two catalysts 1wt% AuPd/ZSM-5 and 1wt% AuPd_(0.975)Cu_(0.025)/ZSM-5 (0.17 and 0.13% respectively), no detected leaching of Au and Cu, and no detected leaching of any metal

after the second use for H₂O synthesis. A 0.17% metal loss from the 1wt% AuPd/ZSM-5 catalyst, is equivalent to 6x10⁻⁸ g less Pd upon reuse, and a 0.13% metal loss from the 1wt% AuPd_(0.975)Cu_(0.025)/ZSM-5 catalyst, is equivalent to 3.3x10⁻⁸ g less Pd upon reuse. It is therefore unlikely that such a negligible decrease in Pd content during the first reaction would affect the activity of the catalyst in such a way that is seen upon reuse, so this is unlikely to be a main contributor to the loss in synthesis (and degradation) activity upon reuse (for either catalyst).

Table 5.7: Catalyst reusability for H₂O₂ synthesis and metal leaching as determined by ICP-MS analysis of filtered 30-minute reaction solution.

| Catalyst | Productivity / | | Metal Leached / % | |
|--|--|------|-------------------|------|
| | mol _{H₂O₂} kg _{cat} ⁻¹ hr ⁻¹ | | Au | Pd |
| | Fresh | Used | | |
| 1wt% AuPd/ZSM-5 | 69 | 57 | 0 | 0.17 |
| 1wt% AuPd_(0.975)Cu_(0.025)/ZSM-5 | 115 | 64 | 0 | 0.13 |

H₂O₂ synthesis conditions: 0.5 h, 2 °C, P(5% H₂/CO₂) = 420 psi, P(25% O₂/CO₂) = 160 psi, 0.01 g catalyst, 2.9 g water, 5.6 g methanol, 1200 rpm. Catalysts prepared by excess chloride co-precipitation and reduced (5% H₂/Ar, 400 °C, 4 h, 10 °C min⁻¹).

Another factor that could contribute to the changes in activity seen by the catalysts upon reuse is changes in metal nanoparticle size and dispersion of the metal on the catalyst. During use in the H₂O₂ synthesis reaction, changes to the metal nanoparticles can occur such as agglomeration. The correlation between catalytic activity towards H₂O₂ synthesis and particle size has been studied widely, with Tian *et al.*^{21,22} demonstrating that particle size in the sub-nanometre range is crucial for achieving optimal catalytic performance for monometallic Pd catalysts.

Figure 5.13 shows the representative bright field transmission electron micrographs and corresponding particle size histograms of the as-prepared catalysts and the catalysts after use in the direct synthesis of H₂O₂. The particle sizes of the 1wt% AuPd/ZSM-5 and 1wt% AuPd_(0.975)Cu_(0.025)/ZSM-5 catalysts are summarised in Table 5.8 with their corresponding activities towards H₂O₂ synthesis. The measured particle sizes of the fresh 1wt% AuPd/ZSM-

5 (3.7 nm) and 1wt% AuPd_(0.975)Cu_(0.025)/ZSM-5 (4.1 nm) catalysts are comparable, as are the particle sizes after use (4.4 & 4.5 nm respectively). TEM analysis of the used catalyst samples also shows negligible changes in the metal nanoparticle sized from the fresh catalyst samples and the nanoparticle sizes of the catalyst are also comparable to each other. Therefore, loss in catalyst performance of the used catalysts cannot be attributed to nanoparticle agglomeration as particle sizes have remained constant.

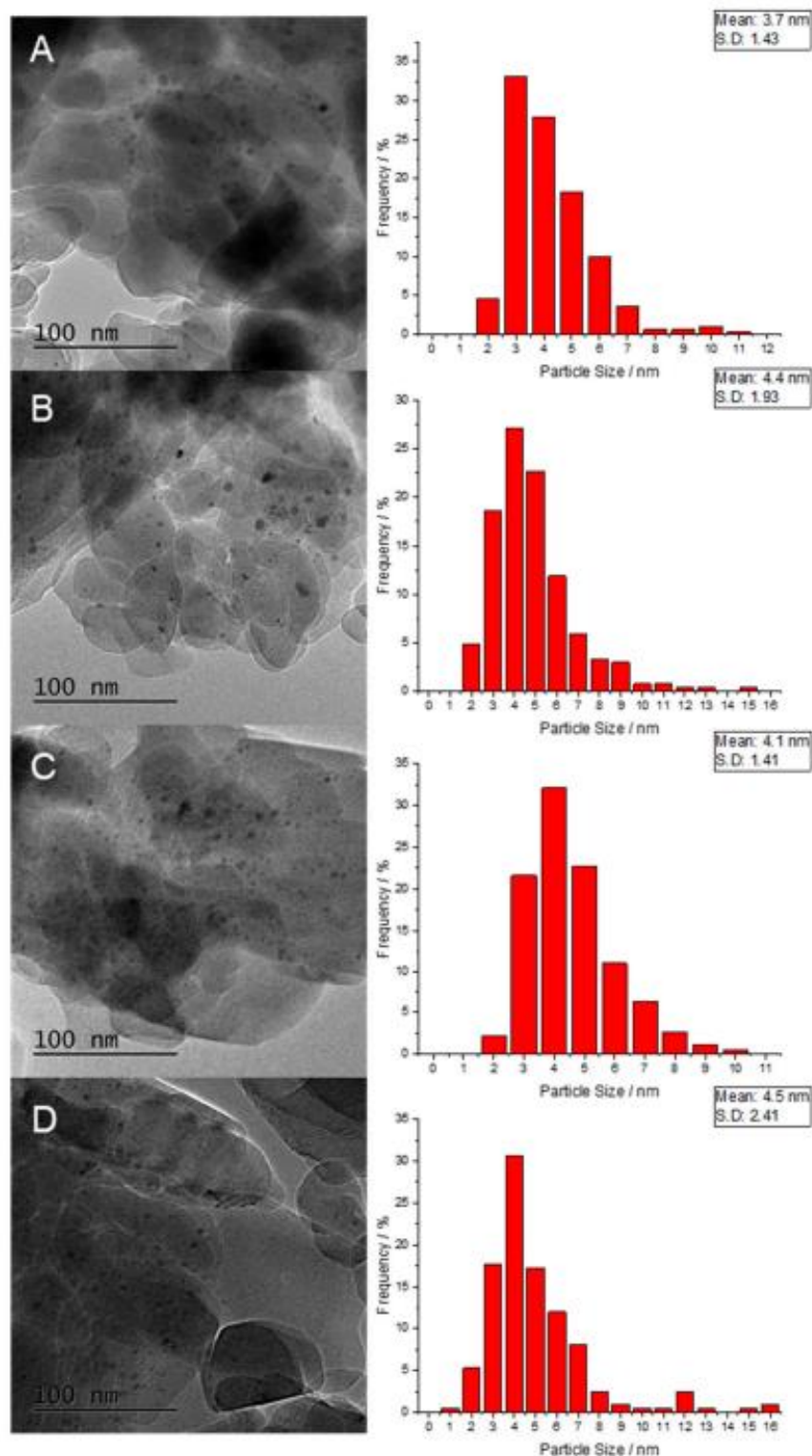


Figure 5.13: Representative bright field transmission electron micrographs and corresponding particle size histograms of as-prepared (A) 1wt% AuPd/ZSM-5 and (C) 1wt% AuPd_(0.975)Cu_(0.025)/ZSM-5 catalysts and analogous (B) 1wt% AuPd/ZSM-5 and (D) 1wt% AuPd_(0.975)Cu_(0.025)/ZSM-5 samples after use in the direct synthesis reaction.¹⁵ H₂O₂ synthesis conditions: 0.5 h, 2 °C, P(5% H₂/CO₂) = 420 psi, P(25% O₂/CO₂) = 160 psi, 0.01 g catalyst, 2.9 g water, 5.6 g methanol, 1200 rpm. Catalysts prepared by excess chloride co-precipitation and reduced (5% H₂/Ar, 400 °C, 4 h, 10 °C min⁻¹).

Table 5.8: Mean particle size and comparative H₂O₂ synthesis productivity from the fresh and used catalysts.

| Catalyst | Mean Particle size | | Productivity | |
|--|----------------------|------------|---|-----------|
| | / nm | | / mol _{H₂O₂} kg _{cat} ⁻¹ h ⁻¹ | |
| | (Standard Deviation) | | (H ₂ O ₂ Concentration / wt%) | |
| | Fresh | Used | Use 1 | Use 2 |
| 1wt% AuPd/ZSM-5 | 3.7 (1.43) | 4.4 (1.93) | 69 (0.14) | 57 (0.11) |
| 1wt% AuPd_(0.975)Cu_(0.025)/ZSM-5 | 4.1 (1.41) | 4.5 (2.41) | 115 (0.23) | 64 (0.13) |

H₂O₂ synthesis conditions: 0.5 h, 2 °C, P(5% H₂/CO₂) = 420 psi, P(25% O₂/CO₂) = 160 psi, 0.01 g catalyst, 2.9 g water, 5.6 g methanol, 1200 rpm. Catalysts prepared by excess chloride co-precipitation and reduced (5% H₂/Ar, 400 °C, 4 h, 10 °C min⁻¹).

From the characterisation of the fresh and used catalysts, it can be deduced that the enhanced catalytic activity towards H₂O₂ synthesis seen by the AuPdCu catalyst (115 mol_{H₂O₂} kg_{cat}⁻¹ h⁻¹) compared to the AuPd catalyst (69 mol_{H₂O₂} kg_{cat}⁻¹ h⁻¹) was achieved through the introduction of Cu into AuPd nanoparticles rather than change in nanoparticle size. It can therefore be proposed that the enhanced activity was as a result of the electronic modification of the Pd species as a result of the introduction of small concentrations of Cu doping, as shown by CO-DRIFTS seen in Figure 5.6 and XPS analysis seen in Figure 5.2. Additionally, there are possible structural changes also indicated by CO-DRIFTS analysis which could be responsible for the enhanced activities seen for the Cu catalyst.

For catalysts prepared by an excess chlorine impregnation method there can be excess chlorine content in the catalysts. The Cl may not be fully removed in the reductive heat treatment step of the catalyst preparation, where hydrogen gas flows over the catalyst at a high temperature and chloride ions can react (forming small quantities of HCl) and hence be removed from the catalyst surface. In comparison catalyst preparation methods, such as sol-immobilisation, involve a thorough washing step with deionised water which removes the majority of unwanted ions prior to heat treatment. It has previously been observed that a loss in surface Cl species during use in the direct synthesis reaction, can result in a decrease in catalytic performance, as Cl is a known promoter of H₂O₂ synthesis activity.²³

However, XPS analysis (Figure 5.14) shows that no signal is observed for any catalyst formulation within the expected energy window for Cl(2p) (approx. 200 eV)²⁴ for the fresh and used samples of 1wt% AuPd/ZSM-5 and 1wt% AuPd_(0.975)Cu_(0.025)/ZSM-5. Therefore, we can deduce that the reduction heat treatment was successful in removing any chlorine content on the surface of the catalyst (to below the XPS detection limit). This contradicts previous investigations into AuPd/TiO₂ catalysts prepared via an similar synthesis technique and possibly indicates the role of the support in retaining halide species (Cl).²³ However, the negligible Cl concentrations observed for these catalysts excludes the possibility of Cl loss during the reaction as the cause of loss in catalytic performance upon reuse.

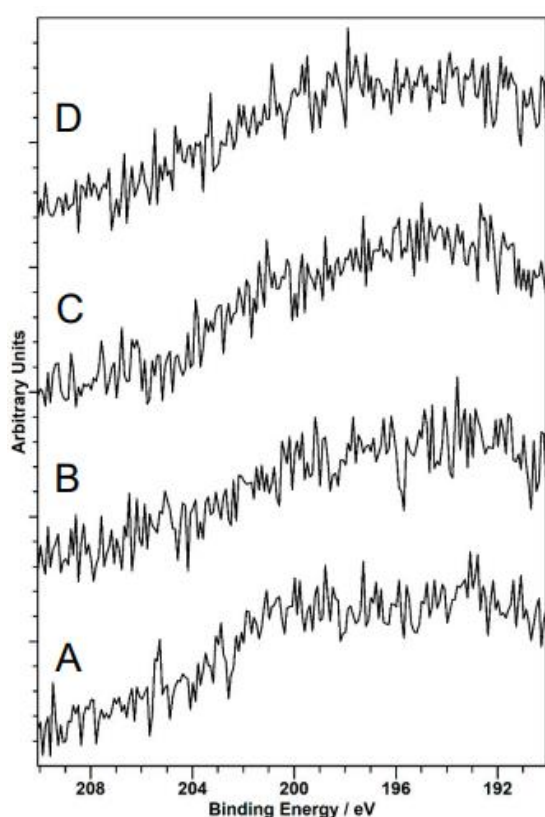


Figure 5.14: Comparison of surface atomic Cl content of the (A) fresh and (B) used 1wt% AuPd/ZSM-5 catalyst and the (C) fresh and (D) used 1wt% AuPd_(0.975)Cu_(0.025)/ZSM-5 analogue.¹⁵ H₂O₂ synthesis conditions: 0.5 h, 2 °C, P(5% H₂/CO₂) = 420 psi, P(25% O₂/CO₂) = 160 psi, 0.01 g catalyst, 2.9 g water, 5.6 g methanol, 1200 rpm. Catalysts prepared by excess chloride co-precipitation and reduced (5% H₂/Ar, 400 °C, 4 h, 10 °C min⁻¹). XPS analysis and images by Dr David Morgan.

Figure 5.15 shows the Pd region of the XPS analysis for the fresh and used AuPd and AuPdCu catalysts. A modification in the Au:Pd ratio for both catalysts after use was observed, which may be indicative of nanoalloy restructuring, with a total shift in the Pd speciation from Pd²⁺ to Pd⁰ also observed, with this latter observation likely due to the high concentration of H₂ present in the reaction. This could also be the cause of the decrease in catalytic performance that is seen for both catalysts (particularly the Cu catalyst) upon reuse. Hence, for future work there is a need to address the stability concerns, particularly around Pd speciation.

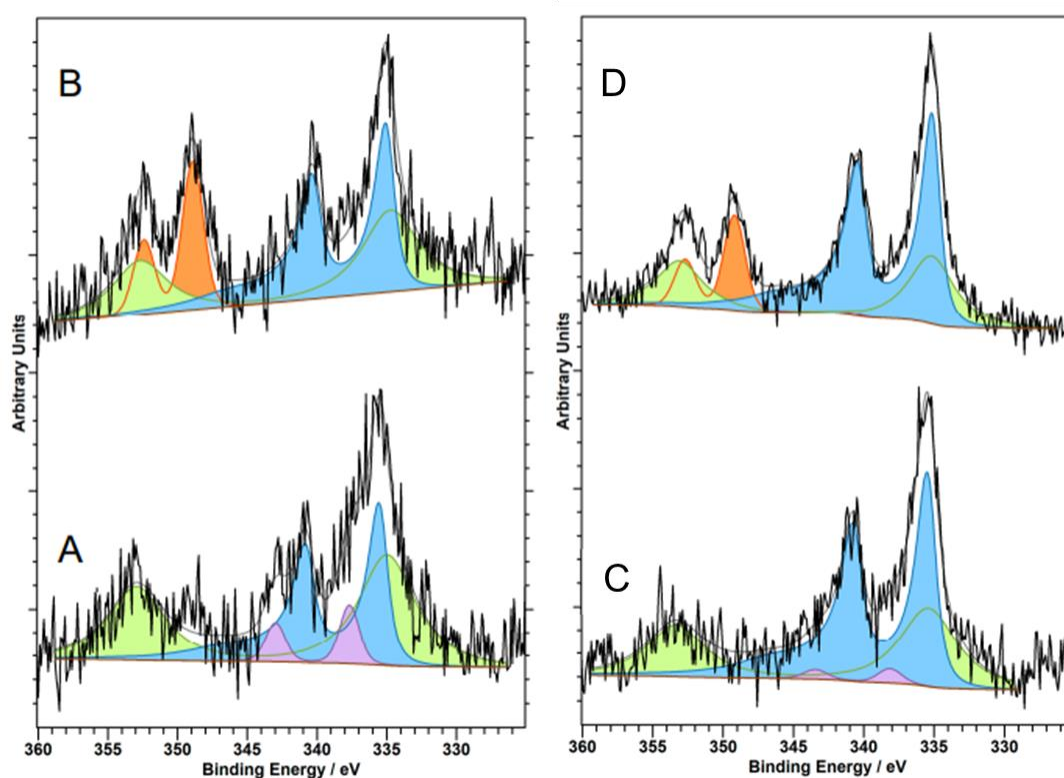


Figure 5.15: XPS spectra of Pd(3d) regions for the (A) as-prepared and (B) used 1wt% AuPd/ZSM-5 catalyst, after use (C) as-prepared and (D) used 1wt% AuPd_(0.975)Cu_(0.025)/ZSM-5 catalyst, after use in the H₂O₂ direct synthesis reaction.¹⁵ Key: Au(4d) (green), Pd⁰ (blue), Pd²⁺ (purple), Ca²⁺ (orange). H₂O₂ synthesis conditions: 0.5 h, 2 °C, P(5% H₂/CO₂) = 420 psi, P(25% O₂/CO₂) = 160 psi, 0.01 g catalyst, 2.9 g water, 5.6 g methanol, 1200 rpm. Catalysts prepared by excess chloride co-precipitation and reduced (5% H₂/Ar, 400 °C, 4 h, 10 °C min⁻¹). XPS analysis and images by Dr David Morgan.

5.3 Conclusions

The direct synthesis of H_2O_2 is an industrially important reaction for its use as a green oxidant. It has been shown that by making very small changes to the catalyst with low levels of metal doping, it is possible to enhance activity and selectivity of metal catalysts for this reaction.

Developing on the work whereby bimetallic AuPd titania supported catalysts were doped with various earth abundant transition metals, a ZSM-5 support has been employed and introduced to low level doping of Cu, Ni and Zn, for use in direct H_2O_2 synthesis. A series of 1wt % $\text{AuPd}_{(0.975)}\text{X}_{(0.025)}/\text{ZSM-5}$ (where X = Cu, Ni, Zn) catalysts were prepared via an excess chloride wet co-impregnation technique and subsequent reductive heat treatment.

It was found that the introduction of all tertiary metals (Cu, Ni, Zn) enhanced the H_2O_2 synthesis activity compared to that seen for the AuPd bimetallic analogue. However, most notably it was seen that that introduction of Cu into the catalyst promoted the activity towards the direct synthesis reaction, far above the catalysts doped with Ni, Zn and outperforms the bimetallic analogue (1wt% AuPd/ZSM-5) by a factor of 1.7. Additionally, this Cu catalyst was shown to be comparable to the activity seen for previously reported catalysts using Pt as a promoter for AuPd nanoalloys.³

It was also observed that the addition of the third metal acts as a stabiliser with respect to metal leaching during the reaction. XPS analysis of the fresh catalysts showed that low levels of doping with Cu, Zn and Ni noticeable shift in Pd species to Pd^{2+} , this mixture of Pd states is known to promote activity towards H_2O_2 synthesis.^{16,17}

A series of Cu doped catalysts were made with Cu loadings ranging from 0.0125 to 0.0375 wt% (total metal loading was fixed at 1wt %). It was observed that there is a small window in the Cu loading where the addition of Cu enhances the activity towards H_2O_2 synthesis. At the highest Cu loading (1wt% $\text{AuPd}_{(0.9625)}\text{Cu}_{(0.0375)}/\text{ZSM-5}$) catalyst activity declined, in keeping with earlier studies that have shown that the alloying of Pd or AuPd nanoalloys with Cu can result in catalyst deactivation.^{4,5}

Further analysis of optimised 1wt% $\text{AuPd}_{(0.975)}\text{Cu}_{(0.025)}/\text{ZSM-5}$ catalyst was performed, using the bimetallic analogue 1wt% AuPd/ZSM-5 as a comparison. Characterisation of the catalysts

by XPS and CO-DRIFTS revealed that the increase in H₂O synthesis activity seen by the Cu doped catalyst, can be attributed to the electronic modification of the Pd species and changes in the surface composition of the nanoalloys as a result of Cu incorporation.

Reuse studies showed that while catalytic stability is an issue due to deactivation which was attributed to the *in situ* reduction of Pd species, and modification of the Au:Pd ratio indicating nanoalloy restructuring, it can be considered that these materials represent a promising basis for future exploration in a range of reactions, particularly where the *in situ* supply of H₂O₂ is required.

5.4 References

- 1 J. M. Campos-Martin, G. Blanco-Brieva and J. L. G. Fierro, *Angew. Chemie - Int. Ed.*, 2006, **45**, 6962–6984.
- 2 R. J. Lewis and G. J. Hutchings, *ChemCatChem*, 2019, **11**, 298–308.
- 3 X. Gong, R. J. Lewis, S. Zhou, D. J. Morgan, T. E. Davies, X. Liu, C. J. Kiely, B. Zong and G. J. Hutchings, *Catal. Sci. Technol.*, 2020, **10**, 4635–4644.
- 4 C. M. Crombie, R. J. Lewis, R. L. Taylor, D. J. Morgan, T. E. Davies, A. Folli, D. M. Murphy, J. K. Edwards, J. Qi, H. Jiang, C. J. Kiely, X. Liu, M. S. Skjøth-Rasmussen and G. J. Hutchings, *ACS Catal.*, 2021, **11**, 2701–2714.
- 5 A. Santos, R. J. Lewis, D. J. Morgan, T. E. Davies, E. Hampton, P. Gaskin and G. J. Hutchings, *Catal. Sci. Technol.*, 2021, **11**, 7866–7874.
- 6 R. J. Lewis, A. Bara-Estaun, N. Agarwal, S. J. Freakley, D. J. Morgan and G. J. Hutchings, *Catal. Letters*, 2019, **149**, 3066–3075.
- 7 J. Kang, P. Puthiaraj, W. seung Ahn and E. D. Park, *Appl. Catal. A Gen.*, 2020, **602**, 117711.
- 8 R. J. Lewis, K. Ueura, Y. Fukuta, S. J. Freakley, L. Kang, R. Wang, Q. He, J. K. Edwards, D. J. Morgan, Y. Yamamoto and G. J. Hutchings, *ChemCatChem*, 2019, **11**, 1673–1680.
- 9 J. Lyu, J. Wei, L. Niu, C. Lu, Y. Hu, Y. Xiang, G. Zhang, Q. Zhang, C. Ding and X. Li, *RSC Adv.*, 2019, **9**, 13398–13402.
- 10 R. J. Lewis, K. Ueura, X. Liu, T. E. Davies, D. J. Morgan, L. Chen, J. Qi, J. Singleton and G. J. Hutchings, *Science (80-.)*, 2022, **376**, 615–620.
- 11 T. Richards, R. J. Lewis, D. J. Morgan and G. J. Hutchings, *Catal. Letters*, 2023, **153**, 32–40.
- 12 E. N. Ntainjua, J. K. Edwards, A. F. Carley, J. A. Lopez-Sanchez, J. A. Moulijn, A. A. Herzing, C. J. Kiely and G. J. Hutchings, *Green Chem.*, 2008, **10**, 1162–1169.
- 13 M. Sankar, Q. He, M. Morad, J. Pritchard, S. J. Freakley, J. K. Edwards, S. H. Taylor, D. J. Morgan, A. F. Carley, D. W. Knight, C. J. Kiely and G. J. Hutchings, *ACS Nano*, 2012, **6**, 6600–6613.
- 14 A. M. Joshi, W. N. Delgass and K. T. Thomson, *J. Phys. Chem. C*, 2007, **111**, 7841–7844.
- 15 A. Barnes, R. J. Lewis, D. J. Morgan, T. E. Davies and G. J. Hutchings, *Catalysts*, 2022, **12**, 1–15.
- 16 A. R. Wilson, K. Sun, M. Chi, R. M. White, J. M. Lebeau, H. H. Lamb and B. J. Wiley, *J.*

- Phys. Chem. C*, 2013, **117**, 17557–17566.
- 17 L. Ouyang, P. F. Tian, G. J. Da, X. C. Xu, C. Ao, T. Y. Chen, R. Si, J. Xu and Y. F. Han, *J. Catal.*, 2015, **321**, 70–80.
 - 18 A. Y. Waziri, A. A. Osigbesan, F. N. Dabai, S. M. Shuwa, A. Y. Atta and B. Y. Jibril, *Appl. Petrochemical Res.*, 2019, **9**, 101–112.
 - 19 K. Duan, Z. Liu, J. Li, L. Yuan, H. Hu and S. I. Woo, *Catal. Commun.*, 2014, **57**, 19–22.
 - 20 D. P. Dissanayake and J. H. Lunsford, *J. Catal.*, 2002, **206**, 173–176.
 - 21 P. Tian, L. Ouyang, X. Xu, C. Ao, X. Xu, R. Si, X. Shen, M. Lin, J. Xu and Y. F. Han, *J. Catal.*, 2017, **349**, 30–40.
 - 22 P. Tian, D. Ding, Y. Sun, F. Xuan, X. Xu, J. Xu and Y. F. Han, *J. Catal.*, 2019, **369**, 95–104.
 - 23 J. Brehm, R. J. Lewis, D. J. Morgan, T. E. Davies and G. J. Hutchings, *Catal. Letters*, 2022, **152**, 254–262.
 - 24 www.harwellxps.guru/knowledgebase/chlorine, (accessed June 2024).

Chapter 6: Conclusions and Future Work

The work in this thesis highlights the importance of the effect of catalyst modification by both thermal treatments and metal doping, to improve both activity and selectivity.

By incorporating a calcination heat treatment prior to reduction for a series of Pt based catalysts it was found that the nanoparticles were anchored to the support, preventing Pt agglomeration during the reduction step and also preventing an SMSI effect that covered the Pt active sites and hence effecting the activity of the catalyst. This modification not only increased the activity of the catalyst but maintained comparable selectivities to the less active reduced only counterparts (that did not undergo the calcination step).

In a novel area of research low concentrations of non-precious transition metals were incorporated into AuPd catalysts for direct H₂O₂ synthesis. Most notably Cu, Ni and Zn were all found to have significant promotional effects on the activity of the reaction over the catalysts in levels of 0.025wt% Cu, Ni or Zn (and lower). Introduction of Cu, Ni and Zn were shown to modify the electronic properties of the AuPd catalysts, most notably by effecting the Pd species of the catalysts.

6.1 Tuning Pt/TiO₂ Catalysts for the Chemoselective Hydrogenation of 3-Nitrostyrene

6.1.1 Conclusions

The synthesis of functionalised anilines such as 3-vinylaniline is important industrially to produce pharmaceuticals, agrochemicals, dyes and fine chemicals. However, the reduction of 3-nitrostyrene to 3-vinylaniline can be difficult due to the presence of the olefin functional group that competes with the nitro group to be reduced. Therefore, it is important to tune catalyst for this reaction to selectively reduce the nitro functional group.

In this thesis, a series of Pt/TiO₂ catalysts, prepared by wet impregnation, were synthesised and underwent specific heat treatments to tune the catalyst sites and enhance the activity of these catalysts. The results of these catalysts for the chemoselective reduction of 3-nitrostyrene to 3-vinylaniline are shown in Table 6.1.

Table 6.1: Chemoselective hydrogenation of 3-nitrostyrene to 3-vinylaniline over Pt/TiO₂ catalysts.

| Catalyst | Heat Treatment | Initial Rate mol _{3NS} kg ⁻¹ min ⁻¹ | TOF hr ⁻¹ |
|-----------------------------|--------------------|---|-------------------------|
| 0.05wt% Pt/TiO ₂ | Reduced | 1.34 x 10 ⁻¹ | 3.12 x 10 ³ |
| | Calcined + Reduced | 2.55 x 10 ⁻² | 5.96 x 10 ² |
| 0.08wt% Pt/TiO ₂ | Reduced | 2.80 x 10 ⁻¹ | 4.10 x 10 ³ |
| | Calcined + Reduced | 2.85 x 10 ⁻¹ | 4.16 x 10 ³ |
| 0.2wt% Pt/TiO ₂ | Reduced | 2.48 x 10 ⁻¹ | 1.45 x 10 ³ |
| | Calcined + Reduced | 9.66 x 10 ⁻¹ | 5.65 x 10 ³ |
| 0.5wt% Pt/TiO ₂ | Reduced | 4.54 x 10 ⁻¹ | 1.06 x 10 ³ |
| | Calcined + Reduced | 1.77 | 4.14 x 10 ³ |

Reaction conditions: 3-NS (0.2 mL), toluene (8 mL), p(H₂): 3 bar, catalyst (50 mg), temperature: 40 °C, stirring throughout. Reduction heat treatment: 5% H₂/Ar, 450 °C, 4 hrs. Calcination heat treatment static air, 450 °C, 4 hrs.

The data showed that for the catalysts with higher Pt loadings (0.2wt% Pt/TiO₂ and 0.5wt% Pt/TiO₂) the calcination treatment prior to the reduction heat treatment, resulted in catalysts that were much more active than their reduced-only counterparts. Through characterisation of these catalysts, it was found that an SMSI effect (strong metal-support interaction) was induced by the reductive heat treatment (at 450°C) where the support covered the catalytic sites, diminishing the activity. It was found that a calcination step prior to the reductive treatment was able to counteract this effect, potentially through anchoring of the Pt on to the support, limiting its mobility. Consequently, the reduced-only catalysts were shown to have larger nanoparticles.

The lower loading catalysts (0.05wt% Pt/TiO₂) did not show this pattern, it was proposed that due to the improved dispersion of metal on these catalysts the prior calcination step was not required to prevent agglomeration of the particles and the resulting size-dependant coverage of the support.

This work presents a highly active and selective 0.2wt% Pt/TiO₂ calcined + reduced catalyst for the chemoselective hydrogenation of 3-nitrostyrene to 3-vinylaniline with 90% selectivity at 99% conversion in 60 minutes.

6.1.2 Future Work

An area that has not been addressed in this work is the reusability of the Pt/TiO₂ catalysts for the chemoselective hydrogenation of 3-nitrostyrene. This is important for any industrial reaction due to the costs of catalyst materials and preparation, but also for the pursuit of processes that support green chemistry. Ideally the catalyst would be reusable without any decreases in activity or selectivity, however, when the catalyst is extracted from the post-reaction solution, if the active species has changed or deactivated the catalyst may need to undergo a reactivation process, and this is an important area that needs to be developed from this work.

One key area that was seen in this work is the effect that SMSI (strong metal support interaction) can have on a catalyst. A number of oxide supports (including Al₂O₃, Fe₃O₄ and SiO₂) have been used in conjunction with Pt for the reduction of nitroarenes, also carbon has been evaluated.¹⁻⁵ By performing a similar study with different supports this metal-support interaction can be further investigated.

Research into the chemoselective hydrogenation of nitroarenes involves more than just nitrostyrene reduction and is therefore a rich area for further research with these tuned catalysts. Nitroarenes can contain a range of additional reducible functionality, aside from the olefin groups, (including -X -C=O -C≡C and -C≡N) and the nitro functional group needs to be preferentially reduced instead of these so that the resulting functionalised anilines can be utilised. Many Pt catalysts have been successfully used for the chemoselective reduction of halo-nitrobenzene (halogen groups: F, Cl, Br, I), achieving high selectivities (up to 99.9%) at 100% conversion.⁶⁻⁸ It has been found that the selectivity of the catalysts can be improved by modifying the metal surface and generating metal-support interactions, which makes the catalysts in this thesis highly promising for this reaction.⁹ Similarly, nitrobenzaldehyde and nitroacetophenone (containing C=O functional group) have had success using Pt-based catalysts for their chemoselective hydrogenation.^{10,11} This reaction has been found challenging as some reducing agents react readily with the carbonyl group without a catalyst present, such as LiAlH₄ and NaBH₂.⁹ Nitrobenzotrile (containing C≡N) and nitrophenylacetylene (containing C≡C) chemoselective reduction has also seen promising results with Pt-based catalysts¹²⁻¹⁴ and again would be another area for which this work can be developed.

6.2 Direct Synthesis of H₂O₂ using Transition Metal Incorporated AuPd Catalysts

6.2.1 Conclusions

An important reaction in the development of heterogeneous catalysts is the direct synthesis of H₂O₂. The production of H₂O₂ on a large scale is vital in the field of green chemistry, as it is a green oxidant with the only by-product of its use being water. The direct synthesis of H₂O₂ is an important field of research and has the potential to replace the Anthraquinone Auto-oxidation Process which is currently the method by which the majority of H₂O₂ is produced worldwide. The direct synthesis of H₂O₂ is well documented using bimetallic AuPd-supported catalysts, which display a synergistic effect that enhances both the activity and selectivity of the catalyst.

In this thesis, small levels of a transition metal dopant were added to a AuPd supported catalyst for the direct synthesis of H₂O₂. The use of trimetallics in this reaction is a novel field and is mainly limited to Pt incorporation to AuPd, with some work using Ru another precious metal.¹⁵⁻¹⁸ The use of small concentrations of a dopant was inspired by the work from Gong *et al*¹⁸ where small concentrations of Pt were used in a 1wt% Au₁Pd₁Pt_{0.1}/TiO₂ catalyst that showed high activity for the direct synthesis of H₂O₂ (112 moles_{H₂O₂} kg_{cat}⁻¹ hr⁻¹) with good selectivity (37% H₂O₂ selectivity at 43% H₂ conversion), when compared to higher Pt loadings such as 1wt% Au₁Pd₁Pt₁/TiO₂ (30 moles_{H₂O₂} kg_{cat}⁻¹ hr⁻¹, 44% H₂ conversion, 15% H₂O₂ selectivity) and its bimetallic AuPd analogue (81 moles_{H₂O₂} kg_{cat}⁻¹ hr⁻¹, 39% H₂ conversion, 31% H₂O₂ selectivity). Transition metals were selected in this work due to their low cost and availability which makes them more favourable than using additional precious metals such as Pt. A range of transition metals have been used successfully when alloyed with Pd for the direct synthesis of H₂O₂, with the exception of Cu incorporation which has previously been shown to have a deleterious effect towards the synthesis reaction. In Chapter 4 a series of 1wt% AuPd_(0.975)X_(0.025)/TiO₂ (where X = Ni, Zn, Cu, In, Co, Ga, Sn, Pt) catalysts were prepared by sol-immobilisation and in Chapter 5 a series of 1wt% AuPd_(0.975)X_(0.025)/ZSM-5 (where X = Ni, Zn, Cu) catalysts were prepared by an excess chloride co-precipitation methodology, and investigated for their performance in the direct synthesis of H₂O₂. The most promising transition metal dopants from the initial testing were Cu, Ni and Zn, and a summary of the key results on both the TiO₂ and ZSM-5 supported catalysts are presented in Table 6.2.

Table 6.2: Comparison of 1wt% AuPd_(0.975)X_(0.025)/TiO₂ and 1wt% AuPd_(0.975)X_(0.025)/ZSM-5 (where X = Cu, Ni, Zn) catalyst series for the direct synthesis of H₂O₂, including H₂ conversion and H₂O₂ selectivity, and H₂O₂ degradation.

| Catalyst / 1wt% | H ₂ O ₂ Synthesis / mol _{H₂O₂} kg _{cat} ⁻¹ h ⁻¹ | H ₂ O ₂ Degradation / mol _{H₂O₂} kg _{cat} ⁻¹ h ⁻¹ | H ₂ Conversion / % | H ₂ O ₂ Selectivity / % |
|--|--|--|----------------------------------|--|
| AuPd₍₁₎/TiO₂ | 61 | 219 | 12 | 59 |
| AuPd_(0.975)Cu_(0.025) /TiO₂ | 94 | 169 | 31 | 40 |
| AuPd_(0.975)Ni_(0.025) /TiO₂ | 107 | 203 | 32 | 41 |
| AuPd_(0.975)Zn_(0.025) /TiO₂ | 100 | 191 | 24 | 50 |
| AuPd₍₁₎/ZSM-5 | 69 | 320 | 12 | 83 |
| AuPd_(0.975)Cu_(0.025) /ZSM-5 | 115 | 529 | 19 | 72 |
| AuPd_(0.975)Ni_(0.025) /ZSM-5 | 81 | 281 | 12 | 81 |
| AuPd_(0.975)Zn_(0.025) /ZSM-5 | 77 | 361 | - | - |

H₂O₂ direct synthesis conditions: 0.5 h, 2 °C, P(5% H₂/CO₂) = 420 psi, P(25% O₂/CO₂) = 160 psi, 0.01 g catalyst, 2.9 g water, 5.6 g methanol, 1200 rpm. Degradation conditions: 0.5 h, 2 °C, P(5% H₂/CO₂) = 420 psi, 0.01 g catalyst, 0.68 g H₂O₂ (50 wt%), 2.22 g water, 5.6 g methanol, 1200 rpm. H₂ conversion and H₂O₂ selectivity from measured from synthesis reaction. TiO₂ supported catalysts prepared by sol-immobilisation and calcined (static air, ramp 10 °C min⁻¹, 400 °C, 3 h). ZSM-5 supported catalysts prepared by excess chloride co-precipitation impregnation and reduced (5% H₂/Ar, 400 °C, 4 h, 10 °C min⁻¹).

When comparing the data sets from Chapters 4 and 5, it is evident that the change in support and catalyst preparation methodology influences the catalysts activities and selectivities. For the TiO₂-supported catalysts, it was found that the incorporation of the tertiary metals (Cu, Ni, Zn) at a loading of 0.025wt% produced the highest activities towards the synthesis of H₂O₂.

It is also interesting that the incorporation of the same concentration of the tertiary metal (0.025wt%) has a substantial promotional effect for the synthesis activity for the ZSM-5-supported trimetallics. To this end, optimisation of the Cu loading in the 1wt%AuPdCu/ZSM-5 catalyst series was found to be in the same range ($\sim 0.025\text{wt}\%$) as the TiO_2 -supported AuPdCu analogue.

Notably, all of the ZSM-5-supported catalysts show a substantial increase in the degradation activities compared to their TiO_2 -supported analogues, for example, the 1wt%AuPd/ TiO_2 catalyst had a degradation activity of $219 \text{ mol}_{\text{H}_2\text{O}_2} \text{ kg}_{\text{cat}}^{-1} \text{ h}^{-1}$ whereas for the 1wt%AuPd/ZSM-5 analogue this value was $320 \text{ mol}_{\text{H}_2\text{O}_2} \text{ kg}_{\text{cat}}^{-1} \text{ h}^{-1}$. Conversely, the ZSM-5-supported catalysts show higher H_2O_2 selectivities (in the synthesis reaction) compared to their TiO_2 -supported analogues, this is most evident for the bimetallic catalysts at a H_2 iso-conversion of 12% where 1wt%AuPd/ TiO_2 gave a H_2O_2 selectivity of 59% and 1wt%AuPd/ZSM-5 gave a H_2O_2 selectivity of 83%. It should be noted that the conditions of the H_2O_2 synthesis and the H_2O_2 degradation reactions are different which could account for this observation.

However, one clear difference between the two catalyst series is that the rate of H_2O_2 synthesis for the trimetallic differs for the specified tertiary metal depending on the support. With the current data it is not evident whether this is due to the choice of support (and the interaction of the metal with it), the catalyst preparation technique, or both.

It is evidenced from the results that the incorporation of small concentrations of transition metals can be used in a trimetallic catalysts with AuPd to enhance the rate of H_2O_2 synthesis, with activities that are comparable to the previously reported Pt trimetallic catalyst. Through the characterisation of the catalysts by XPS and CO-DRIFTS, the enhanced activities of the trimetallic catalysts were attributed to the electronic modification of the Pd species with the addition of low concentrations of tertiary metals found to promote the formation of Pd^{2+} - Pd^0 domains and also changes in the surface composition of the nanoalloy.

A key finding in this work was the effect that Cu incorporation had on the AuPd precious metal catalysts. Contrary to the results seen previously over PdCu catalysts (albeit with higher Cu loadings)^{19,20} and computational studies²¹ that predicted that Cu-containing precious metal nanoparticle catalysts would be unfavourable towards the synthesis of H_2O_2 , these studies have in fact shown that in small concentrations (0.025wt% Cu in a 1wt% AuPd supported

catalyst) Cu can have a substantial promotional effect in combination with Au and Pd precious metals.

6.2.2 Future Work

Developing on the work in this thesis the first key area of future work would be to create catalyst series where the ZSM-5 supported catalysts are prepared by sol-immobilisation, and the TiO₂ supported catalysts are prepared by excess chloride co-precipitation. It is not possible to pinpoint the cause of the discrepancies between the degradation and H₂O₂ selectivities of the two catalyst series without this study. Both the support choice and preparation method have their own influences on the attributes of a catalyst, and from the results in this work it is evident that the transition metal effect in the catalyst is dependent on at least one of these factors, due to the different trends seen in the synthesis activities for each series.

This work was all performed in a batch system, further work could look into using these catalysts in a flow reactor to produce H₂O₂. Many of the catalysts produced, although very active towards the direct synthesis of H₂O₂, showed high degradation rates, in particular the ZSM-5 supported catalysts. In a flow set-up the formed H₂O₂ is removed from the system reducing the opportunity for its degradation can occur over the catalyst.

Additionally, there have been some promising results using PtFe supported catalysts for oxidation reactions where H₂O₂ is produced *in situ*, and therefore another interesting area to investigate would be low level of Fe doping, as this metal was not used in this work.^{19,20}

Another area of importance would be to investigate the introduction of low concentrations of transition metals to Pd-supported catalysts, potentially negating the need for Au, or reducing the quantity of Au needed. This would be beneficial in reducing the amount of noble metals in the catalysts needed for the direct synthesis of H₂O₂.

Further experimental and DFT studies into the promotional effect of Cu in precious metal catalysts for the direct synthesis of H₂O₂ also need to be performed. Although incorporation of the Cu was found to result in electronic modification of the Pd species and changes in surface composition, due to the extremely low levels of doping used in this work, the

techniques employed (TEM, XPS, ICP-MS) were not able to detect the Cu (or other dopant metals) in the catalyst samples. It is therefore not known why Cu incorporation at such low levels has such a significant effect on the trimetallic catalysts, when previous studies (albeit at much higher Cu loadings = 0.5wt%)^{19,20} and computational predictions²¹ have shown and predicted extremely low activities.

The large-scale production of H₂O₂ via the direct synthesis from its constituent gases is a promising alternative to the anthraquinone process. However, the ability to produce H₂O₂ on a smaller scale at the site of use is of huge advantage as this eliminates many costs associated with storage and transportation. Developing on this is the *in-situ* production of H₂O₂ for oxidation reactions. For such reactions the catalyst must not only be active for the direct synthesis of H₂O₂ but must also be active (and selective) for the subsequent oxidation reaction. Another challenge for this is the conditions used for the oxidation may not be optimal for H₂O₂ synthesis. There are a number of established *in-situ* oxidation reactions including benzyl alcohol oxidation and the degradation of phenol that use AuPd and PdX (where X = Mn, Fe, Co, Cu, Ni, Ce) catalysts,^{19,20} and therefore could benefit from the introduction of trimetallic catalysts such as the ones produced in this work.

6.3 References

- 1 J. Li, L. Zhong, L. Tong, Y. Yu, Q. Liu, S. Zhang, C. Yin, L. Qiao, S. Li, R. Si and J. Zhang, *Adv. Funct. Mater.*, 2019, **29**, 1–9.
- 2 Y. Sheng, X. Wang, Z. Xing, X. Chen, X. Zou and X. Lu, *ACS Sustain. Chem. Eng.*, 2019, **7**, 8908–8916.
- 3 H. Wei, X. Liu, A. Wang, L. Zhang, B. Qiao, X. Yang, Y. Huang, S. Miao, J. Liu and T. Zhang, *Nat. Commun.*, 2014, **5**, 1–8.
- 4 Q. Wu, B. Zhang, C. Zhang, X. Meng, X. Su, S. Jiang, R. Shi, Y. Li, W. Lin, M. Arai, H. Cheng and F. Zhao, *J. Catal.*, 2018, **364**, 297–307.
- 5 Y. Pei, Z. Qi, T. W. Goh, L. L. Wang, R. V. Maligal-Ganesh, H. L. MacMurdo, S. Zhang, C. Xiao, X. Li, F. (Feng) Tao, D. D. Johnson and W. Huang, *J. Catal.*, 2017, **356**, 307–314.
- 6 S. Ichikawa, M. Tada, Y. Iwasawa and T. Ikariya, *Chem. Commun.*, 2005, 924–926.
- 7 J. Zhao, L. Ma, X. L. Xu, F. Feng and X. N. Li, *Chinese Chem. Lett.*, 2014, **25**, 1137–1140.
- 8 H. Li, C. Xu, X. L. Mu, P. Zhang, X. M. Zhang and N. Zheng, *ChemNanoMat*, 2018, **4**, 518–523.
- 9 Z. N. Hu, J. Liang, K. Ding, Y. Ai, Q. Liang and H. bin Sun, *Appl. Catal. A Gen.*, 2021, **626**, 118339.
- 10 J. Zhang, L. Wang, Y. Shao, Y. Wang, B. C. Gates and F. S. Xiao, *Angew. Chemie - Int. Ed.*, 2017, **56**, 9747–9751.
- 11 M. Liu, W. Tang, Y. Xu, H. Yu, H. Yin, S. Zhao and S. Zhou, *Appl. Catal. A Gen.*, 2018, **549**, 273–279.
- 12 P. Serna and A. Corma, *ACS Catal.*, 2015, **5**, 7114–7121.
- 13 A. Han, J. Zhang, W. Sun, W. Chen, S. Zhang, Y. Han, Q. Feng, L. Zheng, L. Gu, C. Chen, Q. Peng, D. Wang and Y. Li, *Nat. Commun.*, 2019, **10**, 1–7.
- 14 Ö. Metin, A. Mendoza-Garcia, D. Dalmazrak, M. S. Gültekin and S. Sun, *Catal. Sci. Technol.*, 2016, **6**, 6137–6143.
- 15 E. N. Ntainjua, S. J. Freakley and G. J. Hutchings, *Top. Catal.*, 2012, **55**, 718–722.
- 16 J. K. Edwards, J. Pritchard, L. Lu, M. Piccinini, G. Shaw, A. F. Carley, D. J. Morgan, C. J. Kiely and G. J. Hutchings, *Angew. Chemie - Int. Ed.*, 2014, **53**, 2381–2384.
- 17 J. K. Edwards, J. Pritchard, P. J. Miedziak, M. Piccinini, A. F. Carley, Q. He, C. J. Kiely and G. J. Hutchings, *Catal. Sci. Technol.*, 2014, **4**, 3244–3250.
- 18 X. Gong, R. J. Lewis, S. Zhou, D. J. Morgan, T. E. Davies, X. Liu, C. J. Kiely, B. Zong and G.

- J. Hutchings, *Catal. Sci. Technol.*, 2020, **10**, 4635–4644.
- 19 C. M. Crombie, R. J. Lewis, R. L. Taylor, D. J. Morgan, T. E. Davies, A. Folli, D. M. Murphy, J. K. Edwards, J. Qi, H. Jiang, C. J. Kiely, X. Liu, M. S. Skjøth-Rasmussen and G. J. Hutchings, *ACS Catal.*, 2021, **11**, 2701–2714.
- 20 A. Santos, R. J. Lewis, D. J. Morgan, T. E. Davies, E. Hampton, P. Gaskin and G. J. Hutchings, *Catal. Sci. Technol.*, 2021, **11**, 7866–7874.
- 21 A. M. Joshi, W. N. Delgass and K. T. Thomson, *J. Phys. Chem. C*, 2007, **111**, 7841–7844.